MODELLING THE IMPACT OF CLIMATE CHANGE AND SEA LEVEL RISE ON THE MORPHOLOGY OF LOWER MEGHNA RIVER

RAJIB KAMAL

DEPARTMENT OF WATER RESOURCES ENGINEERING
BANGLADESH UNIVERSITY OF ENGINEERING AND TECHNOLOGY (BUET), DHAKA – 1000

DECEMBER 2011

MODELLING THE IMPACT OF CLIMATE CHANGE AND SEA LEVEL RISE ON THE MORPHOLOGY OF LOWER MEGHNA RIVER

A Thesis Submitted by

Rajib Kamal
(0409162028 P)

In partial fulfillment of the requirements for the degree
of
Master of Science in Water Resources Engineering

Department of Water Resources Engineering
Bangladesh University of Engineering and Technology (BUET)
DHAKA - 1000

December 2011

CERTIFICATION OF APPROVAL

The thesis titled **"Modelling the Impact of Climate Change and Sea Level Rise on the Morphology of Lower Meghna River"**, submitted by Rajib Kamal, Roll No. 0409162028P, Session: April 2009, has been accepted as satisfactory in partial fulfillment of the requirement for the degree of **Master of Science in Water Resources Engineering** on 20th December, 2011.

_____

Dr. Md. Abdul Matin — **Chairman**
Professor
Department of Water Resources Engineering
BUET, Dhaka-1000, Bangladesh

_____

Dr. Umme Kulsum Navera — **Member (Ex-Officio)**
Professor and Head
Department of Water Resources Engineering,
BUET, Dhaka-1000, Bangladesh

_____

Dr. Md. Sabbir Mostafa Khan — **Member**
Professor
Department of Water Resources Engineering,
BUET, Dhaka-1000, Bangladesh

_____

Mr. Abu Saleh Khan — **Member (External)**
Deputy Executive Director,
Institute of Water Modelling (IWM),
Dhaka, Bangladesh

DECEMBER 2011

DECLARATION

It is hereby declared that this thesis work or any part of it has not been submitted elsewhere for the award of any degree or diploma.

Dr. Md. Abdul Matin	**Rajib Kamal**
Countersigned by the Supervisor	Signature of the Candidate

TABLE OF CONTENTS

LIST OF FIGURES

Page No.

LIST OF TABLES

Page No.

LIST OF SYMBOLS

a	Coefficient in resistance equation	-
b	Exponent in resistance equation	-
B	Bankfull width	[L]
B_f	Floodplain width	[L]
c	Volumetric sediment concentration	$[ML^{-3}]$
C	Chezy number	$[L^{1/2}T^{-1}]$
C_f	Dimensionless bed friction coefficient	-
d	Still water depth	[L]
D	Characteristic size of the sediment	[L]
E	Error	-
g	Gravitational acceleration	$[LT^{-2}]$
h	Total water depth	[L]
H	Depth of flow	[L]
I_f	Intermittency Factor	-
n	Porosity of bed deposit	-
P	Precipitation	[L]
q	Discharge per unit width	$[L^2T^{-1}]$
q_t	Sediment discharge per unit width	$[L^2T^{-1}]$
Q	Discharge	$[L^3T^{-1}]$
Q_{bf}	Bankfull discharge	$[L^3T^{-1}]$
Q_{tbf}	Total volume bed material load at bankfull flow	$[L^3T^{-1}]$
R	Submerged specific gravity of the sediment	-
s_b	Streamwise position of the foreset-bottomset break	[L]
s_s	Streamwise position of the topset-foreset break	[L]
s_u	Streamwise position of the bedrock-alluvial break	[L]
S	Channel bed slope	-
S_a	Constant slope of avalanche onto the foreset	-
S_{bb}	Constant slope of the basement	-
S_{sb}	Subaqueous bed slope	-
S_x	Total load transport in the x direction	$[L^3T^{-1}]$
S_y	Total load transport in the y direction	$[L^3T^{-1}]$

t	Time	$[T]$
u	Velocity components in the x dirtection	$[LT^{-1}]$
v	Velocity components in the y dirtection	$[LT^{-1}]$
W	Connection weights of ANN	-
z	Bed level	$[L]$
ε_x, ε_y, ε_z	Turbulent diffusion coefficients	$[L^2T^{-1}]$
ξ	Sea level elevation	$[L]$
η	Alluvial bed elevation	$[L]$
η_{bb}	Bedrock bed elevation	$[L]$
η_{sb}	Subaqueous bed elevation	$[L]$
η_u	Elevation of the bedrock-alluvial break	$[L]$
η_s	Elevation of the topset-foreset break	$[L]$
η_b	Elevation of the foreset-bottomset break	$[L]$
ρ	Density of water	$[ML^{-3}]$
τ^*_{bf}	Bankfull Shields number	-
Ω	Channel sinuosity	-
Λ	Fraction of wash load deposited per unit bed load	-

LIST OF ABBREVIATIONS

AOGCM	Atmospheric-Ocean Global Circulation Model
AR4	Fourth Assessment Report
CEGIS	Centre for Environment and Geographic Information System
GCM	Global Circulation Model
HD	Hydrodynamic
IPCC	Intergovernmental Panel on Climate Change
IWM	Institute of Water Modelling
MAE	Mean Absolute Error
MES	Meghna Estuary Study
MPO	Master Plan Organization
MRE	Mean Relative Error
MSE	Mean Squared Error
NAPA	National adaptation plan of action
NMSE	Normalized Mean Squared Error
SLR	Sea Level Rise
SMRC	SAARC Meteorological Research Centre
SRES	Special Report on Emissions Scenarios
TAR	Third Assessment Report

ACKNOWLEDGEMENT

The author acknowledges his deepest gratitude to his supervisor Dr. Md. Abdul Matin, Professor, Department of Water Resources Engineering, BUET for providing an interesting idea for the thesis and encouraging to work with it. His cordial supervision, valuable suggestion and expertise contributed greatly to this dissertation.

The author is also grateful to Dr. Umme Kulsum Navera, Professor and Head, Department of Water Resources Engineering, BUET, Dr. Md. Sabbir Mostofa Khan, Professor, Department of Water Resources Engineering, BUET and Mr. Abu Saleh Khan, Deputy Executive Director, IWM, who were the members of the Board of Examiners. Their valuable comments on this thesis are duly acknowledged.

Author is in debt to Institute of Water Modelling (IWM), for providing necessary data, information and modelling tools to carry out this research work. The author coveys his deepest and sincerest regards to his family for their understanding and moral support.

Above all, the author is grateful to almighty Allah, Who has given him the opportunity to work hard.

Rajib Kamal
December 2011

ABSTRACT

The impact of climate change on a river may be viewed as a complex interaction between climate, hydrology, hydraulics and morphology of the river system. The anticipated changes in temperature, precipitation and sea level is likely to have a profound impact on the morphology of a river. Altered basin water balance due to precipitation changes and rising levels of sea affects the discharge and water level of the river. The combined effect of such changes disrupts the existing equilibrium of water and sediment transport through the channel and affects various morphologic processes of the river such as change in siltation rate and consequent rise of river bed, progradation of delta along the river etc. In order to assess such complex hydraulic and morphologic response of a river to climate change, application of mathematical modelling is essential.

The present study is an effort to investigate various hydro-morphological changes of Lower Meghna River due to climate change and sea level rise with the application of different mathematical models. The GCM precipitation projections along with the sea level rise scenarios given by IPCC have been used to construct different climate change scenarios namely A1FI, A1B and B1 for the periods of 2020s, 2050s and 2080s. Based on these scenarios, a hydrological Artificial Neural Network (ANN) model and a hydro-morphological MIKE 21 FM model have been developed to assess various hydraulic and morphologic changes of the river. To verify the projections, the ANN model has been calibrated and validated with the available observed data from the year 1975 to 1994. Considering the base period as year 2008, the MIKE 21 FM model has been calibrated for the year 2006 and validated for year 2007. Then the models have used to evaluate the various hydro-morphological changes. In addition, a numerical morphological model has been developed and applied to assess the delta progradation along the river for various climate change scenarios.

The study reveals that the Lower Meghna River exhibits high seasonality with higher discharge during wet season and less discharge in the dry season. For scenario A1FI, maximum monthly discharge has been found as 95539 m^3/s, 132835 m^3/s and 111730 m^3/s for the periods of 2020s, 2050s and 2080s respectively. The backwater effect will be more pronounced during dry seasons and will elevate the water level upto 20.4 cm, 16.9 cm and 13.5 cm for scenarios A1FI, A1B and B1 respectively at the end of 2080s. Such effects will initiate heavy deposition along the river. Siltation increases

progressively at a rate of 1.02 cm/year, 2.29 cm/year and 2.96 cm/year for scenario A1B upto 2080s and the consequent bed level rise has been found as 1.86 m. Due to excess deposition and higher sediment transport the delta front of the river moves seaward. The maximum progradation of delta front towards sea has been found as 26.56 km during 2080s for scenario A1FI.

CHAPTER 1
INTRODUCTION

1.1 General

Climate change is not simply a rising of global average temperature, but will also affect many different processes on the surface of the earth in unknown ways. When investigating the climate as a whole, rivers take up an important place within the wide study of climate. These conduits are some of the most dynamic and complex systems shaping the earth's surface, and are of extreme importance to the human population which rely on rivers in myriad ways. Since climate science is mostly being undertaken to predict the needs of humans in the future, it is necessary to evaluate the possible responses of a river forced by climate change.

The impact of climate change on a river can be identified as a complex interaction between various physical processes related to hydrology, hydraulics and morphology which control the behavior of the river. As a result of climate change, the projected increase in temperature, sea level rise and precipitation variability is likely to affect such processes, resulting in a significant impact on a river basin, associated river systems and overall hydro-morphology of a river.

Change in precipitation is likely to affect the magnitude and frequency of runoff events of a river basin. The runoff of a basin is more sensitive to changes in precipitation than to evapotranspiration and other climate variables and hence small change in precipitation may cause large changes in the runoff and basin water balance. Changed basin water balance may alter the discharge hydrographs of rivers, and such alterations have been projected to cause significant changes in the hydraulics and morphology of the river.

Another consequence of the current global warming is the rising of sea level and the future effect of such sea level rise (SLR) on river system or river morphology is not well known yet. According to Intergovernmental Panel on Climate Change (IPCC), current rate of sea level rise in the coastal areas of Asia is marginally greater than the global average and has been accelerated over the past decade relative to the long term average. This rising sea level influences the flow hydraulics by creating backwater effect.

Backwater effect generally refers to the retardation of a river outflow by a rise in the level of water at the mouth of the river. Mostly it is an estuarial phenomenon. Along with

increased runoff due to climate change, this effect may create drainage condition. The consequence is progressive siltation and increase in the level of channel beds and the floodplains. Another unique phenomenon relevant to the rising sea level is the progradation of river deltas. Under conditions of rising sea level, deltas can be expected to gradually prograde outward, so that the delta front moves towards sea. In reverse sea level rise can also cause the shoreline to move landward creating embayment.

Hence climate change induced precipitation change and sea level rise will cause various hydraulic and morphologic changes in a river resulting in significant impacts on river flow, river water level, siltation rate and bed levels, delta progradation etc.

1.2 Scope and Importance of the Study

Rivers in Bangladesh are morphologically highly dynamic. The main rivers are braided, and forms islands or char in between the braiding channels. These rivers are extremely sensitive to changes in various conditions. Changes in the river flows and sediment transport due to multi-dimensional impacts of climate change are expected to increase the dynamics of these rivers even more. Therefore the country has been identified as one amongst 27 countries, which are the most vulnerable to the impacts of climate change and its possible global warming.

In the southern part of Asia, particularly in Bangladesh there are two extreme events of climate change associated with a river system – extreme dry event and extreme wet event. During wet monsoon, excess rainfall coupled with Himalayan ice-melts will increase runoff and create flood. This Flooding would be exacerbated by climate change induced sea level rise, which would limit the drainage of water due to enhanced backwater effect, as was seen in the floods of 1998. Moreover due to prolonged discharge of floodwaters, the rate of sedimentation will increase. As a result, both the riverbed and adjacent floodplains will rise leading to further drainage congestion, and possibly more intense flooding in the following years. Such a cyclic course of events would intensify the flooding problem more.

The impact of SLR would be most prominent in the southern coastal zone of Bangladesh which is connected to the Bay of Bengal through 710 km coastline. This coastal region is marked by morphologically dynamic river network and estuary system. The Pussur-Sibsa, the Lower Meghna and the Karnafuli are the major river systems of the region. The Lower Meghna River carries the combined flow of Ganges, Brahmaputra and Upper

Meghna and discharges water into the Bay of Bengal through a common terminus known as the Meghna estuary. This massive water carries enormous amount sediment towards the Bay of Bengal. Therefore the impact of SLR would be more prominent for this river. Moreover, increased rainfall runoff in the vast GBM region due to climate change also contributes to enhanced sediment flows along the GBM river systems. This is likely to increase the rate of bed level rise in the channels and the floodplains. The consequence is progressive siltation and decrease of channel depth, thereby increasing the flood ability of the alluvial plain.

In order to assess such complex hydraulic and morphologic response of a river to climate change, application of mathematical modelling is essential. The present study is an effort to investigate such changes of a river due to climate change and sea level rise by studying the Lower Meghna River with the application of different mathematical models. The runoff has been predicted from the future projections of precipitation given by IPCC using a hydrological model. Predicted runoff of Lower Meghna River along with rising sea level data has been incorporated as boundary conditions in other hydro-morphological models to determine backwater effect, siltation rate, bed level change and delta response for various climate change scenarios. For this study, all the analysis has been carried out for A1FI, A1B and B1 scenarios as given by IPCC for the years 2020s, 2050s and 2080s. The main outcome of the present study is to get insight into the river processes associated with climate change and sea level rise. The findings can be useful to assess the various impacts of climate change on a river.

1.3 Specific Objectives of the Study:

Specific Objectives of the study are as follows:

1. To predict the runoff of the river for the selected years under various climate change scenarios.
2. To estimate the magnitude and extent of backwater effect for various climate change scenarios.
3. To assess the effect of climate change on the siltation rate and consequent bed level changes for various scenarios.
4. To evaluate the progradation of delta along the selected reach for different climate change scenarios.

1.4 Organization of the Report

Chapter one gives a brief introduction and the objectives of the present study. In chapter two a short account of previous studies and literature on various aspects of climate change and river morphology has been described. Chapter three describes the theoretical and conceptual development of the models used in the study. Chapter four comprises a detailed description of the development of the models used in this study. Chapter five presents the results of the study and various analyses related to possible responses of a river to climate change. Finally the conclusions and recommendations of the study has been presented in Chapter six.

CHAPTER 2
LITERATURE REVIEW

2.1 General

The climate system which is generated by the five components: atmosphere, hydrosphere, cryosphere, land surface and biosphere – is constantly evolving influenced by various global and local factors. There is sufficient evidence that climate can vary considerably over time. If the present climate is undergoing such a change it is important to recognize the changes and to adapt hydrologic means. Therefore the knowledge of climate and its components, variables, scenarios, projections etc. as well as the various uncertainties associated with them should be well understood for any kind of impact assessment studies related to climate change.

2.2 Climate Variability and Climate Modelling

Climate change reflects the variability or average state of the atmosphere over time scales ranging from decades to millions of years. It encompasses the statistics of different atmospheric and climatic variables and other meteorological elemental measurements in a given region over long periods. Local climate is also influenced by many other factors and forcings. Small changes in any of these features may have a profound impact on climate and weather events, and on the associated systems.

Even though the climate system is extremely complex, current scientific understanding has led to several global climate models that do a reasonable job of reproducing past climate averaged over very large areas. As long as the basic physics in the climate system remain the same, this means that climate change can be partly predictable, particularly over large spatial scales such as continents and the globe. Despite several limitations, there is a progressive development in the scientific understanding of the behavior of atmosphere and ocean and their relations with climate. This knowledge can be represented mathematically and approximated by computer code. Computer models thus allow various climate related experiments (Huntington, 2006).

2.2.1 Climate Variables

The traditional knowledge of weather and climate and their changes focuses on those variables that affect daily life most directly, such as average, maximum and minimum

temperature, wind near the surface of the earth, precipitation in its various forms, humidity, cloud type and amount and solar radiation. However this is only part of the reality that determines weather and climate. The growth, movement and decay of weather and climate systems are also determined by the atmospheric circulation and by its interactions with the large scale ocean currents and the land with its features such as albedo, vegetation and soil moisture. The climate of the Earth as a whole depends on factors that influence the radiative balance, such as for example, the atmospheric composition, solar radiation or volcanic eruptions.

The most common variables applied in impact studies are surface observations of air temperature and precipitation. However, many impact models require a larger set of surface variables as mentioned above. In addition, for certain scenario construction procedures, daily upper air data, mean sea-level or circulation indices may also be needed. Derived variables, such as accumulated temperature, evapotranspiration and runoff, are usually required in regional impact studies, as these are usually computed directly from primary observations. To understand the climate and its variations and to possibly predict the impacts of such changes, one cannot ignore any of these many factors and components that determine the climate.

2.2.2 Climate Models

The behavior of the climate system, its components and their interactions, can be studied and simulated using tools known as climate models. They are used for a variety of purposes from study of the dynamics of the weather and climate system to projections of future climate. Each component or coupled combination of components of the climate system can be represented by models of varying complexity. Usually all climate models balance the incoming energy (as short wave including visible electromagnetic radiation) to the earth with outgoing energy (as long wave including infrared electromagnetic radiation) from the earth. Any imbalance results in a change in the average temperature of the earth. The most widely known applications of these models in recent years have been their use to infer the consequences of increasing greenhouse gases in the atmosphere, primarily carbon dioxide.

2.2.2.1 General Circulation Models

A General Circulation Model (GCM) is a computer based mathematical representation of the earth’s climate system in three dimensions as it evolves in time, based on the

physical properties, interactions and feedback processes of the climate. GCMs depict the climate using a three dimensional grid over the globe, typically having a horizontal resolution of between 250 and 600 km, 10 to 20 vertical layers in the atmosphere and sometimes as many as 30 layers in the oceans. Their time-dependent behaviour is computed by taking time steps typically of 30 minutes (IPCC-TGICA, 2007). A simple general circulation model (SGCM), a minimal GCM, consists of a dynamical core that relates material properties such as temperature to dynamical properties such as pressure and velocity. They are able to capture the broad characteristics of current climate well, including the general circulation patterns, temperature and synoptic scale precipitation, but are not suitable for future climate projections (IPCC, 1997).

2.2.2.2 Coupled Atmosphere Ocean General Circulation Models

Atmospheric GCMs (AGCMs) model the atmosphere (and typically contain a land-surface model as well) and impose sea surface temperatures as boundary conditions. Oceanic GCMs (OGCMs) model the ocean (with fluxes from the atmosphere imposed) and may or may not contain a sea ice model. These two are combined to form Coupled atmosphere-ocean GCMs (AOGCMs) along with the mathematical representations of other components of the climate system, such as the land surface and the cryosphere. The most recent models incorporate representations of aerosol processes, the carbon cycle and in the atmospheric chemistry. The coupled atmosphere-ocean model and the supplementary models are represented schematically in Figure 2.1.

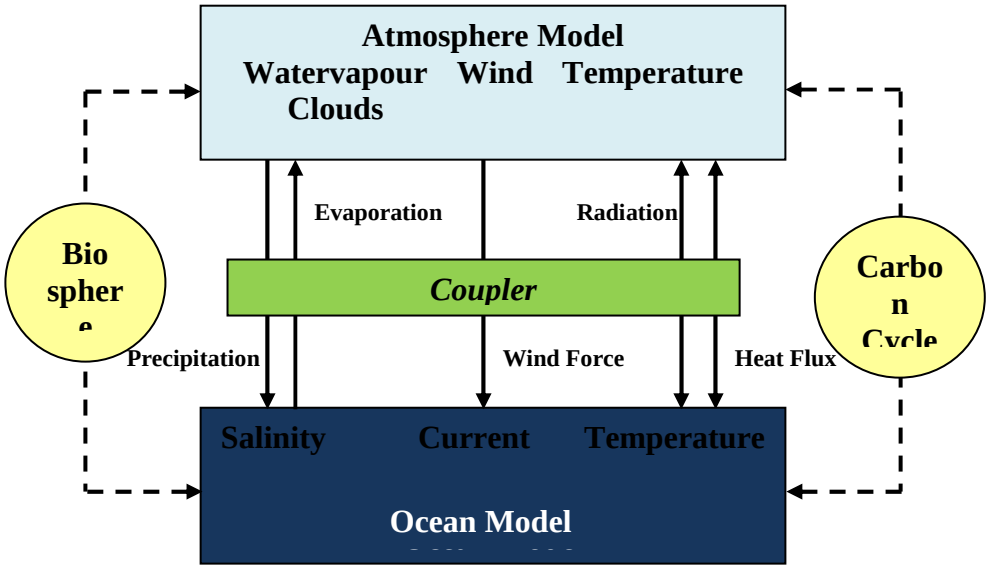

Figure 2.1: Scheme of coupled atmosphere-ocean model and the supplementary models

AOGCMs are used to study the climate system, its natural variability and its response to external forcing. The most important use of the models has been to study how Earth's climate might respond to a doubling of CO2 in the atmosphere, as discussed by the Intergovernmental Panel on Climate Change (IPCC). Much of the literature on climate change is based on studies using such models. While simpler models have been used to provide globally or regionally averaged estimates of the climate response, only AOGCMs, possibly in conjunction with nested regional models, have the potential to provide geographically and physically consistent estimates of regional climate change which are required in impact analysis. Some of the AOGCMs used by IPCC for simulating climate responses are described in Table 2.1.

Table 2.1: Summary of various coupled atmosphere-ocean GCMs (IPCC-TGICA, 2007)

GCM Model	Modelling Centre	Description
ECHAM4	Max Planck Institute for Meteorologie (MPIfM), Germany	Spectral transform model with 19 atmospheric layers and spatial resolution T42 which approximates to about 2.8º longitude/latitude resolution.
HadCM3	Hadley Centre for Climate Prediction and Research (HCCPR), UK	The model has a spatial resolution of 2.5° x 3.75° (latitude by longitude) and the representation produces a surface spatial resolution of about 417km x 278 km.
CSIRO-Mk2	Commonwealth Scientific and Industrial Research Organisation (CSIRO), Australia	The model has horizontal resolution of spectral R21 (approximately 5.6° × 3.2°) with 9 levels in atmospheric component and 21 levels in ocean component.
NCAR-PCM	National Center for Atmospheric Research (NCAR), USA	The model has a resolution of approximately 2° × 2° with 45 vertical levels in the ocean.
CGCM2	Canadian Center for Climate Modelling and Analysis (CCCma), Canada	Atmospheric component has resolution of 3.7º x 3.7º with 10 vertical levels. Ocean component has 29 vertical levels with resolution of approximately 1.8ºx1.8º.
CCSR/NIES	Center for Climate System Research (CCSR) and National Institute for Environmental Studies (NIES), Japan.	The spatial resolution is T21 spectral truncation (5.6º latitude/longitude) with 20 vertical levels for the atmospheric part and roughly 2.8 º horizontal grids with 17 vertical levels for the oceanic part.

2.3 Climate Scenarios and Projections

The climate models simulate the effects of changing climate and their future projections in terms of different climatic variables. The prediction of these variables for the future is practically not possible. Therefore all the projections of climate variables and their changes are made based on some anticipated scenarios of climate that might occur in the future.

2.3.1 Climate Scenarios

Climate change is a dynamic phenomenon where related changes will occur over time, and implications will only be understood in future. It is not possible to define a changing climate that might occur within a defined period in future as no method yet has been developed to provide satisfactory predictions of climate change over a geographic region or a country. An alternative approach is to specify the plausible future climates termed as "Climate Scenarios".

Climate scenarios are coherent, internally consistent and plausible representations of the future climate based on some assumptions that are consistent with future emissions of greenhouse gases and concentrations of other pollutants. Some of the key assumptions are based on ‘plausible socio-econo-political pathways’ which would shape up the future greenhouse gas emission regime. Each pathway identified in the process may be considered to be an element of a scenario. These key assumptions and considerations are often stated in the form of verbose statements, bio-geo-physical equations, and complex models which incorporate both the statements and empirical equations. Climate scenarios are not predictions, since these are based on assumptions, approximations and considerations. Rather, a climate scenario is a plausible indication of what the future could be like over decades or centuries, given a specific set of assumptions.

2.3.2 The SRES Emissions Scenarios

The IPCC published a set of emissions scenarios in 2000 for use in climate change studies (Special Report on Emissions Scenarios – SRES) to replace the earlier IS92 scenarios developed in 1992. The SRES scenarios were constructed to explore future developments in global environment with special reference to the production of greenhouse gases and aerosol emissions. These newer scenarios consider the period 1990 to 2100 and include a range of socioeconomic assumptions (e.g., global population and gross domestic product).

In SRES scenarios, four different narrative storylines, labeled A1, A2, B1 and B2, were developed to describe consistently the relationships between the forces driving emissions and to add context for the scenario quantification. The resulting set of 40 scenarios (35 of which contain data on the full range of gases required to force climate models) cover a wide range of the main demographic, economic and technological driving forces of future greenhouse gas and sulphur emissions. Each scenario represents a specific quantification of one of the four storylines. All the scenarios based on the same storyline constitute a scenario "Family" (Figure 2.2). Six groups of scenarios were drawn from the four families: one group each in the A2, B1 and B2 families, and three groups in the A1 family, characterizing alternative developments of energy technologies, such as A1FI (fossil intensive), A1T(predominantly non-fossil) and A1B (balanced across energy sources). Illustrative scenarios were selected by the IPCC to represent each of the six scenario groups.

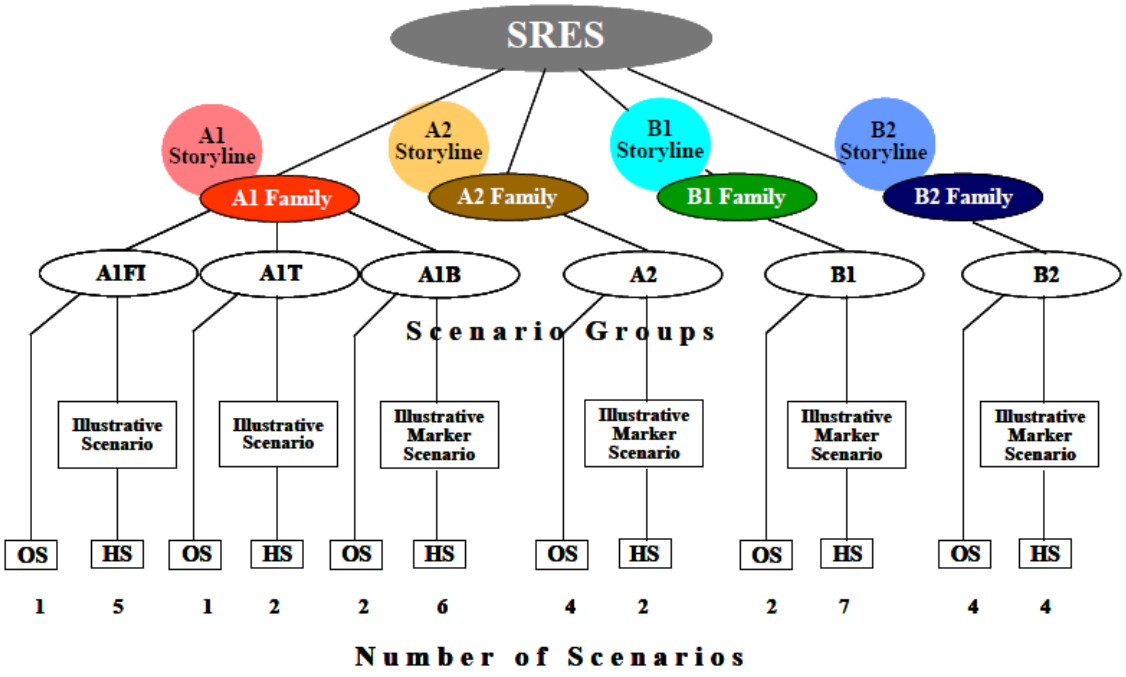

Figure 2.2: Structure of the storylines and scenarios in the IPCC SRES scenarios (Source: Nakicenovic et al., 2000)

In simple terms, the four storylines combine two sets of divergent tendencies: one set varying between strong economic values and strong environmental values, the other set between increasing globalization and increasing regionalization. All scenarios were designated as equally valid, with no assigned probabilities of occurrence. The storylines are summarized as follows (Nakicenovic et al., 2000):

- **A1 storyline and scenario family:** a future world of very rapid economic growth, global population that peaks in mid-century and declines thereafter, and rapid introduction of new and more efficient technologies.
- **A2 storyline and scenario family:** a very heterogeneous world with continuously increasing global population and regionally oriented economic growth that is more fragmented and slower than in other storylines.
- **B1 storyline and scenario family:** a convergent world with the same global population as in the A1 storyline but with rapid changes in economic structures toward a service and information economy, with reductions in materials intensity, and the introduction of clean and resource efficient technologies.
- **B2 storyline and scenario family:** a world in which the emphasis is on local solutions to economic, social, and environmental sustainability, with continuously increasing population (lower than A2) and intermediate economic development.

2.3.3 Climate Change Projections

Climate models are used to simulate and quantify the climate response to present and future climate conditions. In order to have a basis for assessing future impacts of climate change, it is necessary to characterize the present day or recent climate in a region – often referred to as the climatological baseline. Most climate models project the future climate for some defined periods with reference to the baseline period. Usually thirty year periods are used to define the baseline and future time periods since averaging over this length of time gives a better indication of the longer-term trend in climate. The GCMs consider the baseline period as 1961 – 1990. The IPCC recommends that three fixed time horizons in the future – the 2020s (i.e., 2010-2039), the 2050s (2040-2069) and the 2080s (2070-2099) should be considered in impacts studies (IPCC-TGICA, 2007).

To project the future climate, the first step is to simulate the present climate for baseline period considering no change in external climate forcing. The quality of these simulations is assessed by systematically comparing the simulated climate with observations of the present climate. In this way the model is evaluated and its quality is established. This step is essential to gain confidence in and provide a baseline for projections of climate change. Once the quality of the model is established, two different strategies can be applied to make projections of future climate change. The first, so-

called equilibrium method is to change (e.g. double) the carbon dioxide concentration and to run the model again to a new equilibrium. The second, so-called transient method, is to force the model with a greenhouse gas and aerosol scenario. Transient simulations are based on artificially constructed scenarios, so-called idealized scenarios. Most of the recent studies of climate change using transient simulations are based on the SRES Emissions Scenarios. Climate simulations based on such idealized scenarios may provide insight in to the climate response to potential sector under concern. The projection of climate change relies mainly on the choice of such scenarios.

2.3.4 Uncertainties in Climate Change Projections

Uncertainty in climate change projections has always been a subject of various impact assessments. Several steps from emissions to climate response contribute to the overall uncertainty of a climate model projection (Figure 2.3). These uncertainties can be quantified through a combined effort of observation, process understanding, a hierarchy of climate models and ensemble simulations.

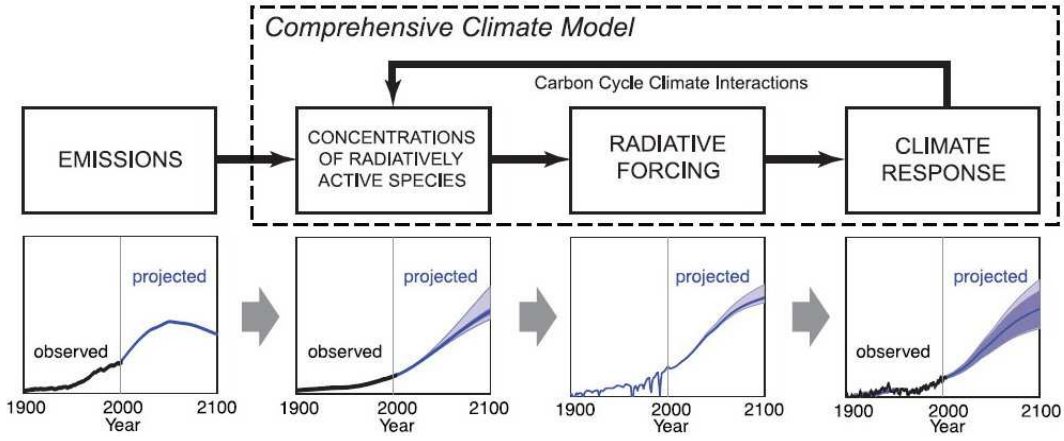

Figure 2.3: Uncertainties in climate change projections (after IPCC 2001a)

For a given emissions scenario, various biogeochemical models are used to calculate concentrations of constituents in the atmosphere. Various radiation schemes and parametrizations are required to convert these concentrations to radiative forcing. Finally, the response of the different climate system components (atmosphere, ocean, sea ice, land surface, chemical status of atmosphere and ocean) is calculated in a comprehensive climate model. In addition, the formulation and interaction of the carbon cycle in climate models also introduces important feedbacks which produce additional uncertainties (IPCC 2001a).

2.4 Climate Variables Affecting River and Future Projections

Water is involved in all components of the climate system (atmosphere, hydrosphere, cryosphere, land surface and biosphere). Therefore, climate change affects water through a number of mechanisms. Climate warming observed over the past several decades is consistently associated with changes in a number of components of the hydrological cycle and hydrological systems such as: changing precipitation patterns, intensity and extremes; changes in cloud cover and atmospheric water vapour; increasing evaporation and changes in soil moisture; melting of ice caps and glaciers and reduced snow cover; and increases in ocean temperatures and ocean acidity. Sea level rise, associated with thermal expansion of water and widespread melting of ice caps and glaciers, has a significant impact on the hydrological cycle of a basin. These variables and processes may affect a river system directly or indirectly in many ways. However, when considering a particular river basin, the impact of precipitation change and sea level rise is pronounced (Bates et al., 2008). This section discusses observations of recent changes in such water-related variables and their projections for future changes.

2.4.1 Role of Precipitation and Sea Level

There is significant natural variability in all components of the hydrological cycle, often masking long-term trends. However, substantial uncertainty holds in trends of the hydrological variables because of large regional differences and limitations in the spatial and temporal coverage of monitoring networks (Huntington, 2006). A major advance in climate change projections is the large number of simulations available from a broader range of climate models for various emissions scenarios. Continued greenhouse gas emissions at or above current rates under SRES scenarios would cause further warming and induce many changes in the global climate system during the 21st century. Projected global average temperature change for 2090–2099 (relative to 1980–1999), under the SRES illustrative marker scenarios, ranges from 1.8°C (likely range 1.1°C to 2.9°C) for scenario B1 to 4.0°C (likely range 2.4°C to 6.4°C) for scenario A1FI (IPCC, 2007b). Variables like precipitation and sea level will change according to those individual scenarios with substantial spatial and temporal variation.

The IPCC Fourth Assessment Report mentions with high likelihood that observed and projected increases in temperature, sea level rise and precipitation variability are the

main causes for reported and projected impacts of climate change on water resources, resulting in a significant impact on a river basin and associated river systems.

Change in precipitation is likely to affect the magnitude and frequency of runoff events of a river basin. The runoff of a basin is more sensitive to changes in precipitation than to evaporation and other climate variables and hence small change in precipitation may cause large changes in the runoff and basin water balance. Changed basin water balance may alter the discharge hydrographs of rivers, and such alterations have been projected to cause significant changes in the flooding patterns of low latitude flood pulse systems (Mirza et al., 2003). There is increasing recognition that changes in precipitation are likely to alter the magnitude and frequency not only of extreme floods but also moderate floods. They are usually responsible for transporting more than 80% of the sediment load carried by a river over a prolonged period (Blum and Tornqvist, 2002). Hence changes in precipitation will affect the flow characteristics and sediment regime of a river, leading to various hydraulic and morphological changes in response to climate change.

Sea level rise, resulting from thermal expansion of water and melting of glaciers, also contributes significantly on the regional basin water balance. The rising level of sea, which is a concern particularly in the river deltas, will create high inland water levels. The riverine and coastal flooding will also increase due to sea level rise, because it causes more backing up of the river flows along the delta through backwater effects (Ericson et al., 2006). Such effect will also introduce various hydro-morphological changes in the rivers.

2.4.2 Observed and Projected Changes in Precipitation

Theoretical and climate model studies suggest that, in a climate that is warming due to increasing greenhouse gases, a greater increase is expected in extreme precipitation, as compared to the mean. Taken together, the observational and modelling studies lead to an overall conclusion that an increase in the frequency of heavy precipitation events is likely to have occurred over most land areas over the late 20th century.

Observed Changes in Precipitation

Trends in land precipitation have been analyzed using a number of data sets; notably the Global Historical Climatology Network (GHCN), the Precipitation Reconstruction over Land (PREC/L), the Global Precipitation Climatology Project (GPCP), the Global Precipitation Climatology Centre (GPCC) and the Climatic Research Unit (CRU). Figure

2.4 shows the spatial variation of precipitation over land for different AOGCM model simulations along with the observed indicating different trends in different parts of the world, with a general increase in Northern Hemisphere mid and high latitudes (particularly in autumn and winter) and a decrease in the tropics and subtropics in both hemispheres (IPCC, 2001b).

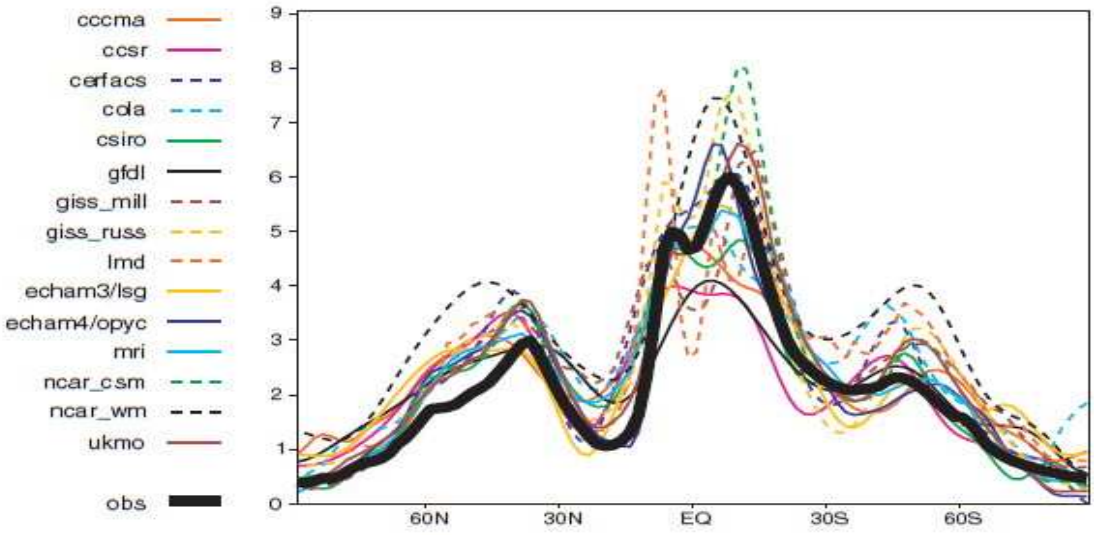

Figure 2.4: Simulated and observed zonal mean precipitation (IPCC, 2001b)

Long-term trends in precipitation amounts from 1900 to 2005 have been observed in many large regions. Significantly increased precipitation has been observed in the eastern parts of North and South America, northern Europe and northern, central and south Asia. Inter-seasonal, interannual and spatial variability in rainfall has been observed during the past few decades across all of Asia. Annual mean rainfall exhibits increasing trends in western and the south-eastern coast of China, the Arabian Peninsula, Bangladesh and along the western coasts of the Philippines (IPCC, 2007a).

Substantial increases in heavy precipitation events have been observed in many land regions since about 1950, even in those regions where there has been a reduction in total precipitation amount (IPCC, 2007b). Generally, the frequency of occurrence of more intense rainfall events in many parts of Asia has increased, while the number of rainy days and total annual amount of precipitation has decreased. In tropical Asia, hills and mountain ranges cause striking spatial variations in rainfall. Approximately 70% of the total annual rainfall over the Indian subcontinent is confined to the southwest monsoon season (June-September). Recent decades have exhibited an increase in extreme rainfall events over northwest India during the summer monsoon (IPCC, 2001a).

Projected Changes in Precipitation

Based on patterns emerging from a limited number of studies with current AOGCMs, older GCMs and regional studies, there is a strong correlation between precipitation and projected global warming. Future increases in temperature will likely to change the variability of mean precipitation and extreme precipitation events. Climate projections using multi-model ensembles show increases in globally averaged mean precipitation over the 21st century and projects an overall increase in future as shown in Figure 2.5.

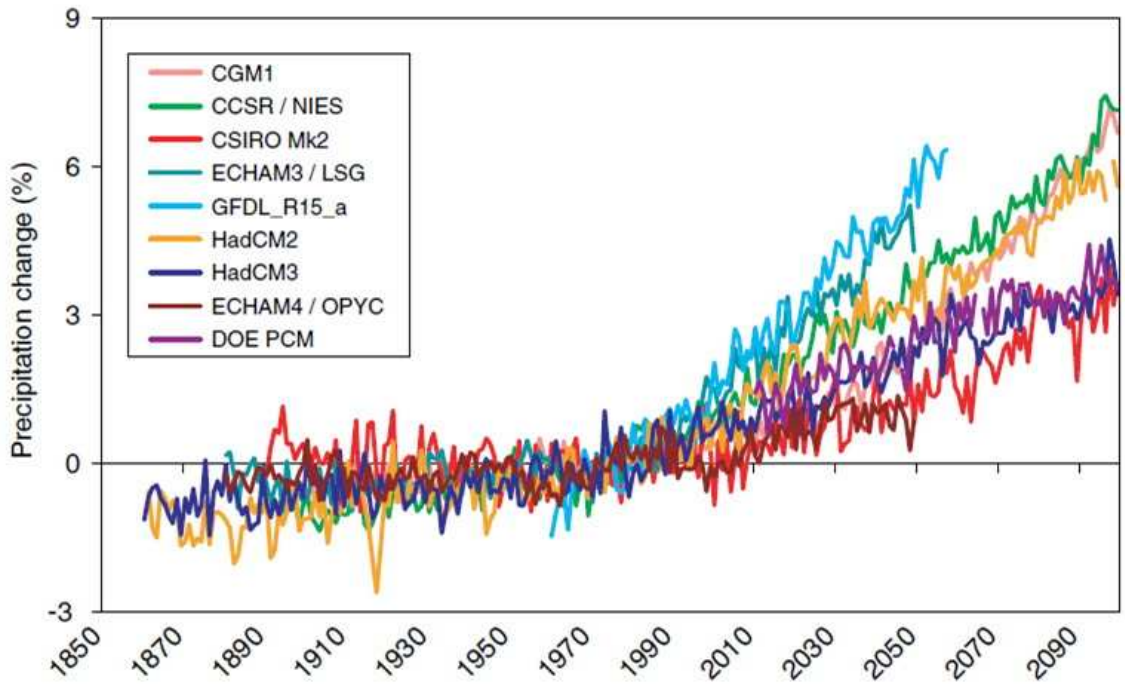

Figure 2.5: Time series of global averaged precipitation change (%) from various GCMs (Source: IPCC, 2007b)

For a future warmer climate, the current general circulation models (GCMs) indicates that precipitation generally increases in the areas of regional tropical precipitation maxima (such as the monsoon regimes) and over the tropical Pacific in particular, with general decreases in the subtropics, and increases at high latitudes as a consequence of a general intensification of the global hydrological cycle. Results (Figure 2.6) from recent AOGCM simulations forced with SRES A2 and B2 emissions scenarios indicate that precipitation is likely to increase in both summer and winter over high-latitude regions. In winter, increases are also seen over northern mid-latitudes, tropical Africa and Antarctica, and in summer in southern and eastern Asia. Australia, Central America and southern Africa show consistent decreases in winter rainfall.

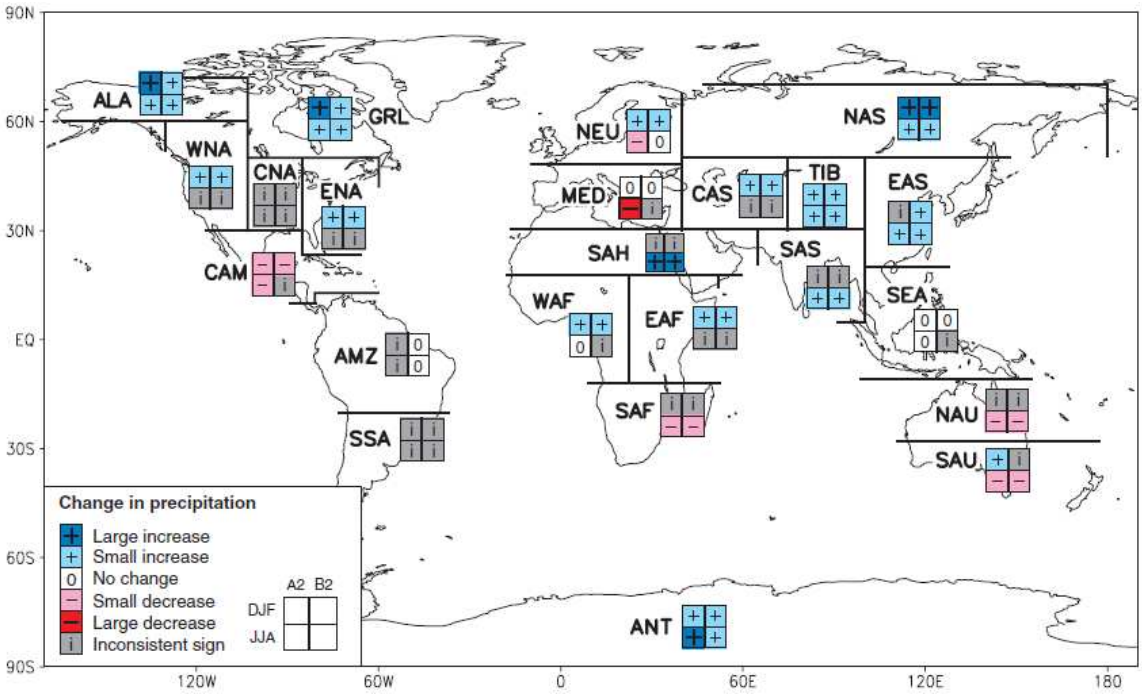

Figure 2.6: Inter-model consistency in regional precipitation change (IPCC, 2001a)

In general, all AOGCMs simulate an enhanced hydrological cycle and an increase in annual mean rainfall over most of Asia. An area-averaged annual mean increase in precipitation of 3±1% in the 2020s, 7±2% in the 2050s, and 11±3% in the 2080s over the land regions of Asia is projected as a result of future increases in the atmospheric concentration of greenhouse gases (GHGs). Under the combined influence of GHGs and sulfate aerosols, the projected increase in precipitation is limited to 2±1% in the decade 2020s, 3±1% in the 2050s, and 7±3% in the 2080s (IPCC, 2001c). The models show high uncertainty in projections of future winter and summer precipitation over South Asia. Table 2.2 shows the precipitation changes over South and Southeast Asia.

Table 2.2: TAR results of precipitation changes over Asia

Regions	Precipitation Change (%)								
	2020s			2050s			2080s		
	Annual	Winter	Summer	Annual	Winter	Summer	Annual	Winter	Summer
Asia	3.6	5.6	2.4	7.1	10.9	4.1	11.3	18.0	5.5
South Asia	2.9	2.7	2.5	6.8	-2.1	6.6	11.0	-5.3	7.9
Southeast Asia	2.4	1.4	2.1	4.6	3.5	3.4	8.5	7.3	6.1

Since the TAR, there is an improving understanding of projected patterns of precipitation. According to the Fourth Assessment Report (AR4), precipitation in summer is likely to increase in Northern Asia, East Asia, South Asia and most of Southeast Asia, but is likely to decrease in central Asia. Precipitation increases over the tropical oceans and in some of the monsoon regimes, e.g., the South Asian monsoon in summer (June to August) and the Australian monsoon in summer (December to February), are notable. Projections of precipitation over South Asia at the end of the 21st century (2090 to 2099) for scenario A1B has been given in Table 2.3.

Table 2.3: Precipitation projections over South Asia according to AR4

Region	Season	Precipitation Change (%)				
		Min	25%	50%	75%	Max
South Asia	DJF	-35	-9	-5	1	15
	MAM	-30	-2	9	18	26
	JJA	-3	4	11	16	23
	SON	-12	8	15	20	26
	Annual	-15	4	11	15	20

The table shows the minimum, maximum, median (50%), and 25 and 75% quartile values among the 21 models for precipitation (%) change over South Asia. Most of the A1B models project a decrease in precipitation in DJF (the dry season), and an increase during the rest of the year. The median change is 11% by the end of the 21st century, and seasonally is –5% in DJF and 11% in JJA, with a large inter-model spread.

Precipitation during the coming decades is projected to be more concentrated into more intense events, with longer periods of little precipitation in between. There is very likely to be an increase in the frequency of intense precipitation events in parts of South Asia and in East Asia. Extreme rainfall and winds associated with tropical cyclones are likely to increase in East Asia, Southeast Asia and South Asia. There is a tendency for drying in mid-continental areas during summer, indicating a greater risk of droughts in these regions. Therefore, intense and heavy episodic rainfall events with high runoff amounts are interspersed with longer relatively dry periods with increased evapotranspiration, particularly in the sub-tropics (IPCC, 2007c).

Bangladesh Context

In Bangladesh, the mean annual rainfall is about 2300mm, but there exists a wide spatial and temporal distribution. Annual rainfall ranges from 1200mm in the extreme west to over 5000mm in the east and north-east (Ahmed, 2006). Generally, the eastern parts of the country enjoy higher rainfall than the western parts. Trend analysis shows that decadal departures were below long-term averages until 1960; thereafter they have been much above normal (Mirza and Dixit, 1997).

The future precipitation pattern of Bangladesh cannot be obtained directly from the 3rd or 4th IPCC report. However, a number of attempts have been made to project the precipitation pattern over Bangladesh due to climate change. Ahmed and Alam (1998) produced the climate change scenarios for Bangladesh by downscaling various GCM outputs. It was reported that the winter rainfall would decrease at a negligible rate in 2030, while in 2075 there would not be any appreciable rainfall. On the other hand, monsoon precipitation would increase at a rate of 12% and 27% for the two projection years respectively. Mirza (2002) considered an ensemble of GCMs, instead of validating outputs of any specific model. There have been huge variations in output results, varying from 0.8% to 13.5% increase in mean annual rainfall for the Ganges basin and -0.03% to 6.4% change for the same for the Brahmaputra basin for a 2^{o}C temperature rise. Agrawala et al. (2003) used another ensemble of GCMs. A total of 17 GCMs have been run initially for model validation for Bangladesh's observed data sets. The results indicate that annual precipitation increases upto 9.7% for the year 2100.

The National Adaptation Programme for Action (NAPA) for Bangladesh has been the latest attempt to develop a climate change scenario for the country. Instead of developing one or more scenarios, the NAPA Core Team adopted the results obtained by Agrawala et al. for changes in temperature and modified the results regarding changes in precipitation (GOB, 2005). These projections are given in Table 2.4.

Table 2.4: Precipitation Projection over Bangladesh according to NAPA

Year	Precipitation Change (%)		
	Annual	DJF	JJA
2030	5	-2	6
2050	6	-5	8
2100	10	-10	12

2.4.3 Observed and Projected Changes in Sea Level

One of the key factors to evaluate for many impact studies is the present level of the sea relative to the land. Globally, eustatic sea level (the volume of water in the oceans) appears to have been rising during the past century (UNFCCC, 2001). However, there are large regional deviations in relative sea level from this global trend due to local land movements. Subsidence, due to tectonic movements, sedimentation, or human extraction of groundwater or oil, enhances relative sea-level rise. Uplift, due to post glacial isostatic rebound or tectonic processes, reduces or reverses sea-level rise (IPCC, 2001c).

Observed Changes in Sea Level

The main source of information on relative sea level is tide gauge records. Recent techniques of satellite altimetry and geodetic leveling have enhanced and standardized baseline determinations of relative sea level over large areas of the globe.

Analyses of sea-level records having at least 25 years of hourly data from stations installed around the Pacific Basin show an overall average mean relative sea-level rise of 0.7 mm/yr. Focusing only on the island stations with more than 50 years of data, the average rate of sea-level rise is 1.6 mm/yr (IPCC, 2001a). According to AR4 of IPCC, global mean sea level has been rising and the rate of rise has increased between the 19th and 20th centuries (Figure 2.7). The average rate was 1.7 ± 0.5 mm/ yr for the 20th century, 1.8 ± 0.5 mm/yr for 1961–2003 and 3.1 ± 0.7 mm/yr for 1993–2003.

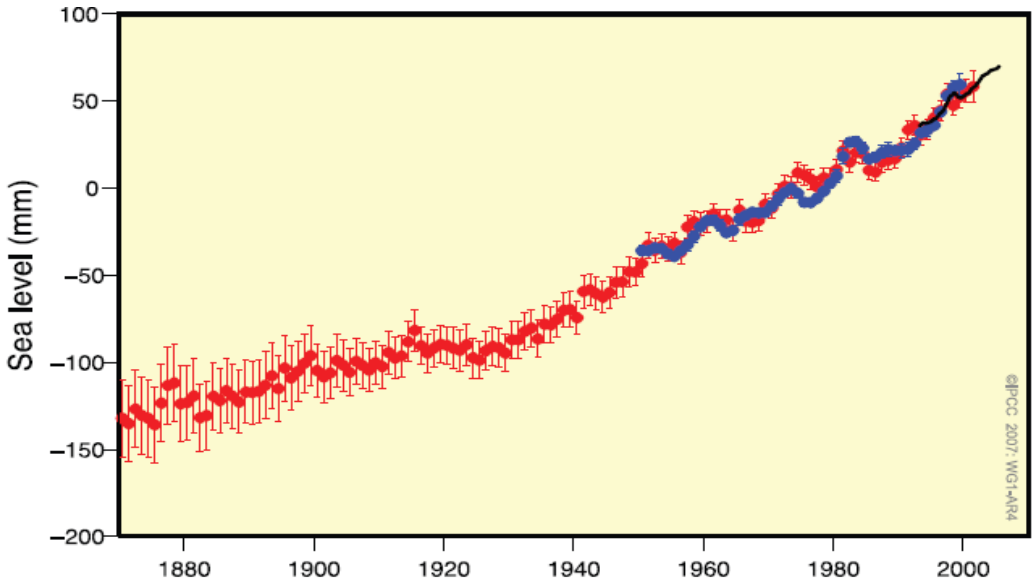

Figure 2.7: Annual averages of the global mean sea level based on reconstructed fields since 1870 (red), tide gauge measurements since 1950 (blue) and satellite altimetry since 1992 (black). Values are relative to the average for 1961-1990 (Source: IPCC, 2007a)

The average thermal expansion contribution to sea level rise for the 1961 to 2003 period was 0.42 ± 0.12 mm/yr, while the contribution from glaciers, ice caps and ice sheets is estimated to have been 0.7 ± 0.5 mm/yr. The global average rate of sea level rise measured by TOPEX/Poseidon satellite altimetry during 1993 to 2003 is 3.1 ± 0.7 mm/yr. This observed rate for the recent period is close to the estimated total of 2.8 ± 0.7 mm/yr for the climate-related contributions due to thermal expansion (1.6 ± 0.5 mm/yr) and changes in land ice (1.2 ± 0.4 mm yr–1) (IPCC, 2007a).

Precise satellite measurements since 1993 provide unambiguous evidence of regional variability of sea level change. In some regions, rates of rise during this period are up to several times the global mean, while in other regions sea level is falling (IPCC, 2007c).

Projected Changes in Sea Level

Although some components of future sea-level rise can be modeled regionally by using coupled ocean-atmosphere models, the most common method of obtaining scenarios is to apply global mean estimates from simple models. More recently, some studies have begun to express future sea-level rise in probabilistic terms, enabling rising levels to be evaluated in terms of the risk of exceeding a critical threshold of impact.

Projections of global average sea level rise from 1990 to 2100, using a range of AOGCMs following the IS92a scenario, lie in the range 0.11 to 0.77 m (Figure 2.8). This range reflects the systematic uncertainty of modelling.

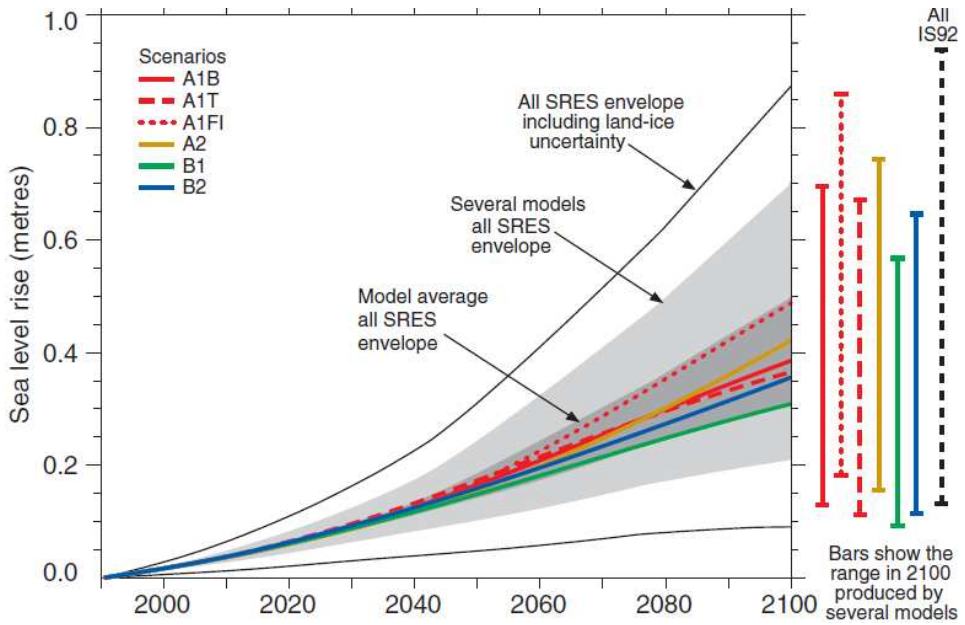

Figure 2.8: Global average sea level rise for 1990 to 2100 for the SRES scenarios (Source: IPCC, 2001b)

According to TAR, a sea level rise of 0.09 to 0.88 m is projected for 1990 to 2100 for the full set of SRES scenarios primarily from thermal expansion and loss of mass from glaciers and ice caps. The central value is 0.48 m, which corresponds to an average rate of about two to four times the rate over the 20th century. The range of sea level rise presented in the SAR was 0.13 to 0.94 m based on the IS92 scenarios. The Fourth Assessment Report of IPCC projected global-average sea level rise at the end of the 21st century (2090 to 2099) relative to 1980 to 1999 are of the order of 0.18 to 0.59 m, based on the spread of AOGCM results and different SRES scenarios. Despite higher temperature change projections in this assessment, the sea level projections are slightly lower, primarily due to the use of improved models which give a smaller contribution from glaciers and ice sheets.

The IPCC TAR (2001) provides a time series of sea-level projections through the 21st century with maximum, minimum and models average projections for the potential dynamic response of the Greenland and Antarctic Ice Sheets. While AR4 projections have been for the period of 2090 to 2099. These projections are given in Table 2.5. However recent reports indicate greater SLR projections than the TAR and AR4.

Table 2.5: Sea level rise projections according to TAR and AR4

Scenario	Sea Level Rise (cm)								
	TAR (relative to 1990)								AR4 (relative to 1980-1999)
	2020		2050		2080		2100		2090-2099
	Model Range	Best Estimate	Model Range	Best Estimate	Model Range	Best Estimate	Model Range	Best Estimate	Model Range
A1B	2.2 – 10.3	6.1	6.3 – 28.4	16.7	10.7 – 52.7	30.1	12.9 – 69.4	38.7	21 – 48
A1T	2.2 – 10.4	6.6	6.6 – 29.1	17.5	13.7 – 61.2	29.8	18.2 – 85.9	36.7	20 – 45
A1FI	2.4 – 11.0	6.1	6.4 – 29.9	17.2	9.9 – 52.9	35.6	11.1 – 67.1	49.1	26 – 59
A2	2.1 – 10.4	6.1	5.8 – 26.9	15.7	11.3 – 52.6	30.4	15.5 – 74.3	42.4	23 – 51
B1	2.2 – 10.5	6.2	5.2 – 25.9	15.0	8.0 – 44.4	24.9	9.2 – 56.7	31.0	18 – 36
B2	2.3 – 10.9	6.4	5.6 – 27.7	16.0	9.1 – 48.8	27.5	11.4 – 64.6	35.8	20 – 43

For each scenario shown in table, the midpoint of the range for AR4 is within 10% of the TAR model average for 2090-2099. The ranges are narrower than in the TAR mainly because of improved information about some uncertainties in the projected contributions.

Thermal expansion is the largest component, contributing 70–75% of the central estimate in these projections for all scenarios. Glaciers, ice caps and the Greenland ice sheet are also projected to contribute positively to sea level (IPCC, 2007b). Figure 2.9 shows the contribution of different components on the global average sea level rise for the six SRES marker scenarios. The uncertainties denote 5 to 95% ranges, based on the spread of model results, and not including carbon cycle uncertainties.

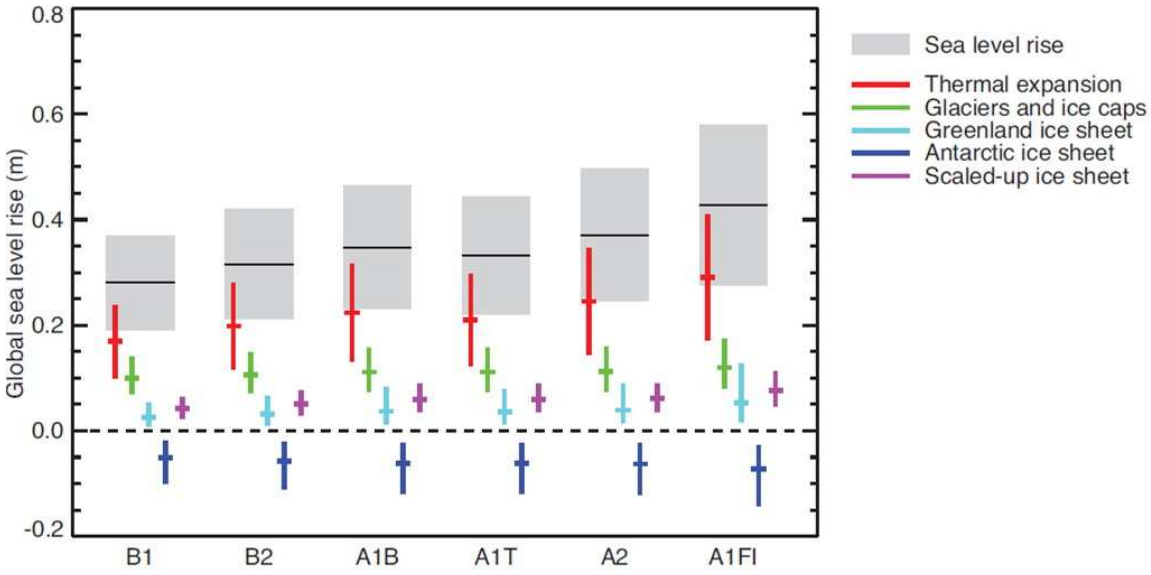

Figure 2.9: Projected global average sea level rise and its components in 2090 to 2099 (relative to 1980–1999) for the six SRES marker scenarios (Source: IPCC, 2007b)

In all the SRES marker scenarios except B1, the average rate of sea-level rise during the 21st century is very likely to exceed the 1961–2003 average rate (1.8 ± 0.5 mm/yr). During 2090 to 2099 under A1B, the central estimate of the rate of rise is 3.8 mm/yr, which exceeds the central estimate of 3.1 mm/yr for 1993 to 2003. The 1993 to 2003 rate may have a contribution of about 1 mm/yr from internally generated or naturally forced decadal variability. These sources of variability are not predictable and therefore the actual rate during any future decade might be more or less than the projected rate.

Bangladesh Context

Sea-level rise during the 21st century is projected to have substantial geographical variability and such variation may occur along the coast of Bangladesh. IPCC-IV study

has referred to various researchers who have reported that in the coastal areas of Asia, the current rate of SLR (1 to 3 mm/yr) is marginally greater than the global average. In addition to this, the rate of sea level rise of 3.1 mm/yr as reported over the past decade has been accelerated relative to the long term average taken over the 20th century as a whole (1.7 to 2.4 mm/yr) (CCC, 2009a).

The SAARC Meteorological Research Centre (SMRC) analyzed sea level changes of 22 years historical tide data at three tide gauge locations in the coast of Bangladesh. The study revealed that the rate of sea level rise during last 22 years is many fold higher than the mean rate of global sea level rise over 100 years. They also revealed the regional variation in the rate of sea level changes. SMRC projected figures of sea level rise are 18 cm, 30cm and 60 cm for the year 2030, 2050 and 2100 respectively (CCC, 2009b).

National Adaptation Programme for Action (NAPA) has predicted the sea level rise for Bangladesh based on 3rd IPCC report and projected SLR for the year 2030 and 2050 would be 14 cm and 32 cm respectively (GOB, 2005). The sea level projections for Bangladesh are summarized in Table 2.6.

Table 2.6: Sea level Projections for Bangladesh

Year	Sea Level Rise (cm)		
	3rd IPCC (upper range)	SMRC	NAPA
2030	14	18	14
2050	32	30	32
2100	88	60	88

2.5 Climate Change Impacts on the Hydro-morphology of a River

Climate change is likely to lead to an intensification of the global hydrological cycle and to have a major impact on regional water resources system. The IPCC Fourth Assessment Report mentions with high likelihood that observed and projected increases in temperature, precipitation variability and sea level rise are the main causes for the reported and projected impacts of climate change on water resources, resulting in a significant effect on the hydro-morphological characteristics of a river basin and relevant river system.

2.5.1 Impacts on a River Basin

A river basin can be divided into three zones based on various geomorphic contexts and different hydro-morphological behavior and processes of the river. In the upper part of the basins, rivers are formed by erosion of the bedrock; their course incises progressively (zone 1 as shown in Figure 2.10). Flow carries the products of the incision and eroded soil towards the lower zones. In zone 2 some equilibrium exists between sediment transport capacity of the flow and the sediment supply; it is the transfer zone. In zone 3, the sediments are deposited by lack of transport capacity, in deltas or estuaries. Any changes in climate and hydro-meteorology will affect the soil erosion, hydraulic regime (discharge and sediment transport) and evolution of river courses throughout the basin.

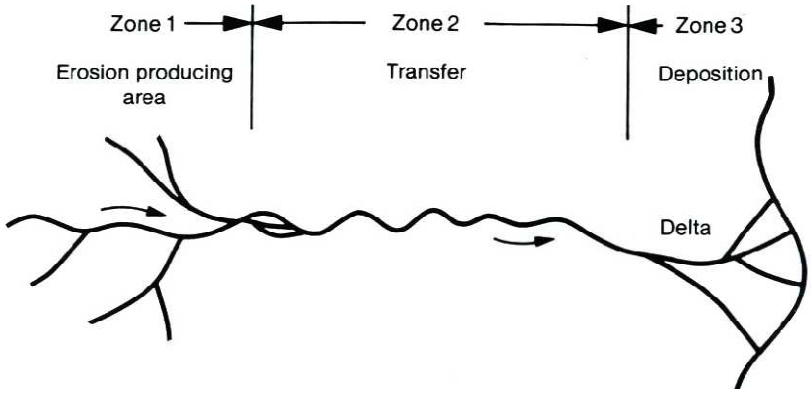

Figure 2.10: Geomorphic zones of a river basin

As a result of climate change and global warming, excess precipitation is likely to affect the magnitude and frequency of runoff events resulting in changes in flow and sediment regime of a river basin. Such changes may influence the conveyance capacity and morphological behavior of rivers through:

a. Bed erosion or deposition;

b. Channel widening or narrowing;

c. Changes in planform.

Which of these occurs depends upon the extent to which changes in flow are accompanied by changes in sediment delivery. In the upper reaches, an increase in runoff is likely to trigger bed erosion, increasing channel capacity and enhancing sediment supply for the lower reaches. In the middle reaches, in average, sediments will be in transit with limited erosion or deposition. In the lower reaches, geomorphologic context due to climate change may be quite diversified, depending on topography and on the presence of sediment sources. Increased streamflow accompanied by high sediment

supply from the upper reaches may result in aggradation, reducing channel slope and conveyance capacity of the river. Channel widening and changes in planform may also occur due to non-equilibrium conditions of water and sediment supply. Finally, at the outlet, rivers with high sediment load fill up the drowned valley and then deposit sediment beyond the coastline, creating delta (Zhu et al., 2008).

The impact of sea level rise will also be prominent in the lower reaches (zone 3) of a river basin. Rising levels of sea will affect the evolution of delta as well as the aggradation of rivers through backwater effect. Therefore, the flow regime and morphology of the rivers located in the lower reach of a basin will be more responsive to climate change.

2.5.2 Impacts on the GBM River System

Climate change affects the regional river basin system by varying the basin water balance through temperature and precipitation changes and raising sea level, which is a concern particularly in the river deltas. Among the river systems, the impact of climate change on the Ganges-Brahmaputra-Meghna (GBM) basin is expected to be particularly strong. The basin is one of the most vulnerable areas in the world as it is subject to the combined effects of glacier melt, extreme monsoon rainfall and sea level rise.

It is expected that climate change induced alterations in temperature would affect the timing and rate of snow melt in the upper Himalayan reaches. Study shows that the 30.2 km long Gangotri glacier has been receding alarmingly in recent years. Some other glaciers in Asia, such as glaciers in the Tibetan Plateau and the glaciated areas located in the headwaters of the Changjiang River are projected to decrease (Gain, 2011). Such trends of glacial melts suggest an increased summer flows in the Ganga, Indus, Brahmaputra and other rivers that criss-cross the northern Indian plain.

Again, the GBM basin is highly influenced by extreme monsoon rainfall (Mirza, 2002). Intensification of the monsoon rainfall coupled with increased glacier melts is likely to contribute to flood disasters in Himalayan catchments. In the longer term, global warming could lead to serious impacts on the 7 main rivers in Asia fed by melt water from the Himalayas.

The anticipated sea level rise due to global warming will create a profound impact on the rivers of GBM basin, because it causes more backing up of the rivers along the delta. This will result in increased drainage congestion due to higher water levels which will be

exacerbated by other factors associated with climate change, such as siltation of estuary branches in line with increased surface runoff and higher riverbed levels.

2.5.3 Impacts on the Rivers of Bangladesh

Bangladesh has been sharing a total of 54 transboundary rivers, which are mostly originated from Himalayan glaciers located on upper riparian countries. The country, being only 7 percent of GBM catchment area, receives over 90 percent of the water from the basin which discharges through the Ganges-Brahmaputra-Meghna river system (CCC, 2009b). The confluences between the Brahmaputra and the Ganges (known as the Padma) and the Meghna become two huge water pools during the peak seasons and cause flooding, particularly in the central part of the country. Due to climate change, excess rainfall coupled with Himalayan ice-melts will increase runoff and create more intense flooding in these rivers. The situation may become worse if it is associated with global warming accelerated sea level rise.

The impact of sea level rise would be most prominent in the southern coastal zone of Bangladesh which is connected to the Bay of Bengal through 710 km coastline. This coastal region is marked by morphologically dynamic river network and estuary system. The Pussur-Sibsa, the Lower Meghna and the Karnafuli are the major river systems of the region. The Lower Meghna River carries the combined flow of Ganges, Brahmaputra and Upper Meghna and discharges water into the Bay of Bengal through a common terminus known as the Meghna estuary. This massive water also carries enormous amount sediment towards the Bay of Bengal.

Due to climate change, a synchronization of peak flows of the major rivers, accompanied by increased discharge and sea level rise, will induce an unusual situation where the entire drainage system in the floodplain fails to drain all the incoming waters and suffer severe floods of very high intensity. Due to prolonged discharge of floodwaters, the rate of sedimentation will increase. Moreover, increased rainfall runoff in the vast GBM region due to climate change also contributes to enhanced sediment flows along the rivers (CCC, 2009b). As a result, both the riverbed and adjacent floodplains will rise leading to further drainage congestion. The consequence is progressive siltation and decrease of channel depth, thereby increasing the flood ability of the alluvial plain and possibly more intense flooding in the following years. Such a cyclic course of events would intensify the flooding problem more.

2.6 Response of the Flow Regime and Morphology of a River to Climate Change

There is substantial evidence that climate variables and their change will affect the hydro-morphological characteristics and processes of a river. The main issues of climate change that may affect the morphology of a river are – (i) changes in flow regime due to changes in precipitation pattern and (ii) changes in base level due to sea-level rise.

A major change in the hydrologic regime would trigger a response that would completely change the morphology of rivers. Therefore the rivers may take long periods for adjustment in fluvial processes and morphological forms due to climate change. Different analytical, empirical and conceptual models such as Schumm (1969), De Vries (1975), Klaassen (1995) has been developed to assess such long term morphological changes. These changes are associated with a complex series of independent variables, but the discharge of water and sediment integrates most of the other independent variables (Verhoog, 1987).

The nature and quantity of water and sediment moving through the channel largely determines various morphological variables of stable alluvial channels such as width, depth, widthdepth ratio, slope of the bed etc. Therefore climate change will affect the river morphology by changing the discharge of water and sediment. Schumm prepared a conceptual model (Table 2.7) giving the consequences of such long term changes which can be used to assess the morphological response of river to climate change.

Table 2.7: Schumm's Conceptual Model

Independent Variables		**Dependant Variables**			
Discharge (Q)	**Sediment Discharge (Q_S)**	**Width (b)**	**Depth (d)**	**Slope (S)**	**Width-depth ratio (F=b/d)**
+	+	+	+/-	+/-	+
-	-	-	+/-	+/-	-
+	-	+/-	+	+	-
-	+	+/-	-	+	+

Schumm's relations indicate that width and depth responses occur in different fashions depending on the nature of the causal changes in discharge and/or sediment load. This is consistent with the ideas on stable channel geometry and can be used to assess the response of the rivers to changes of different variables related to climate change.

As a result of climate change, variation in precipitation may alter the discharge and sediment characteristics of a river. Sea level rise is likely to introduce backwater effect leading to high inland water level and drainage congestion. Such conditions will be exacerbated by other morphological processes associated with climate change such as higher riverbed levels, siltation of estuary branches, delta progradation etc.

2.6.1 Change in Streamflow

The runoff of a basin is more sensitive to changes in precipitation than to evapotranspiration and other climate variables and hence small changes in precipitation may cause large changes in the discharge of rivers. For a catchment with a low runoff ratio (the annual volume of discharge divided by the annual volume of precipitation), the effect of a 10% reduction in precipitation may range from a 50% reduction in river discharge with no direct CO_2 effect, to a 70% increase in discharge with a maximum direct CO_2 effect (Verhoog, 1987). For higher runoff ratios the ranges of possible discharge changes is much less.

Changed basin water balance due to variation of precipitation and glacier melts may alter the discharge hydrographs of rivers, and such alterations have been projected to cause significant changes in the hydraulics of a river. An increase in precipitation in the head waters will not only cause an increase in annual discharge, but through reduction of vegetation density, it will increase peak discharge and greatly increase the amount of sand load. These excess sediments will be deposited progressively along the river resulting in decrease of the slope of the river (Figure 2.11).

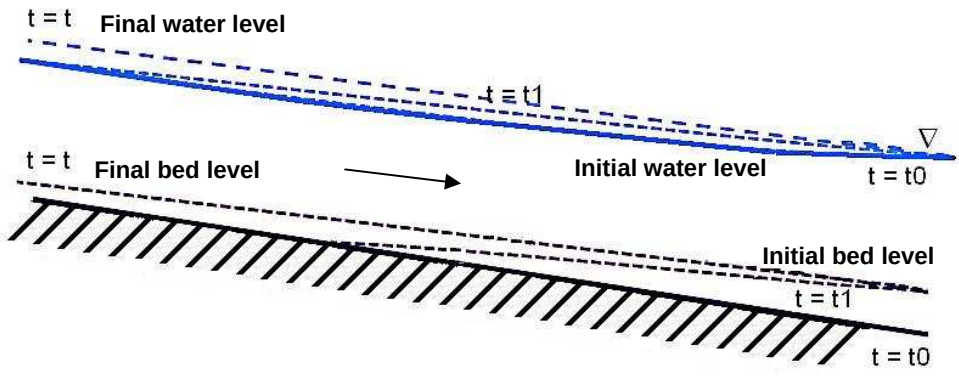

Figure 2.11: Effect of increased discharge on a river

The effect can be better conceptualized using Schumm's model. As a consequence of higher discharge and sediment load, the channel will become wider and shallower leading to a greater width-depth ratio and the channel slope will become much flatter. To accommodate the increased discharge, water surface will rise resulting in flooding of the rivers and adjacent floodplains.

2.6.2 Backwater Effect and Drainage Congestion

Back water effect (BWE) generally refers to the retardation of a river outflow by a rise in the level of water at the mouth of the river. Mostly it is an estuarial phenomenon, but will also be felt in rivers and adjacent floodplains further upstream. The effect may be from a main river to a tributary or from sea to a river. Not only do conditions at the mouth of the river retard the outflow, but often a flow reversal occurs—that is, water may flow from the sea to a river.

BWE in Bangladesh arises as a result of a number of dynamic conditions/causes in the Bay of Bengal. The principal ones are: (1) southwest monsoon wind during the rainy season, (2) astronomical tides and (3) storm surges (Ali, 1999). Another non-dynamic and long-term BWE is likely to be caused by the sea level rise, which will raise the level of water at the mouth (estuary) of a river. There will be a permanent increase of water level within the delta area, and the increase may vary spatially across the river to further upstream (Figure 2.12).

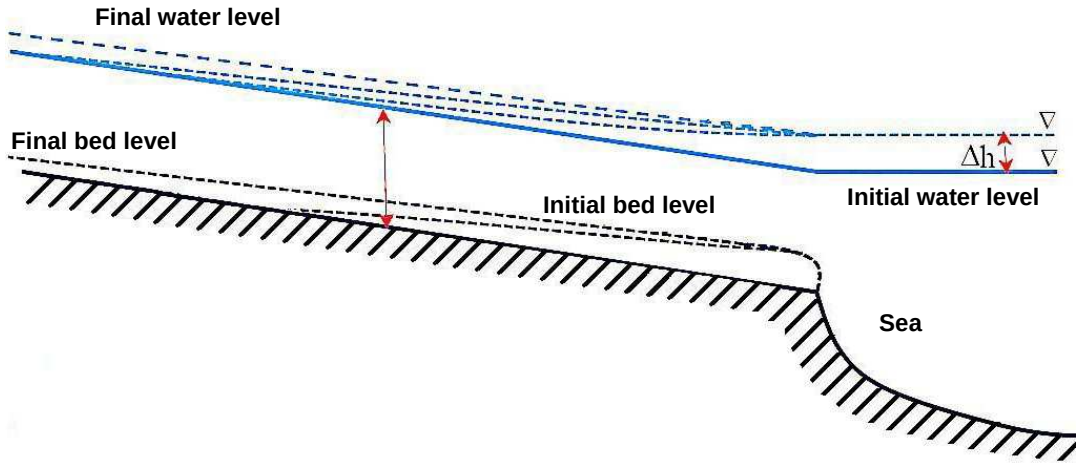

Figure 2.12: Backwater effect due to sea level rise

The combined effect of higher sea water levels along with increased discharge will create water-logging and drainage congestion. The morphologically highly dynamic rivers in

Bangladesh are expected to adapt to such changes in water levels in a period of time, which falls within the considered time horizon of 100 years. According to Schumm's model, the result would be gradual decrease of channel slope as well as water level gradient. As a consequence, floodwater inside the country continues to accumulate, bringing more areas under inundation and increasing the length and depth of inundation in areas already inundated, thus further aggravating the flood situation that already exists.

2.6.3 Sedimentation and Bed Level Change

Disturbance of the morphological processes of a river will also become a significant problem under climate change. Climate change is expected to affect the river morphology with two main (related) processes involved:

(i) Increased morphological activity with increased river flow and sediment load

(ii) Disturbance of the balance between sediment transport and deposition in rivers

There will be a substantial increase of river flow carrying large amount of sediment load. Decrease in water level gradients due to sea level rise will result in lower flow velocities and reduced sediment carrying capacities of the rivers. As a result, the rate of sedimentation will increase leading to rise in both the riverbed and the bed of the adjacent floodplains. These changes in bed levels will in turn cause additional changes in river levels, which effect will propagate the impact of sea level rise in the upstream direction (Figure 2.13).

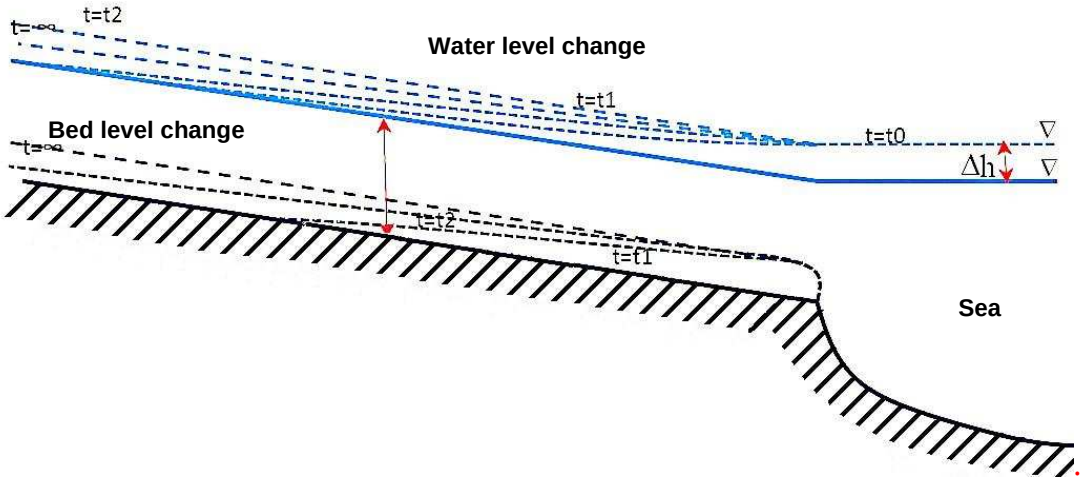

Figure 2.13: Change of bed level

According to Schumm's model, constant interactions between the bed and bank material, flowing water and sediment load will lead to significant changes in channel geometry by making the channel wider and shallower.

2.6.4 Delta Progradation

Rivers form deltas wherever they flow into standing water such as a lake, a reservoir or the ocean. Due to climate change induced global warming, variations in sea levels can exert a significant influence on depositional patterns at river mouths and river deltas. Under conditions of constant base level of standing water, i.e. constant sea level, deltas can be expected to move seaward resulting in gradual progradation of the river delta. However under conditions of sea level rise as anticipated to occur, the behavior of the delta changes dramatically leading to more complex evolutions of deltaic shorelines.

Deltas commonly display three distinct zones; (a) a low-slope topset deposit that forms as the coarse sediment load deposits on the river bed, (b) a high-slope foreset deposit that forms as the coarse sediment load avalanches down the delta face into deeper water and (c) a low-slope bottomset deposit that forms as the fines settle out on the bed of the lake or estuary. The concept of delta evolution can be explained in the context of Figure 2.14. Water and sediment are released at the upstream end of the reach over a bedrock basement with sufficiently high slope. The effect of standing water downstream causes the river-borne sediments to deposit and form an alluvial topset. The alluvial bed slope decreases downstream as sediment deposits out. The sediment load remaining at the shoreline (topset-foreset break) is supplied to an avalanching subaqueous foreset, which progrades outward over the basement.

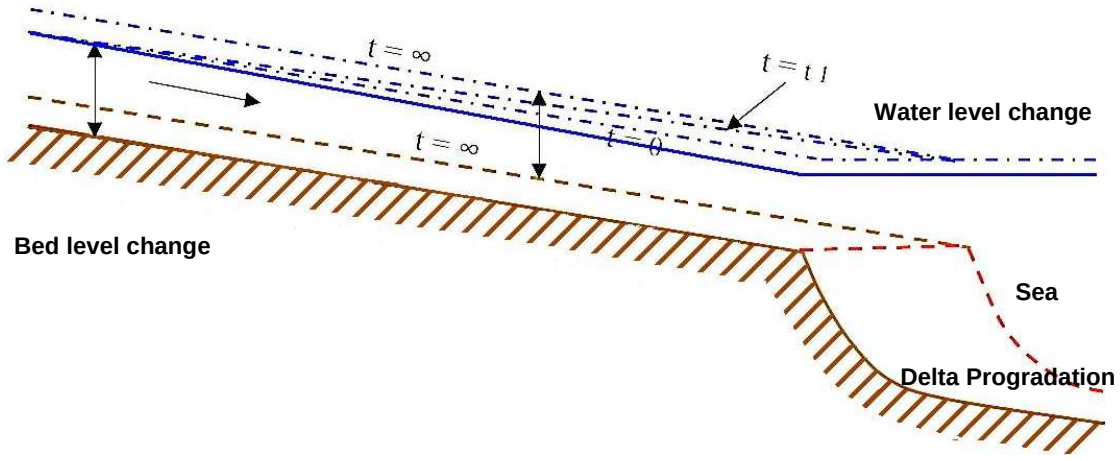

Figure 2.14: Progradation of river delta

The effect of rising levels of sea on the progradation of delta will be better understood from Figure 2.15.

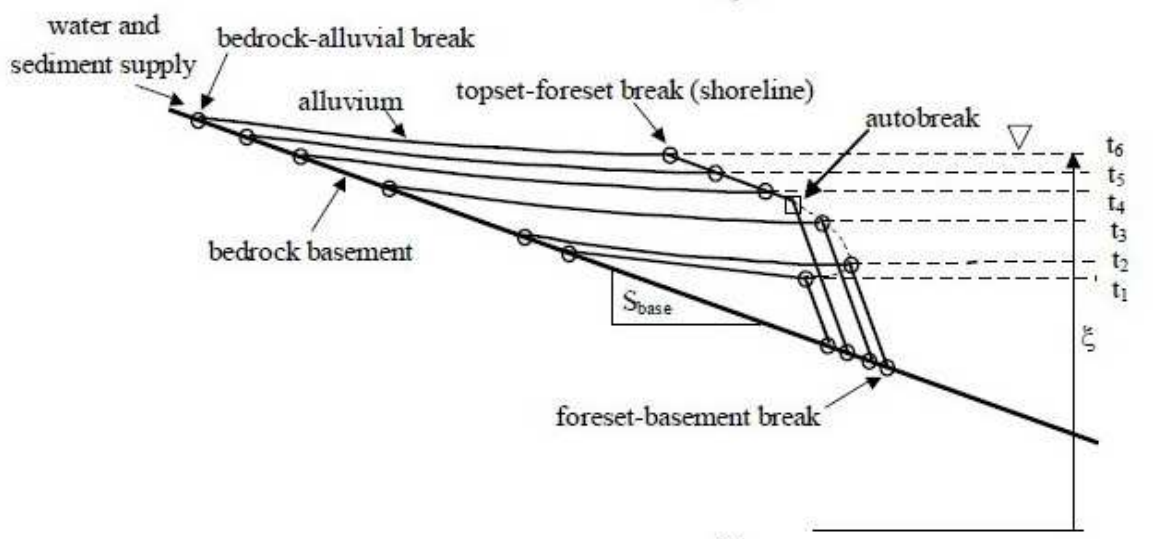

Figure 2.15: Delta evolution with rising sea level (Source: Parker and Muto, 2003)

In Figure 2.15 shows that the sea level is rising in time. In the early stages of delta development, a steady water and sediment supply will at first lead to a delta that progrades seaward (regresses). The river must fill the topset space created by rising sea level which causes the sediment transport to decrease more rapidly downstream, leaving less sediment delivery at the shoreline to supply to the foreset. As a result, the shoreline progrades ever more slowly, until it reverses and moves upstream (transgresses). At some point, i.e. "autobreak," there is no longer any sediment left at the shoreline to supply to the foreset. After this time the subaqueous delta is abandoned and the shoreline begins to transgress rapidly, creating a zone of deep water (embayment) behind it. Muto (2001) called this transgression due to sea level rise "autoretreat." The process of autoretreat begins as soon as the shoreline starts to move landward.

A key feature of the delta evaluation process is sediment supply. Whether or not a delta goes into autoretreat depends on sediment supply and the rate and duration of base level rise. For any given rate and duration of rise, the delta goes into autoretreat for a sufficiently low sediment supply. As long as sediment is still being delivered to the delta face no embayment is created. Therefore under the right conditions a sufficiently high sediment supply can prevent river mouths from being drowned due to sea level rise.

2.7 Modelling and Assessment of Climate Change Impacts on a River

The process of changing climate and their interaction with different features of the earth are extremely complicated. Understanding the effects of climate change and their subsequent variables on a specific sector requires large quality information. To incorporate this large amount of information into the complex processes of climate, use of various modelling tools and techniques becomes essential. Hence analyzing the impact of climate change on the complex river system requires the application of various assessment models. Extensive use of a number of assessment models, tools and methodologies as well as various scenarios, including those provided by the IPCC, can help to provide an assessment of the future impacts of climate change on a river.

2.7.1 Impact Modelling

When considering the impact of climatic change on the morphology of river basins and river systems, first it is necessary to estimate the impact of climate change on precipitation and evaporation, secondly on basin runoff and resulting streamflow and lastly on the hydraulics and morphology of the rivers. However, such processes become much complex when associated with global warming induced sea level rise. The river responses in a number of ways to these effects like change in river flow, high inland water level, increased siltation and consequent bed level changes, delta progradation etc. A variety of studies have done to study such responses using different modelling tools, techniques and methods.

2.7.2 Modelling to Estimate Streamflow

Climate change means variation in temperature and precipitation and changes in evaporation, air humidity, wind speed, cloudiness etc. When considering a particular river basin system, interest should be placed upon the basin runoff resulting from these variables. The relation of existing regional climate to runoff is not always straightforward. The basin runoff is usually more sensitive to precipitation changes, since they have an amplified effect on runoff.

To establish a rainfall-runoff relation for a river basin, the effect of evapotranspiration is also very crucial. Other important geophysical factors affecting the process are: the nature of geological formation (crystalline or sedimentary); the density of the natural vegetation, the nature of the drainage pattern and the formation of floodplains. Floodplains have high infiltration losses and evapotranspiration losses, which reduce

streamflow. While precipitation is the input, the soil cover complex plays the role of the discriminating element of the precipitation-runoff relations. These factors are interconnected to each other and their circular relations are difficult to introduce. Therefore hydrologic mathematical models are used to study changes in runoff caused by various factors and processes due to changes in climate.

For hydrologic climate impact modelling, the ideal model would be a distributed deterministic model with the following sub-models: an unsaturated zone model, a root zone model, a saturated flow model, a snowmelt model, a canopy interception model, an evapotranspiration model, an overland and channel flow model. Examples of such model are MIKE SHE (Systems Hydrologic European), Sacramento Soil Moisture Accounting Model etc. With these tools it is possible to model changes in vegetation and land use, but it is not possible to model secondary details. Moreover such information for a huge basin is very difficult to gather. Therefore the widely used model technologies are based on the assumption that physical basin boundary conditions do not change, thus vegetation, soil properties and channel morphology are kept constant.

In the view of above, system theoretic approaches have been considered an alternate to the physically based models, due to their simplicity relative to minimizing the need for collecting detailed watershed data. Examples of such model are ARMAX (Auto Regressive Moving Average with Exogenous Inputs), ANN (Artificial Neural Network) models etc. Nowadays, ANNs are getting more popular as an alternative for the conventional physical models because of its ability to simulate nonlinear complex system without any priori assumption about the hydrologic processes involved in a basin.

Over the past few years there have been numerous studies of the hydrologic effects of climate change. These studies primarily have focused on the effects of changes in temperature and precipitation on mean monthly, seasonal or annual runoff.

McCabe and Wolock (1997) studied the statistical likelihood of detecting a trend in annual runoff given an assumed change in mean annual runoff, the underlying year-to-year variabihty in runoff and serial correlatlon of annual runoff. Means, standard deviations, and lag-l serial correlations of annual runoff were computed for 585 stream gages in the United States. Assuming a linear 20% change in mean annual runoff over a 100 yr period and a significance level of 95%, the average probability of detecting a significant trend was 28% among the 585 stream gages.

Bronstert et al (2002) indicated that changes in land cover may have influenced the hydrological regime of various river basins. The altered timing of snow accumulation and snowmelt combined with a time shift in the rainfall regime may result in an unfavorable superposition of snowmelt and high precipitation resulting in considerable increase of 55% of the peak discharge during flood season. Various land surface and meteorological boundary conditions yielded increases in peak discharge that varied between 0 and 30% even for events with the same return period of about 3 years.

Nohara et al. (2006) investigated the projections of river discharge for 24 major rivers in the world during the twenty-first century simulated by 19 coupled atmosphere–ocean general circulation models based on the Special Report on Emissions Scenarios A1B scenario. To reduce model bias and uncertainty, a weighted ensemble mean (WEM) is used for multimodel projections. Results indicated that the discharge increases in high-latitude rivers (Amur, Lena, MacKenzie, Ob, Yenisei, and Yukon) and the peak timing shifts earlier because of an earlier snowmelt caused by global warming. Discharge tends to decrease for the rivers in Europe to the Mediterranean region (Danube, Euphrates, and Rhine), and southern United Sates (Rio Grande).

Christensen and Lettenmaier (2006) assessed the impact of climate change on Colorado River basin using a multimodel ensemble approach in which downscaled and bias corrected output from 11 General Circulation Models (GCMs) was used. Downscaled climate scenarios (ensembles) were used as forcings to the Variable Infiltration Capacity (VIC) macroscale hydrology model. Results for the A2 and B1 climate scenarios were divided into period 1 (2010–2039), period 2 (2040–2069), and period 3 (2070–2099). Analyses showed that runoff changes were mostly the result of a dominance of increased evapotranspiration over the seasonal precipitation shifts, with ensemble mean runoff reductions of −1, −6, and −11 percent for the A2 ensembles and 0, −7, and −8 percent for the B1 ensembles for the respective periods. Hamlet and Lettenmaier (1999) applied the same methodology to evaluate the climate change impacts on Columbia River basin.

Li et al (2008) developed a distributed hydrologic model of the Yellow River based on observed data in order to investigate the impact of temperature and precipitation change on runoff. Data derived from the results of seven general circulation models (GCMs) under two climate change scenarios A2 and B2 were used as future climate scenarios. Simulated runoff corresponding to climate scenarios indicated that the runoff amount would change lightly before 2020 and then would decrease approximately 5% per year.

Large variability in annual runoff in the future implied a high probability and severity of flooding as well as droughts.

Besaw et al (2010) developed artificial neural networks (ANNs) model to forecast streamflow in ungauged Winooski River basin, USA. The model inputs included time-lagged records of precipitation and temperature. To predict streamflow in an ungauged basin, the recurrent ANNs were trained on climate-flow data from one basin and used to forecast streamflow in a nearby basin with different (more representative) climate inputs. The successful demonstration of these flow prediction methods showed that the ANNs, trained on a climate-discharge record from one basin, prove capable of predicting streamflow in a nearby basin as accurately as in the basin on which they were trained. This suggests that the proposed methods are widely applicable, at least in the humid, temperate climate zones.

Chen et al (2008) evaluated the impacts of climate change on water resource in the Bosten Lake basin, China using an artificial neural network model. The model was trained using the error backpropagation algorithm and validated for a major catchment that covers 82% of the Bosten Lake basin and has the only available weather and streamflow data. After validating the model it was used to examine the surface hydrology responses to changes of regional temperature and precipitation. Major results showed that because of an additional effect on glacier melt in the upper reach of the basin temperature increase can cause large increases of streamflow. Model results also showed that if the current climate trend continues, the annual streamflow would increase by 38% of its current volume, and the summer and winter streamflow would increase by 71.8 and 11.4% of their respective current volume in the next 50–70 years, highlighting challenges for the basin's water resources management and flood protection.

Similar type of studies were also carried out by various researchers to estimate the variation in streamflow due to climate change using neural network approach due to its simplicity and easier applicability.

2.7.4 Modelling the Hydraulic and Morphologic Response of a River

A major change in the hydrologic regime would trigger a response that would completely change channel morphology. Channel morphology reflects a complex series of independent variables such as: geology, paleoclimatology, relief, valley dimensions, vegetation, hydrology, channel morphology, water discharge, sediment discharge and

flow hydraulics. These variables are not independent of each other. Eventual climate change directly influences the vegetation and the hydrology of the basin, which in turn influences the channel morphology, which influences valley dimensions, which influences relief. Relief again influences the hydrology of the basin, etc (Verhoog, 1987).

When considering the impact of climate change on a river, the channel morphology becomes the independent variable. In a natural stream, over longer periods of time, the discharge of water and sediment integrates most of the other independent variables and their nature and quantity largely affects the river behavior. Therefore the observed water and sediment discharge become independent variables which determine the morphologic characteristics of the stream and therefore the flow hydraulics. All other variables become independent then. When the impact of sea level rise is incorporated, the high water levels of the rivers also become an independent variable determining the hydro-morphologic characteristics of a river.

In order to assess such complex hydro-morphological changes, application of mathematical modelling is essential. There are a number of modelling tools available to simulate such long term morphological changes of a river due to climate change. Examples of some notable hydrodynamic and morphologic model are MIKE 21, DELFT, SOBEK, SMS, CCHE2D etc. Although these models have different computational techniques and methodologies, all of them are capable of incorporating various scenarios and impacts of climate change on a river system and consequently able to produce various responses of a river to such changes.

In order to simulate the complex long term hydraulic and morphologic responses of a river to climate change, various researchers had undertaken several studies with the application of models. Most of them are related to inundation and backwater effect. Only few studies were done to assess the morphological activities due to climate change.

Huang et al (2004) examined the increased potential risk of tidal inundations in the Pearl River delta, China, due to future rises in sea level. The research was based on tidal records of 54 tide gauges distributed across the delta plain and employs mathematical calculations to predict potential rises of water level in different parts of the delta under a number of flood scenarios given by IPCC. After assessing a 72-year tidal and factors such as estuarine backwater effects and long-term geological subsidence, it suggested that a 30 cm rise in relative sea level at the mouth of the estuary is possible by 2030.

Based on the prediction and five freshwater discharge scenarios, the potential impacts in water level across the delta plain were calculated. The impacts were also translated into return periods of water level. It is suggested that in a large part of the delta plain, return periods will be shortened and hence will be increasingly vulnerable to tidal inundation.

Vastila et al (2010) assessed the impacts of climate change, both in terms of changed basin water balance and sea level rise, on the Lower Mekong flood pulse. The impacts were simulated by a three-dimensional hydrodynamic model EIA 3D using the projected changes in sea level and the Mekong mainstream discharge under the influence of climate change as boundary conditions. The model simulations projected that average and maximum water levels and flood duration increase in 2010–2049. The most consistent and notable changes occurred in the average and dry hydrological years. Sea level rise had the greatest effects in the Mekong Delta, whereas the impacts of changed basin water balance were more notable in the upper areas of the Mekong floodplains. Hanh and Furukawa (2007) undertook similar studies for the coastal zone of Vietnam.

Springer et al (2009) presented a record of Holocene hydroclimatology for a humid, temperate watershed in the Appalachian Mountains of eastern North America. They used river-deposited cave sediments to construct a history of incision, aggradation and morphological change in the surface channel. They found that the Greenbrier River had aggraded by 4 m during or prior to the Halocene and adopted an alluvial morphology, probably due to the mobilization of hillslope sediments accumulated during the colder, drier full-glacial conditions of the Late Pleistocene. As climate moistened during the Holocene, the Greenbrier River incised through channel-filling sediments and back onto bedrock. Therefore, the bedrock morphology of many streams in the Appalachian Mountains may not have existed for much of the Holocene, which highlights the effect of climate variability on channel processes. The base-level rise was more evidence that bedrock incision by rivers is often episodic and that slow, long-term incision rates are probably not representative of short-term incision rates.

Scott and Jia (2010) developed a two-dimensional hydrodynamic and sediment transport model CCHE2D for addressing sediment transport problems in the Mississippi and Arkansas Rivers due to climate change. Traditionally, because of the computational time requirements of multi-dimensional simulations, models are run for relatively short periods of time on relatively short river reaches. Although this provides an indicator of initial channel response, it does not provide an indicator of long-term changes in river

morphology. To reduce simulation time requirements, a quasi-steady approach was undertaken for long-term simulations like climate change for the selected river systems with gradually varying hydrographs. The study results indicated that although riverine sediment transport and hydrodynamics are inherently unsteady in nature, the quasi-steady approach could provide adequate solution for supporting long term simulations of river due to climate change. A study was also carried by Promny (2011) to evaluate the effects of climate change on the morphology of German waterways using SOBEK.

2.7.5 Modelling to Evaluate Delta Progradation

Climate change and global warming accelerated sea level rise will have a profound effect on morphological processes of a river and its associated delta system. In this case the progradation of delta depends not only on the water and sediment discharge supplied by the associated river basin, but also on the rising level of sea water. Hence the water and sediment discharge along with the increasing sea level become independent variables that determine morphology of the river and evolution of river delta.

A variety of conceptual, experimental and numerical models have been developed to predict the response of a river to sea level rise and the process of delta evolution associated with such rise. However, such computational methods are still under developed and continuous research is undergoing. Among them, the Numerical Model developed by Parker and Muto (2003) is widely used for various field conditions to assess the process of delta evolution due to climate change.

Parker and Muto (2003) developed a numerical model is to study delta evolution, including autoretreat, and is compared against a set of experiments. The model also encompasses the migration of a bedrock-alluvial transition at the upstream end of the delta. Akamatsu, Parker and Muto (2005) applied this model to explore the effect of rising sea level on river deltas and long profiles for the Fly-Strickland River System, Papua New Guinea for smooth and punctuated eustatic sea level rise. The results indicated that sediment supply during floods plays a key role in determining the delta response to the sea level rise. The results also suggested that (1) this river delta experienced autoretreat during the most recent postglacial sea-level rise, (2) the effect of the sea-level rise likely extended far upstream of the present-day river delta, (3) the present Fly-Strickland estuary partially represents the aftermath of, and is in recovery from the effect of the last postglacial sealevel rise, (4) the predicted final position of

shoreline at the present day in the case of punctuated sea level rise is approximately same as in the case of smooth sea level rise and (5) a change of sediment supply has a drastic influence on the bed profile.

The numerical model verifies Muto's (2001) concept of autoretreat at field scale, and quantifies it for the Fly-Strickland River System, Papua New Guinea. The model suggests that Holocene sea level rise likely had a profound effect on both the river delta (drowning it) and the river profile itself (increasing concavity of the long profile and forcing the upstream end of the sand-bed reach landward.

Parker, Akamatsu, Muto and Dietrich (2004) also analyzed the passive margin of the East Coast of the US. The coastline from New Jersey to North Carolina shows a series of embayments, including Delaware Bay, Chesapeake Bay and Albemarle Sound. Evidently the mouths of the rivers flowing into this region were drowned by sea level rise. The margin of the northern Gulf of Mexico near the Mississippi River delta, on the other hand, presents a very different picture. Evidence suggests that the Mississippi Delta was able to continue to prograde throughout Holocene sea level rise. The experiments of Muto (2001) allowed interpretation of the difference between these scenarios. Apparently the sediment supply to the Appalachian-sourced streams was not sufficient to prevent autoretreat and delta drowning due to 120 m sea level rise over 12000 years. The sediment supply to the Mississippi Delta, however, appears to have been sufficient to allow progradation over the same period. They concluded that if the sediment supply is sufficient then the delta front continues to move seaward, and the speeds of progradation of the new deltas after stabilization depend on the sediment feed rate from upstream.

Lai and Capart (2007) envisioned the delta evolution as a one-dimensional diffusion process, with different diffusivities acting along the topset and foreset, and the resulting equation is solved by finite differences. Computations were first validated against analytical solutions derived earlier for the case of constant base level. Numerical simulations for the case of rising base level were then presented, and compared with small-scale laboratory experiments. The numerical, analytical and experimental results were found to be in good agreement with each other, and exhibit various features of interest. The results indicated that deltas starting from a uniform slope first prograde, then retreat under the influence of a rising base level. However, a rising base level can cause erosion along the upper face of the foresets of the river delta.

2.7.6 Impact Assessment Studies in Bangladesh

Various literatures have been found that describes the impact of climate change and sea level rise on the rivers of Bangladesh. However, very few of them consider the hydraulic and morphologic responses of the river that might occur due to the anticipated changes in climate. Some of the notable works are described here.

Mirza and Dixit (1997) estimated that a 2°C warming combined with a 10 percent increase in precipitation would increase runoff in the Ganges-Brahmaputra-Meghna Rivers by 19, 13 and 11 percent respectively. Increased depth of flooding will be pronounced in the lowlands and depressions in the Faridpur, southwest Dhaka, Rajshahi, Pabna, Comilla and Sylhet-Mymensingh greater districts. Mirza (1997) also mentioned that due to change in precipitation as a result of 4°C temperature increase, mean annual discharge of the Ganges River could increase by 15 to 27% and the mean annual discharge of the Brahamaputra River may change by 2 to 13%.

Gain et al (2011) investigated the effect of climate change on both low and high flows of the lower Brahmaputra River. They applied a novel method of discharge-weighted ensemble modeling using model outputs from a global hydrological models forced with 12 different global climate models (GCMs). Based on the GCM outputs and long-term records of observed flow at Bahadurabad station, their method resulted in a multi-model weighted ensemble of transient stream flow for the period 1961–2100. Using the constructed transients, they subsequently projected future trends in low and high river flow. The analysis showed that extreme low flow conditions are likely to occur less frequent in the future. However a very strong increase in peak flows was projected, which may, in combination with projected sea level change, might have devastating effects for Bangladesh.

IWM and CEGIS (2007) assessed the potential impacts of climate change by considering the sea level rise, changes in intensity of cyclones and precipitation for both low (B1) and high (A2) greenhouse gas emission scenarios according to the 3rd IPCC predictions. The result showed that about 13% more area will be inundated in monsoon due to 62cm sea level rise for high emission scenario A2. Due to increased rainfall in addition to 62cm sea level rise, the inundated area will be increased upto 16% in the year 2080. Such studies are limited to the inundation of coastal areas due to SLR and its possible impacts on livelihood. Only a few literatures have been found that studied the morphological change of a river system.

Rahman and Alam (2003) showed an interesting result at the bifurcations of the Jamuna river with its distributaries Dhaleswari river and Old Brahmaputra river. They found that the bed level will rise 0.08, 0.12 and 0.41 m at the mouth of the Dhaleswari river and 0.05, 0.08 and 0.27 m at the mouth of the Old Brahmaputra river for the years 2015, 2025 and 2095 respectively. This will probably result in a considerable increase in the discharges in the distributaries and a small decrease of the discharges in the Jamuna and Padma rivers. The discharge distribution at the tributaries of the Ganges and the Padma rivers (Gorai and Arial Kahn rivers) will change also due to the considered sedimentation. These changes might be of important consequences for the course of the main river channels in Bangladesh.

GEGIS (2010) assessed the impact of different aspects of climate change on the morphological processes of some major rivers such as the Jamuna, the Ganges and the Padma. The study assessed various aspects of river morphology and climate change qualitatively. They found that the flooding in the Jamuna and Ganges floodplain would not be a major threat, because with the increasing discharge rivers will adjust their dimensions. Hence increase in bank erosion and scour was expected. Due to high sediment yield from the basin and mild slope, the response of the river was expected to be rapid one.

Matin and Kamal (2010) used 1D mathematical model to analyze the impacts of rising sea level on the Pussur-Sibsa River system and found progressive siltation of the river. The study also projected that the sedimentation rate will increase for the river if the sea level changes according to the IPCC scenario. From the study it was found that for sea level rise of 12%, 58%, 70% and 78%, the sedimentation rate in the lower reach of Pussur River increases upto 25%, 49%, 64% and 74% for the years 2020, 2030, 2040 and 2050 respectively.

No research has so far been attempted to examine how sedimentation would be affected due to increased flood vulnerability under climate scenarios. One may, however, take note that rate of sediment deposit along the river bed and adjacent floodplains might increase if duration of high intensity floods increase as a consequence of sea-level induced stronger backwater effect on receding flood water. This requires further hydro-morphological analysis. The present study is an attempt to undertake such study considering various hydraulic and morphologic aspects that might be affected due to climate change.

2.8 The Lower Meghna River

The Lower Meghna River is the widest and one of the most dynamic rivers of Bangladesh. It one of the three rivers that forms the Ganges Delta, the largest on earth fanning out to the Bay of Bengal. Being a part of the Surma-Meghna River System, Meghna is formed inside Bangladesh by the joining of different rivers originating from the hilly regions of eastern India. The river meets Padma River in Chandpur District. The river ultimately flows into the Bay of Bengal in Bhola District.

2.8.1 Course of the River

The Lower Meghna River originates from the Surma-Meghna River System in Bangladesh. It rises in the Manipur Hills of northeast India as the Barak River and flows west becoming the Surma River. The Meghna is formed inside Bangladesh above Bhairab Bazar by the combination of the Surma and Kushiyara rivers. Down to Chandpur, Meghna is hydrographically referred to as the Upper Meghna. After the Padma joins, it is referred as the Lower Meghna and moves down 145 kilometers to the Bay of Bengal (MoWR, 1998).

Figure 2.16: The Lower Meghna River

In her course from Chandpur to Bay of Bengal, the Lower Meghna braids into a number of little rivers including the Pagli, Katalia, Dhonagoda, Matlab and Udhamodi, but the

main flow is towards Meghna Estuary. Near Bhola, the river falls into the Bay of Bengal through a number of channels: the Tetulia River, the Shahbazpur channel and the Hatia channel (Figure 2.16). The Shahbazpur channel carries the major portion of the flow.

A larger number of settlements, towns, ports and industries have sprung up on both the banks of Lower Meghna. Narsingdi, Chandpur, Barisal and Bhola are the district towns that stand on the banks of the river. Kuliarchar, Bhairab Bazar, Chandpur, Ramdaspur, Kalupur and Daulatkhan are important river ports and business centers.

2.8.2 Planform and Channel Development

The main channel of the Lower Meghna River is located between the Chandpur and the northern head of Bhola. This channel is very dynamic in nature. Frequent natural shifting of the channel, development of large chars, formation of subchannels and submerged zones are the extensive features of the river. During monsoon, the water flows through the main channel and subsequent floodplains. When the water recedes, numerous subchannels and slack water areas are exposed. Such features are identifiable on Figure 2.17 as barren sediment accumulation zones. The River is notorious for its alluvial islands, called chars. Some of the notable are Char Haim near Chandpur, Char Munshi and Char Gazaria near Bhola. These chars are formed and reworked during each year of flooding.

Figure 2.17: Satellite image of Lower Meghna River

2.8.3 Hydrodynamic Condition of the River

The combined flow of the Ganges-Brahmaputra (Jamuna)-Meghna rivers is drained into the Bay of Bengal through the Lower Meghna River. It is ranked third among the big rivers in the world in terms of river flow and pours nearly a trillion (10^{12}) m^3 of water pours into the estuary annually (CCC, 2009b). Due to the variation in precipitation between the two main seasons (dry and monsoon seasons), the river experiences wide variation of hydrological conditions and consequent physical processes. While the discharge within the Lower Meghna (the part downstream of the confluence near Chandpur) typically varies between 8,000 m^3/s in February/March and 100,000 m^3/s in July to September, the peak discharge exceeds 120,000 m^3/s in the year of severe flood (MWR, 2001). The discharge variation of Lower Meghna River is given in Table 2.8.

Table 2.8: Discharge variation of Lower Meghna River (CCC, 2009b)

Discharge for different Return Periods (m^3/s)		**Average Annual Discharge (m^3/s)**	
100 yr	1,28,720	Maximum	89,788
20 yr	1,15,327	Mean	28,565
2 yr	88,622	Minimum	5,070

The stages along the Lower Meghna are subjected to tidal influence. The average daily water level at Chandpur varies between 0.56m and 4.99m. During low flows in the Lower Meghna River the tidal range near the confluence with the Upper Meghna River is about 0.4 m. The tidal range also varies spatially along the river, from approximately 1.5 m in Chandpur to 4 m in Hatiya. Hence a Micro-to-Meso tidal environment prevails in the area. The average water level slope of the Lower Meghna River varies between 1 cm/km (during low flows) and almost 4 cm/km (during flood conditions). Recorded maximum velocity ranges from 1.14 – 2.2 m/s during monsoon. The character of the estuary channels is determined by the combined influence of tidal and river flows. The Lower Meghna River is clearly dominated by fluvial (river) processes (MoWR, 2001).

2.8.4 Morphologic Condition of the River

Heavy rainfall in the Himalayas and the exposure of the catchment to the weathering actions contribute enormous amount of sediment load in the Ganges-Brahmaputra-Meghna rivers. Nearly 1.5 to 2 billion tons of sediment enters through these rivers and

passes through the Lower Meghna River annually. Therefore the river forms an extensive floodplain and contributes sediment to the delta. A study shows that amount of floodplain sedimentations is about one-third of the sediment that is carried by the major rivers. The other one-third enters the Meghna Estuary through the Lower Meghna River and contributes to the land formation and delta development. The rest is transported towards the ocean. The part of the sediment that is carried by Lower Meghna River, governs the morphologic behavior of the river.

Sediment concentration of Lower Meghna River is slightly higher near the bottom than at the surface of the estuary, indicating the water columns are vertically well mixed. During the survey of Meghna Estuary Study, all collected and analyzed sediment samples in the area showed the depth-averaged concentration ranged between 0.5 and 9.0 gm/L (Ali, 2007). The size of the sediments also varies spatially and the representative grain size for the river was found in the range of 0.09 to 0.13 mm (Figure 2.18).

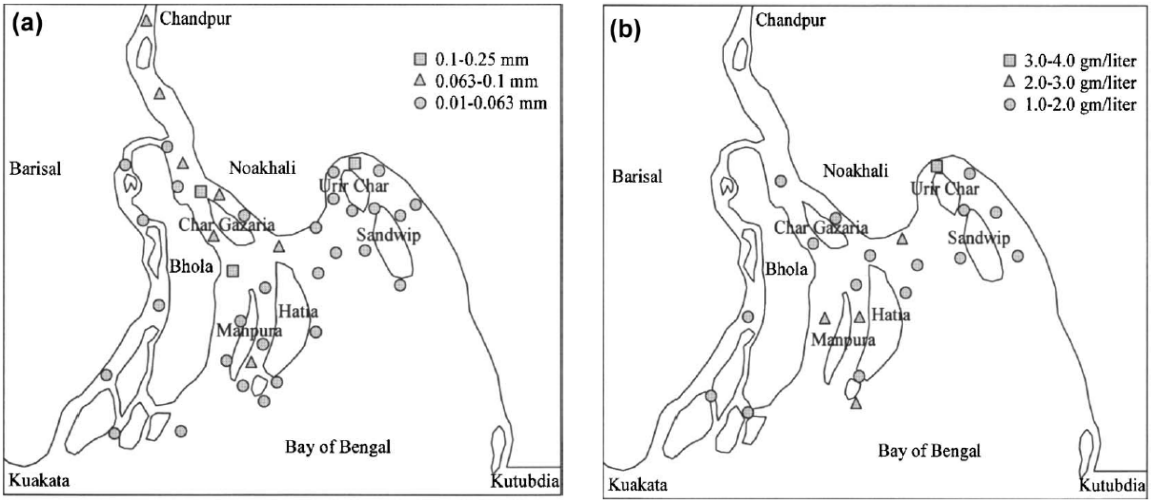

Figure 2.18: Grain size distribution (a) and suspended sediment concentration (b) of Lower Meghna River (Source: MoWR 2001)

2.8.5 Climate Change and Lower Meghna River

The Lower Meghna River carries the combined flow of Ganges, Brahmaputra and Upper Meghna and discharges water into the Bay of Bengal through a common terminus known as the Meghna estuary. The annual discharge of Lower Meghna River is expected to increase due to climate change. A huge inflow of water from upstream GBM basin areas coinciding with heavy monsoon rainfall will increase the peak discharge of the river.

This massive water carries enormous amount sediment towards the Bay of Bengal. Major sources of the sediments carried by the Lower Meghna are the rivers in the upstream areas of India, China, Nepal and Bhutan and the average annual sediment load that passes through this river to the Bay of Bengal ranges between 0.5 billion to 1.8 billion tons (CCC, 2009a). Therefore the impact of SLR would be more prominent for this river. Ali (1999) indicated that the present slope of the Meghna River from about 100 km inland near Chandpur, a river port to its mouth is about 1.136 cm/km. If the sea level rises by 1.0 m, the resultant river slope will become 0.136 cm/km. Moreover, increased rainfall runoff in the vast GBM region due to climate change also contributes to enhanced sediment flows along the GBM river systems. This is likely to increase the rate of bed level rise in the channels and the floodplains. The consequence is progressive siltation and decrease of channel depth, thereby increasing the flood ability of the alluvial plain.

The process of delta evolution will be significant in the deltaic zone of Bangladesh, which discharges billion tons of sediment through the Meghna Estuary. An enhanced sediment flow due to increased rainfall runoff along with gradual deforestation in the vast GBM region is likely to affect such process. Recent remote sensing analysis of CEGIS revealed that the land areas have been increasing due to huge sedimentation and subsequent land development scenarios (Char Nangulia, Noler Char and Caring Char of Noakhali district) in the coastal zones of Bangladesh (CCC, 2009b).

CHAPTER 3
METHODOLOGY

3.1 General

The impact of climate change on a river can be identified as a complex interaction between various physical processes related to hydrology, hydraulics and morphology which control the behavior of the river. As a result of climate change, the projected increase in temperature, sea level rise and precipitation variability is likely to affect such processes, resulting in a significant impact on a river basin, associated river systems and overall hydro-morphology of a river. In order to assess such complex hydraulic and morphologic response of a river, application of mathematical modelling is essential. In the present study, various hydro-morphological changes of Lower Meghna River due to climate change and sea level rise have been analyzed with the application of different mathematical models.

3.2 Modelling the Responses of the River due to Climate Change and Sea Level Rise

The anticipated climate change and sea level rise is likely to initiate various hydraulic and morphologic changes in the Lower Meghna River resulting in significant impacts on river flow, river water level, siltation rate and bed levels, delta progradation etc. These effects have been assessed and analyzed using different modelling tools and techniques. These are discussed here.

3.2.1 Prediction of Discharge

To predict the discharge of Lower Meghna River due to climate change, a relationship has been developed to covert the future precipitation projections into discharge. Since the precipitation over Ganges-Brahmaputra-Meghna basin affects the river flow of the basin and contributes most of the flow, a precipitation-discharge relationship was established. The discharge-precipitation relationship can be expressed as follows –

$$Q = f(P) \tag{3.1}$$

where, Q is the discharge and P is the precipitation. To establish such relationship, an Artificial Neural Network (ANN) model has been developed for the present study. This model uses feedforward backpropagation method to predict discharge and has the ability to adapt and train.

3.2.2 Estimation of Backwater Effect

Backwater effect resulting from the sea level rise retards the river outflow by raising the water level along the river. The magnitude and extent of backwater effect of Lower Meghna River can be determined by comparing the water levels of the projected periods with the base condition. The water level variations can be determined by solving the continuity and momentum equations. For two dimensional cases, the depth integrated continuity equation can be written as follows –

$$\frac{\partial h}{\partial t} + \frac{\partial h\bar{u}}{\partial x} + \frac{\partial h\bar{v}}{\partial y} = hS \tag{3.2}$$

where, t is the time; $h = \eta + d$ is the total water depth; η is the surface elevation; d is the still water depth; $\bar{u}$ and $\bar{v}$ are the depth average velocity components in the x and y dirtection and S is the magnitude of the discharge due to point sources. This equation along with the momentum equations have been solved simultaneously using the MIKE 21 Flow Model FM to obtain the water level variations.

3.2.3 Assessment of Bed level Changes and Siltation Rate

The morphology of the Lower Meghna River reacts to changes in the upstream input of water and sediment resulting in a change in the process of erosion and deposition. As a result the bed level changes with time. The bed level changes of the river can be calculated by using the sediment continuity equation. The equation can be written as follows –

$$-(1-n)\frac{\partial z}{\partial t} = \frac{\partial S_x}{\partial x} + \frac{\partial S_y}{\partial y} - \Delta S \tag{3.3}$$

where, n is bed porosity, z is bed level, t is time, S_x and S_y are total load transport in the x and y direction and ΔS is sediment sink or source rate. The contribution from the bed load transport to the bed level change rate is obtained by taking the divergence of the sediment fluxes at a particular section. These calculations have been performed by MIKE 21 Flow Model FM.

The siltation rate of the river has been calculated considering the bed level changes with time. The net deposition or erosion has been calculated by determining the overall cross sectional changes. These changes with respect to time give the long term siltation rate of the river due to climate change.

3.2.4 Evaluation of Delta Progradation

The channel aggrades and regression of delta occurs when the river is at bankfull flow for time I_f, i.e. when it is morphologically active. Then the progradation of the delta can be determined using the modified equation of sediment continuity –

$$(1-n)\frac{\partial \eta}{\partial t} = -\Omega \frac{I_f(1+\Lambda)}{B_f}\frac{\partial Q_{tbf}}{\partial x} \tag{3.4}$$

where Q_{tbf} is the total sediment load at bankfull flow with floodplain width B_f , Ω is channel sinuosity and Λ is the fraction of wash load deposited per unit bed material load in the channel-floodplain complex .

Along with the sediment continuity equation, flow and sediment transport equations are used. After applying moving boundary conditions and finite difference approximation, the numerical model can be used to evaluate the progradation of delta.

3.3 Models and Model Linkages

The complex changes in the hydraulic and morphologic behavior of the Lower Meghna River as a result of climate change and sea level rise is very difficult to assess. To analyze such intricate relationships, it is necessary to employ various climate, hydrologic, hydraulic and morphologic models. Therefore for the present study, climate change impacts on the Lower Meghna River have been simulated with the combination of three models. They are –

- Artificial Neural Network (ANN) model, which can be considered as a hydrological model, can be used to convert precipitation changes into runoff and discharge of a river.
- MIKE 21 Flow Model FM, which consists of both hydrodynamic and morphologic module, can be operated to assess various hydraulic and morphologic changes of a river.
- Numerical Delta Progradation model, which is an analytical model, can be used to simulate the movement of delta fronts along the long profile of a river.

Among many variables, the precipitation outputs of HadCM3 atmospheric–ocean general circulation model (AOGCM) runs projected by Hadley Centre for Climate Prediction and Research have been used as the input parameter representing climate change under the influence of increasing greenhouse gas concentration. At first, the Artificial Neural

Network (ANN) will be developed to investigate the impacts of precipitation changes due to climate change on the river discharge. The resulting discharge will again affect the river hydraulics and morphology along with sea level rise. This scenario will be analyzed using MIKE 21 Flow Model FM. Finally the various climate change impacts will be incorporated in the numerical Delta progradation model to study the movement of delta front along river profile. However, these models are interrelated and linked, as the results of ANN model will be used in MIKE 21 FM. Again, the findings of both these models will be included in the Delta Progradation model. The mentioned models along with their interrelations, links and outputs are shown in Figure 3.1.

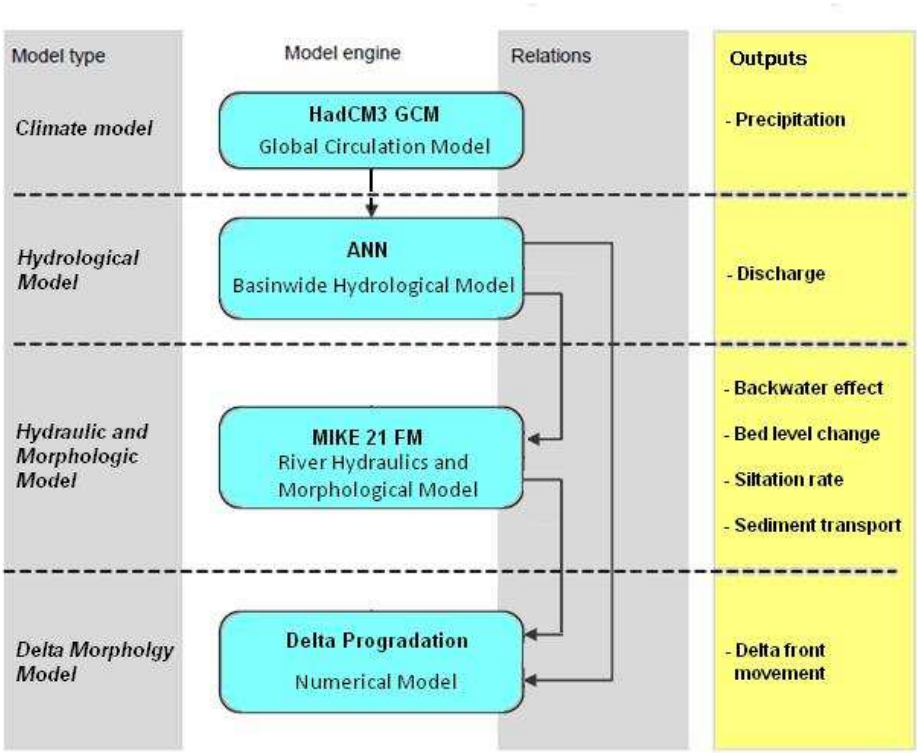

Figure 3.1: Linkage of models

The description of the models along with their various mathematical aspects and modelling features are discussed in chapter four.

3.4 Selection of Climate Change Scenarios

As a result of climate change, various responses of a river such as increased flow, high water level, sedimentation and bed level changes, delta progradation etc. have been assessed and linked using different types of models. Once the models are developed, calibrated and validated adequately, it would be ready to simulate future scenarios using envisaged boundary condition of some conceivable hydrologic years. Hence all the

models, affected directly or indirectly by various climate change processes, have been developed and analyzed for the scenarios given in Table 3.1.

Table 3.1: Climate change scenarios considered for the study

Climate Change Scenario	Qualitative change in Precipitation	Qualitative change in Runoff	Sea level rise (cm)		
			2020	2050	2080
A1FI	+	+	6.1	17.2	35.6
A1B	+	+	6.1	16.7	30.1
B1	+	+	6.2	15.0	24.9

Scenario A1FI and B1 represents the upper and lower extremities among various climate change scenarios. The projection of A1B is more moderate compared to them and have been used in many impact studies for Bangladesh.

3.5 Data Collection and Processing

The observed precipitation data over the GBM basin has been collected from the global database developed by Climate Research Unit (CRU). The CRU provides gridded dataset of resolution $3.75^0 \times 2.5^0$ all over the world. Considering the GBM basin, 32 grids were selected to obtain the monthly precipitation data for the period of 1975 to 1994. The observed data of precipitation over GBM basin was only available for the period of 1975 to 1994. Therefore the present study was conducted based on these available data sets. A sample set of data are shown in Figure 3.2.

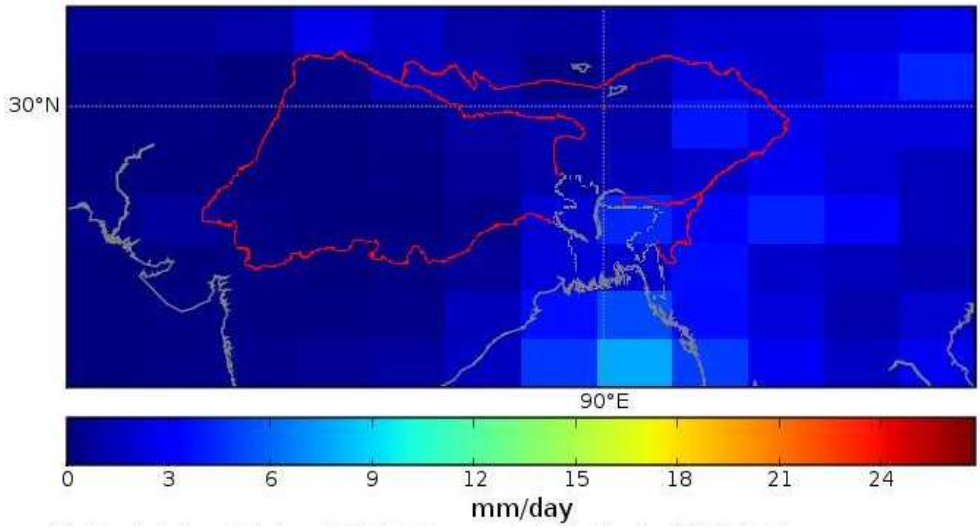

Figure 3.2: Observed precipitation over GBM basin for October, 1975

The projected precipitations of HadCM3 GCM models for different periods were retrieved from the IPCC data distribution web site. These projections have been developed by Hadley Center for Climate Prediction and Research (HCCPR) for various climate change scenarios. The sea level rise projections were considered according to IPCC predictions for different scenarios. Details of the observed and projected precipitation have been given in Appendix A.

Various hydrographic data of the Lower Meghna River was collected from Bangladesh Water Development Board (BWDB) for different stations. Discharge data of Bhairab Bazar and Baruria station and water level data for Chandpur, Hatiya and Doulatkhan station were collected for the period of 1975 to 2008. The cross sectional and bathymetry data of Lower Meghna River were collected from BWDB and BIWTA. The lists of data gathered for the present study are enlisted in Table 3.2.

Table 3.2: List of data collected for the study

Data Type	Data Variable	Source	Location	Collection Period
Climate data	Observed precipitation	CRU	GBM basin	1975 to 1994
	Projected precipitation	HCCPR, UK	GBM basin	2020s, 2050s and 2080s
	Sea level rise projection	IPCC	-	2020s, 2050s and 2080s
Hydrographic data	Discharge	BWDB	Baruria	1975 to 2008
	Discharge	BWDB	Bhairab Bazar	1975 to 2008
	Water level	BWDB	Chandpur	1975 to 2008
	Water level	BWDB	Hatiya	1975 to 2008
	Water level	BWDB	Doulatkhan	1975 to 2008
	Bathymetry	BWDB, BIWTA	Lower Meghna	2006

Discharge is usually not measured at Chandpur station. Therefore the discharge of Padma at Baruria station and the discharge of Upper Meghna at Bhairab Bazar were incorporated into 1-D hydrodynamic model HEC-RAS to obtain the discharge of Lower Meghna River. The water level corresponding to discharge was then compared with the water level measured at Chandpur. The discharge at Baruria, Bairab Bazar and Chandpur are given in Figures 3.3 (a) to (c).

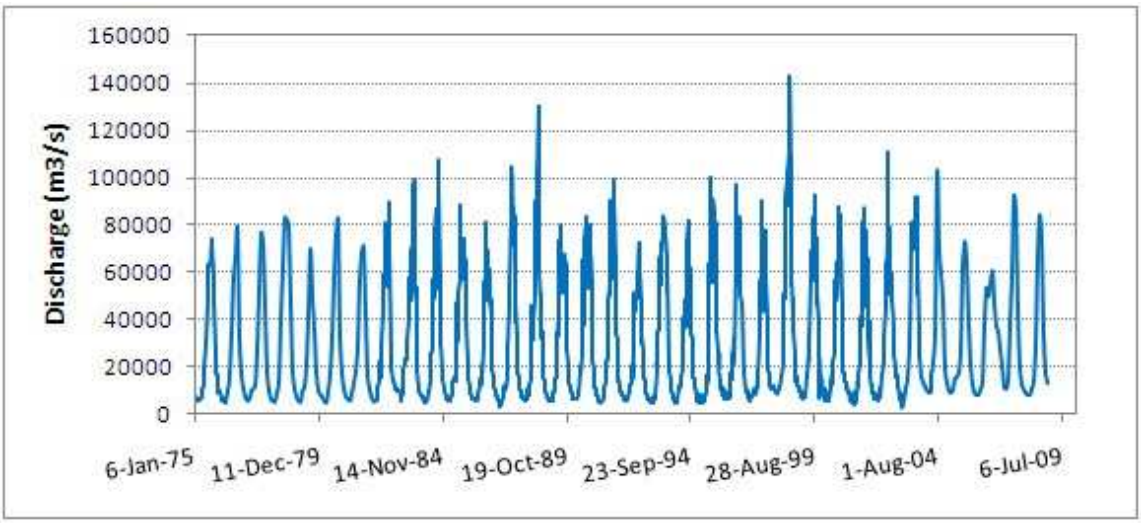

(a)

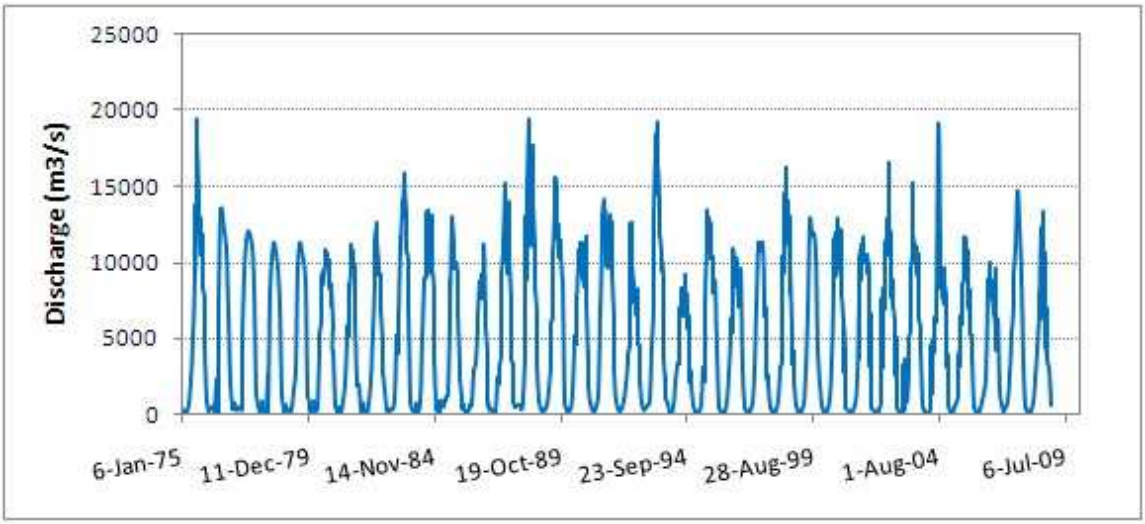

(b)

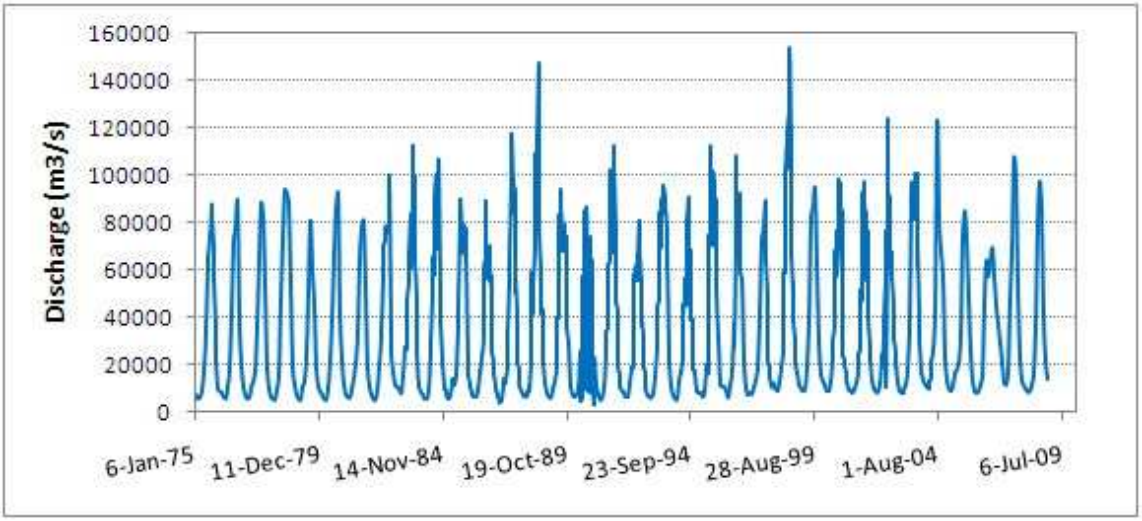

(c)

Figure 3.3: Time series hydrographs of (a) Padma at Baruria (b) Upper Meghna at Bhairab Bazar and (c) Lower Meghna at Chandpur

The bathymetry data of Lower Meghna River was collected from Bangladesh Inland Water Transport Authority (BIWTA) for the pre monsoon (April) and post monsoon (November) periods of year 2006. Cross sectional data of the river was also collected from BWDB. The bathymetry of Lower Meghna River according to the collected data is shown in Figure 3.4.

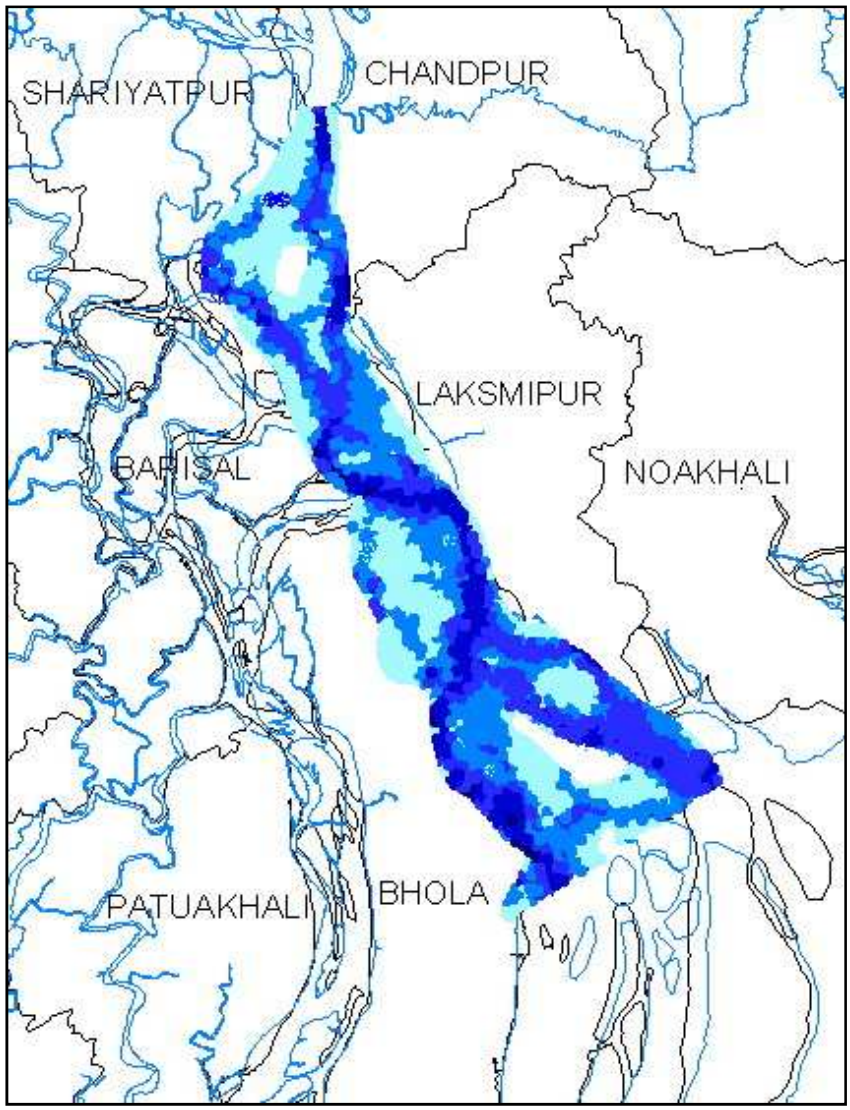

Figure 3.4: Observed bathymetry of the study area

The surveyed data of BIWTA during April 2006 was used to set-up the initial bathymetry of MIKE 21 FM model. These data covered almost all the areas of the river, except some data were missing near Chandpur. These gaps were adjusted and filled with the BWDB measured data. These data were then geo-referenced and processed to prepare it as input in the model. However, the Tentulia channel was not considered for the present study.

3.6 Method to Estimate River Flow using ANN Model

To predict the discharge of Lower Meghna River due to climate change, a rainfall-runoff (precipitation-discharge) ANN model over the GBM basin was developed by using the precipitation data of GBM basin and discharge data of Lower Meghna River. The step-by-step procedure of the model development is as follows –

- **Setting of GBM Basin Grids:** The precipitation data was set and processed so that they can be used conveniently in the neural network architecture. The basin grids were selected in such a way that they match the resolution of the precipitation data.
- **Processing of Input Data:** For the neural network model considered for the present study, the observed precipitation and discharge were taken as the input variables. The time series data of precipitation and discharge were incorporated on the GBM basin grids using neural network method.
- **Development of Neural Network Model:** There is no specific method or rules for the development of ANN architecture that will produce the best result. The numbers of input and output nodes are problem dependent. The flexibility lies in selecting the number of hidden layers and in assigning the number of nodes to each of these layers as well as in the number of iteration. For the present study a trial-and-error procedure was applied to decide the optimal neural network architecture by adjusting the number of hidden layers and number of nodes in each hidden layer. The activation function and number of iteration were also specified in this stage.
- **Calibration of the Model:** The model was calibrated to obtain the desired discharge of Lower Meghna River from the precipitation inputs by comparing the ANN predicted discharge and the observed discharge of the river. The error was calculated in terms of Mean Squared Error (MSE). If the error is significant and unable to produce desired results, the weights were corrected through backpropagation algorithm.
- **Validation of the Model:** After calibration, the model was validated by introducing a new set of data. The validation was done in terms of various statistical indicators. If satisfactory validation was not obtained, new trial was performed by changing the architecture of the neural network.
- **Application of the Model:** The network that gave the best statistical performance could be selected as the designed model. This developed model was then applied to predict the discharge of Lower Meghna River for various climate change scenarios.

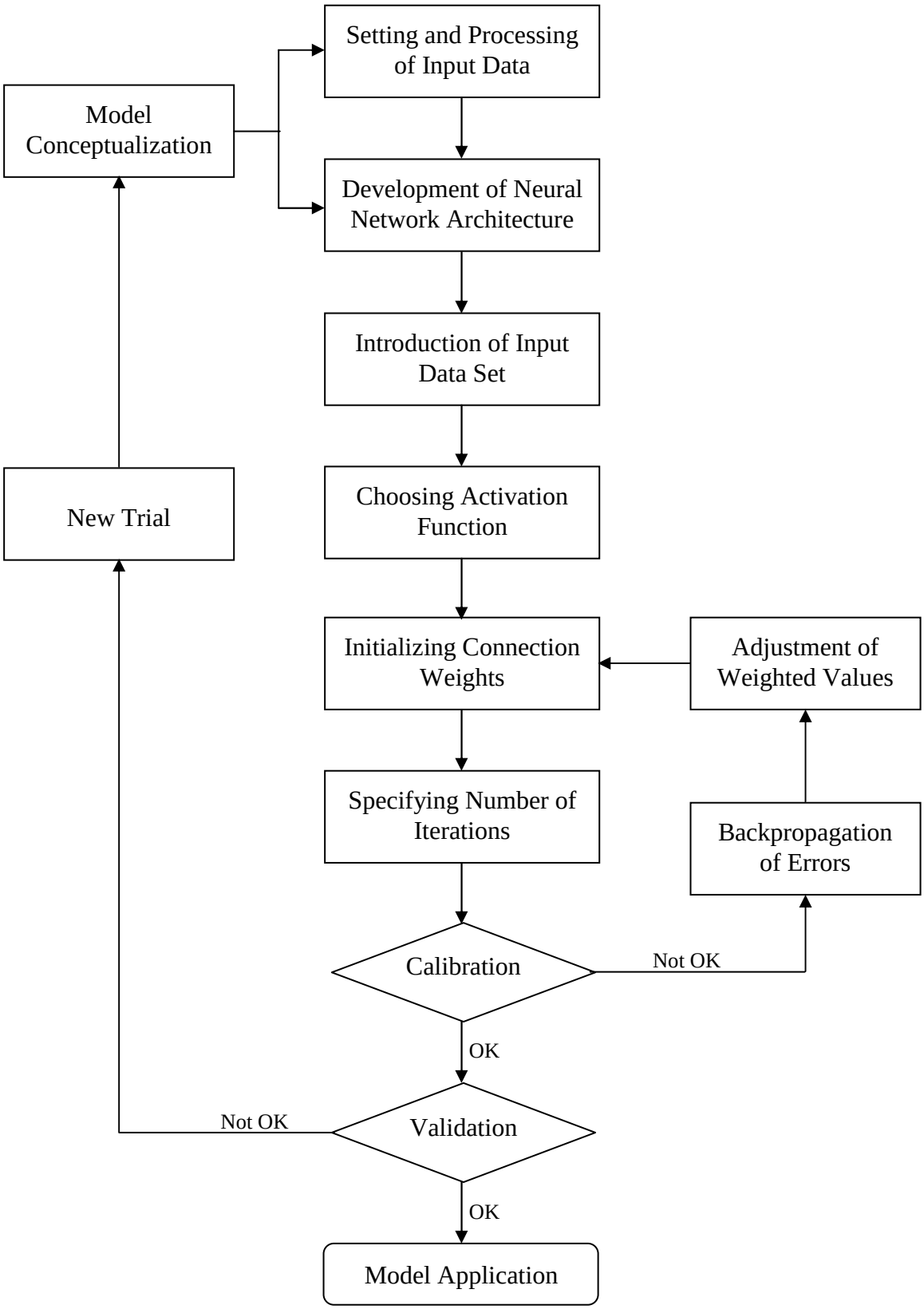

Figure 3.5: Flowchart showing the steps of ANN model development

3.7 Method to Analyze Hydro-Morphologic Responses using MIKE 21 Flow Model

In order to determine various hydro-morphologic changes of Lower Meghna River such as water level variation due to backwater effect, change in bed level and siltation rate, a two dimensional mathematical model of the river was developed using MIKE 21 Flow Model FM. This modelling works were performed at Institute of Water Modelling (IWM), Dhaka. The modelling process is described here briefly –

- **Model Conceptualization:** The model domain and modelling period was set carefully at the preliminary stage of modelling. The selected portion of Lower Meghna River between Chandpur and Hatiya was considered as the model domain. The modelling periods were selected in such a way that they can link the present day condition with the future projected periods.
- **Initial and Boundary Conditions:** The model domain of Lower Meghna River had two closed boundaries. The model had a discharge boundary at the upstream at Chandpur and a water level boundary at the downstream at Hatiya. Water level data was incorporated as the initial condition in the model.
- **Various Inputs in Hydrodynamic and Sand Transport Module:** Various inputs and parameters contribute in adjusting the solution technique of the hydrodynamic module and sand transport module of MIKE 21 Flow Model FM. The inputs in the hydrodynamic module are wetting-drying parameter, Eddy viscosity, bed resistance or roughness parameter etc. Various inputs and parameters associated with the sand transport module are sediment transport predictors, alluvial resistance, grain size of soil etc.
- **Calibration and Validation of the Model:** The model was calibrated and validated for both the wet and dry conditions under different periods. During this process, the various inputs and parameters were adjusted in such a way that the model could represent the real condition of the river. The roughness parameter Chezy's C is mainly a calibration parameter in the hydrodynamic module and the alluvial resistance is the calibration parameter for morphologic simulation.
- **Model Simulation and Application:** After calibration and validation of the model, the projected discharge and rising water level due to sea level rise was incorporated for different climate change scenarios to estimate the possible hydraulic and morphologic changes of Lower Meghna River due to climate change. The whole modelling process is summarized in the flowchart of Figure 3.6.

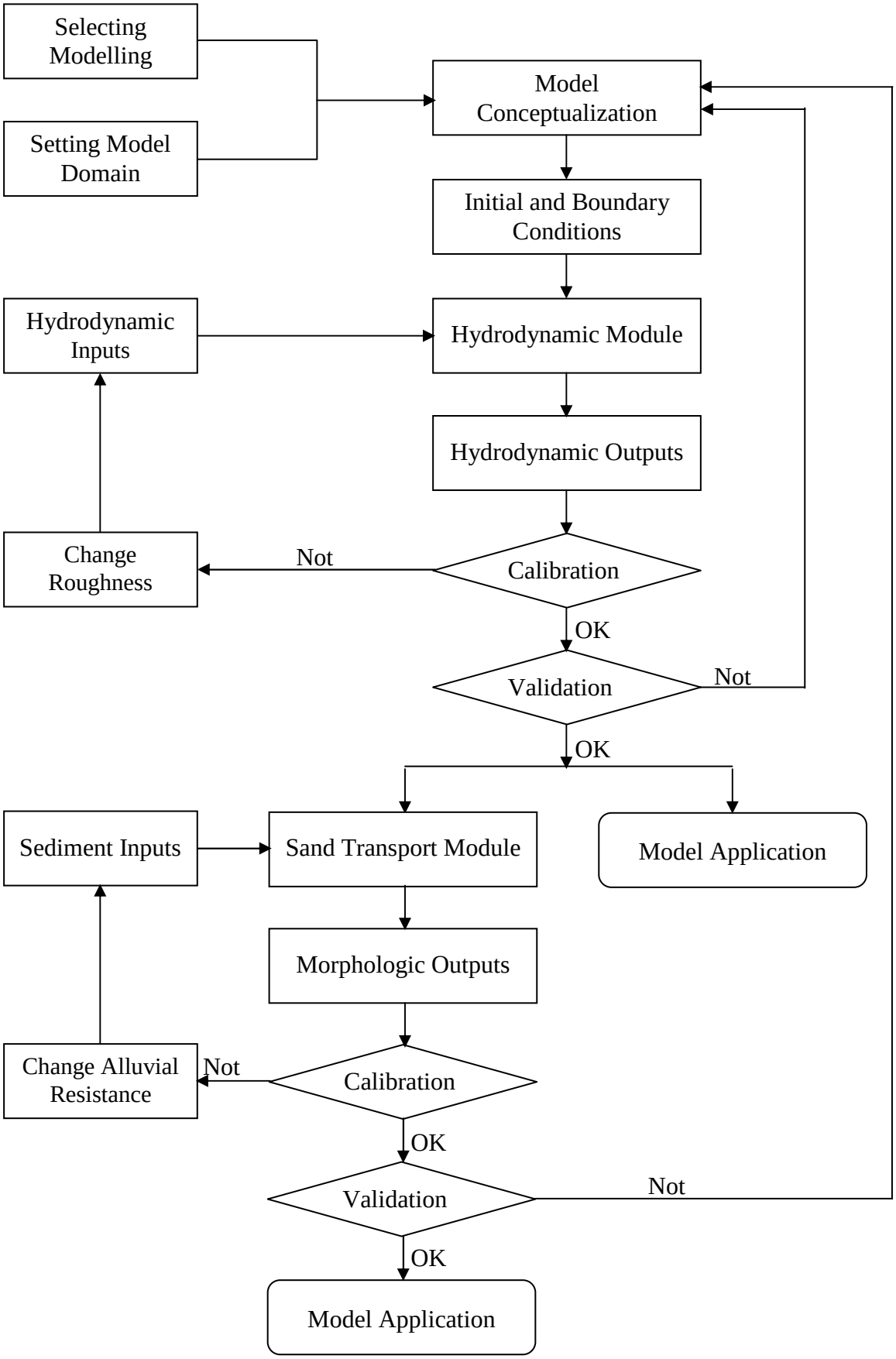

Figure 3.6: Flowchart of modelling process using MIKE 21 Flow Model FM

3.8 Method to Assess Delta Progradation using Numerical Model

The progradation of delta along the lower reach of Meghna had been assessed using the Numerical Model developed based on Parker and Muto's theory. This model had been applied to the longitudinal profile of the river to analyze the process of delta progradation due to sea level rise. The various steps involved during the computational procedure of the numerical model are described below –

- **Model Conceptualization:** The numerical model is based on one dimensional sediment continuity equation. Hence the reach was selected along the long profile of Lower Meghna River. Along with the sediment continuity equation, the numerical model was formulated by using the flow and sediment transport equations. Then the moving boundary conditions were added. The details of the numerical formulation have been described in chapter four.
- **Specifying Auxiliary Inputs:** After the numerical formulation and discretization of the model, various input auxiliary data for the formulated equation was specified for the Lower Meghna River. These data include intermittency factor, Chezy's roughness coefficient, grain size of sediments, bed slope etc. The geometric inputs involved in the computation were determined from the cross-sections collected from BWDB and BIWTA.
- **Introducing Primary Variables:** For the developed numerical model, three variables govern the process of delta progradation. These are discharge, sediment discharge and rising levels of sea. These variables are set and processed to apply in the numerical model for different conditions.
- **Model Adjustment:** The numerical model was developed and adjusted for the base condition. These adjustments are very difficult due to lack of data. However, effort was made to adjust and verify the model by considering the model results of MIKE 21 Flow Model FM. Usually the auxiliary parameters were changed and modified to adjust the numerical model.
- **Model Application to Incorporate Climate Change Scenarios:** The climate change and global warming is likely to affect the process of delta progradation by changing river flow, sediment transport and raising sea water level. The discharge data was taken from the results of neural network model and the sediment transport rates were considered from the simulations of MIKE 21 FM for various climate change scenarios. Sea level rise was incorporated according to the IPCC projections.

- **Developing Delta Progradation Profile:** The numerical model was used to determine changes of delta progradation process. The results were then incorporated in the long profile of the river to visualize the gradual progradation of delta in the Lower Meghna River. This process was repeated for various climate change scenarios for selected periods. Figure 3.7 shows the various steps to assess delta progradation using the numerical model.

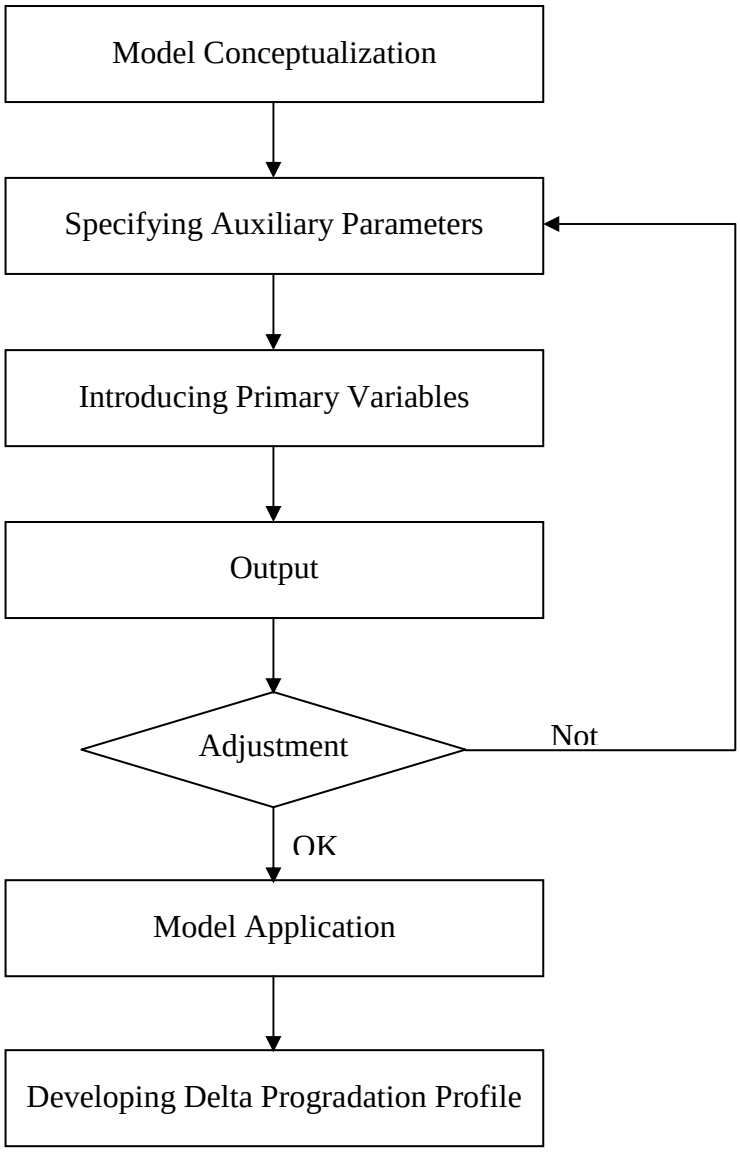

Figure 3.7: Flowchart to assess delta progradation using numerical model

CHAPTER 4
BACKGROUND OF THE MODELS

4.1 General

Modelling is the modern technique to determine both short-term and long-term river channel responses to any change in the environment. Physical experiments testing the effect on climate of (for example) changing amounts of greenhouse gas concentrations in the atmosphere would require observed multiple copies of earth with differing concentrations of greenhouse gases for many years, conditions that are obviously not attainable. This knowledge can be represented mathematically and thus approximated by computer code. When modeled on a computer, the experiment described above becomes feasible, as the conditions of the experiment can be met in computer based simulations of the earth. Hence, the process of impact modelling is becoming famous day by day.

4.2 Models used for the Study

For the present study, climate change impacts on the Lower Meghna River have been simulated with the combination of three models. They are –

- Artificial Neural Network (ANN) model, which can be considered as a hydrological model.
- MIKE 21 Flow Model, which consists of both hydrodynamic and morphologic module.
- Numerical Delta Progradation model, which is a one dimensional analytical morphologic model.

The description of the models along with their various mathematical aspects and modelling features are discussed in the following sections.

4.3 Artificial Neural Network

Artificial neural networks (ANN) are computing systems that relate an input to an output and are made of a number of simple but highly interconnected processing units. ANN has been developed as a generalization of mathematical model of human cognition or neural biology. Within the last decade, it has experienced a huge resurgence due to the development of more sophisticated algorithms and the emergence of powerful computation tools. Since the early nineties, ANN has been successfully used in

hydrology related areas such as rainfall-runoff modeling, stream flow forecasting, ground-water modeling, water quality, water management policy, precipitation forecasting, hydrologic time series, and reservoir operations (ASCE, 2000a, 2000b).

4.3.1 ANN for Stream Flow Prediction

Traditional physical based hydrologic models that are based on mathematical representation of watershed processes can be applied to stream flow predictions. These models typically require detailed watershed data such as landuse characteristics, elevation, soil characteristics and river morphology. This information for a huge basin (e.g. the GBM basin) is very difficult to gather (Islam et al., 2008). Additional efforts are needed for assessing model parameters and performing model calibration and verification. Models based on the principle of artificial neural networks (ANNs) can be considered an alternate to physically based models, due to its simplicity relative to minimizing the need for collecting detailed watershed data. This methodology offers a promising alternative to the use of hydrologic models that require modeling the internal processes of a watershed. ANN models are capable of learning and abstracting the essential characteristics from inputs that might contain irrelevant information. They are extremely useful for solving problems without existing algorithmic solutions or with algorithms that are too complex to implement. Current research on ANN hydrologic applications ranges from the predictions of peak discharge and time to peak from a single rainfall event, to the forecast of hourly or daily river stages or discharges (Dawson and Wilby, 2002; Jeong and Kim, 2005).

4.3.2 Architecture of ANN

Artificial Neural Networks (ANNs) consist of large number of processing elements with their interconnections. They can be characterized by three components:

- Nodes: Information processing occurs at many single elements called nodes, also referred to as units, cells, or neurons.
- Weights: Signals are passed between nodes through connection links and each connection link has an associated weight that represents its connection strength.
- Activation function: Each node typically applies a nonlinear transformation called an activation function to its net input to determine its output signal.

A neural network is characterized by its architecture that represents the pattern of connection between nodes, its method of determining the connection weights, and the activation function (ASCE, 2000a).

4.3.3 Feedforward Neural Networks

In a feedforward network, nodes are generally arranged in layers, starting from a first input layer and ending at the final output layer. There can be several hidden layers, with each layer having one or more nodes. Information passes from the input to the output side. The term "feedforward" means that nodes in one layer are connected to those in the next, but not to those in the same layer. Thus, the output of a node in a layer is only a dependent on the inputs it receives from previous layers and the corresponding weights. A typical three-layer feedforward ANN, consisting of a layer of input nodes, a single layer of hidden nodes and a layer of output nodes is shown in Figure 4.1.

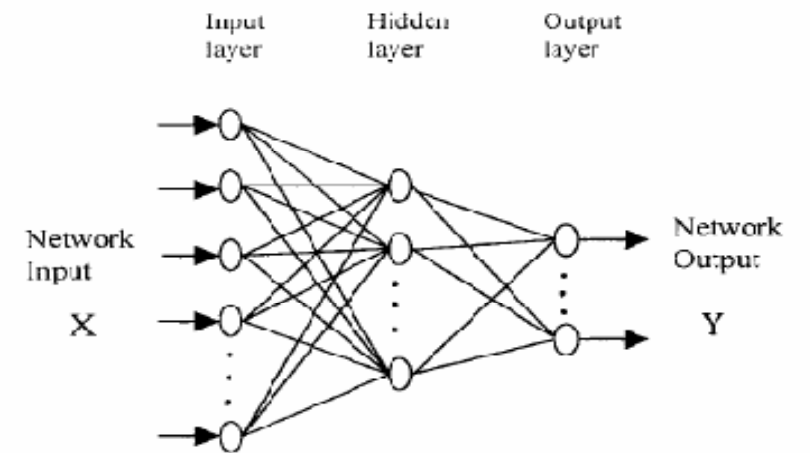

Figure 4.1: Configuration of a typical three layer feedforward artificial neural network

In most networks, each node in the input layer receives an input variable for the problem at hand and passes it to the nodes in the hidden layer. The last or output layer consists of values predicted by the network and thus represents model output. Number of hidden layers and number of nodes in each hidden layer are usually determined by a trial-and-error procedure. Nodes within neighboring layers of the network are fully connected by links. A synaptic weight is assigned to each link to represent the relative connection strength of two nodes at both ends in predicting the input-output relationship. In this figure, *X* is a system input composed of a number of causal variables that influence system behavior and *Y* is the system output composed of a number of resulting variables that represent the system behavior.

4.3.4 Backpropagation of Neural Networks

Backpropagation models, similar to feedforward architecture, contain three components. They are an input layer, an output layer and at least one hidden layer. All those layers are fully connected to each other as shown in Figure 4.2.

In backpropagation algorithm there are two main steps. The first step is a forward pass, which is also called as activation phase. In that step, inputs are processed to reach the output layer through the network. After the error is computed, a second step starts backward through the network, which is also called as error backpropagation. The errors at the output layer are propagated back toward the input layer with weights being modified.

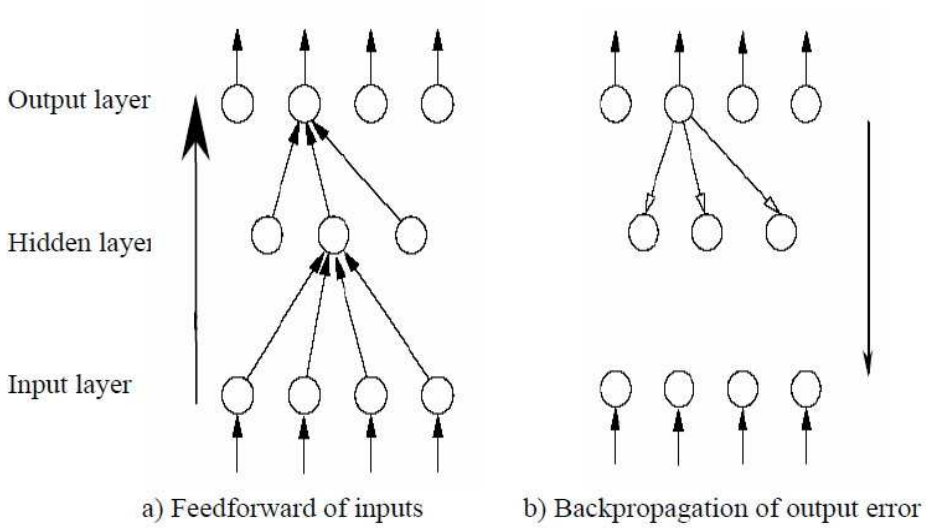

Figure 4.2: Backpropagation of neural networks

Most of the backpropagation models employ a delta learning rule, which requires the continual backpropagation of an error term from the output layer back to the input layer. The delta rule is one of the most commonly used learning rules. For a given input vector, the output vector is compared to the correct answer. Then, the weights are adjusted to reduce this difference. This procedure is applied until the difference between the actual and predicted outputs is less than preassigned value of maximum error.

4.3.5 Training and Testing of Neural Networks

Training and testing concept can be understood as calibration and validation process respectively. The purpose of training, also called learning, is to determine the set of connection weights that cause the ANN to estimate outputs within the given tolerance

limits to target values. The data should contain sufficient patterns so that the network can learn the underlying relationship between input and output variables adequately.

During the training phase, an error value, usually mean square error (MSE) is calculated between the desired output and the actual output. The MSE is then propagated backwards to the input layer and the connection weights between the layers are readjusted. This adjustment continues until a weight space is found, which results in the smallest overall prediction error. Then the network is considered learned enough and trained.

After training, the learning algorithm of the network is often deactivated and the weights are frozen. Then the test data is presented to the ANN, which it has never encountered before, enabling a validation of its performance. This is referred to as testing or validation of the ANN. Depending on the outcome, either the ANN has to relearn the examples with some examples or it can be implemented for its designated use.

During training and testing, errors for both data sets decrease initially. After an optimal amount of training has been achieved, the errors for the training set continue to decrease, but those associated with the test data set begin to rise as shown in Figure 4.3. This is an indication that further training will likely result in the network overfitting the training data. The process of training is stopped at this time, and the current set of weights is assumed to be the optimal values. The network is ready for use as a predictive tool.

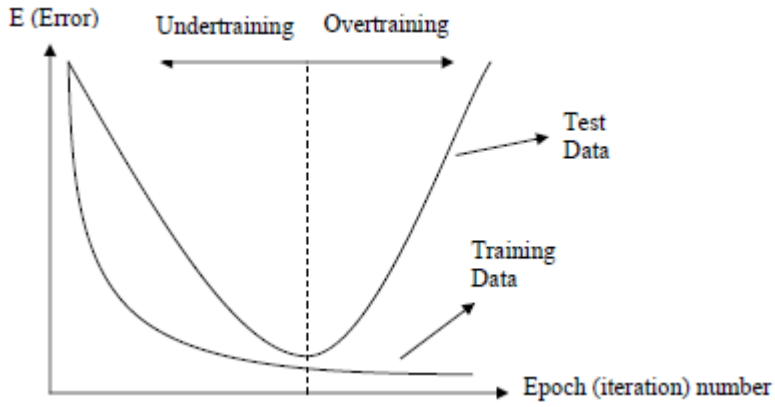

Figure 4.3: Error distributions during testing and training

If the available data set is too small for partitioning into training and testing data, the simplest way to prevent overtraining is to stop training when the mean squared error (MSE) stops to decrease significantly.

4.3.6 Mathematical Aspects of Feedforward Backpropagation Algorithm

A schematic diagram of a typical *j*-th node of the hidden layer or output layer is displayed in Figure 4.4. The inputs to such a node may come from system input variables or outputs of other nodes, depending on the layer that the node is located in. These inputs form an input vector $X = (x_1, \ldots, x_i, \ldots, x_n)$. The sequence of weights leading to the node form a weight vector $W_j = (w_{1j}, .., w_{ij}, .., w_{nj})$, where w_{ij} represents the connection weight of the *i*-th node from the preceding layer to this node.

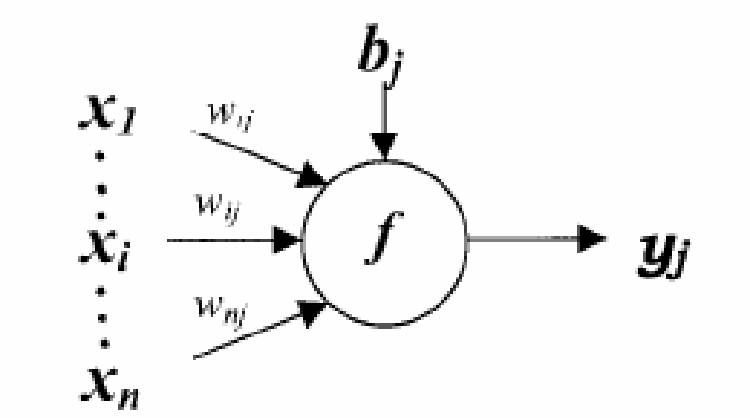

Figure 4.4: A typical node in the hidden layer or the output layer

The input to the node *j*, designated as S_j. S_j is the weighted sum of all the incoming inputs, which are the outputs from the nodes in the previous layer. It can be mathematically represented as –

$$S_j = \sum_{i=0}^{n}(x_i w_{ij} - b_j) \tag{4.1}$$

Here, b_j is the threshold value, also called the bias, associated with this node. The output of node *j*, y_j, is obtained by computing the activation function that determines the response of a node to the total input signal it receives. The most commonly used activation function is the sigmoid function (ASCE, 2000a), given as –

$$y_j = f(S_j) = \frac{1}{1+e^{(-sj)}} = logsig(S_j) \tag{4.2}$$

The sigmoid function is a bounded, monotonic, non-decreasing function that provides a graded, nonlinear response. This function enables a network to map any nonlinear process. The popularity of the sigmoid function is partially attributed to the simplicity of its derivative that will be used during the training process. A number of such nodes are

organized to form an artificial neural network. A logsig transfer function is given in Figure 4.5.

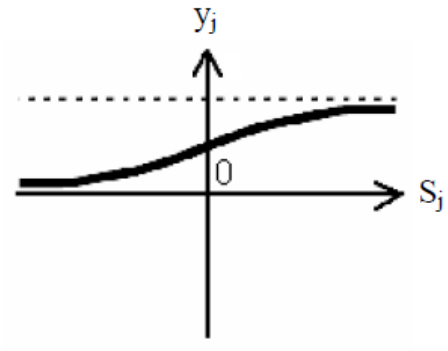

Figure 4.5: Logsig transfer function

In order for an ANN to generate an output vector $Y = (y_1, y_2, \ldots, y_p)$ that is as close as possible to the target vector $T = (t_1, t_2, \ldots, t_p)$, a training process is employed to find optimal results that minimize a predetermined error function that usually has the form –

$$E = \sum_P \sum_p (y_i - t_i)^2 \quad (4.3)$$

Here, p is the number of output nodes and P is the number of training patterns. This error is propagated backward through the network to each node, and correspondingly the connection weights are adjusted based on the equation 4.4.

$$\Delta w_{ij}(n) = -\varepsilon^* \frac{\partial E}{\partial w_{ij}} + \alpha^* \Delta w_{ij}(n-1) \quad (4.4)$$

Where, $\Delta w_{ij}(n)$ and $\Delta w_{ij}(n\text{-}1)$ are the weight increments between node i and j during the n-th and (n-1)-th pass, or epoch. A similar equation is written for correction of bias values. In equation 4.4, ε and α are called learning rate and momentum, respectively. The momentum factor can speed up training in very flat regions of the error surface and help prevent oscillations in the weights. A learning rate is used to increase the chance of avoiding the training process being trapped in a local minima instead of global minima.

4.3.7 Performance Indicators of ANN

In order to improve the efficiency and reliability, it is necessary to judge performance of neural network in both training and validation stages. Various statistical indicators are commonly used to determine performances of the neural network. In this study, five commonly used statistical indicators are used which are briefly described in Table 4.1.

Table 4.1: Statistical indicators of the performance of ANN

Name	Formula	Remarks
Coefficient of Determination	$r = \frac{\sum(x-\bar{x})(y-\bar{y})}{\sqrt{\sum(x-\bar{x})^2\sum(y-\bar{y})^2}}$	Here, x = observed value $\bar{x}$ = average of observed value y = model predicted value $\bar{y}$ = average of model predicted value n = number of observations
Mean Squared Error	$MSE = \sqrt{\frac{\sum(x-y)^2}{n}}$	
Normalized Mean Squared Error	$NMSE = \frac{MSE}{varience}$	
Mean Absolute Error	$MAE = \frac{\sum\lvert(x-y)\rvert}{n}$	
Mean Relative Error	$MRE = \frac{1}{n}\sum\left\lvert\frac{x-y}{x}\right\rvert$	

Higher value of r indicates that the model simulated data fits better with the observed data. Models with least MSE, NMSE, MAE and MRE can provide better estimation between observed and predicted values. The simulated values can also be plotted against observed data to validate the performance of the model.

4.3.8 ANN toolbox of MATLAB™

The Neural Network Toolbox™ of MATLAB is used to train feedforward neural networks to solve specific problems. Typically, neural networks are adjusted, or trained, so that a particular input leads to a specific target output as illustrated in Figure 4.6.

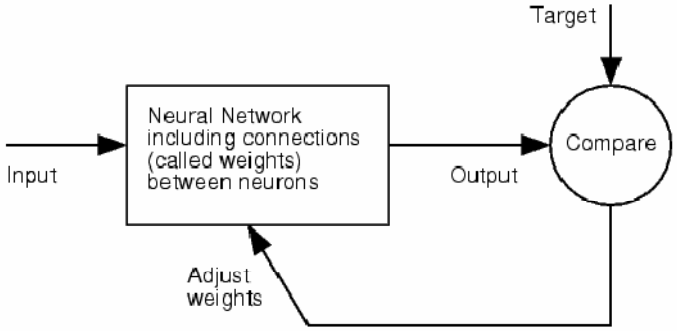

Figure 4.6: Overview of the functionality of neural network in MATLAB

The graphical user interface (GUI) is designed to be simple and user friendly (Figure 4.7). This window has its own work area, separate from the more familiar command-line workspace. Thus, when using the GUI, the GUI results to the (command-line) workspace might be exported. Similarly, it is also possible to import results from the workspace to the GUI.

There are generally four steps in training process of this tool: (a) Assemble the training data, (b) Create the network object, (c) Train the network and (d) Simulate the network response to new inputs. Once the Network/Data Manager window is up and running, network can be created, reviewed, trained, simulated, and exported the final results to the workspace. Similarly, it is possible to import data from the workspace for use in the GUI.

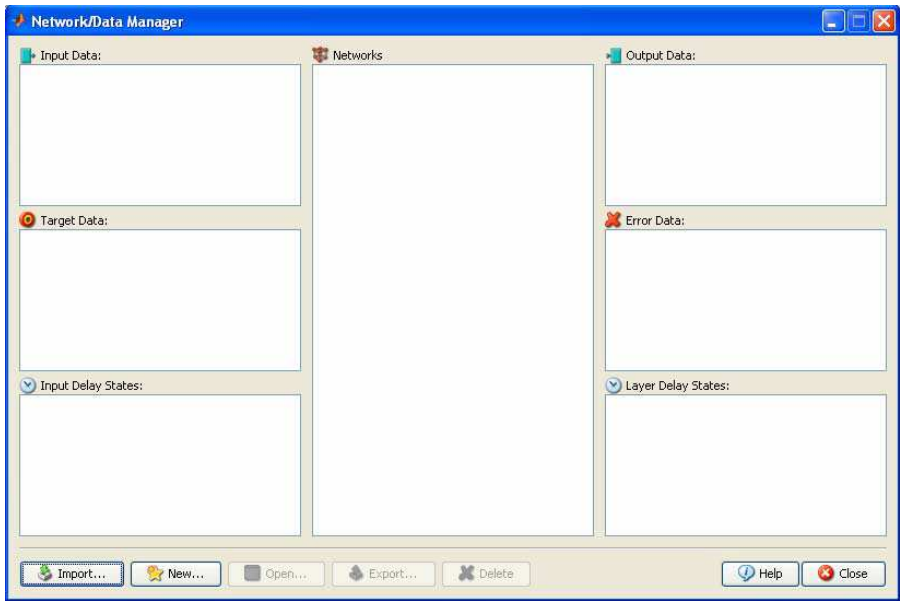

Figure 4.7: Graphical user interface of neural network tool of MATLAB

Feedforward neural networks can be used without needing any explicit mathematical equation relating inputs and outputs. This shows the computational superiority of ANNs. Also, feedforward network with a hidden layer or hidden layers without considering the number of sigmoidal hidden nodes can approximate any continuous function (ASCE, 2000a). This feature of ANNs points the high capacity in establishing relations between inputs and outputs.

4.4 MIKE 21 Flow Model FM

MIKE 21 Flow Model FM is a modelling system based on a flexible mesh approach. The modelling is composed of different modules such as Hydrodynamic Module, Transport Module, ECO Lab Module, Mud Transport Module, Sand Transport Module, Particle Tracking Module etc. The Hydrodynamic Module is the basic computational component of the entire modelling system providing the hydrodynamic basis for other modules.

4.4.1 Application of the Model

The MIKE 21 Flow Model FM modelling system has been developed for various applications of riverine and coastal problems within oceanographic and estuarine environments. The application areas are generally problems where flow and transport phenomena are important with emphasis on coastal and marine applications, where the flexibility inherited in the unstructured meshes can be utilized.

4.4.2 Hydrodynamic Module

The hydrodynamic module calculates the resulting flow and distributions of salt, temperature, subject to a variety of forcing and boundary conditions. Salt and temperature variations are considered as subordinated to the HD module.

4.4.2.1 Governing Equations

The modelling system is based on the numerical solution of the two-dimensional shallow water equations - the depth-integrated incompressible Reynolds averaged Navier-Stokes equations (DHI, 2007). Thus, the model consists of continuity, momentum, temperature, salinity and density equations. In the horizontal domain both Cartesian and spherical coordinates can be used. The local continuity equation is written as –

$$\frac{\partial u}{\partial x} + \frac{\partial v}{\partial y} = S \tag{4.5}$$

And the two horizontal momentum equations for the x- and y- component, respectively

$$\frac{\partial u}{\partial t} + \frac{\partial u^2}{\partial x} + \frac{\partial vu}{\partial y} = fv - g\frac{\partial \eta}{\partial x} - \frac{1}{\rho_0}\frac{\partial P_a}{\partial x} - \frac{g}{\rho_0}\int_z^n \frac{\partial \rho}{\partial x}dz - \frac{1}{\rho_0 h}\left(\frac{\partial s_{xx}}{\partial x} + \frac{\partial s_{xy}}{\partial y}\right) + F_w + u_s S \tag{4.6}$$

$$\frac{\partial v}{\partial t} + \frac{\partial v^2}{\partial y} + \frac{\partial uv}{\partial x} = -fu - g\frac{\partial \eta}{\partial y} - \frac{1}{\rho_0}\frac{\partial P_a}{\partial y} - \frac{g}{\rho_0}\int_z^n \frac{\partial \rho}{\partial y} dz - \frac{1}{\rho_0 h}\left(\frac{\partial s_{yx}}{\partial x} + \frac{\partial s_{yy}}{\partial y}\right) + F_v + v_s S \quad (4.7)$$

Where t is the time; x,y and z are the Cartesian co-ordinates; η is the surface elevation; d is the still water depth; $h = \eta + d$ is the total water depth; u and v are the velocity components in the x and y dirtection; f is the Coriolis parameter; g is the gravitational acceleration; ρ is the density of water; s_{xx} ,s_{xy} , s_{yx} and s_{yy} are components of the radiation stress tensor; v_t is the vertical turbulent (or eddy) viscosity; P_a is the atmospheric pressure; ρ_0 is the reference density of water. S is the magnitude of the discharge due to point sources and u_s , v_s is the velocity by which the water is discharged into the ambient water.

4.4.2.2 Numerical Scheme of the Model

The spatial discretization of the primitive equations is performed using a cell-centered finite volume method. The spatial domain is discretized by subdivision of the continuum into non-overlapping element/cells. In the horizontal plane an unstructured grid is used comprising of triangles or quadrilateral element. An approximate Riemann solver is used for computation of the convective fluxes, which makes it possible to handle discontinous solutions. For the time integration an explicit scheme is used (DHI, 2007).

Spatial Discretization

The discretization in solution domain is preformed using a finite volume method. The spatial domain is discretized by subdivision of the continuum into non-overlapping cells/elements. In the two-dimensional case the elements can be arbitrarily shaped polygons. However, here only triangles and quadrilateral elements are considered. The discretization is illustrated in Figure 4.8.

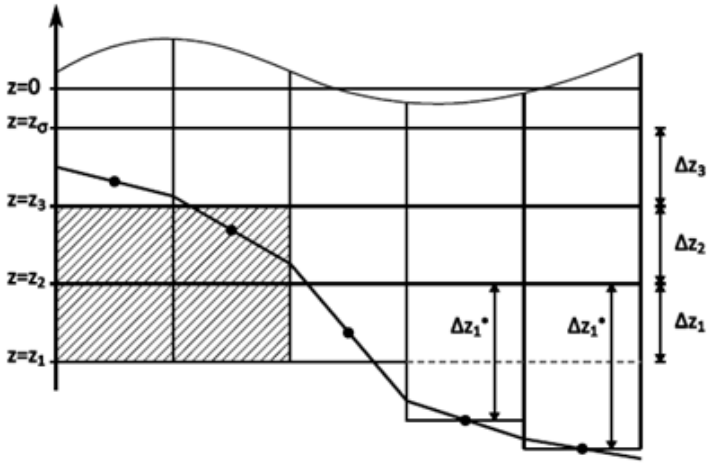

Figure 4.8: Simple bathymetry adjustment approach

In the z-level domain the discretization is given by a number of discrete z-levels $\{z_i , i = 1, (N_z+1)\}$, where N_z is the number of layers in the z-level domain. z_1 is the minimum z-level and z_{N_z+1} is the maximum z-level, which is equal to the sigma depth, z_σ. The corresponding layer thickness is given by

$$\Delta z_i = z_{i+1} - z_i \qquad i = 1, N_z \tag{4.8}$$

Discretization of Governing Equations

The integral form of the system of shallow water equations can be written as

$$\frac{\partial U}{\partial t} + \nabla . F(U) = S(U) \tag{4.9}$$

Where U is the vector of conserved variables, F is the flux vector function and S is the vector of source terms.

In Cartesian co-ordinates the system of 2D shallow water equations can be written as

$$\frac{\partial U}{\partial t} + \frac{\partial (F_x^I - F_x^V)}{\partial x} + \frac{\partial (F_y^I - F_y^V)}{\partial y} = S \tag{4.10}$$

Where the superscripts I and V denote the inviscid (convective) and viscous fluxes respectively.

Integrating Eq. (4.9) over the i-th cell and using Gauss's theorem to rewrite the flux integral gives

$$\int_{A_i} \frac{\partial U}{\partial t} d\Omega + \int_{\Gamma_i} (F.n)\, ds = \int_{A_i} S(U)\, d\Omega \tag{4.11}$$

Where A_i is the area/volume of the cell Ω is the integration variable defined on A_i , Γ_i is the boundary of the i-th cell and *ds* is the integration variable along the boundary. *N* is the unit outward normal vector along the boundary. Equation (4.11) can be written

$$\frac{\partial U_i}{\partial t} + \frac{1}{A_i}\sum_j^{NS} F.n\Delta\Gamma_j = S_i \tag{4.12}$$

Here U_i and S_i , respectively, are average values of *U* and *S* over the i-th cell and stored at the cell center, *NS* is the number of sides of the cell, n_j is the unit outward normal vector at the j-th side and $\Delta\Gamma_j$ is the large area of the j-th interface.

Both a first order and a second order scheme can be applied for the spatial discretization. For the 2D case an approximate Riemann solver is used to calculate the convective fluxes at the interface of the cells.

Time Integration

Consider the general form of equations

$$\frac{\partial U}{\partial t} = G(U) \tag{4.13}$$

For 2D simulations, there are two methods of time integration for both the shallow water equations and the transport equations: A low order method and a higher order method. The low order method is a first order explicit Euler method.

$$U_{n+1} = U_n + \Delta t G(U_n) \tag{4.14}$$

where Δt is the time step interval. The higher order method uses a second order Runge Kutta method on the form:

$$U_{n+\frac{1}{2}} = U_n + \frac{1}{2}\Delta t G(U_n)$$

$$U_{n+1} = U_n + \Delta t G\left(U_{n+\frac{1}{2}}\right) \tag{4.15}$$

4.4.3 Sand Transport Module

The Sand Transport Module calculates the resulting transport of non-cohesive materials based on the flow conditions found in the hydrodynamic calculations and, if included, wave conditions from wave calculations. The sand Transport calculations are carried out using a mean horizontal velocity component. The sediment transport rates are calculated for sand fractions without taking inertia effects into account.

4.4.3.1 Sediment Transport

For morphological development of alluvial rivers with interaction between bed bathymetry and hydrodynamics, only bed material transport is of interest. Thus, only bed load and the part of the suspended load originating from the bed material is considered.

Bed load transport

The interaction between the bed load and the alluvial bed is one of the most fundamental aspects of the morphological behaivour of a river. When discussing the local bed load sediment transport capacity of a flow, it is convenient only to consider sediment transport in uniform shear flow. In principle, two approaches have been adopted. The first modifies the critical stress for initiation of motion:

$$\theta_c = \theta_{c0}\left(1 + \frac{\partial z_b}{\partial s}\right) \tag{4.16}$$

Where, θ_c is the modified critical Shield's parameter, θ_{c0} is the critical Shield's parameter in uniform flow, z_b is the bed level and s is the sream wise coordinate. For this kind of formula, the following correction can be applied:

$$S_s = \left(1 - \alpha.\frac{\partial z_b}{\partial s}\right) S_{bl} \tag{4.17}$$

Where α is model calibration parameter, S_{bl} is bed load as calculated from sediment transport formula and S_s is bed load along streamlines. This equation is implemented in the present modeling system.

Suspended load transport

Modelling of non-cohesive suspended sediment in a fluid can be described by a transport equation for the volumetric sediment concentration. In the general case the sediment balance contains contributions from the three transport mechanisms: advection, settling and diffusion. This can be expressed:

$$\frac{\partial c}{\partial t} + \frac{\partial (uc)}{\partial x} + \frac{\partial (vc)}{\partial y} + \frac{\partial (wc)}{\partial z} = \frac{\partial}{\partial x}\left(\varepsilon \frac{\partial c}{\partial x}\right) + \frac{\partial}{\partial y}\left(\varepsilon \frac{\partial c}{\partial y}\right) + \frac{\partial}{\partial z}\left(\varepsilon \frac{\partial c}{\partial z}\right) + w_s \frac{\partial c}{\partial z} \tag{4.18}$$

where c is the volumetric concentration, t is time, x and y are spatial horizontally coordinates, z is a vertical coordinate, u,v and w are flow velocities in the x, y and z direction, respectively. ε_x, ε_y and ε_z are turbulent diffusion coefficients and w_s is the settling velocity of the suspended sediment.

4.4.3.2 Sediment Transport Formula

The model by Engelund and Hansen is a total load model that needs user-specified information in order to divide the sediment transport into bed load and suspended load. The bed load (S_{bl}) and suspended load (S_{sl}) transport rate are obtained from the relations:

$S_{bl} = k_b.S_{tl}$ and $S_{sl} = k_s.S_{tl}$

where k_b and k_s are bed load and suspended load calibration factor. The total sediment transport (S_{tl}) is obtained by:

$$S_{tl} = 0.05\frac{C^2}{g}\theta^{\frac{5}{2}}\sqrt{(s-1)gd_{50}^3} \quad (4.19)$$

where C is the Chezy number. The equilibrium concentration is simply specified as the suspended load divided by the water flux and converted from volumetric concentration to mass concentration.

4.4.4 Morphology

A morphological model is a combined hydrodynamic/sediment transport model. The hydrodynamic flow field is updated continuously according to the changes in bed bathymetry. Morphological models are traditionally divided into coupled and uncoupled models. In coupled models, the governing equations for flow and sediment transport are merged into a set of equations, which are solved simultaneously. In uncoupled models, the solution of the hydrodynamics is solved at a certain time step prior to the sediment transport equations. Subsequently a new bed level is computed and a hydrodynamic model proceeds with the next time step. The latter approach is applied in the present modelling system.

4.4.4.1 Sediment Continuity Equation

The key parameter for determination of the bed level changes is the rate of bed level change $\partial z/\partial t$ at the element cell centers. This parameter can be obtained in a number of ways, but in general all methods are based on the Exner equation (sediment continuity equation), which can be written:

$$-(1-n)\frac{\partial z}{\partial t} = \frac{\partial S_x}{\partial x} + \frac{\partial S_y}{\partial y} - \Delta S \quad (4.20)$$

Where, n is bed porosity, z is bed level, t is time, S_x is bed load or total load transport in the x direction, S_y is bed load or total load transport in the y direction, x, y are horizontal Cartesian coordinate and ΔS is sediment sink or source rate.

4.4.4.2 Alluvial bed resistance

In MIKE environment, the morphology module includes an alluvial bed resistance term which is the Chezy's number (C) and can be defined as follows –

$$C = aH^b \tag{4.21}$$

where, H is local water depth, a is the resistance coefficient and b is the resistance power. Inclusion of the resistance affects simulated scour and deposition patterns. Flow is deflected more over shallow parts, and sediment transport increases due to increased bed shear stresses. If hydrodynamic calibration of the bed resistance shows a certain relationship between local depth and Chezy number, when running the morphological model an alluvial roughness coefficient should be specified using the same parameters.

4.4.4.3 Morphological Bed Update

The bed is updated continuously through a morphological simulation (at every HD-time step) based on the estimated bed level change rates. New values for the bed level change rates are estimated at every N-th HD-time step, where n is a user defined time step factor. The new bed levels are obtained with a forward in time difference scheme stating:

$$z_{new} = z_{old} + \frac{1}{1-n}\frac{\partial z}{\partial t}\Delta t_{HD} \tag{4.22}$$

For this reason, it is only necessary to calculate the bed load transport at the same time step as $\partial z/\partial t$, while the advection-dispersion equation for the concentration of the suspended needs to calculated at every time step. The morphological update also offers to speed-up the morphological evolution in the following way.

$$z_{new} = z_{old} + \frac{1}{1-n}\frac{\partial z}{\partial t}\Delta t_{HD}.Speed - up \tag{4.23}$$

In which *Speed-up* is a dimension less factor which updates the bed level at this rate.

4.4.5 Numerical Stability of the Model

The time integration of the shallow water equations and transport equations is performed using explicit scheme. Due to the stability restriction using an explicit scheme the time step interval must be selected so that the Courant criterion is fulfilled. In Cartesian coordinates, the Courant-Freidrich-Levy (CFL) number is defined as

$$CFL_{HD} = \left(\sqrt{gh} + |u|\right)\frac{\Delta t}{\Delta x} + \left(\sqrt{gh} + |v|\right)\frac{\Delta t}{\Delta y}) \quad (4.24)$$

where h is the total water depth, u and v are the velocity components in x and y direction, g is the gravitational acceleration, Δx and Δy are characteristic lengths for an element and Δt is the time step interval.

For transport equations in Cartesian coordinates, the CFL number is defined as

$$CFL = |u|\frac{\Delta t}{\Delta x} + |v|\frac{\Delta t}{\Delta y} \quad (4.25)$$

The stability of the numerical scheme should be secure if the CFL number is less than 1. However, the calculation based on this value can create stability problems. Therefore the value of CFL is usually set to the range between 0 and 0.8. During model set-up, the time step interval should be selected in such a way that the CFL number falls within this range. The criteria can also be met by adjusting the characteristic length of the elements.

4.5 Numerical Delta Progradation Model

The progradation of delta and consequent movement of delta front can be considered as a one dimensional problem due to simplicity. However, such processes are very difficult to incorporate in a multi-dimensional modelling system. Hence, in the present study a one dimensional numerical morphological model was developed and applied to assess the delta progradation of Lower Meghna River due to climate change. The model formulated here is based on the approach established by Parker and Muto (2003).

4.5.1 Application of the Model to Study Delta Progradation

The numerical model discussed here is based on the Exner's sediment continuity equation which incorporates a separate sediment transport module. Under conditions of rising sea level, this model can be applied from deltaic zone to further upstream of the river for alluvial conditions and thus can be applicable for a wide range of rivers.

4.5.2 Outline of the Numerical Model

The present analysis allows for three moving boundaries; the topset-foreset break (shoreline), the foreset- bottomset break (foreset-basement break in the present case) and the bedrock-alluvial transition point shown in Figure 4.9.

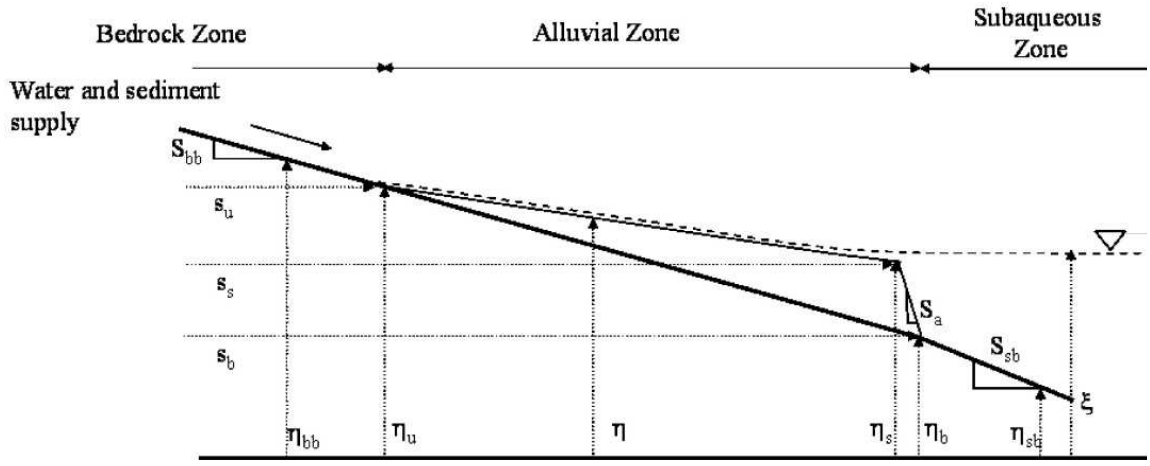

Figure 4.9: Definition sketch for the numerical formulation

The key parameters of the analysis are defined as follows: η = alluvial bed elevation; η_{bb} = bedrock bed elevation; η_{sb} = subaqueous bed elevation; x = streamwise distance; t = time; S_{bb} = constant slope of the basement on which the sediment deposits; S_a = constant slope of avalanche onto the foreset; S_{sb} = subaqueous bed slope; s_u = streamwise position of the bedrock-alluvial break; s_s = streamwise position of the topset-foreset break (shoreline); s_b = streamwise position of the foreset-bottomset break; η_u =elevation of the bedrock-alluvial break; η_s = elevation of the topset-foreset break; η_b = elevation of the foreset-bottomset break; and ξ = sea level elevation.

4.5.3 Governing Equation of the Model

Rivers are morphologically active during floods. To capture this in a simple way, the river is assumed to be at bankfull flow for fraction of time I_f , when it is morphologically active; otherwise the river is assumed to be morphologically inactive. As the channel aggrades in response to sea level rise the deposit is spread across the floodplain through migration and avulsion and progradation of delta occurs based on various conditions. Such scenario can be explained by Exner's equation of sediment continuity –

$$(1-n)\frac{\partial \eta}{\partial t} = -\Omega \frac{I_f(1+\Lambda)}{B_f}\frac{\partial Q_{tbf}}{\partial x} \tag{4.26}$$

where, Q_{tbf} is the total volume bed material load at bankfull flow; B_f is floodplain width; n is porosity of bed deposit; Ω is channel sinuosity and Λ is the fraction of wash load deposited per unit bed material load in the channel-floodplain complex.

4.5.4 Solving Various Equations

For the application of any morphological model of river, seven equations are needed to be solved. These are boundary condition equations, water and sediment continuity equation, equation for channel slope, Manning or Chezy's equation, roughness predictor, sediment transport predictor etc.

Computation of Flow

Channel hydraulics at bankfull flow is described in terms of a quasi-steady backwater formulation. The full form of the backwater equation can be written as –

$$U\frac{dU}{dx} = -g\frac{dH}{dx} + gS - C_f\frac{U^2}{H} \tag{4.27}$$

where U is the flow velocity, H is flow depth, S is bed slope and C_f is a dimensionless bed friction coefficient described in terms of a constant value. The boundary condition on (4.27) is one of specified elevation of standing water $\xi(t)$. Thus if $x = s_s(t)$ is the position of the topset-foreset break (shoreline):

$$(\eta + H)_{x=s_S} = \xi(t) \tag{4.28}$$

The case of interest here is that of constant rate of base level rise $\dot{\xi}$ (e.g. 10 mm/year).

Computation of Sediment Transport

In the case of a sand-bed river sediment mobility is governed by the Shields number τ^*_{bf} of the bankfull flow, which is defined as –

$$\tau^*_{bf} = \frac{C_f U^2}{RgD} \tag{4.29}$$

where R denotes the submerged specific gravity of the sediment and D denotes the characteristic size of the sand in the river bed. Considering the bankfull width as B, sand transport is described in terms of the total bed material relation of Engelund and Hansen which can be written as follows –

$$Q_{tbf} = B\sqrt{Rg}D^{3/2}\frac{0.05}{C_f}(\tau^*_{bf})^{5/2} \tag{4.30}$$

Downstream Varying Bankfull Channel Geometry

A simple way to describe the bankfull characteristics of a channel is in terms of a specified bankfull Shields number τ^*_{bf}. Parker et al. have found that the following approximate closure is appropriate for sand bed streams:

$$\tau^*_{bf} = 1.86 \tag{4.31}$$

The following relation is found for U by transforming (4.29):

$$\frac{U}{\sqrt{RgD}} = \left(\frac{\tau^*_{bf}}{C_f}\right)^{1/2} \tag{4.32}$$

Thus for constant values of τ^*_{bf}, C_f, grain size D and sediment submerged specific gravity R, (4.32) specifies a bankfull flow velocity that remains constant in the downstream direction. Substituting (4.32) into (4.27) and reducing:

$$\frac{dH}{dx} = S - S_{fric} \quad , \; S = -\frac{\partial \eta}{\partial x} \quad , \; S_{fric} = R\tau^*_{bf}\frac{D}{H} \tag{4.33}$$

For a river profile $\eta\ (x,\ t)$ at any time t, (4.33) can be solved subject to (4.28) to determine the streamwise variation in depth H. It is here assumed that the river has no tributaries over the reach of interest, so that bankfull water discharge Q_{bf} is constant in the streamwise direction. Water continuity requires that:

$$Q_{bf} = BUH \tag{4.34}$$

in which case the streamwise varying bankfull width is given from (4.32) and (4.34) as:

$$B = \left(\frac{C_f}{\tau^*_{bf}}\right)^{1/2}\frac{Q_W}{\sqrt{RgD}H} \tag{4.35}$$

Once the streamwise variation of H and B at bankfull flow are computed for a given bed profile, the streamwise variation in total bed material load Q_{tbf} at bankfull flow is computed from (4.30).

Computation of Bed Variation

Considering the channel sinuosity and the fraction of wash load deposited per unit bed material load as unity, the Exner equation of sediment continuity takes the form –

$$(1-n)\frac{\partial \eta}{\partial t} = -I_f\frac{\partial q_t}{\partial x} \tag{4.36}$$

where now q_t refers specifically to the sediment transport rate during flood discharge Q_{bf}.

4.5.5 Continuity and Shock Conditions

Two continuity conditions must hold: at x = s_u (t) the bedrock elevation must match the alluvial bed elevation, and at x =s_b (t) the foreset elevation must match the subaqueous basement elevation. In addition, a shock condition for the foreset is obtained by integrating (4.36) over the foreset. The results are as follows:

$$\dot{s}_u = -\frac{1}{(S_{bb} - S_u)} \frac{\partial \eta}{\partial t}\Big|_{x=s_u} \quad S_u = -\frac{\partial \eta}{\partial x}\Big|_{x=S_u} \quad S_{bb} = -\frac{\partial \eta_{bb}}{\partial x} \tag{4.37}$$

$$\dot{s}_b = -\frac{S_a - S_s}{S_a - S_{sb}} \dot{s}_s + \frac{1}{S_a - S_{sb}} \frac{\partial \eta}{\partial t}\Big|_{x=s_s} \quad , \; S_s = -\frac{\partial \eta}{\partial x}\Big|_{x=S_s} \tag{4.38}$$

$$(1 - n)(s_b - s_s)\left[(S_a - S_S)\dot{s}_S + \frac{\partial \eta}{\partial t}\Big|_{x=S_s}\right] = I_f q_t|_{x=S_s} \tag{4.39}$$

The above three relations specify the migration speeds $\dot{s_u}$, $\dot{s_b}$ and $\dot{s_s}$ of the three transition points.

4.5.6 Transformation to Moving Boundary Coordinates

In order to include the dynamics of the moving boundaries, the following transformations are introduced:

$$\bar{X} = \frac{X - S_u}{S_S - S_u} \quad , \; \bar{t} = t \tag{4.40}$$

The Exner equation thus transforms to

$$(1 - n)\left\{\frac{\partial \eta}{\partial \bar{t}} - \left[\frac{\bar{X}\dot{S}_S + (1 - \bar{X})\dot{S}_u}{S_S - S_u}\right]\frac{\partial \eta}{\partial \bar{X}}\right\} = -\frac{I_f}{(S_S - \dot{S_S})} \frac{\partial q_t}{\partial \bar{X}} \tag{4.41}$$

Equations (4.37) – (4.39) are similarly transformed to moving coordinates and reduced with (4.40) before solving Equation (4.41). Using the above numerical formulation progradation of delta along the river profile can be assessed.

CHAPTER 5
MODEL SETUP AND ANALYSIS

5.1 General

The complex changes in the hydraulic and morphologic behavior of the Lower Meghna River can be assessed by linking different types of models. To simulate these linkages, three types of models have been developed to investigate such responses. The hydrological model, developed by Artificial Neural Network (ANN) method, was employed to simulate the changes precipitation (as projected in GCM models) in the GBM Basin to obtain the changes in the discharge of the Lower Meghna River. This discharge and the rising sea level data are the boundary conditions of MIKE 21 hydro-morphological model, which was used to simulate the water level variations, sedimentation and bed level changes of the river. The sediment transport rate along with the discharge and rising sea water level have been incorporated in the numerical model to evaluate delta progradation.

5.2 Modelling Approach

As stated earlier, three different types of model have been used for the present study. In every step of these model developments, various climate change impacts, projections and scenarios was used. At first, the Artificial Neural Network (ANN) was developed to investigate the impacts of precipitation changes due to climate change on the river discharge. The resulting discharge affects the river hydraulics and morphology along with sea level rise. These were the boundary conditions of the MIKE 21 FM hydrodynamic and morphologic model, which was used to simulate various responses of a river such as higher water level due to backwater effect, siltation and bed level changes etc. The sediment transport rate, obtained from the MIKE 21 FM simulations, along with the discharge and rising sea water level was incorporated in the numerical morphological model to evaluate delta progradation.

All the models were developed by considering a baseline condition. Once the models are developed, calibrated and validated adequately, it would be ready to simulate future climate change scenarios using envisaged boundary condition of some conceivable hydrologic years. For the present study, the projections were carried out for the periods of 2020s, 2050s and 2080s under scenario A1FI, A1B and B1.

5.3 Estimation of River Flow using ANN Model

In this study, a rainfall-runoff (precipitation-discharge) ANN model over the GBM basin has been developed by using the precipitation data of GBM basin and discharge data of Lower Meghna River. Time series data of precipitation and discharge were imposed on the GBM basin grids using neural network method. The developed model was then calibrated and verified to obtain the desired discharge of Lower Meghna River from the precipitation inputs for different observed and projected scenarios of climate change.

5.3.1 Setting of GBM Basin Grids

Since the model area covers the whole GBM basin along with a major portion of Bangladesh, the concerned area was divided into total of 32 grids. The resolution of each grid is $3.75^0 \times 2.5^0$ (latitude by longitude) and the representation produces a surface spatial resolution of about 417 km x 278 km area. This was done to maintain consistency among the grids and the resolution of precipitation inputs. Figure 5.1 shows the selected grids over GBM basin and Bangladesh.

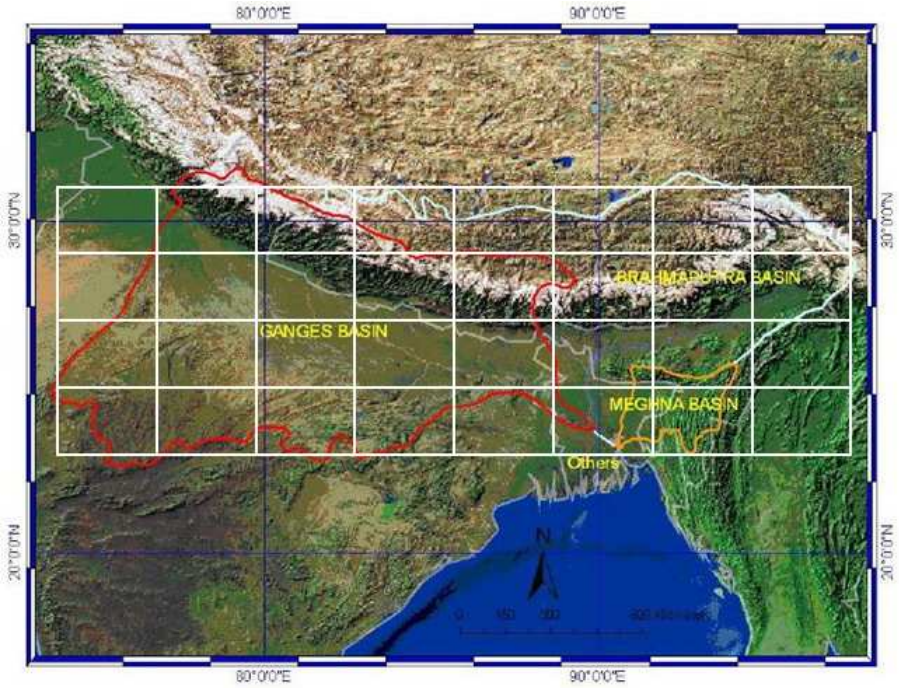

Figure 5.1: Selected grids over GBM basin and Bangladesh

United States Geological Survey (USGS) produced GBM basin grids of 0.5 degrees resolution along with major river networks and drainage direction of the region. Later these were modified and updated several times by comparing known catchment areas, drainage directions etc. Figure 5.2 shows both the flow network and grids of GBM basin

with the polygon of Bangladesh. Flow network was constructed such a way that it carries water (runoff) from one cell to the next discharging cell based on the drainage directions.

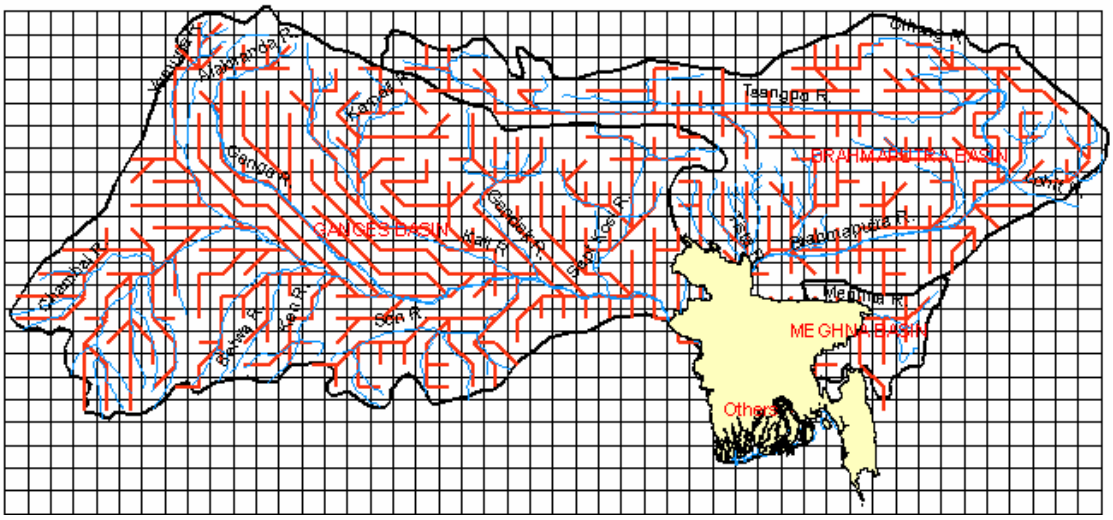

Figure 5.2: Grid superimposed on the flow network of GBM basins

These grids with superimposed flow network have been modified and simplified for the present study. The grids of fine 0.5×0.5 degree resolution was converted into 3.5 × 2.75 degree resolution in order to match with the precipitation inputs over GBM basin. The corresponding flow network was also simplified (Figure 5.3) in order to indicate the drainage direction of water from one cell to next discharging cell.

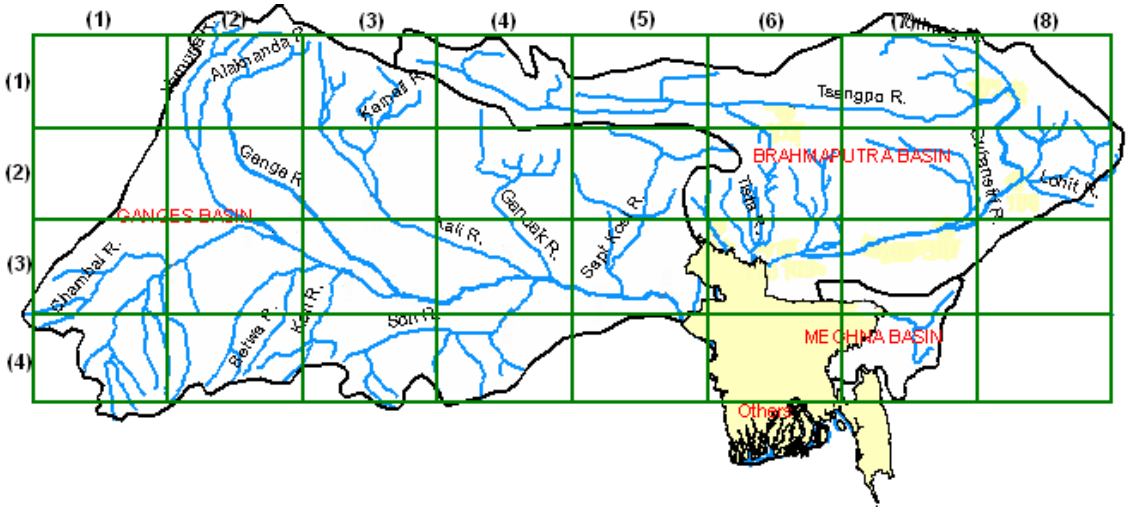

Figure 5.3: Simplified GBM grids and flow network

5.3.2 Processing of Input Data

In order to use ANN structures effectively, input variables in the phenomenon must be selected with great care. This highly depends on the better understanding of the problem.

In a firm ANN architecture, key variables must be introduced and unnecessary variables must be avoided in order to prevent confusion in calibration and validation process.

The input node for the present study is the precipitation over GBM basin. Based on the flow direction on the grids shown in Figure 5.3, a total of 26 out of 32 grids were selected as input nodes. These input nodes were selected such a way that water carries from every cell of the GBM grid and travel towards the outlet. As seen from the figure, 6 grids (grid number 11, 12, 54, 64, 83 and 84) do not contribute to the flow and hence they were excluded from the analysis. Figure 5.4 shows the location of the precipitation input nodes.

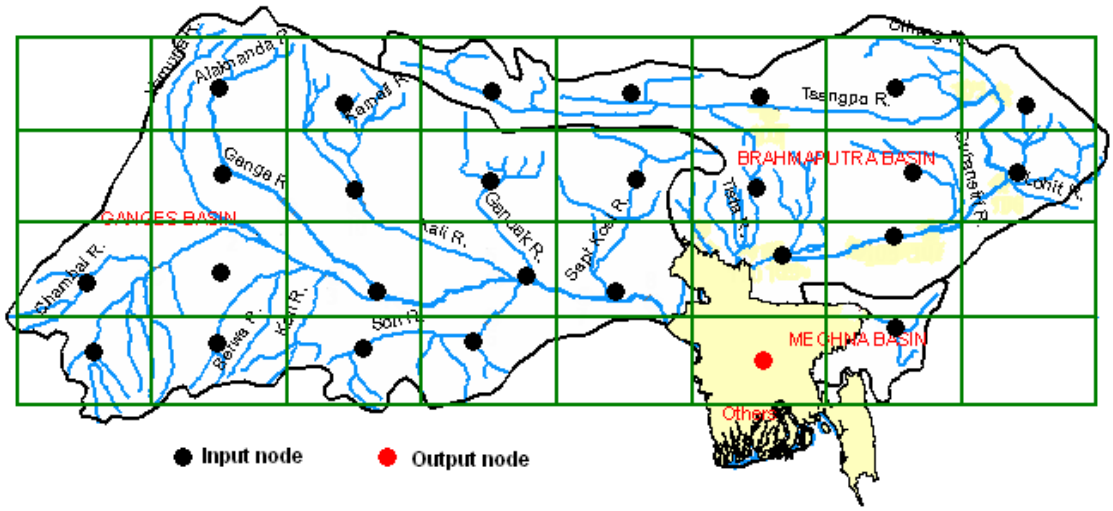

Figure 5.4: Input and output nodes of the neural network model

Assuming all the precipitation over GBM contributes to the basin runoff and the resultant combined flow drains out through the Ganges, Brahmaputra and Meghna River system, the Lower Meghna River can be considered as the outlet of the basin. Therefore the discharge of Lower Meghna River at Chandpur was taken as the output node of the neural network model (Figure 5.4). Both the input and output nodes, i.e. precipitation and discharge, were the input variables of the model.

The neural network model was calibrated and validated using the monthly precipitation and discharge data for the period of 1975 to 1994. The monthly accumulated precipitation over GBM basin (sum of precipitation of all the grids) and the discharge of Lower Meghna River are shown in Figure 5.5.

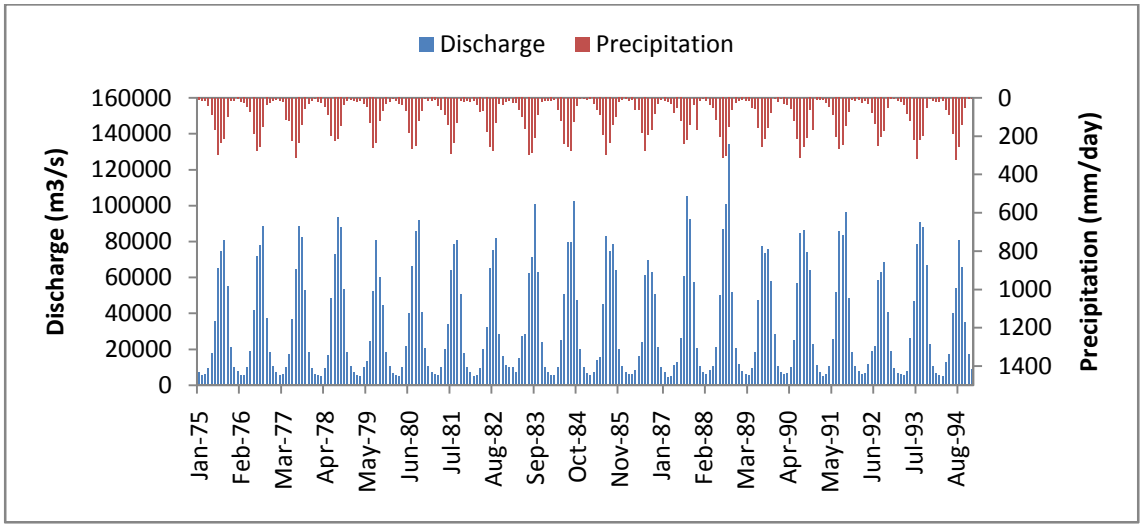

Figure 5.5: Monthly precipitation and discharge data for neural network model

5.3.3 Development of Neural Network Model

The determination of the ANN architecture and selection of a training algorithm is an important step for the development of neural network model. An optimal architecture may be considered the one giving the best performance in terms of minimum error, while retaining a simple and compact structure. There is no specific information for determination of such an optimal ANN architecture. Often, more than one ANN can generate similar results. The numbers of input and output nodes are problem dependent. The flexibility lies in selecting the number of hidden layers and in assigning the number of nodes to each of these layers as well as in the number of iteration. A trial-and-error procedure is generally applied to decide on the optimal architecture.

In this study, Feedforward neural network model has been developed for the GBM basin. Among various neural network techniques, this technique is closely related to statistical models that are a data-driven approach and more suited for forecasting applications. Therefore, Feedforward neural network was used to predict discharge of Lower Meghna River. The feedforward network was trained using the backpropagation algorithm which is known as an optimization technique for Feedforward.

A total of 26 nodes representing precipitation and a single node representing discharge were used in the input and output layer of the model respectively. The number of hidden layers and their nodes depend on the performance of the model and is determined by trial and error basis. For this study, six trials have been performed to obtain the best network that predicts discharge from precipitation inputs. For each trial, different networks were

used by changing number of hidden layers, number of processing elements or nodes in each hidden layer, number of runs for each trial, number of iterations or epochs during each run etc. Additionally, sigmoid function was assigned in each node of the hidden layers. Because this type of function usually gives better solution for non-linear complex problems, such as the precipitation-discharge relationship.

The network that gives minimum error is the best performing neural network. The summery of the different networks for each trial are provided in Table 5.1.

Table 5.1: Summary of different neural networks used for trials

Trial No.	No. of Hidden Layers	No. of Nodes in each Hidden Layer	No. of Runs in each Trial	No. of Iterations
1	5	13, 11, 9, 7, 5	10	10000
2	5	13, 11, 9, 7, 5	20	20000
3	5	13, 11, 9, 7, 5	30	10000
4	5	13, 11, 9, 7, 5	20	30000
5	7	15, 13, 11, 9, 7, 5, 3	20	20000
6	10	30, 27, 24, 21, 18, 15, 12, 9, 6, 3	20	20000

The network that shows the best performance during calibration and validation can be chosen as the desired network of the model. The neural network model used in the final trial has been illustrated in Figure 5.6.

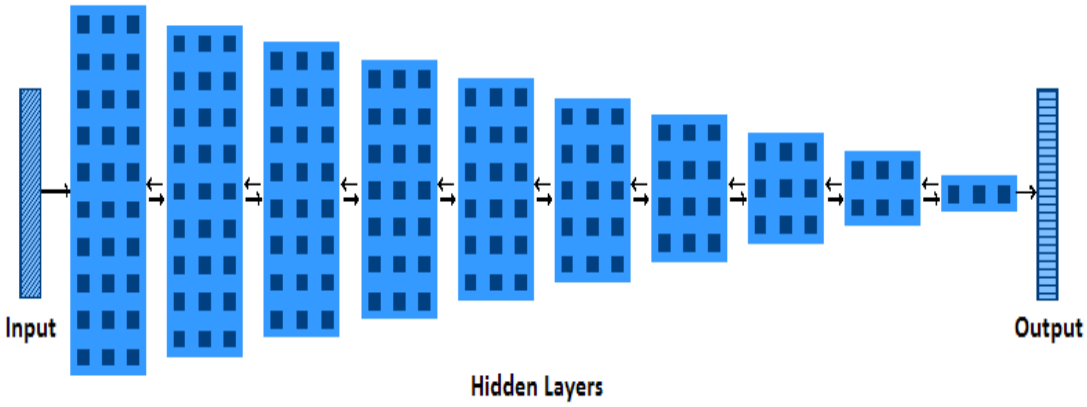

Figure 5.6: Designed neural network for final trial

5.3.4 Calibration of the Model

Calibration is a process of adjusting the connection weights in the neural network so that the network's response best matches the desired response. The calibration of a neural

network can be understood as the combination of two processes – training and testing. The purpose of such process is to determine the set of connection weights that cause the ANN to estimate outputs within the given tolerance limits to target values.

The different networks designed for trials were calibrated for the period of 1975 to 1990 using the monthly precipitation and discharge as inputs and outputs respectively. The data was divided into two parts for calibration and testing. For each trial, the weights are assigned small random values initially. During calibration, these are adjusted based on the mean squared error (MSE) between the ANN outputs and the observed discharges. This adjustment continues until a weight space is found, which results in the minimum mean squared error (MSE) and best overall prediction of discharge. The results of MSEs during calibration and testing for different trials are given in Table 5.2.

Table 5.2: Model Performance during Calibration

Trial	Calibration Minimum MSE	Calibration Standard Deviation	Testing Minimum MSE	Testing Standard Deviation
1	0.0074	0.00026	0.0086	0.00036
2	0.0063	0.00048	0.0081	0.00041
3	0.0070	0.00064	0.0086	0.00045
4	0.0061	0.00052	0.0086	0.00029
5	0.0062	0.00057	0.0084	0.00031
6	0.0050	0.00099	0.0078	0.00037

From the table it is seen that the value of MSE is minimum for the network used in trial 6. Therefore this network produces the best results for predicting discharge. The variation of MSEs for different runs and iteration numbers (epochs) for trial 6 are shown in Figure 5.7(a) and (b). From Figure 5.7(c), it is evident that initially the mean squared error with respect to standard deviation for calibration was low but testing was high. It means that the network learned the process well but was not able to predict well for a new sets of data. As the number of iteration increases with different runs, the values were minimum for both calibration and testing. Hence the network was able to learn as well as to predict with the increasing number of runs. For this trial, the best network was obtained in run 18 with 20000 iterations. So the weighted values during this run give the best result.

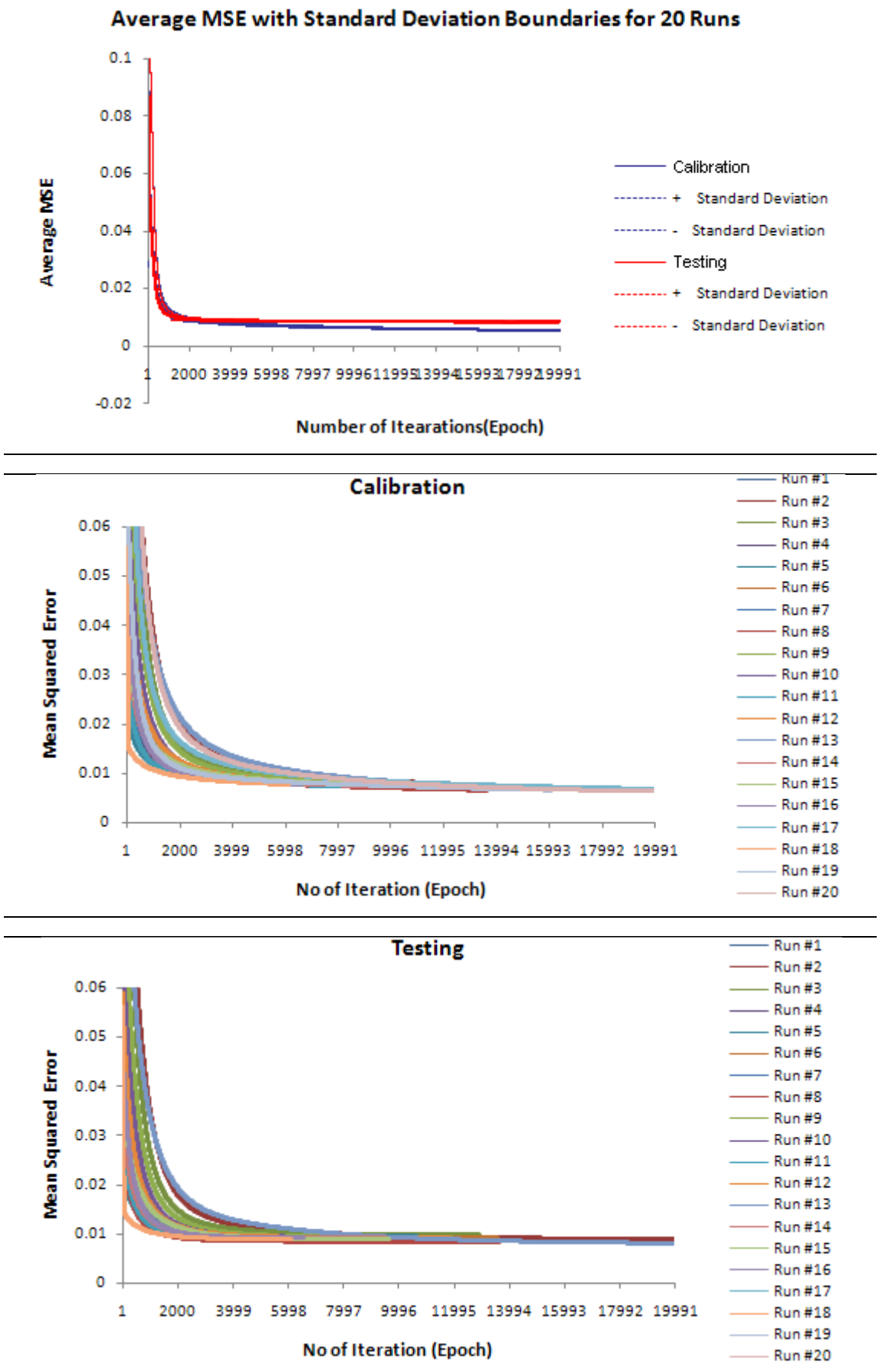

Figure 5.7: Performance of the model network for final trial during calibration

5.3.5 Validation of the Model

Validation is the process of investigating the performance of the model to predict output for new set of inputs. In this process, new inputs are imposed on the developed calibrated model to predict output and this output in then compared with the observed known outputs.

In the present study, the developed neural network model for each trial was verified to see which network predicts better discharge after comparing with the observed discharge. For all the trials, the calibrated networks were verified for the period of 1991 to 1994 by imposing the monthly precipitation data that were not used during calibration. The simulated results of discharge were compared with the observed discharge of Lower Meghna River. Various statistical indicators such as correlation coefficient (R^2), normalized root mean square error (RMSE), mean absolute error (MAE) and mean relative error (MRE) were applied to validate the model networks for each trial. The results are summarized in Table 5.3.

Table 5.3: Model Performance during Validation

Trial	Normalized Mean Squared Error	Mean Absolute Error	Mean Relative Error	Correlation Coefficient
1	0.255	10986.73	0.697	0.863
2	0.240	10854.87	0.632	0.872
3	0.254	10902.16	0.717	0.864
4	0.255	10788.88	0.699	0.863
5	0.251	10866.05	0.625	0.867
6	0.231	8676.31	0.289	0.882

The results indicate that the neural network used in trial 6 produces the best output when compared with the observed discharge. Various statistical indicators give the best estimate for this trial. Figure 5.8 shows the model simulated discharge and actual observed discharge for the validation period 1991 to 1994 along with the correlation between them. It is evident that the developed, calibrated and validated neural network used in trial 6 produces the optimum output that matches the observed discharge. The model is able capture the rising and falling limb of discharge, i.e., it predicts discharge for both wet and dry season with considerable accuracy. Therefore the network

developed in the final trial will be used to predict discharge for different precipitation inputs due to various scenarios of climate change.

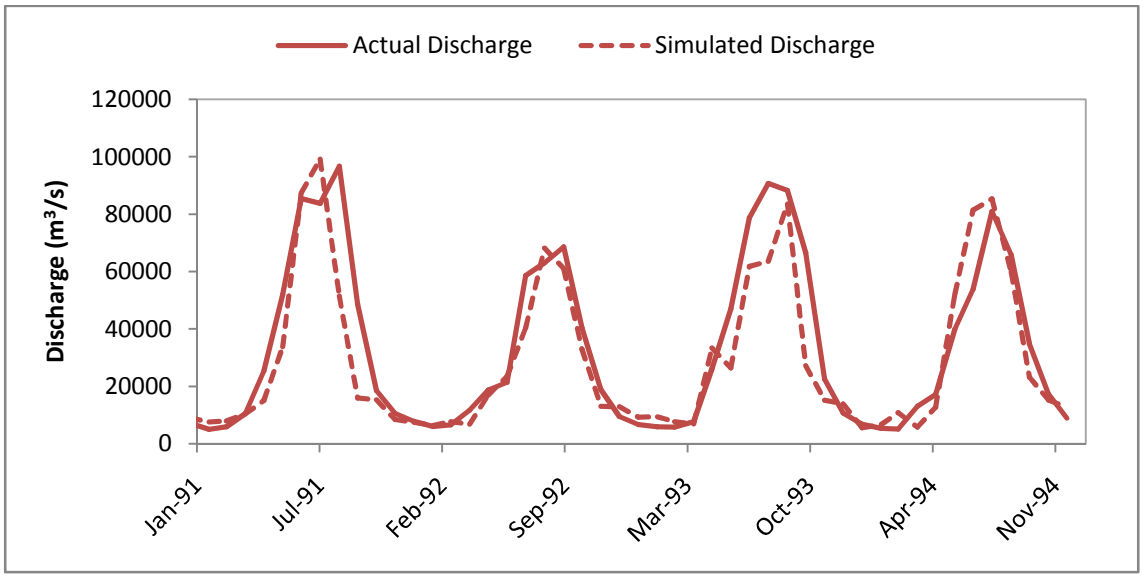

(a)

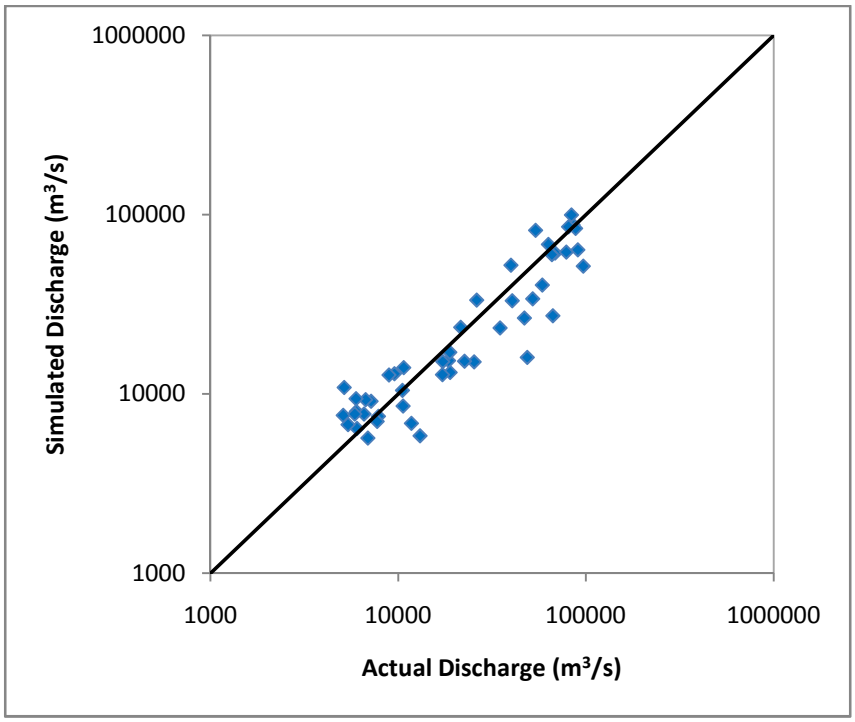

(b)

Figure 5.8: Comparison between observed and simulated discharge during validation (a) and correlation between them (b)

The details of other trials performed for the present study during calibration and validation have been given in Appendix B.

5.4 Analyzing Hydraulic and Morphologic Responses of River Using MIKE 21

A two dimensional mathematical model had been developed using MIKE 21 FM in order to assess various hydraulic and morphologic changes of Lower Meghna River due to climate change. This modelling works were performed at Institute of Water Modelling (IWM), Dhaka. At first the model was set-up using various data such as discharge, water level etc. for present day conditions. After calibration and validation of the model, the projected discharge and rising water level due to sea level rise was incorporated for different climate change scenarios to estimate the possible hydraulic and morphologic changes of the river due to climate change.

5.4.1 Selection of Modelling Period

While setting up the model, two distinct periods were selected for various hydraulic and morphologic computations. At first, the calibration and validation of the model was done for the year 2006. Because the bathymetry data of the river collected from BWDB was for the year of 2006. Two separate months representing different hydraulic condition were chosen for the process. The month of August 2006 representing wet season and the month of March 2006 representing dry season was selected for calibration of the model. After that the model was validated for the months of March and August of the year 2007. When the model is ready for analysis, the initial or base condition was simulated for the whole year of 2008. Hence the modelling period can be summarized as follows –

- Calibration period: the month of August 2006 representing wet season and the month of March 2006 representing dry season
- Validation period: the months of March and August of the year 2007
- Initial or base period: the whole year of 2008 from January to December

5.4.2 Setting-up Model Domain

The model domain for the present study was the Lower Meghna River from Chandpur at the upstream to upper portion of Hatiya at the downstream. This domain was prepared using the bathymetry data collected from BIWTA. The preparation of the domain consisted of two steps – mesh generation and bathymetry development.

5.4.2.1 Mesh Generation

The hydrodynamic module is the core of all other modules such as sediment transport in the MIKE 21 environment. Mesh generated under this module is used for rest of the

modules. Mesh generation is the most important task in any model application. In the MIKE environment, a separate module is assigned called mesh generator. This module creates .mdf files that are used for mesh generation.

First a satellite image of the study area was imported on the mesh generator module as background information. Using this image, the boundary of the model was created. This polygon was assigned with triangular mesh after defining the size of the individual mesh. Then a series of mesh of generated with a total of 14669 elements and 7593 nodes. It had got two open boundaries. Using different tools and features, the generated mesh was checked to minimize error and create more smooth mesh. After several checking and modification, mesh was finally ready to be incorporated with various model input. The final mesh generated for the present study region is shown in Figure 5.9.

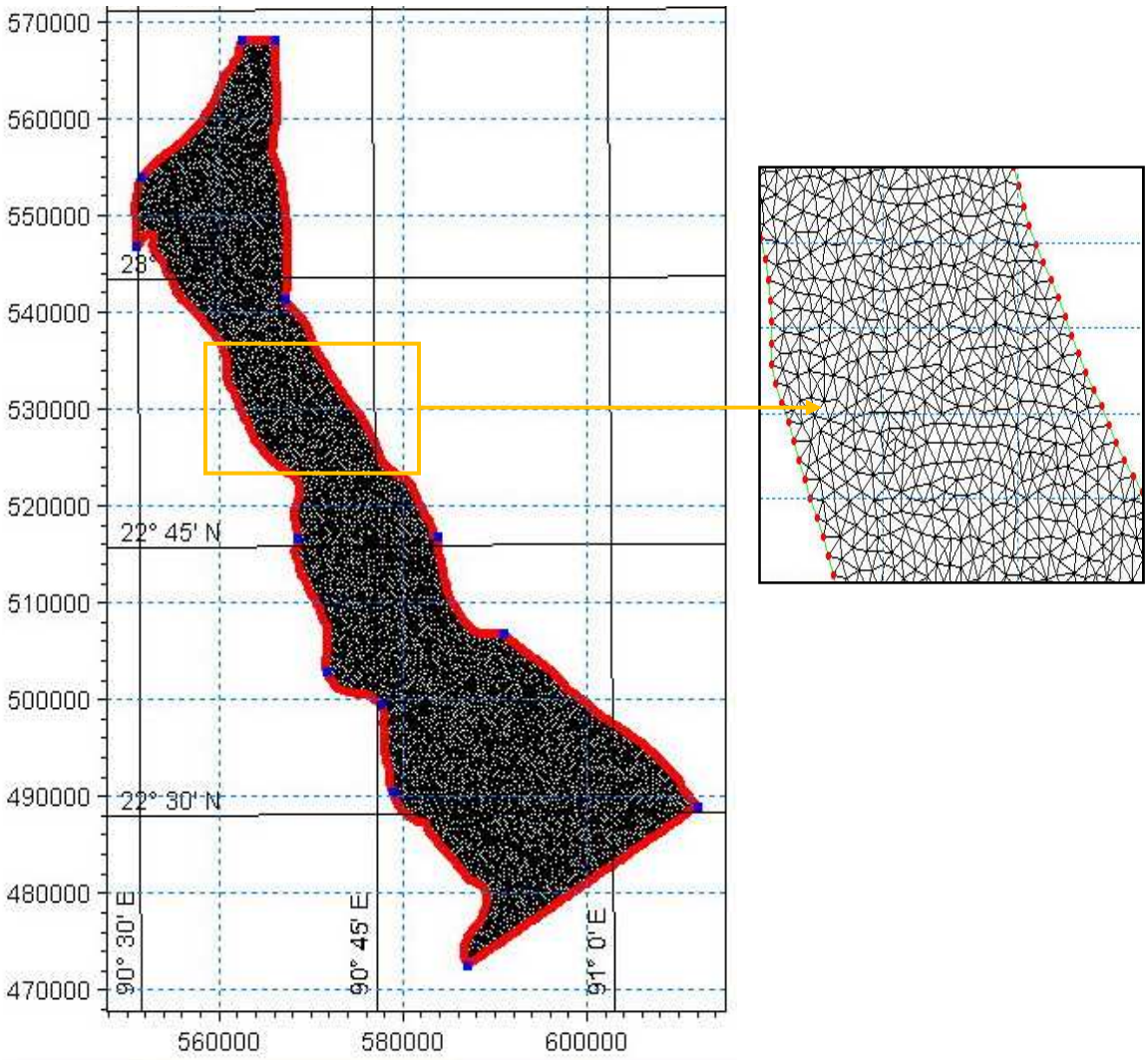

Figure 5.9: Generated mesh of the study area

5.4.2.2 Bathymetry Development

Scattered survey data on bathymetry are interpolated to mesh nodes using scatter module in the MIKE environment. Normally bathymetry data are measured in random fashion. Mesh can be generated using these measured bathymetric points. But mesh generated in this way would not give better quality model. Therefore the study area was developed with good quality meshes and then surveyed bathymetric data were interpolated into those mesh nodes. The developed bathymetry of the study area is shown in Figure 5.10.

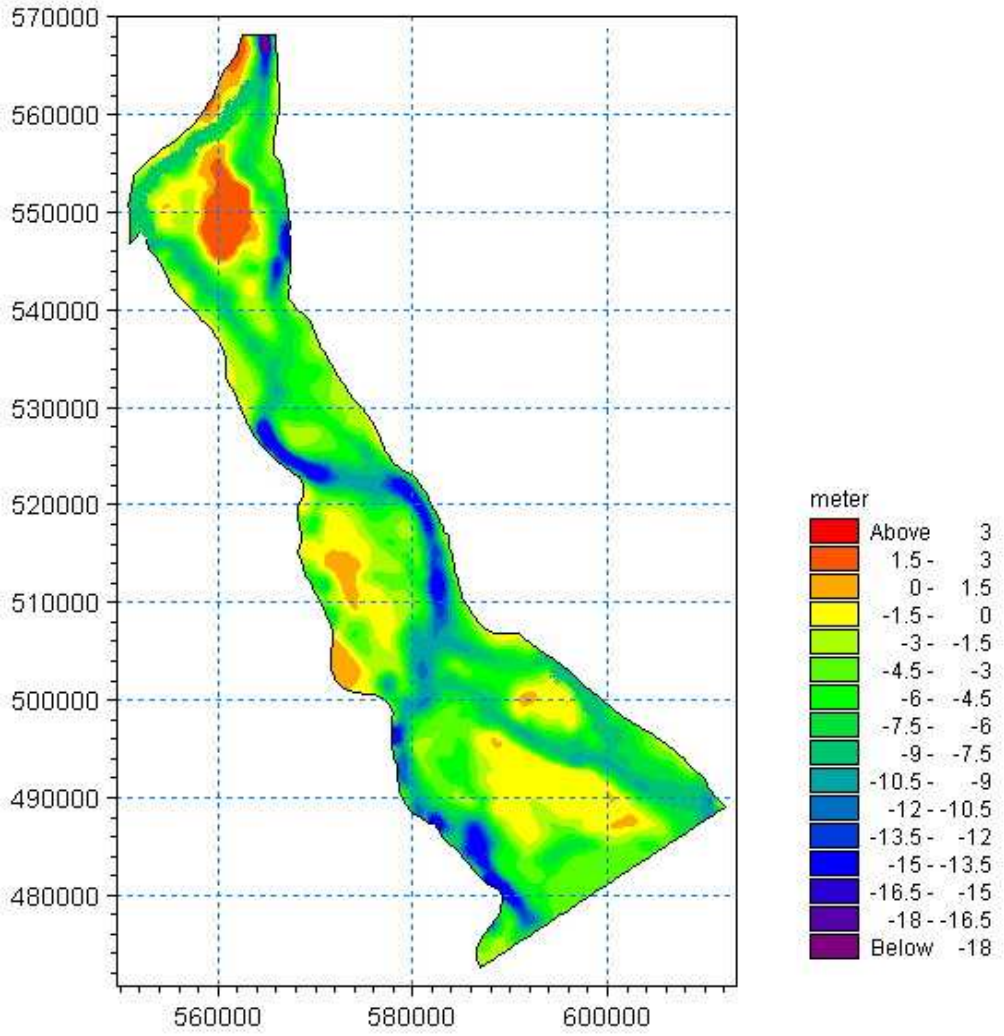

Figure 5.10: Model bathymetry of the study area

5.4.3 Boundary Conditions and Initial Conditions

5.4.3.1 Boundary Conditions

Boundary condition is an essential component for hydrodynamic modelling. Normally discharge is assigned at the upstream inflow boundary and water level or rating curve at

downstream boundary. The model of Lower Meghna River had a discharge boundary at the upstream at Chandpur and a water level boundary at downstream at Hatiya. In MIKE 21 FM, boundary conditions can be assigned to every node or in line of that boundary.

The discharge at Chandpur had been generated from discharges of Padma at Baruria and Upper Meghna at Bhairab Bazar using 1-D Hydrodynamic model HEC-RAS and was incorporated as upstream boundary. Interpolated water level from Hatiya has been applied to downstream boundary. All the boundaries were applied for two distinct periods – for the month of March and August of the years 2006 and 2007 during calibration and validation and for the year 2008 for base condition simulation. The discharge and water level data for these periods are shown in Figure 5.11.

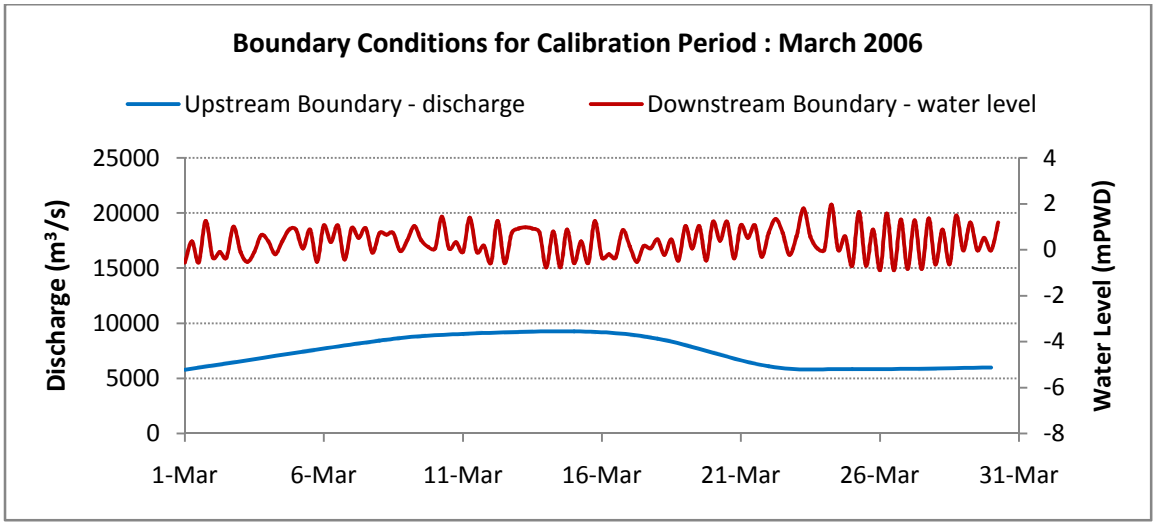

(a)

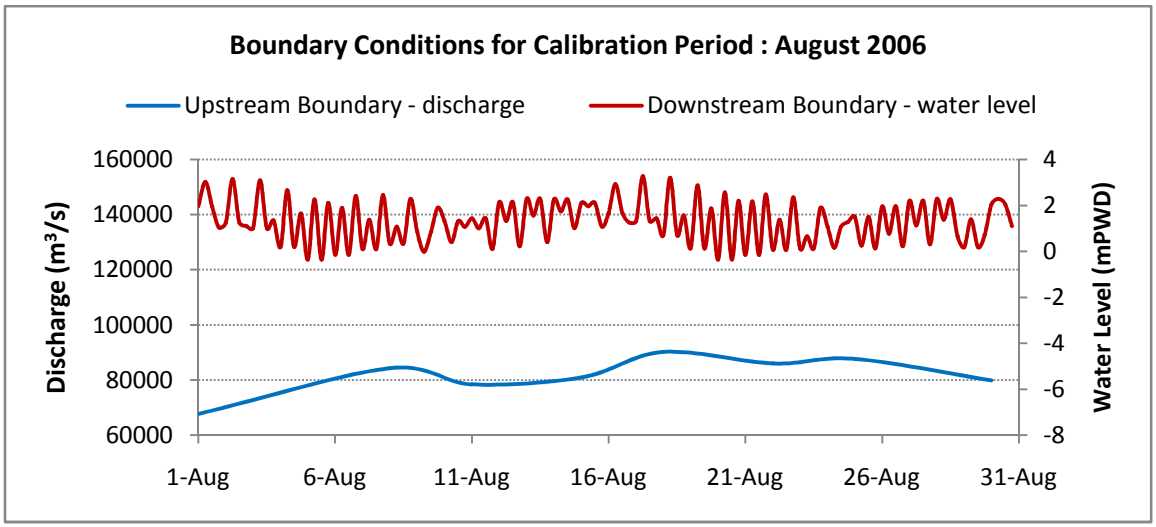

(b)

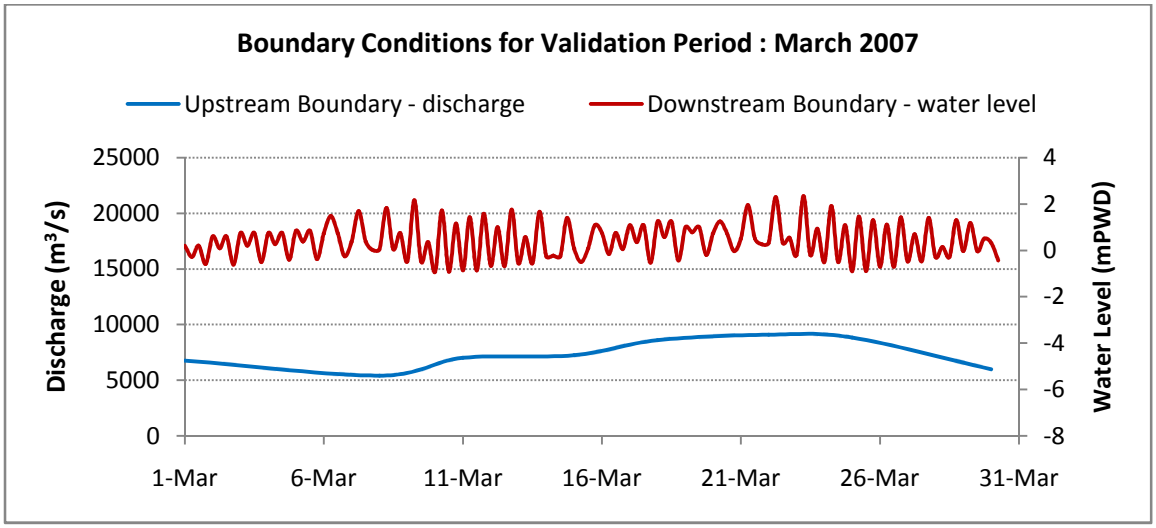
Boundary Conditions for Validation Period : March 2007
Upstream Boundary - discharge
Downstream Boundary - water level
Discharge (m³/s)
Water Level (mPWD)
25000
20000
15000
10000
5000
0
4
2
0
-2
-4
-6
-8
1-Mar
6-Mar
11-Mar
16-Mar
21-Mar
26-Mar
31-Mar

(c)

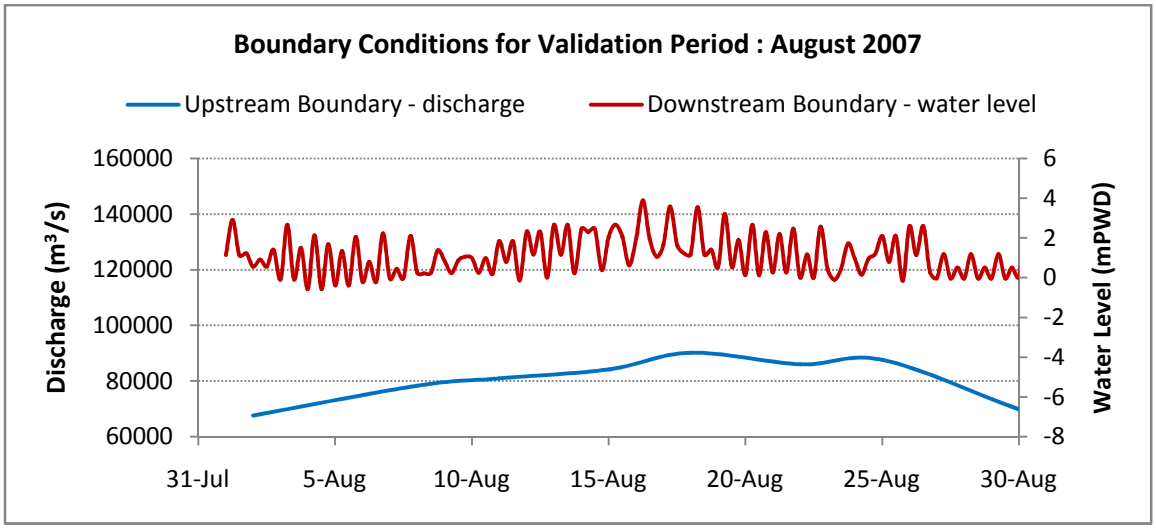
Boundary Conditions for Validation Period : August 2007
Upstream Boundary - discharge
Downstream Boundary - water level
Discharge (m³/s)
Water Level (mPWD)
160000
140000
120000
100000
80000
60000
6
4
2
0
-2
-4
-6
-8
31-Jul
5-Aug
10-Aug
15-Aug
20-Aug
25-Aug
30-Aug

(d)

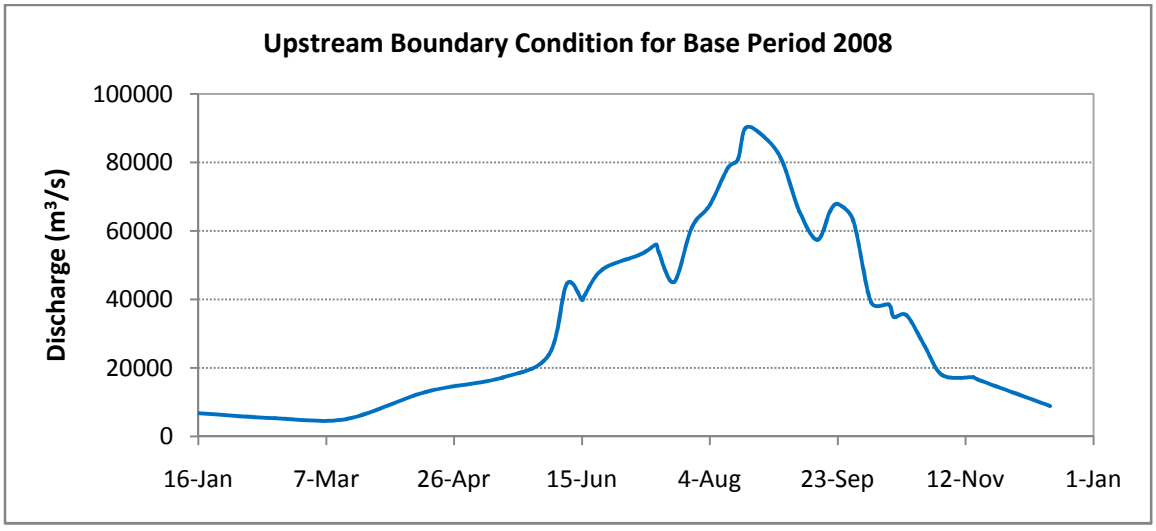
Upstream Boundary Condition for Base Period 2008
Discharge (m³/s)
100000
80000
60000
40000
20000
0
16-Jan
7-Mar
26-Apr
15-Jun
4-Aug
23-Sep
12-Nov
1-Jan

(e)

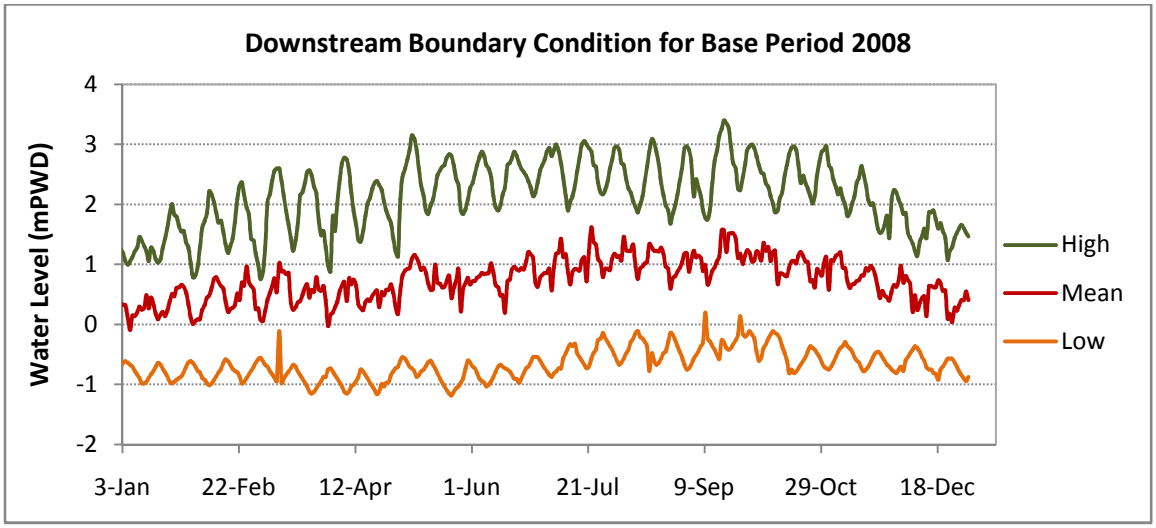

(f)

Figure 5.11: Boundary conditions for calibration period (a, b), validation period (c, d) and base period (e, f)

5.4.3.2 Initial Conditions

Initial conditions, which state the hydrodynamic condition at the start of simulation, need to be defined for all models. Usually the time series boundary conditions at specified upstream and downstream ends are available from various sources. Other than these, discharge or water level data at all the other points at model are not available. So, for defining the initial conditions at all the points at the model, it becomes essential to run a steady hydrodynamic model with a specified discharge and water level in defined upstream and downstream ends. The resulting water level obtained from this has been applied at all other points as initial conditions during unsteady simulation. For simplicity, the initial water level for the whole model domain was assumed same as the downstream water level boundary, and accordingly velocity was assumed zero at all the nodes.

5.4.4 Various Inputs in Hydrodynamic Module

Various inputs and parameters contribute in adjusting the solution technique of the hydrodynamic module of MIKE 21. These are wetting-drying parameter, Eddy viscosity, bed resistance or roughness parameter etc.

- The wetting-drying parameters are used to represent real world scenario where portions of an area may become devoid of water and later become wet again. Any nodes or points become wet or dry respectively when water depth become higher or lower than the threshold values.

- The turbulence parameter coefficient of eddy viscosity is used for the distribution of flow by exchanging lateral momentum of flow. In MIKE 21 FM environment, the eddy viscosity can be specified by using constant eddy formulation or applying Smagorinsky formulation.
- Roughness parameter such as Chezy's C is an important parameter in hydrodynamic module since it provides some control over the fluid velocity magnitude and direction.

For the present study, the drying depth, below which any nodes will be treated as dry, is given as 0.005 m and the wetting depth, depth above which any node will become wet again, is given as 0.1 m. To define eddy viscosity, the Smagorinsky coefficient was taken 1 estimated on the basis several studies. The Chezy's C is mainly a calibration parameter in the hydrodynamic module and was taken in the range of 60 to 70 $m^{1/2}/s$ based on various conditions of the domain.

5.4.5 Various Inputs in Sand Transport Module

The sand transport module is used to capture various morphological changes of the river. This module simulates various features based on the results obtained during hydrodynamic calculations. Various inputs and parameters associated with this module are sediment transport predictors, alluvial resistance, grain size of soil etc.

Engelund and Hansen formula was applied for Sediment transport prediction in this study. The grain size of Lower Meghna River was varied between 0.09 mm to 0.13 mm along the domain. The alluvial resistance is also a calibration parameter for morphologic simulation. A value 30 for the coefficient and 0.5 for exponent was used for the study.

5.4.6 Calibration and Validation of the Model

During model development, many uncertainties exists related to input as model geometry, boundary conditions, roughness, eddy viscosity etc. which can have momentous impact on model solutions. Once geometry and boundary conditions have been obtained with reasonable accuracy from the field, it is common practice to set them out of preview of the calibration process. Validation is a multi-step process of model adjustments and comparisons, leavened with careful consideration of both the model and the data. During validation, a new set of observed data have been incorporated to justify wheather the calibrated parameters produces satisfactory result for a new condition.

5.4.6.1 Hydrodynamic Calibration

For hydrodynamic calibration, mostly roughness and eddy viscosity are the parameters to play with to obtain an adequate match with the observed field conditions. For the present study, the water levels at Doulatkhan station located 35 m upstream of Hatiya were compared with the simulated water levels of the model for the same location. This calibration was undertaken for both wet and dry season for the periods of March and August of year 2006. The roughness parameter (Chezy's C) was adjusted to get the best result. From calibration results it was found that the computed values show good agreement with the observed water levels for both wet and dry months (Figure 5.12).

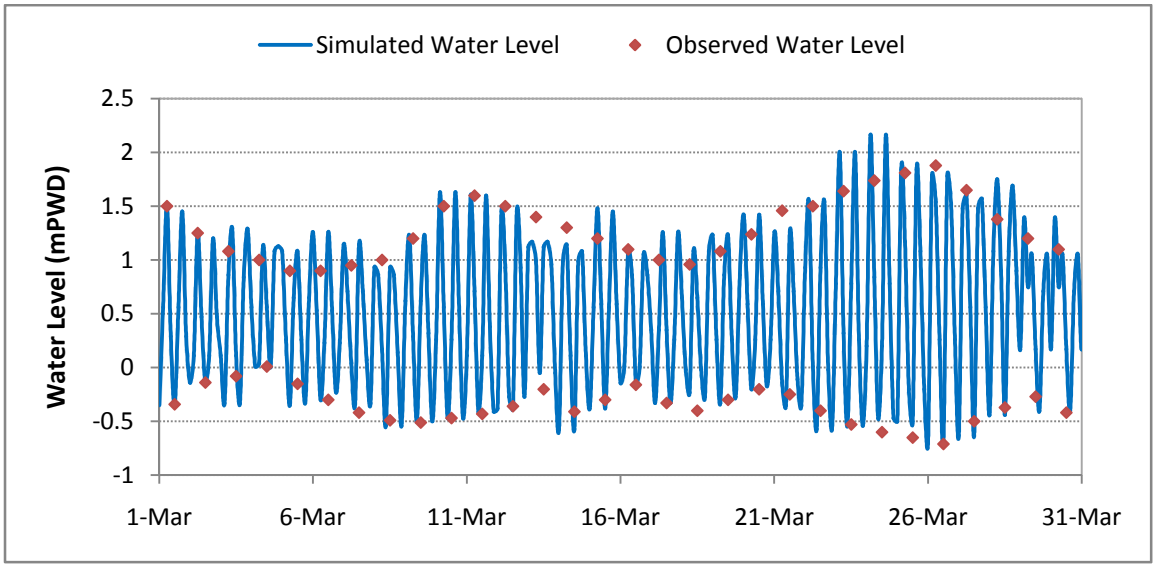

(a) March 2006

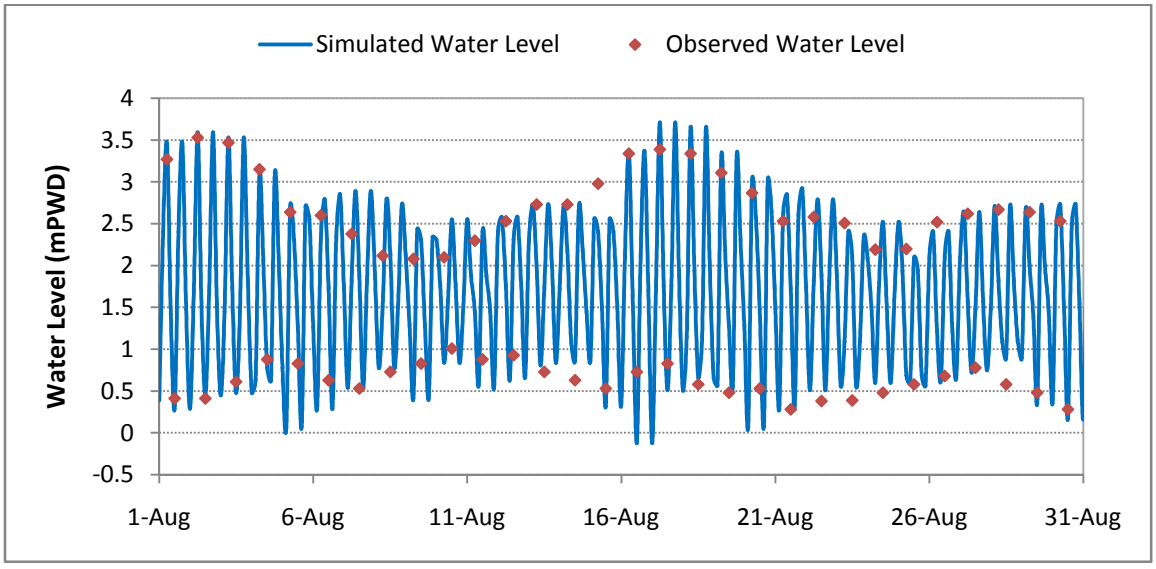

(b) August 2006

Figure 5.12: Simulated and observed water level during calibration

5.4.6.2 Hydrodynamic Validation

The computed water surface elevations by the model were validated with observed water surface elevations at Doulatkhan station for the months of March and August of year 2007. This comparison has been shown in Figure 5.13. Good agreement between the observed and simulated water levels indicates satisfactory performance of the model.

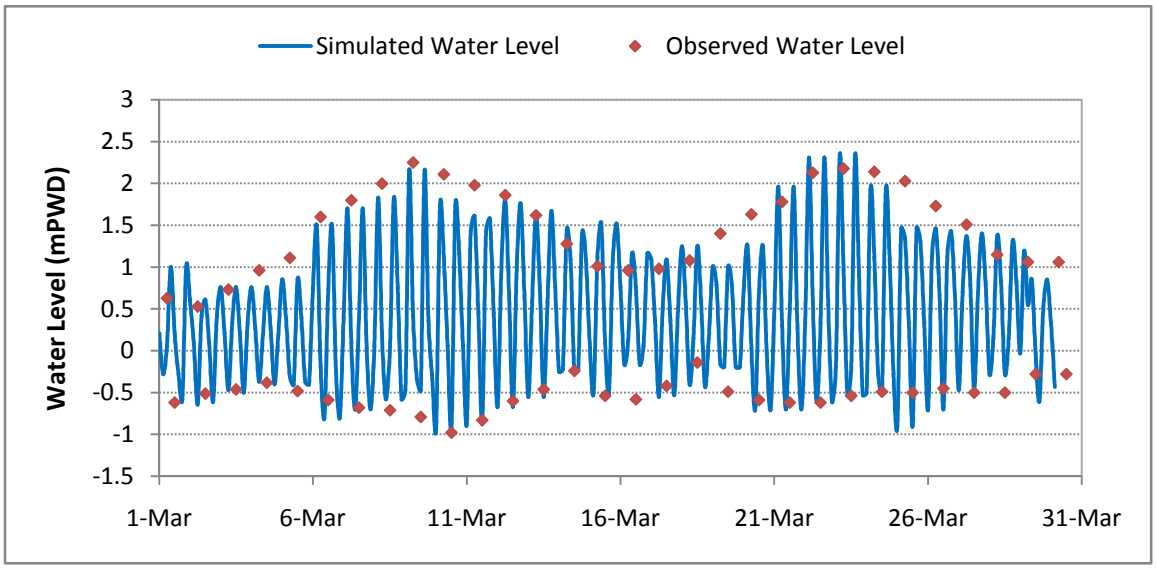

(a) March 2007

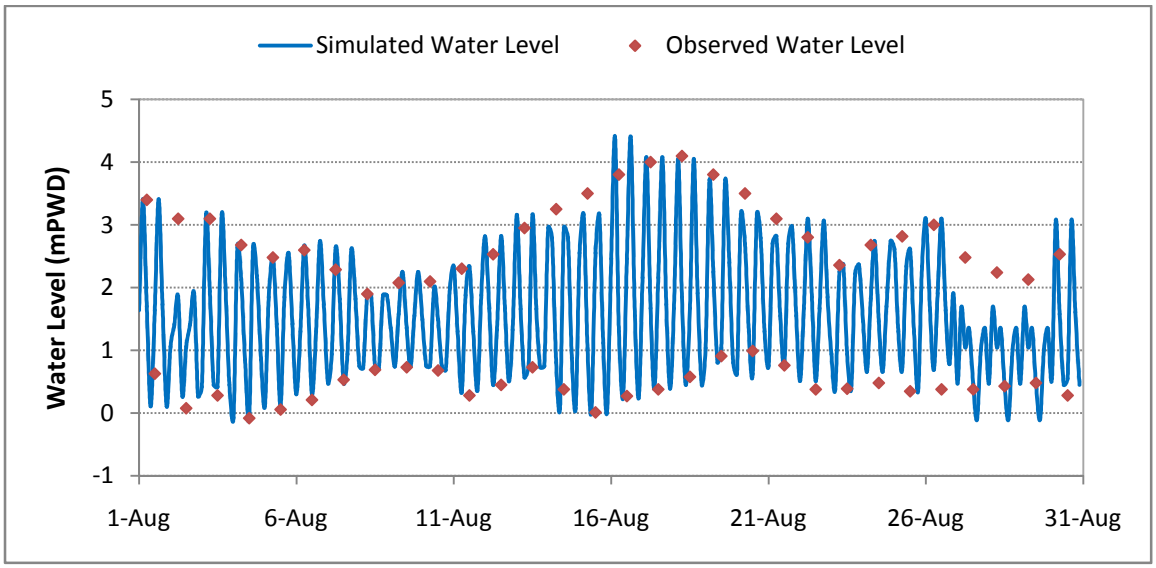

(b) August 2007

Figure 5.13: Simulated and observed water level during validation

During the calibration and validation process, the model showed good agreement with observed data for both dry and wet periods. Therefore the model was capable to simulate different conditions and scenarios used in the present study.

5.4.6.3 Morphologic Calibration

Due to lack of sediment data, it is very difficult to undertake morphological calibration of a river. However, an alternate approach is the implication of sediment rating curve. A sediment rating-curve of Lower Meghna River had been generated based on the relationship given in Meghna Estuary Study (MES) (MWR, 2001). This rating curve was then utilized to verify the model computed sediment transport rates. The simulated sediment transport rates matched closely with the rating curve (Figure 5.14).

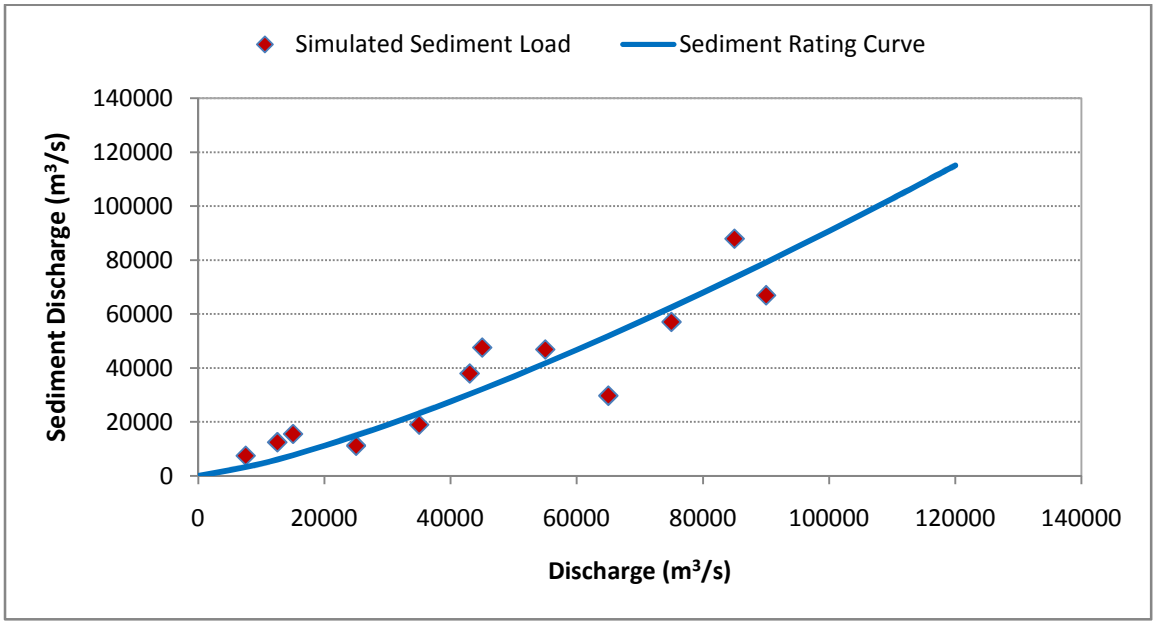

Figure 5.14: Comparison between simulated sediment rates with developed rating curve

River bed is assumed consisting of effective sand grain diameter of 0.09 to 0.13 mm. This grain size along with parameters of alluvial resistance used, is found satisfactory during calibration for the morphology.

5.4.6.4 Morphologic Validation

The developed sand transport module of the model was validated by comparing the model simulated bathymetry with the observed bathymetry of Lower Meghna River. Considering the initial bathymetry of April 2006, the model was simulated for period of November 2006. The model simulated bathymetry of November 2006 was then compared with the observed bathymetry of the same period. Results are presented as the bed elevations for three selected cross-sections (each one upper, middle and lower part of the river) in Figure 5.15. From the results it is found that simulated bed elevations adequately matched the observed bed elevations.

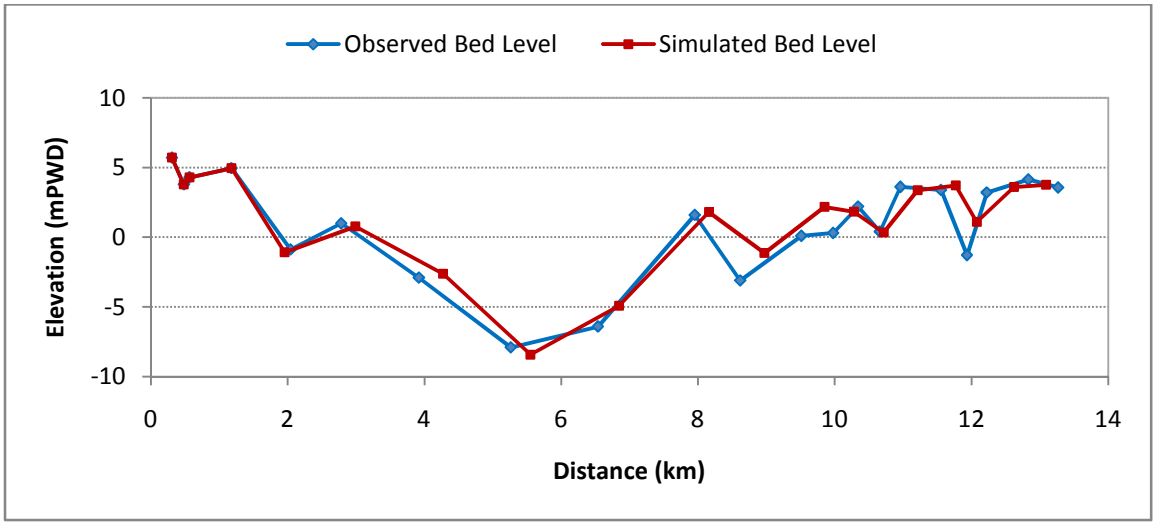

(a) Upper section

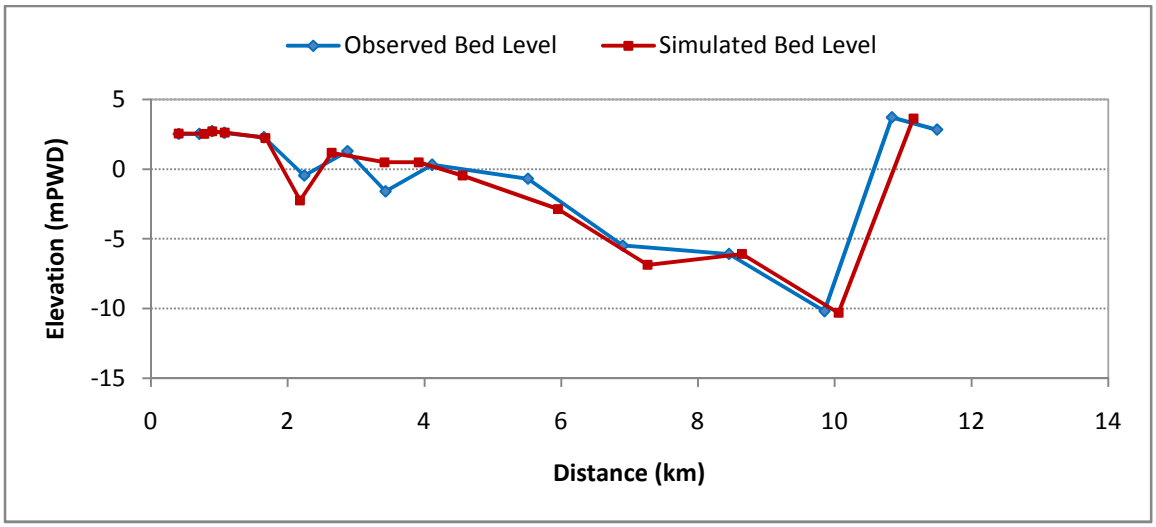

(b) Middle section

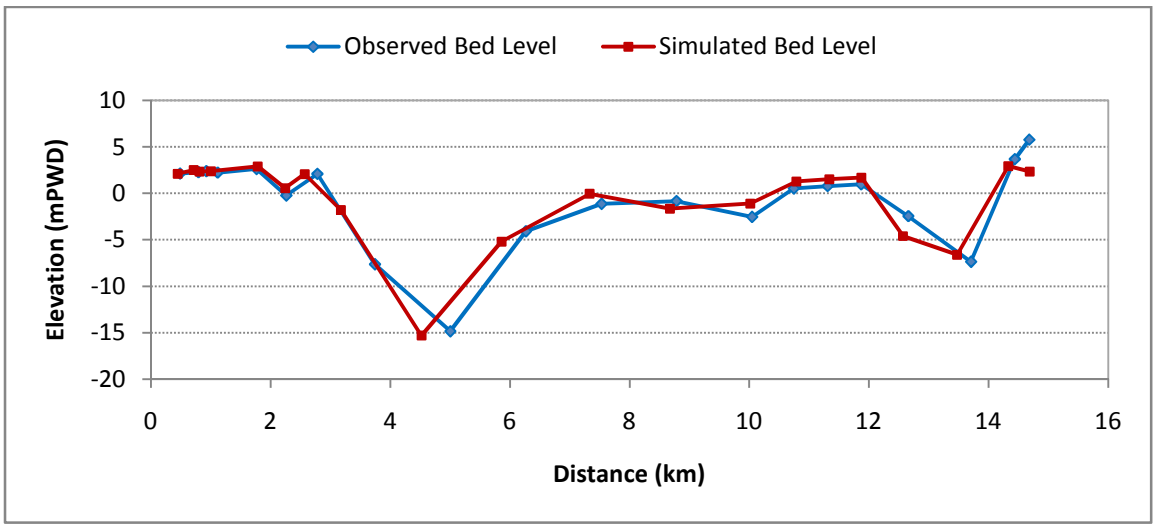

(c) Lower Section

Figure 5.15: Morphologic validation for the selected cross sections

5.4.7 Stability of the Model

Selection of proper time-step is a key parameter in any hydrodynamic model. In explicit schemes time-step is restricted by stability criteria, which requires fulfillment of stringent Courant condition (in this case Courant-Freidrich-Levy number or CFL number). However, accuracy of the results may have an impact on selecting the time-steps. The required computational time-step may be dependent upon element sizes, strength of flows, flow patterns and the rate of change in boundary conditions. Usually the time-step of a model is determined by trial and error basis. The procedure of choosing a time-step is that, a test simulation is performed in which the time-step size is adjusted until the solution does not change and the model remains stable numerically. Then the adjusted final interval can be used as the time-step.

To reduce the computational time for a simulation, the time-step should be as large as possible to capture the extremes of the dynamic boundary conditions and maintain numerical stability. In this study 120 seconds was taken as a computational interval for unsteady simulation. Considering an element of size 500 m × 500 m, whose velocity in x and y direction were 0.56 m/s and -0.43 m/s respectively, the corresponding CFL number was found 0.24. Similarly, for various conditions this value was in the range between 0.2 and 0.4. Hence the model fulfilled the criteria for numerical stability for different conditions and scenarios. Figure 5.16 shows the variation of CFL number along the river profile at the end of simulation during the base period. The CFL numbers at the end of the simulation for various climate change scenarios are given in Figure C1 of Appendix C. It was found that the model was numerically stable for those simulations.

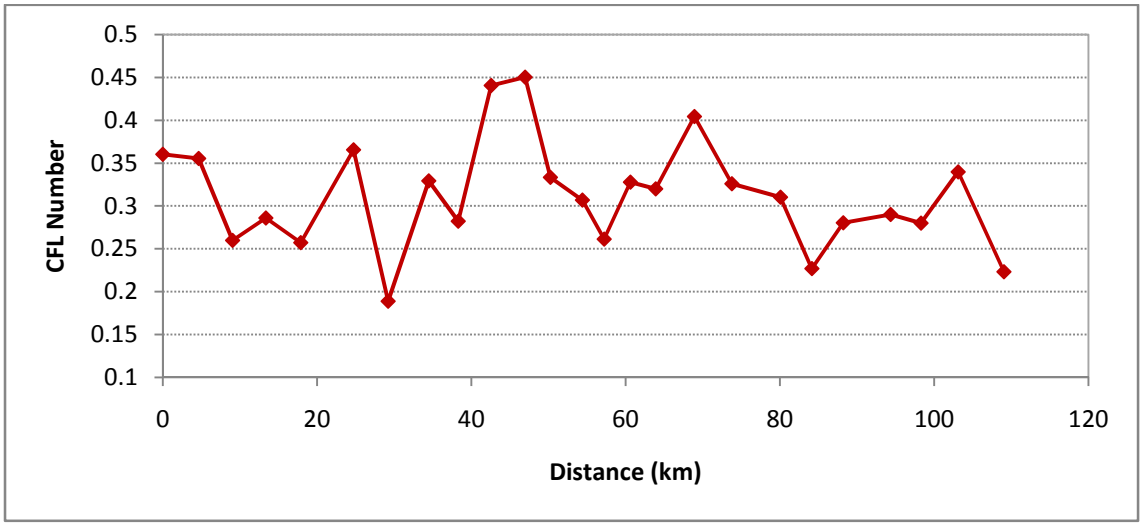

Figure 5.16: Variation of CFL number at the end of base period simulation

5.4.8 Simulation of the Model

When satisfactory results are obtained in calibration and validation, the model was considered ready for simulation and various analyses. First the model was run for the base period of year 2008. Then the predicted discharge of Lower Meghna River, which can be found from the neural network analysis, along with sea level rise scenario was incorporated on the upstream and downstream boundaries respectively. The model was simulated for various climate change scenarios to assess the hydraulic and morphologic responses of the river. Such simulation was performed only for the projected years of 2020s, 2050s and 2080s. Because it was not possible to simulate continuously upto 2080 due to limitation of the model. The analysis was carried out for the river profile as well as for the selected cross sections. The selected cross sections are shown in Figure 5.17.

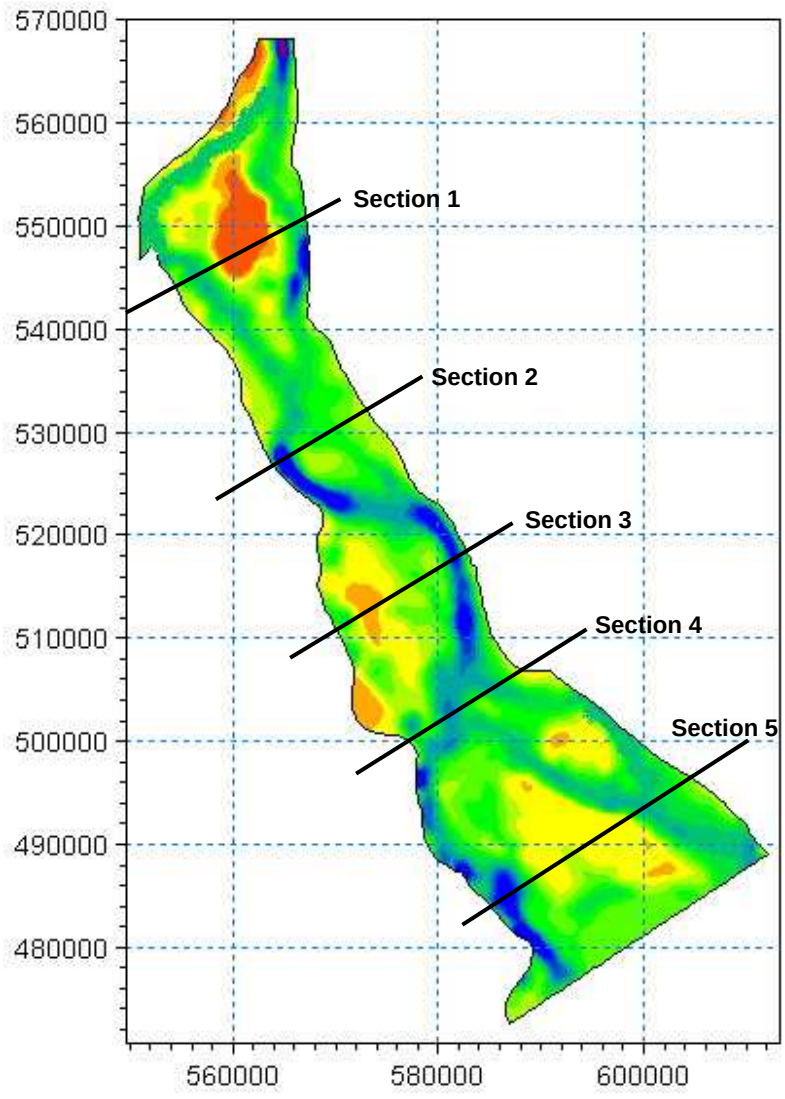

Figure 5.17: Selected cross sections for various analyses

5.5 Evaluation of Delta Progradation along River using Numerical Model

The process of delta progradation of Lower Meghna River was assessed using the one dimensional Numerical model. This model was applied to the longitudinal profile of the river to analyze the process of delta progradation due to sea level rise.

5.5.1 Specification of Auxiliary Inputs

After the numerical formulation and discretization of the model, various input auxiliary data for the formulated equations were specified for the Lower Meghna River. These data include Chezy's roughness coefficient, grain size of sediments, porosity, submerged specific gravity, bed slope etc. The values are given in Table 5.4.

Table 5.4: Various inputs in the numerical model

Input Parameter	Unit	Value
Chezy Resistance Coefficient	$m^{1/2}/s$	60
Grain Size of Sediment	mm	0.11
Submerged Specific Gravity of Sediment	-	1.65
Porosity	-	0.4
Initial Bed Slope	cm/km	2.3

Other inputs related to channel geometry such as initial length of the fluvial zone of the river, initial elevation of the top and bottom of foreset etc. were also incorporated before the application of the model.

5.5.2 Computation of Intermittency Factor

Actual rivers tend to be morphologically active only during floods. That is, most of the time they are not doing much to modify their morphology. The simplest way to take this into account is to assume an intermittency (I_f) such that the river is in flood of a fraction of the time, during which the discharge equals the bankfull discharge. Considering the flood season as June-July-August, the Intermittency Factor was taken as 0.25 for Lower Meghna River.

5.5.3 Introducing Primary Variables

For the developed numerical model, three variables govern the process of delta progradation. These are discharge, sediment discharge and downstream water level due

to rising levels of sea. At first these variables were set for the baseline condition considering the base period as 2008. All the analyses were carried out with respect to this base period.

5.5.4 Adjustment of the Model

The numerical model was developed and adjusted for the base condition. These adjustments are very difficult due to lack of data. However, effort was made to adjust and verify the model by considering the model results of MIKE 21 Flow Model FM. The auxiliary parameters were changed and modified to adjust the numerical model.

5.5.5 Incorporating Climate Change Scenarios

The process of delta progradation was analyzed by changing river flow, sediment transport and water level resulting from the effect of climate change and sea level rise. The discharge data was taken from the results of ANN model and the sediment transport rates were considered from the simulations of MIKE 21 Flow Model FM for various climate change scenarios. Sea level rise was incorporated according to the projections of IPCC. All the projections were made for scenarios of A1FI, A1B and B1 for the selected periods.

5.5.6 Developing Delta Progradation Profile

The numerical model was used to determine the movement of delta front of Lower Meghna River. The results were then incorporated in the long profile of the river to visualize the gradual progradation of delta in the Lower Meghna River. This process was repeated for various climate change scenarios for selected periods.

CHAPTER 6
RESULTS AND DISCUSSIONS

6.1 General

To predict the discharge of Lower Meghna River, observed precipitation over GBM basin and discharge of Lower Meghna River were incorporated in the ANN model. The developed model was then applied to convert projected future precipitation into discharge for different climate change scenarios namely A1FI, A1B and B1 for the periods of 2020s, 2050s and 2080s. The predicted discharge along with the sea level rise projections were imposed in MIKE 21 FM to assess various hydraulic and morphologic changes such as water level variation due to backwater effect, changes in siltation rate and consequent bed level changes for various scenarios. Finally, the progradation of delta along the lower reach of the river was analyzed using a numerical model. The predicted discharges, increased water levels due to sea level rise and changed sediment transport capacities was used into this model to evaluate the movement of delta front along the river under various climate change scenarios for the stated periods.

6.2 Prediction of River Flow

The streamflow of the rivers of Ganges-Brahmaputra-Meghna basin can be affected by four primary factors – temperature, precipitation, evapotranspiration and soil moisture. Among them precipitation becomes the governing factor due to the basin's tropical climate. The total volume change in precipitation primarily increases the total volume of runoff in the basin, which in turn affect the discharge or flow through the rivers of the basin. Due to climate change, a potential increase in precipitation over GBM basin is likely to alter the flow characteristics of Lower Meghna River.

Figure 6.1 shows the ANN model results of projected discharges of Lower Meghna River under climate change scenarios A1FI, A1B and B1 respectively for the period of 2020s, 2050s and 2080s. It is seen that for almost every scenarios except scenario A1FI, the discharge increases with time resulting from increased precipitation due to climate change. Seasonal variation of precipitation, i.e., extreme precipitation in monsoon and lack of precipitation in the dry season affects the timing of peak discharge and overall flow variation of the river. The variation of flow in dry and wet season is also affected the by the spatial and temporal change precipitation pattern over the basin.

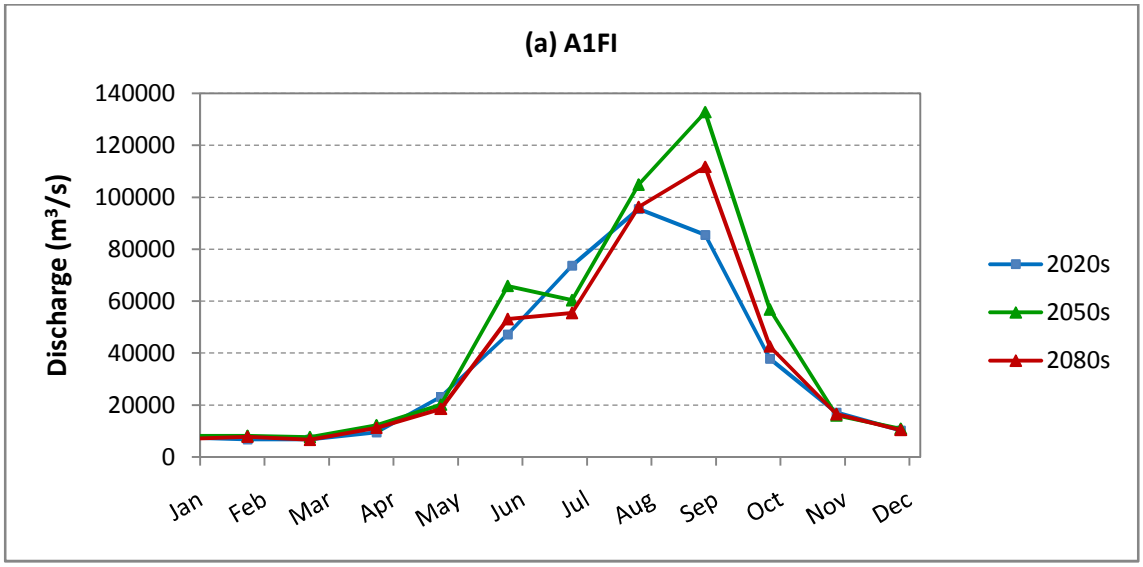

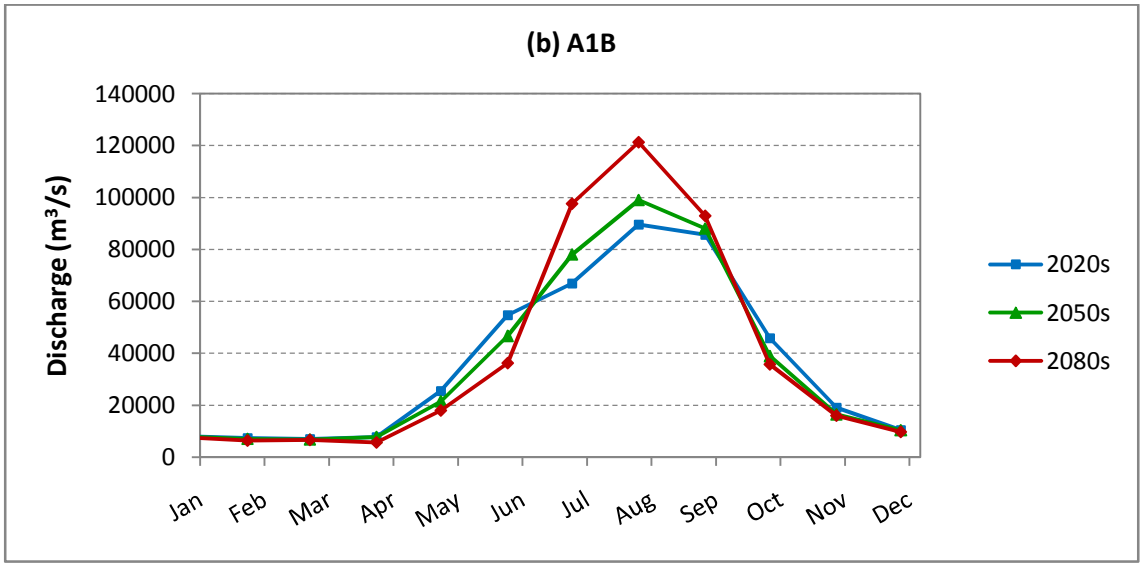

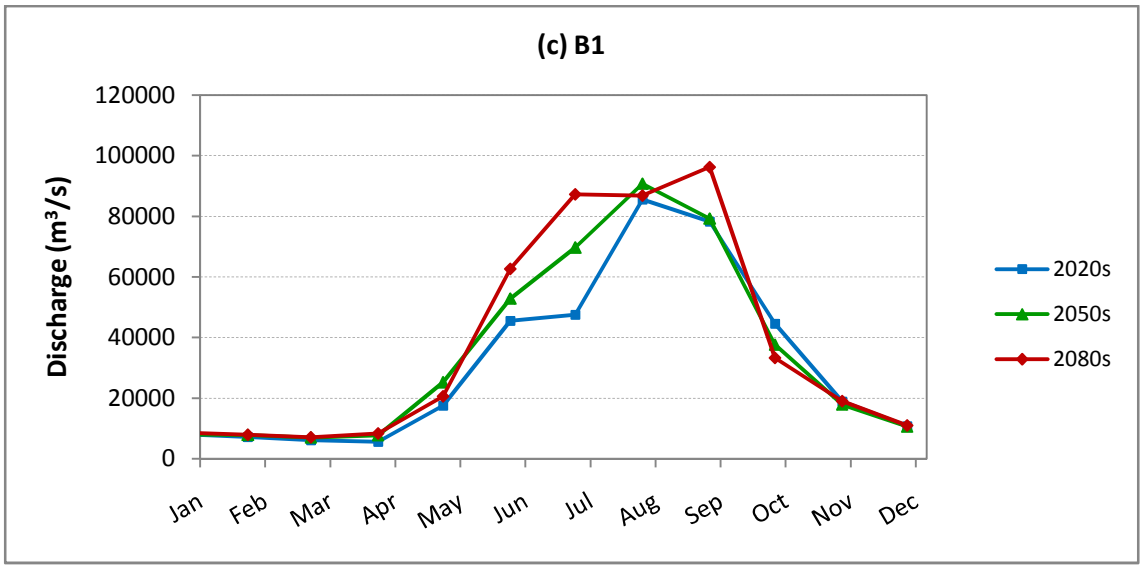

Figure 6.1: Projected discharge hydrographs for different climate change scenarios

For scenario A1FI (Figure 6.1a), discharge in monsoon increases significantly for the periods of 2020s and 2050s but decreases for 2080s. As the temperature rises, more of the precipitation falls as rain and less water is stored as snow. Therefore the peak discharge increases for 2020s and 2050s but decreases in 2080s due to lesser contribution from base flow. The discharge hydrographs seem to move towards right which indicates the occurrence of late monsoon as a result of longer dry season due to climate change.

The maximum monthly discharge of the river increases progressively upto 2080s for the scenarios A1B and B1 (Figure 6.1b and 6.1c). In both cases, moderate temperature rise causes more precipitation. This excess rainfall increases the discharge of the river in monsoon. However, for scenario A1B, this increased discharge is more concentrated within the shorter period of monsoon. The discharge decreases for the other periods of the year. It means that the dry months become drier and wet months become wetter as a result of climate change.

On the other hand, discharge increases in monsoon for scenario B1 for the periods of 2020s, 2050s and 2080s. In this case the rising limbs of the hydrographs tend to shift leftward which means the occurrence of early monsoon. This prolonged monsoon is caused mainly by the huge contribution from the base flow along with the increased precipitation. The magnitude of discharge for monsoon period is not as high as scenarios A1FI and A1B, but longer period of monsoon affects the flow characteristics of the river.

The change of discharge and flow characteristics of Lower Meghna River can be better understood when compared with the base condition which represents the present state of the river. Table 6.1 shows the projected discharges of the river for different climate change scenarios and their comparison with the base period of 2008. Observing the monthly projected discharges for different scenarios and comparing with the base condition, it is seen that the discharge may increase upto 40% in monsoon and decrease upto 23% in dry season indicating high seasonal variation due to climate change.

For scenario A1FI, maximum discharge has been found as 95539 m^3/s, 132835 m^3/s and 111730 m^3/s for the periods of 2020s, 2050s and 2080s respectively which are 7.7%, 39.7% and 32% higher than the base condition. During dry months, the discharge can decrease 14.7%, 20.5% and 18% respectively for the stated periods. The change is also pronounced for scenario A1B. The maximum discharge increases 6.4%, 17.6% and 34% during monsoon and may reduce 17.7%, 18.4% and 20.5% during dry season for the

periods respectively. For scenario B1, maximum discharge can be found as 85611 m^3/s, 90830 m^3/s and 96274 m^3/s for the respective periods which is 1.6%, 7.8% and 18.5% higher when compared with base condition.

Table 6.1: Projected discharges and their comparison with the base condition

Month	Scenario	2020s		2050s		2080s	
		Discharge (m^3/s)	Change (%)	Discharge (m^3/s)	Change (%)	Discharge (m^3/s)	Change (%)
Jan	A1FI	7509.4	-8.2	8224.8	-15.3	6923.4	0.6
	A1B	8140.2	-5.1	8039.8	-6.3	7765.8	-9.5
	B1	8173.1	-4.7	8044.7	-1.6	8659.2	5.9
Feb	A1FI	6870.3	-6.8	8129.8	6.6	7854.0	10.3
	A1B	7412.1	0.6	7045.4	-4.4	6496.7	-11.9
	B1	7160.4	-2.9	7888.6	7.0	7924.7	7.5
Mar	A1FI	6756.5	-4.9	7659.0	-6.6	6635.9	7.8
	A1B	7084.7	-0.3	6813.4	-4.1	6657.6	-6.3
	B1	6124.7	-13.8	7017.0	-1.3	7134.9	0.4
Apr	A1FI	9527.1	-12.4	12293.0	-13.6	11271.5	-17.7
	A1B	7818.2	-18.7	7750.9	-18.4	5737.0	-19.6
	B1	5627.6	-23.7	7783.4	-18.0	8407.1	-11.5
May	A1FI	23164.5	17.9	20174.4	2.7	18501.2	-5.8
	A1B	25551.1	19.5	21515.2	9.5	18075.3	-8.0
	B1	17527.4	-10.8	25257.5	28.6	20669.6	5.2
Jun	A1FI	47209.4	17.4	65901.6	33.8	53118.0	20.0
	A1B	54745.1	21.1	46695.1	16.0	36323.9	-9.7
	B1	45577.3	13.3	52873.7	19.7	62686.7	32.1
Jul	A1FI	73774.4	13.3	60389.2	-7.2	55458.2	-14.8
	A1B	66924.1	2.8	78100.8	20.0	97616.2	39.9
	B1	47603.4	-16.9	69706.4	7.1	87255.7	34.0
Aug	A1FI	95539.3	7.7	104870.0	18.2	96324.6	8.6
	A1B	89586.2	6.4	99009.2	17.6	121271.0	34.0
	B1	85610.8	1.7	90829.9	7.8	86829.9	3.1
Sep	A1FI	85626.8	9.8	132835.0	39.7	111729.7	32.0
	A1B	85712.5	9.3	88044.2	12.3	92919.6	15.5
	B1	78323.5	1.1	79281.3	4.9	96273.8	18.5
Oct	A1FI	37834.1	-21.1	56822.2	-1.8	42566.6	-8.5
	A1B	45846.8	-6.4	38955.2	-15.4	35799.1	-23.9
	B1	44583.8	-8.3	37625.4	-18.6	33256.1	-19.2
Nov	A1FI	17172.5	-14.7	16012.6	-20.5	16511.4	-18.0
	A1B	19172.5	-4.8	16511.4	-18.0	16012.6	-20.5
	B1	18896.5	-6.1	17890.9	-11.1	19025.3	-5.5
Dec	A1FI	10235.9	-3.3	10883.7	2.8	10405.8	-1.7
	A1B	10461.6	-1.2	10373.3	-2.0	9745.2	-8.0
	B1	10792.7	1.9	10677.6	0.9	11064.4	4.5

The seasonal variation of discharge is also a significant feature under various climate change scenarios. The projected discharges for most of the scenarios indicate an increased discharge during wet season and lesser discharge in the dry season compared to base condition (Figure 6.2). For scenario A1FI, the annual discharge as well as the discharge in wet months increases but the discharge in dry months decreases considerably. For A1B, discharges in wet months increase 6.8, 6.9 and 13.3% and decrease 4.2, 10.1 and 16.6% for the periods of 2020s, 2050s and 2080s respectively with respect to base scenario. For B1, the discharges decreases in 2020s followed by increased annual discharge as well as discharges in wet months and decreased discharges in dry months.

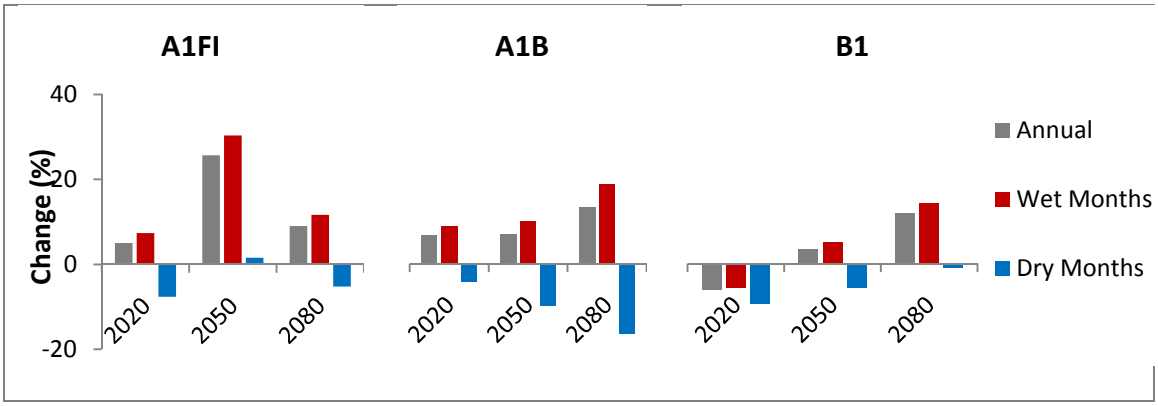

Figure 6.2: Comparison of annual, wet and dry discharges with base condition for different climate change scenarios

6.3 Estimation of Backwater Effect

Coastal rivers like the Lower Meghna River will be significantly affected by the global warming induced sea level rise and associated backwater effect. Due to backwater effect, the water level along the river will rise and this change will be felt in the adjacent floodplains and further upstream of the river. The combined effect of rising sea water levels along with increased discharge due to climate change will cause higher water levels in those areas. Therefore for the present study, two conditions have been considered to analyze backwater effect along the Lower Meghna River –

- Condition 1 (C1): effect of sea level rise with less discharge during dry season
- Condition 2 (C2): effect of sea level rise and increased discharge during monsoon

The Lower Meghna River shows considerable spatial variation in water level. During the monsoon of base period 2008, the average water level varies from 1.22 mPWD near Hatiya to 4.62 mPWD near Chandpur with an average water surface gradient of 3

cm/km. In the dry period, the water level ranges between – 0.5 mPWD to 2.0 mPWD along various locations of the river. Variation of water levels of Lower Meghna River during the dry and monsoon season of base period is shown in Figure 6.3.

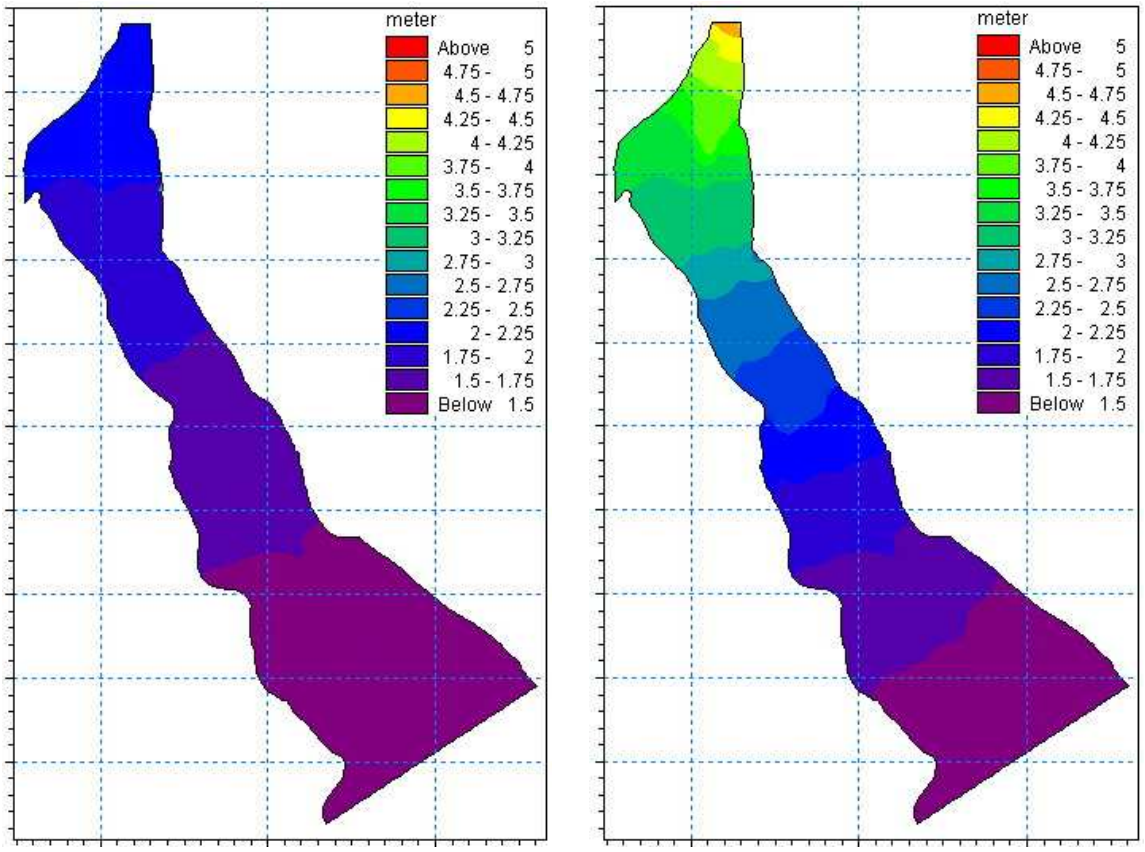

Dry season Wet season

Figure 6.3: Water level variation in the base period

Due to the combined effect of changed discharge and sea level rise, the water level increases and exhibits a substantial variation along different parts of the river for various climate change scenarios. Such variations of water level for the conditions mentioned above have been given in Figure C2a to C2c of Appendix C under scenarios A1FI, A1B and B1 respectively for different periods.

From the figures it is found that the water level slightly increases and remains almost same as base period for the dry season (Condition 1). Small variation occurs only due to the effect of sea level rise only under various climate change scenarios. However during monsoon (Condition 2), where both the effect of higher discharge and sea level rise have been considered, the water level increases significantly under different scenarios. For scenario A1FI, water level range of the river during monsoon raises upto 1.36 – 5.09 mPWD, 1.47 – 5.74 mPWD and 1.67 – 6.55 mPWD during the periods of 2020s, 2050s

and 2080s respectively. Similarly, these ranges for the monsoon season have been found as 1.35 – 4.85 mPWD, 1.46 – 5.25 mPWD and 1.61 – 6.12 mPWD for scenario A1B and 1.35 – 4.68 mPWD, 1.44 – 4.92 mPWD and 1.54 – 5.16 mPWD for scenario B1 during the same periods respectively.

The rise of water level due to the combined effect of discharge and sea level rise can be estimated by comparing the water levels of individual scenario and the water levels of the base period. This comparison can be made for both the dry and wet periods under various climate change scenarios. Such rises in water levels for the condition 1 (dry) and condition 2 (wet) have been illustrated in Figure 6.4 to 6.6 under scenarios A1FI, A1B and B1 respectively for 2020s, 2050s and 2080s.

A striking feature can be observed from the figures after comparing the water level rise due to backwater effect for both the conditions under various scenarios. It is seen that water level change due to backwater effect is more prominent in the dry season (condition 1) than the wet season (condition 2). During dry periods, the discharge is less for various scenarios, but the sea level continues to rise. The higher water level in the downstream propagates upward and elevates the water level considerably compared to base condition. In this case water level rise is directly affected by the sea level rise.

On the other hand during monsoon, the projected discharges are much higher compared to base period for various climate change scenarios. Therefore both the increased discharge and sea level rise contributes to the water level rise of the river. Although the rising levels of sea continue to increase, the higher discharge prevents the backing up of water due to sea level rise. Hence water level change is less during the monsoon when compared with the base period for various climate change scenarios.

Comparing the figures it is also evident that the water level rise at the downstream of the river remains same for both conditions and directly depends on the rising sea level. However in the middle and upper reach of the river, the change in discharge as well as the sea level rise contributes to raise the water levels and hence the variation between dry periods (condition 1) and wet periods (condition 2) are higher in these parts. In the upper part, the variation decreases as the effect of rising sea level, i.e. backwater effect is less in those regions.

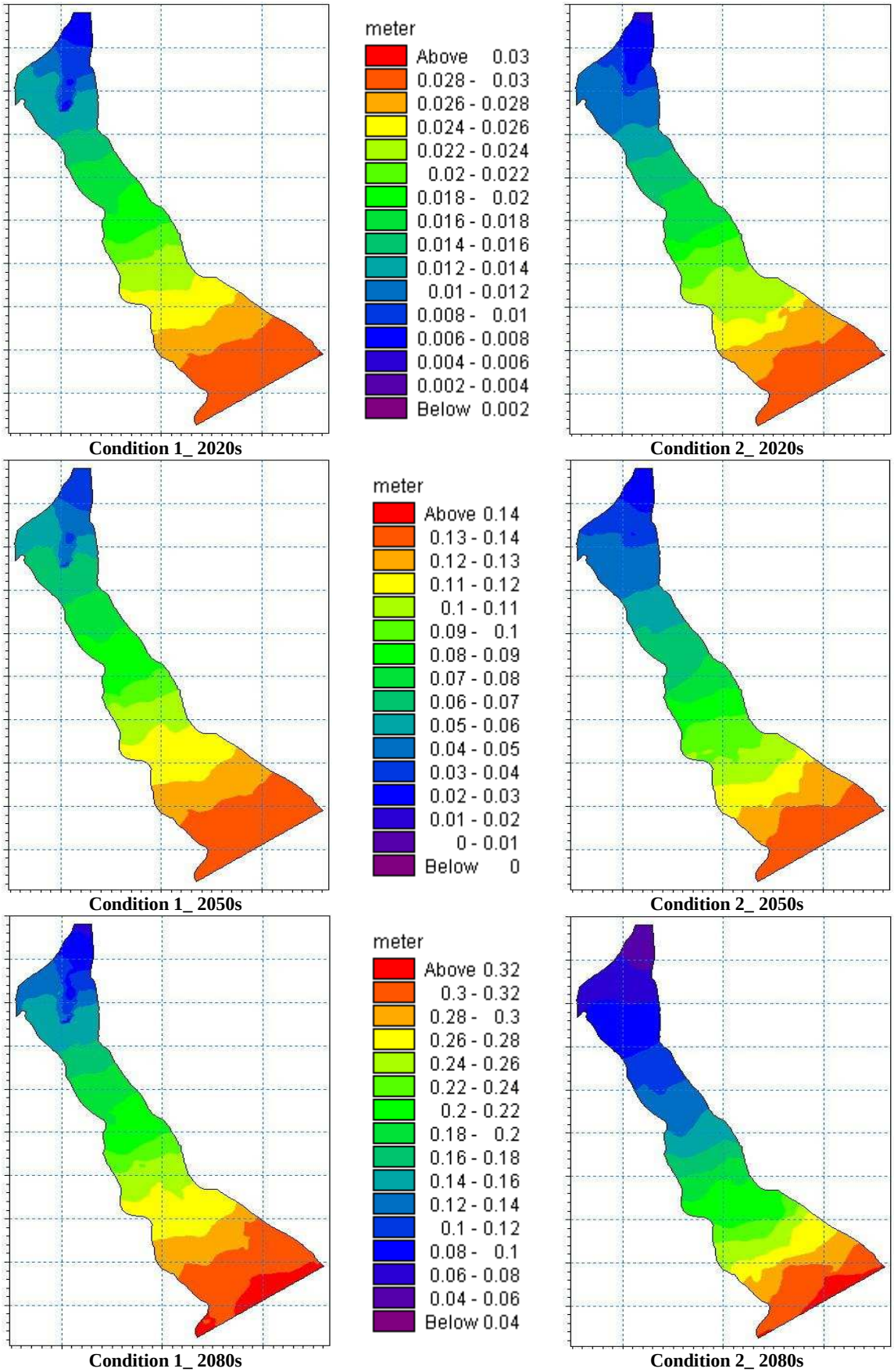

Figure 6.4: Backwater effect under scenario A1FI for different periods

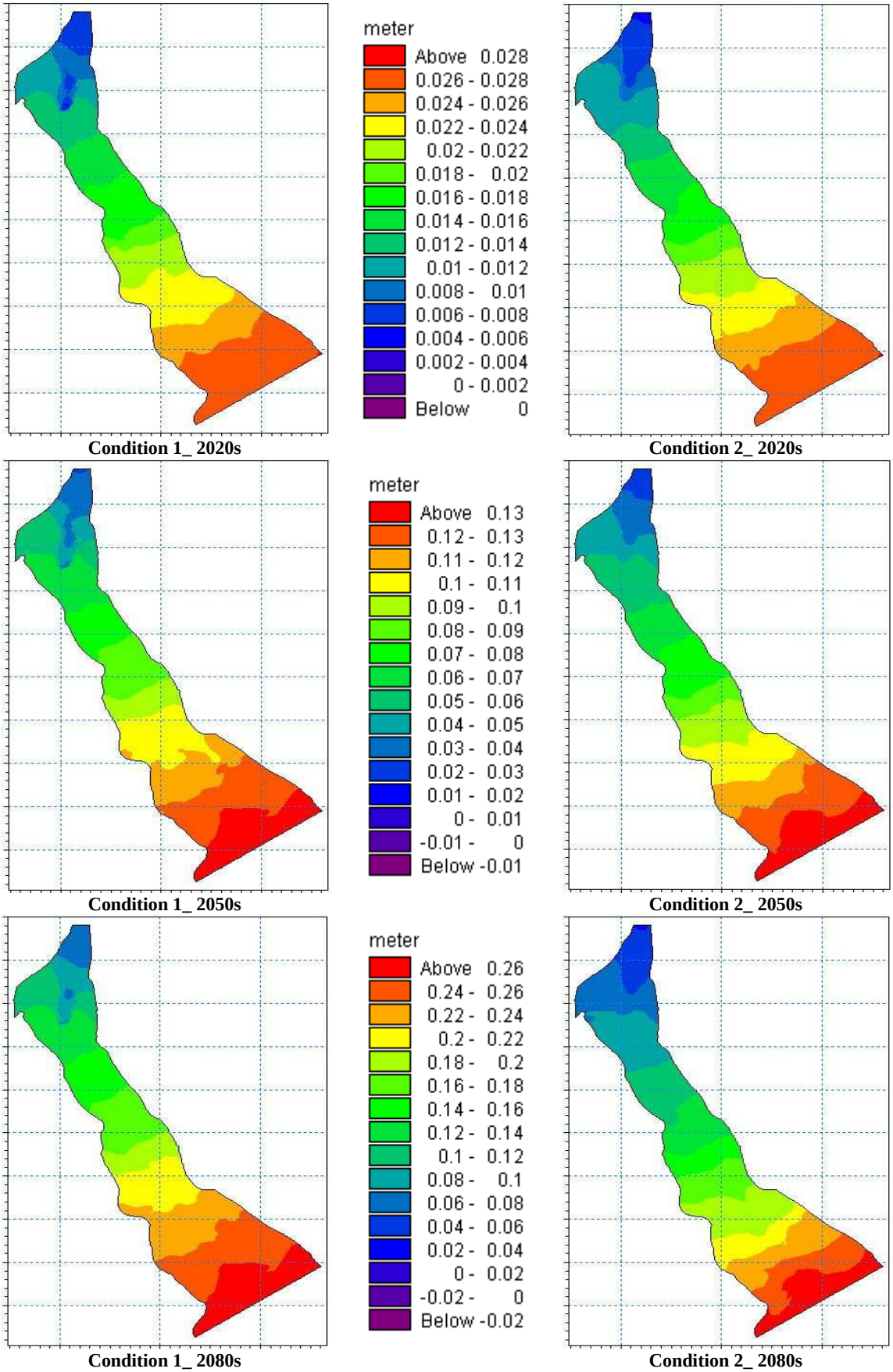

Figure 6.5: Backwater effect under scenario A1B for different periods

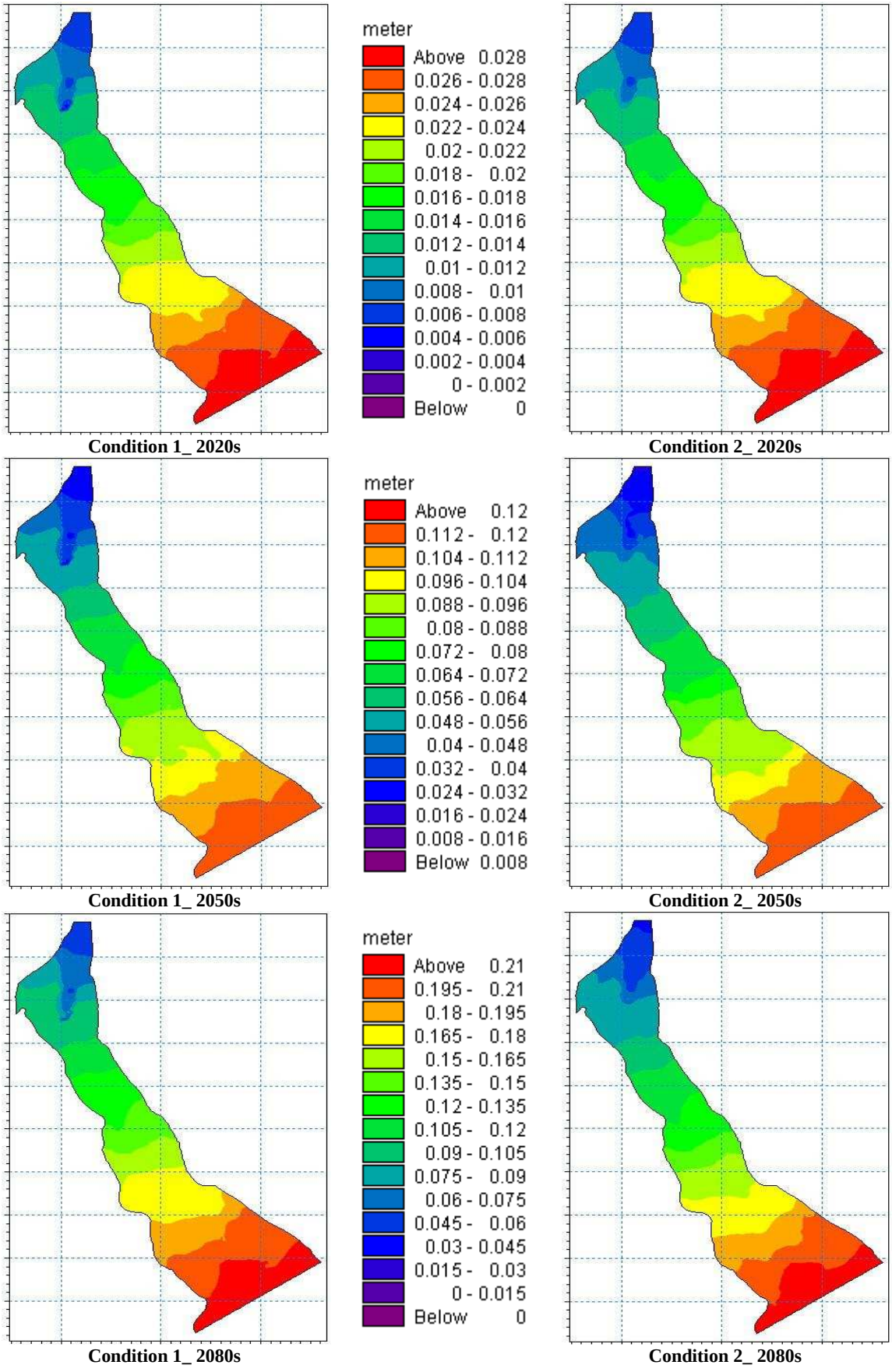

Figure 6.6: Backwater effect under scenario B1 for different periods

In the light of above discussion it can be said that the backwater effect will be more prominent during dry periods resulting in higher water levels along the river. Figure 6.7 shows the water level rise due to backwater effect along the river profile considering both conditions for the scenarios A1FI, A1B and B1. From this figure it can be found that the water level rise for both conditions during 2020s is almost same for all the scenarios. During 2050s and 2080s, the water level rise for condition 1 (dry period) is greater than condition 2 (wet period). This is because during 2020s, the discharge is not too higher compared to base condition and sea level rise is the dominant factor to produce higher water levels along the river. After that during 2050s and 2080s, the discharge increases considerably with respect to base period and contributes greatly to raise the water levels. This decreases the backwater effect considerably. Hence the backwater effect due to the combined effect of higher discharge and sea level rise is much lower when compared with the effect of the sea level rise with low discharge.

For scenario A1FI, considering sea level rise during dry season (condition 1) the average water level rise is 1.8 cm, 8.6 cm and 20.4 cm during the periods 2020s, 2050s and 2080s respectively. Imposing both higher discharge and sea level rise during monsoon (condition 2), the values can be found as 1.7 cm, 7.3 cm and 15.5 cm respectively. Likewise, scenario A1B and B1 shows that the water level rise for condition 1 is greater than that of condition 2. Maximum water level rise has been found as 16.9 cm for scenario A1B and 13.5 cm for scenario B1 during the dry periods of 2080s. These results are shown in Table 6.2.

Table 6.2: Average water level rise (cm) due to backwater effect

Scenario	2020s		2050s		2080s	
	Dry period	Wet period	Dry period	Wet period	Dry period	Wet period
A1FI	1.8	1.7	8.6	7.3	20.4	15.5
A1B	2	1.7	8.3	7.9	16.9	13.8
B1	2.1	1.8	7.3	7.1	13.5	12.9

From Table 6.2 and Figure 6.7 it is clear that the water level rise due to rising sea level rise induced backwater effect is maximum for scenario A1FI as a result of higher discharge and greater rate of sea level rise. For scenario A1B and B1, these rises are less resulting from lower discharge and slower rate of sea level rise compared to scenario A1FI.

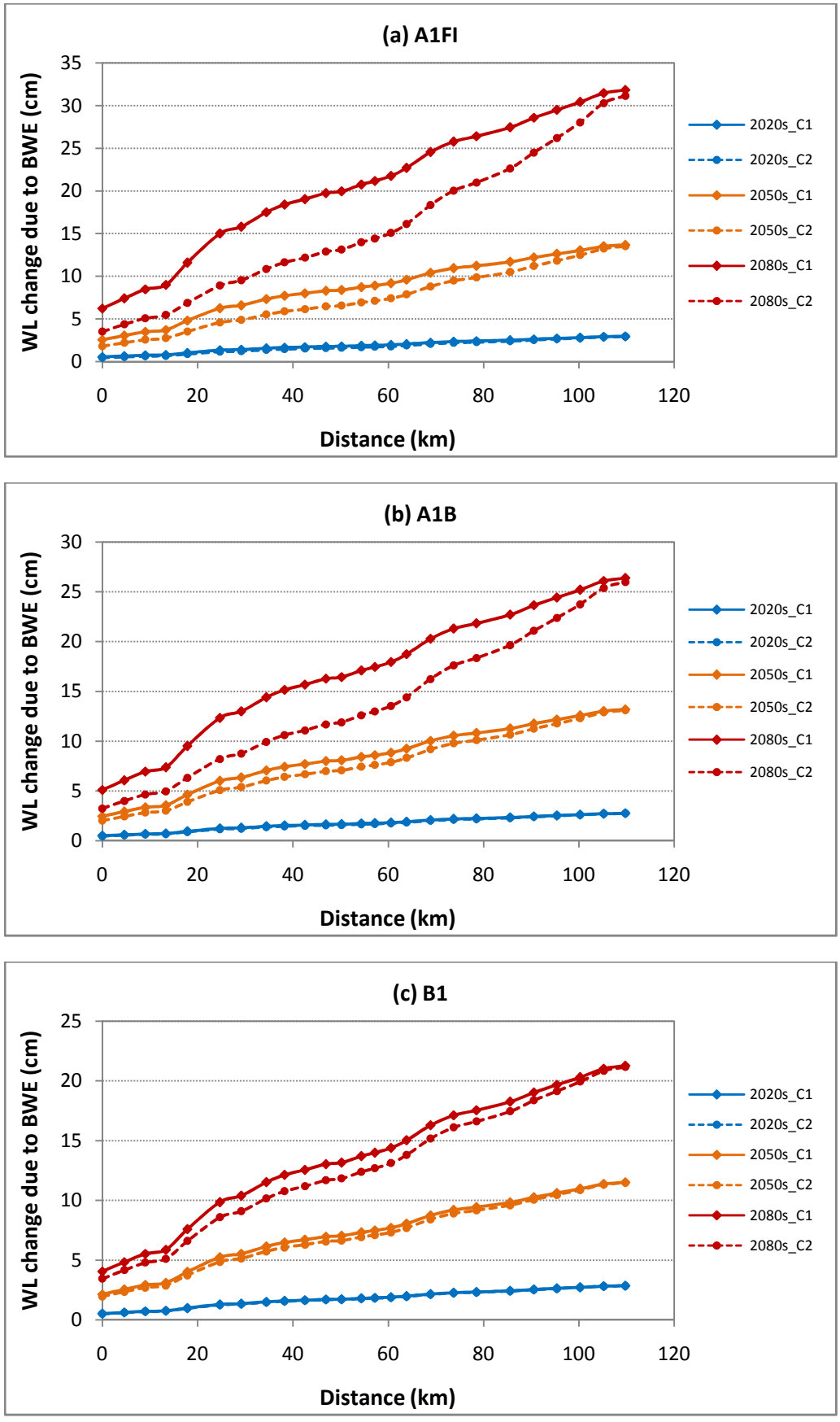

Figure 6.7: Water level change due to backwater effect for different scenarios

From Table 6.2 and Figure 6.7 it is clear that the water level rise due to rising sea level rise induced backwater effect is maximum for scenario A1FI as a result of higher discharge and greater rate of sea level rise. For scenario A1B and B1, these rises are less resulting from lower discharge and rate of sea level rise compared to scenario A1FI.

As the water level of the river rises, the water surface gradient also changes for various climate change scenarios. The discharge associated with sea level rise causes the water levels to rise in the middle and upper reach of the river. The result is the gradual change of water surface gradient for various climate change scenarios. The water surface gradient is much flatter during the dry periods as a result of lower discharge and higher level of sea. These gradients decrease gradually with time due to progressive sea level rise. Therefore backwater effect becomes prominent in this period. During monsoon, increased discharge elevates the upstream water level and causes the water surface to become much steeper. In this case backwater effect is less. The changes in water surface gradients due to backwater effect for various scenarios have been given in Table 6.3.

Table 6.3: Change of water surface gradient due to backwater effect

Scenario	Water Surface Gradient (cm/km)					
	Dry period			Wet period		
	2020s	2050s	2080s	2020s	2050s	2080s
A1FI	2.98	2.91	2.78	3.40	3.89	4.44
A1B	2.99	2.91	2.82	3.19	3.45	4.11
B1	2.98	2.92	2.86	3.04	3.17	3.29

The extent of backwater effect depends on these gradients. From Figure 6.7 and Table 6.3 it is evident that the extent of backwater effect increases from downstream of the river. This extent of such effect can be felt further upstream of the river.

6.4 Assessment of Bed Level Changes and Siltation Rate

The morphology of the Lower Meghna River reacts to changes in the upstream input of water and sediment resulting in a change in the intensity of erosion and deposition. The channel is very dynamic due to the active processes of accretion and erosion of the channel beds and banks. Natural shifting of the channel, development of large chars, formation of deep pocket zones, shoaling effect etc. are the important features of morphologic changes along with the overall erosion-deposition process. These processes

affect the siltation rate and cause long term morphologic changes of the river. Figure 6.8 shows the bathymetry of Lower Meghna River for the base period of 2008.

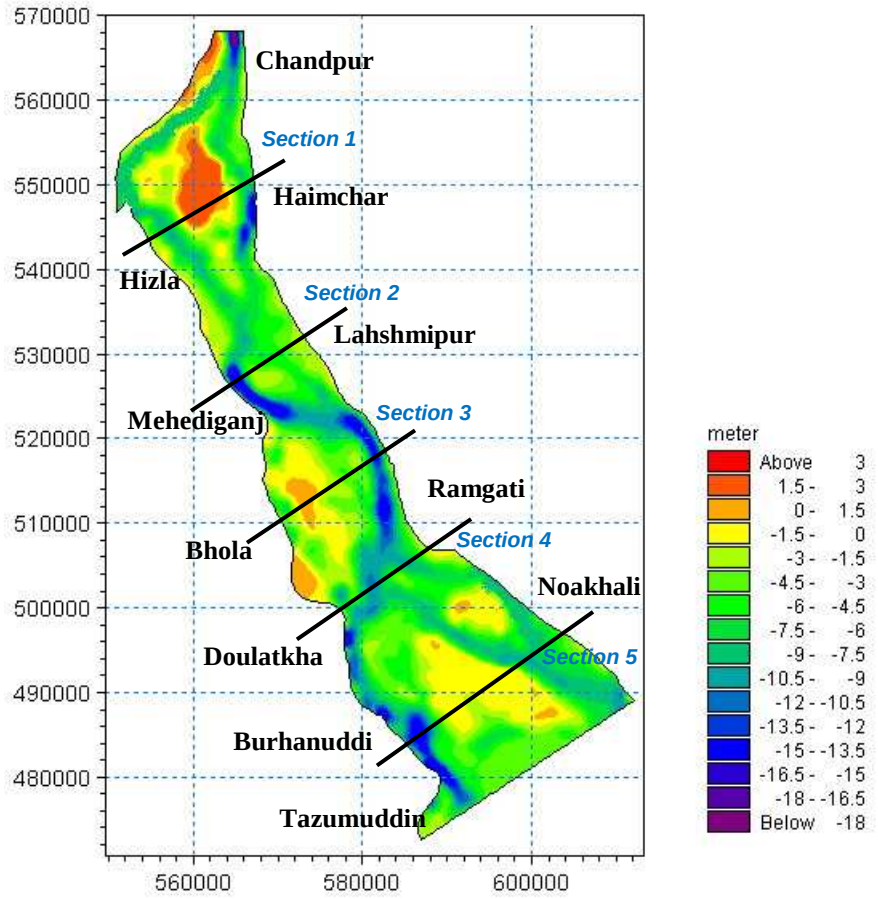

Figure 6.8: Bathymetry of the river for base period and selected cross sections

The figure shows that the river gets divided into two branches in its upstream near Chandpur. Near Mehediganj these two branches meet again and the main channel follows a curved path upto Bhola. At Doulatkhan there exist three channels due to presence of Char Gazaria and some other small islands. These features play an important role on the morphology of the river. For a clear understanding of erosion-deposition patterns and consequent bed level changes for different periods, five cross sections have been selected and analyzed. These are also shown in Figure 6.8.

Due to climate change and sea level rise, the discharge and water level of the Lower Meghna River will be affected. Such changes will disrupt the existing equilibrium of water and sediment transport through the channel and will trigger new hydraulic and morphologic state of the river. The process of deposition-erosion and consequent bed level changes of the river will vary according to the conditions of water and sediment

movement through the channel for various climate change scenarios. Such process is also influenced by the velocity pattern of the river. The velocity variation along with their direction of Lower Meghna River for the base period is shown in Figure 6.9a.

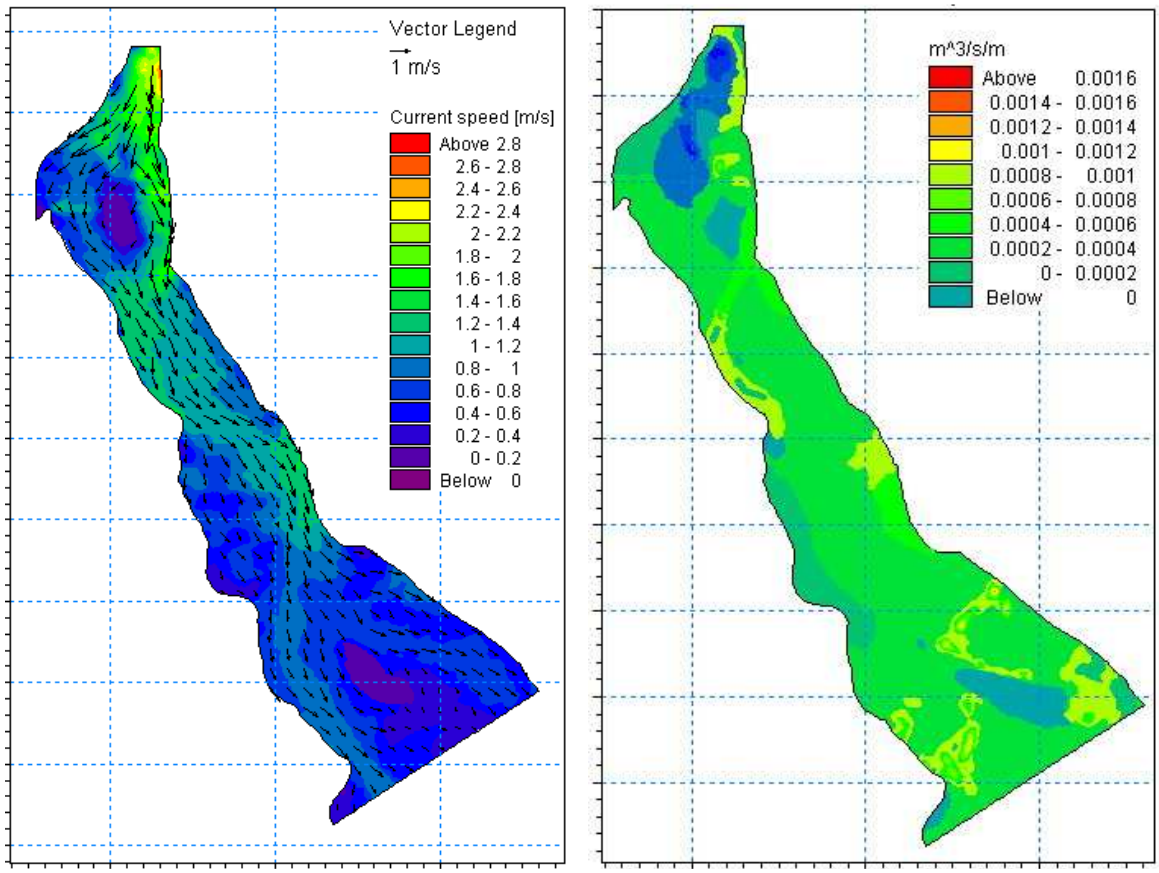

(a) Velocity (b) Sediment Transport

Figure 6.9: Velocity and sediment transport variation of the river for base period

From the figure it is evident that the velocity is very high near the left bank of the river at Chandpur. Higher velocity is also observed along the curved main channel near Mehediganj, Bhola and Ramgati. Then the channel gets divided and main channel passes through the right bank at Burhanuddin. These are the zones which are expected to be eroded. On the other hand, the right bank of Char Haim, the lower middle and lower part of the river shows comparatively less velocities. Specially the lower reach of the river near Char Gazaria shows significant reduction of velocity. These are the zones where deposition is expected to be the dominant morphologic process. The erosion-deposition induced morphological changes are also affected by the sediment transport capacities of the river. Higher discharge and resulting greater velocities carry large amount of sediment and hence increase the sediment transport capacities of the river. These sediments are deposited where the velocity is low resulting in bed level rise of the

channel. Figure 6.9b shows the total sediment transport rate of Lower Meghna River for the base period 2008.

From the figure it is seen that the sediment transport of the river varies spatially and this process is influenced by the local bathymetry and associated discharge and velocity. For the base condition, the transport rate varies between 0.0002 m^2/s and 0.006 m^2/s with an average of 0.00031 m^2/s. This rate changes if the discharge and other conditions are changed. The average sediment transport rate of Lower Meghna River for various climate change scenario are given in Table 6.4.

Table 6.4: Sediment transport rate of the river for various climate change scenarios

Scenario	Sediment Transport Rate ($m^3/s/m$)		
	2020s	2050s	2080s
A1FI	0.00052	0.00094	0.00078
A1B	0.00041	0.00075	0.00081
B1	0.00031	0.00037	0.00039

The morphology of Lower Meghna River is affected by the variation of discharge, velocity and sediment transport capacities as mentioned above. For various climate scenarios, these variables change resulting in different morphologic responses of the river to climate change. However such changes were assessed only for the projected years of 2020s, 2050s and 2080s rather than considering continuous years upto 2080 due to the limitation of the model.

Scenario A1FI is characterized by both erosion-deposition of the river. Due to high discharge, severe erosion takes place along the main channel of the river. The excess discharge also carries large amount of sediments which are deposited on other parts of the river. As seen from Figure 6.10, gradual deposition occurs upto period 2080s. Deposition near the char areas, formation of deep pocket zones and development of deep channels are the significant morphologic features for this scenario. These processes can be better understood by analyzing the selected cross sections on the river. These sections along with their projected bed levels for different periods are shown in Figure 6.11.

In the upper reach of the river, there is a small island (char) near Haimchar. This island normally remains dry during low flows and flooded during monsoon seasons. For the base condition, the main channel was passing through the left side of the river. In the

subsequent years, i.e. for 2020s, 2050s and 2080s, it is clear from the Figure 6.10 that the left channel of the island has undergone severe erosion and the right channel has become more silted. Deposition occurs along the right side of the island increasing the area of the island. Section 1 (Figure 6.11a) also indicate the same finding that the left channel has gone about 8 m erosion for the period 2080s with respect to base period. The left bank of the island has showed a lowering of its surface by 0.5 to 1 m, while the right bank showed 1.5 m deposition. So the island tends to move towards right bank of the river due to progressive erosion along the left side and deposition on the other side.

The main channel exhibits meandering behavior and forms bends along the middle reach of the river. Due to bends, severe erosion takes place on the right bank near Mehediganj and left bank near Ramgati. Zones of deep pockets are formed in these parts. Consequently, deposition occurs on the opposite banks of the river. Near Mehediganj (Section 2, Figure 6.11b) deep pockets are formed due to 6 m erosion along the right bank. Around 4 to 5 m deposition has been observed near the left bank of the river. This deposition enforces the main flow of the river through its left and middle side resulting in large erosion and formation of deeper channel in the middle portion. A similar but opposite pattern of deposition-erosion has been observed in Section 3 (Figure 6.11c) near Ramgati. The right side of the channel near Bhola was almost silted up due to heavy deposition. This diverts the flow towards left side of the channel resulting in erosion of approximately 3 m and 5 m in the middle and left portion respectively. The bed level of left side may lower upto 18 mPWD creating deep pockets along the left bank of the river.

Huge deposition takes place along the lower reach of the river as was observed from Figure 6.7. This occurs due to reduced sediment transport capacity of the river as well as strong backwater effect. Near Doulatkhan (Section 4, Figure 6.11d), the middle portion of the river gets around 5 m higher during 2080s compared to base condition. Siltation of about 3 m is also observed along the left bank of the river. The right bank undergoes approximately 3 m erosion in this case. After Doulatkhan, the main channel splits and water flows along three channels towards downstream of the river. At further downstream huge deposition occurs around Char Gazaria and the surface of the island becomes 1 to 2 m higher (Figure 6.11e). Deposition also takes place along the left bank of the river. To compensate this deposition, most of the flow is concentrated towards the right channel which undergoes severe erosion of about 5 m. Therefore deep pockets are formed along the right bank of the river near Burhanuddin.

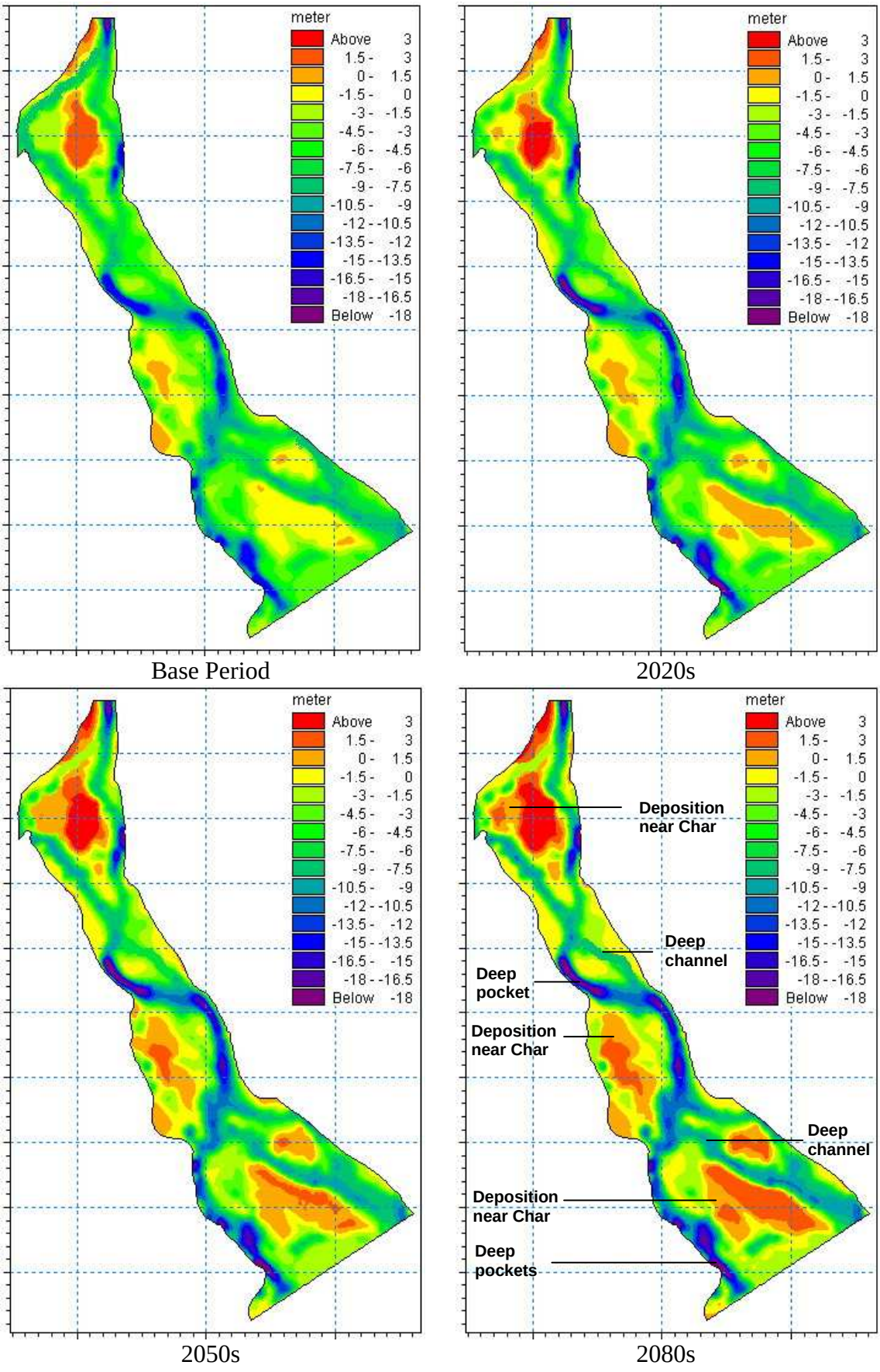

Figure 6.10: Bed level changes under scenario A1FI for different periods

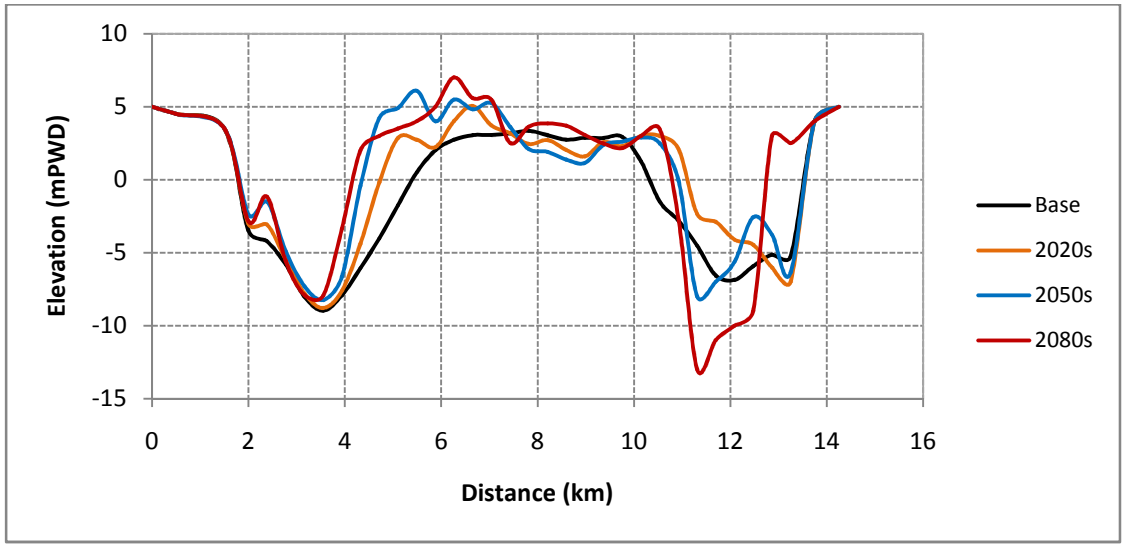

(a) Section 1

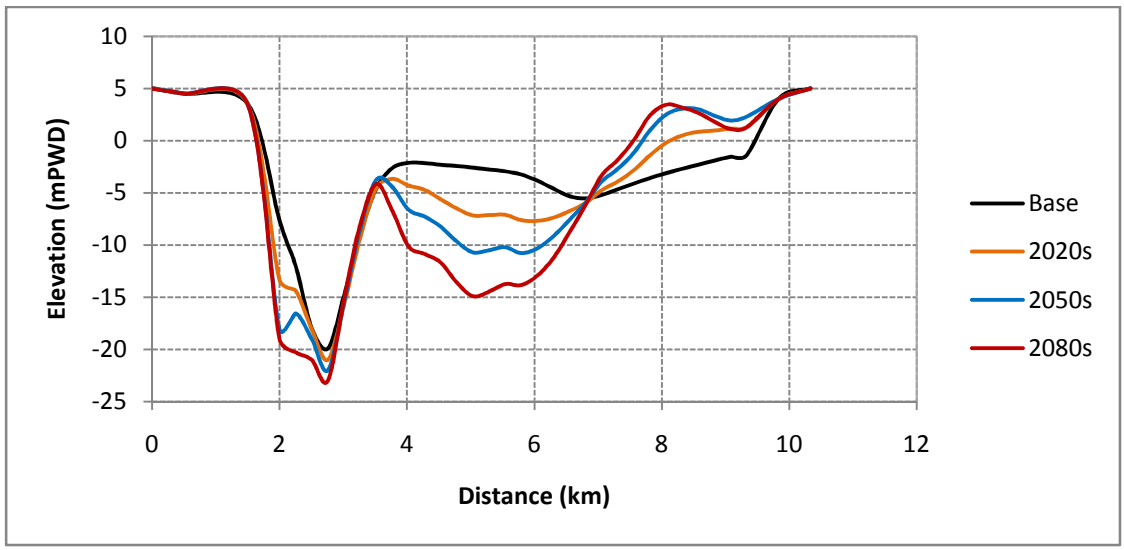

(b) Section 2

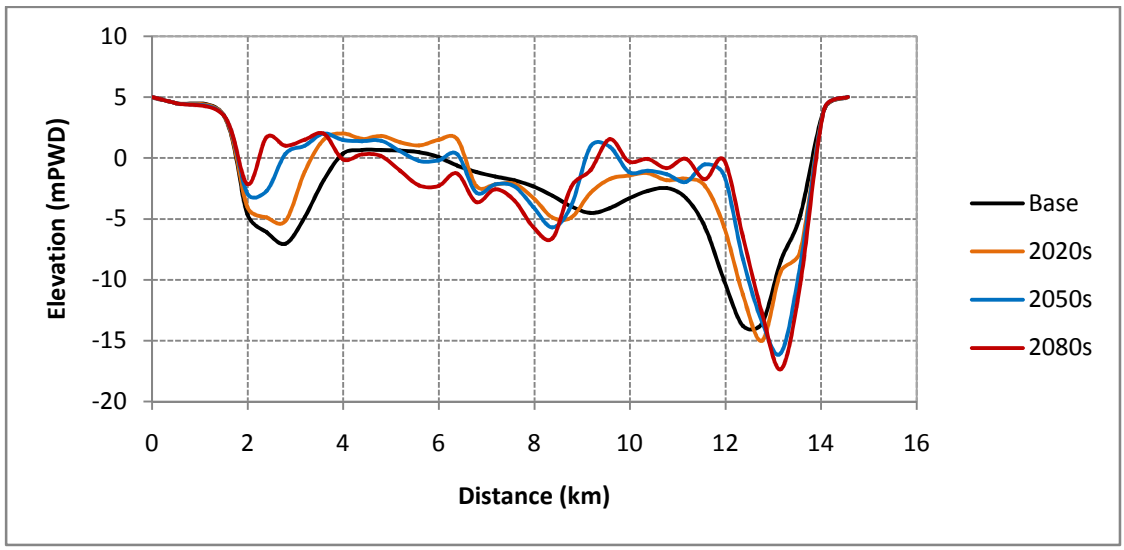

(c) Section 3

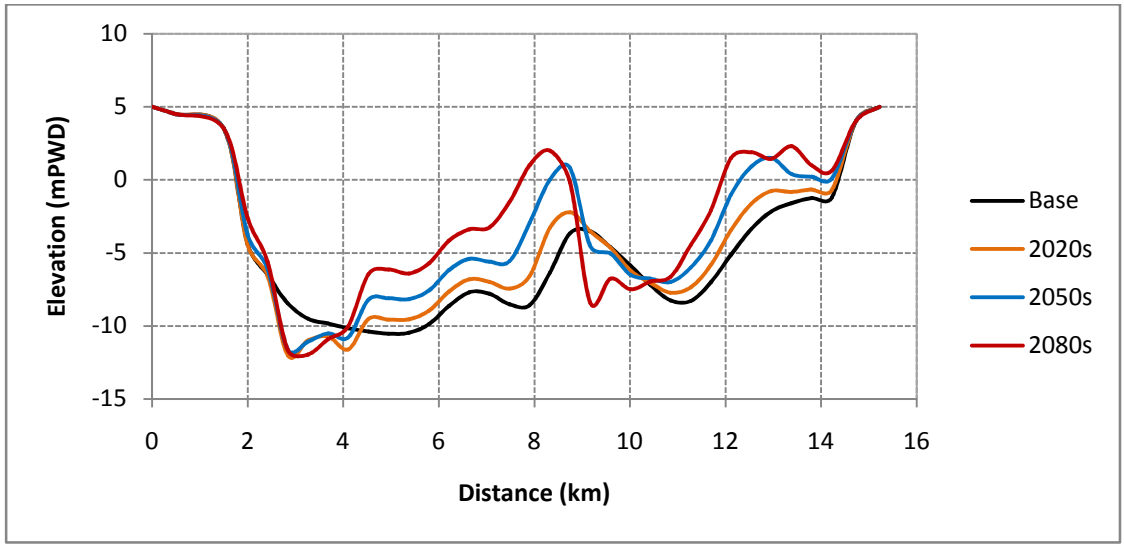

(d) Section 4

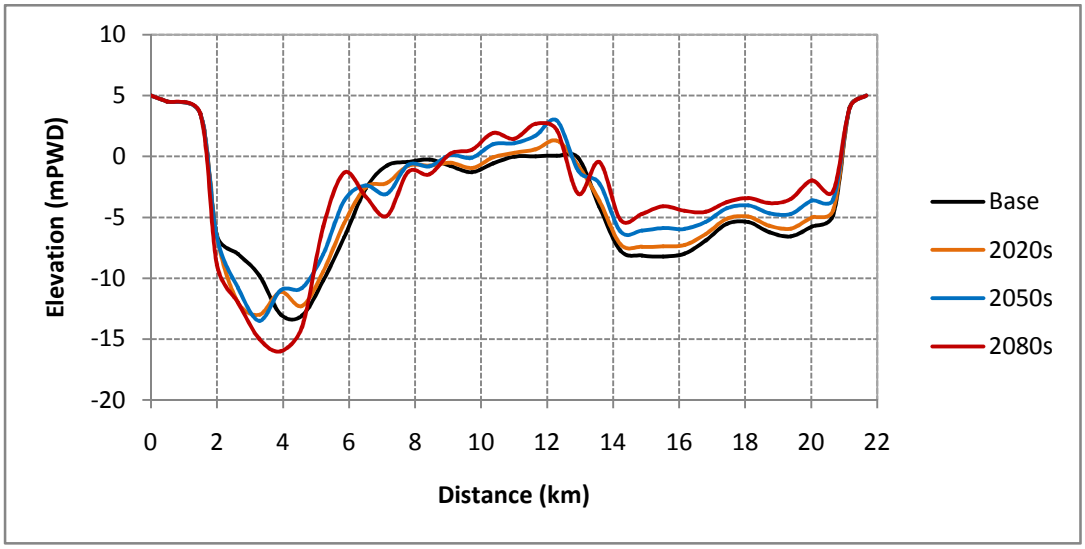

(e) Section 5

Figure 6.11: Cross sectional changes under scenario A1FI for different periods

For scenario A1B, deposition is the dominant process with less erosion for different periods compared to A1FI. The reduced discharge relative to A1FI with high sediment input causes heavy deposition along different parts of the river. As seen from Figure 6.12, deposition around Char areas, development of new Chars and formation of point bars and alternative bars are the significant morphologic changes for this scenario. These processes along with the resulting bed level changes with time under scenario A1B have been illustrated in Figure 6.13 for the selected cross sections of the river.

Near Haimchar in the upper portion of the river, huge deposition takes place in the right channel as well as along the right side of the Char. The right channel near Hizla is silted

upto 5 m and right side of the char becomes 2 to 3 m higher compared to base condition (Section 1, Figure 6.13a). Hence the Char area increases considerably upto period 2080s. The main channel flow is diverted towards the left channel resulting in an erosion of 4 to 5 m. From Figure 6.9 it is also evident that the Char increases in length downward due to continuous deposition in the lower part of the char.

In the middle reach of the river, formation of different types of channel bars such as point bars and alternative bars are observed near Lakshmipur, Mehediganj, Ramgati and Bhola as a result of progressive deposition along the banks of those regions (Figure 6.12). Section 2 located near Lakshmipur shows that the left portion of the river is almost silted upto 2 to 3 m forming channel bar along the left bank of the river (Figure 6.13b). The water flows through the right and middle portion of the section causing slight erosion in the right side and 3 to 4 m erosion along the mid portion of the river. At Ramgati (Section 3, Figure 6.13c) deposition occurs in the right channel as well as around the Char areas near Bhola. The right channel bed raises upto 2 to 3 m and the surface of the Char increases upto 1 mPWD due to this deposition.

The process of deposition increases in the lower part of the river as a result of reduced sediment transport capacity and backwater effect. Near Doulatkhan the river bed rises upto 5 m due to heavy siltation in the middle portion of the section (Section 4, Figure 6.13d). The left channel undergoes excess deposition of about 3 m along the left bank indicating the formation of a channel bar near Ramgati. Near Burhanuddin (Section 5, Figure 6.13e), the surface of Char Gazaria becomes approximately 1 m higher due to sediment deposition. Both the left channel and right channel of this char undergoes a deposition of about 2 to 3 m with respect to base period. Siltation of about 4 m is also observed along the left bank of the river. This indicates the development of a channel bar along the left bank near Noakhali which verifies the same findings as was seen from Figure 6.12. As a result of such formation of channel bar and large deposition in the river beds, the conveyance area decreases and most of the flow is concentrated towards the right channel which undergoes erosion of about 1.5 m.

From Figure 6.12 it is also evident that extreme deposition occurs at lower part of the river specially at the downstream of Char Gazaria. The backwater effect and higher water levels due to sea level rise impedes the natural drainage of the river in those regions. Therefore the sediment transport capacity of the river reduces considerably which enforces the sediments to deposit around the lower parts of the river.

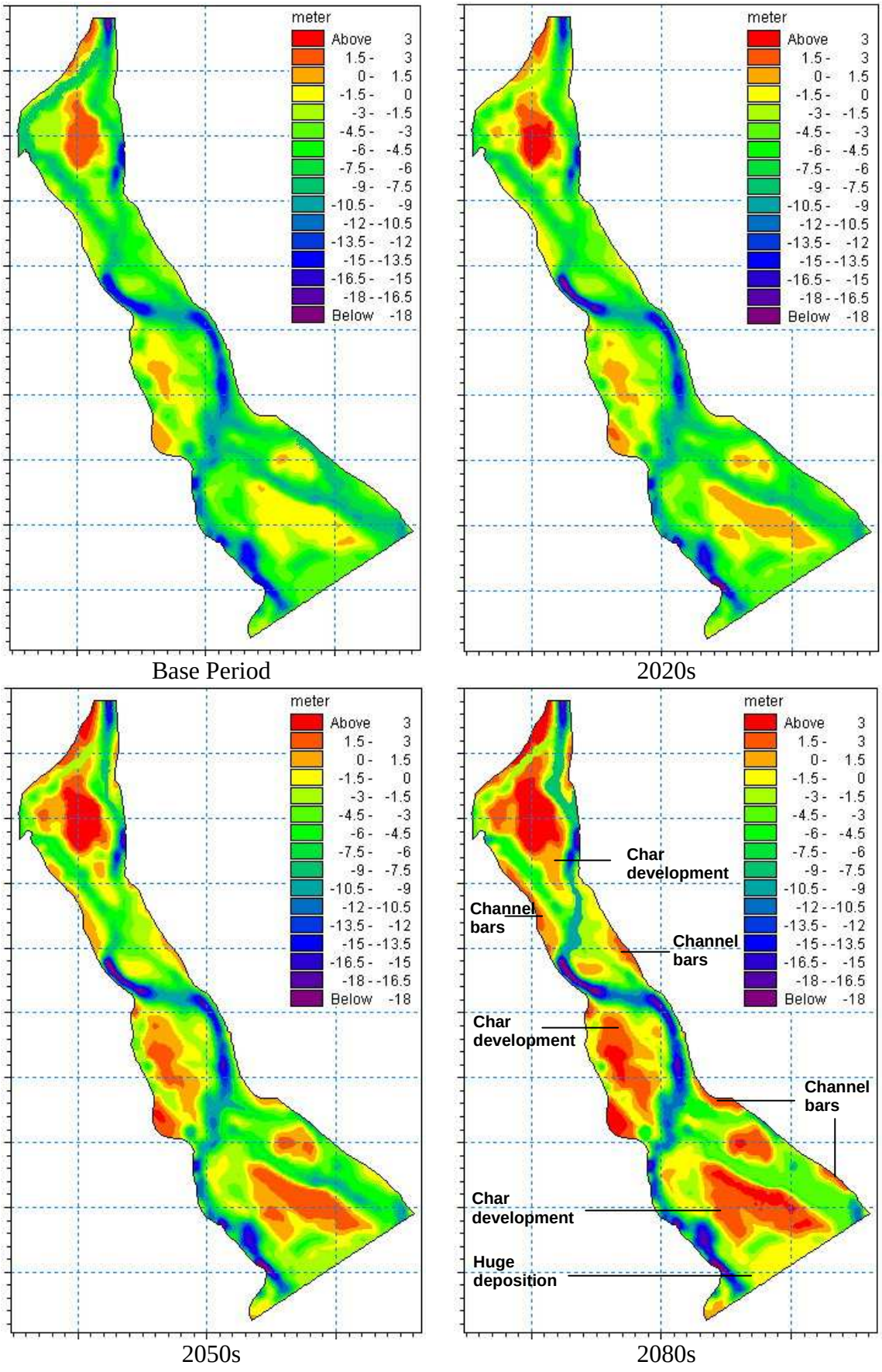

Figure 6.12: Bed level changes under scenario A1B for different periods

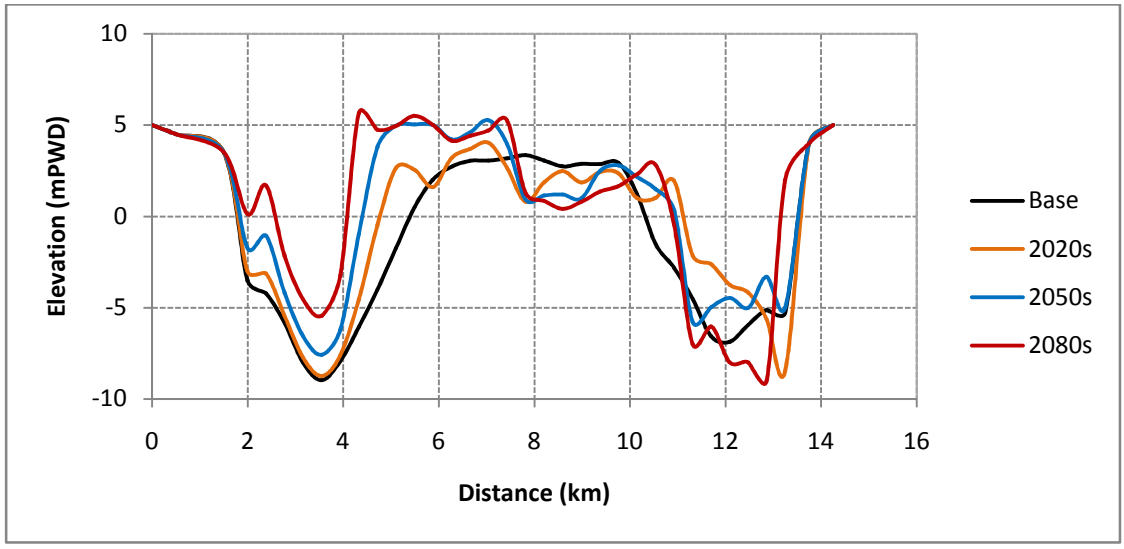

(a) Section 1

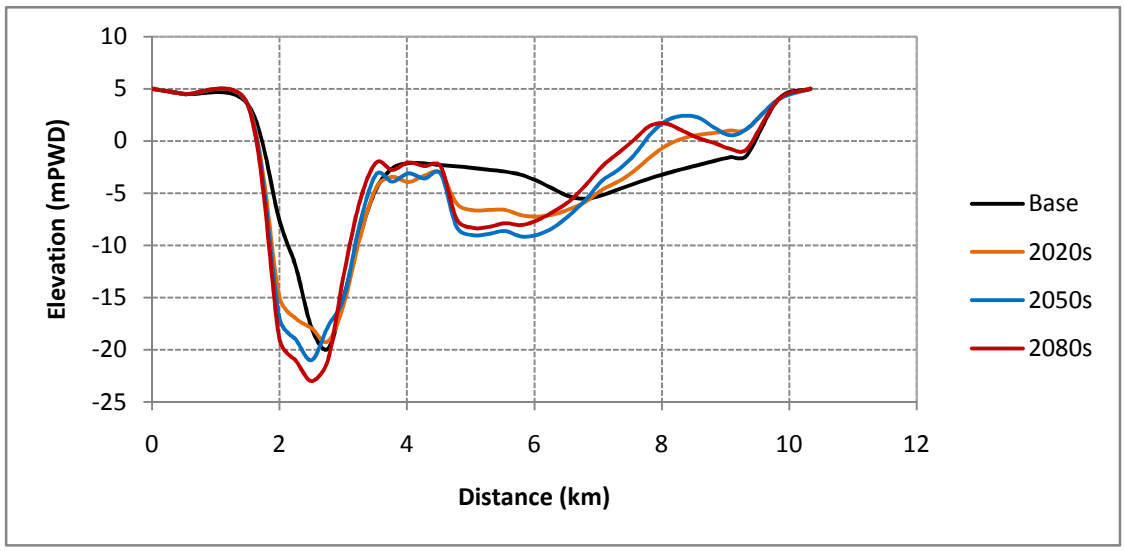

(b) Section 2

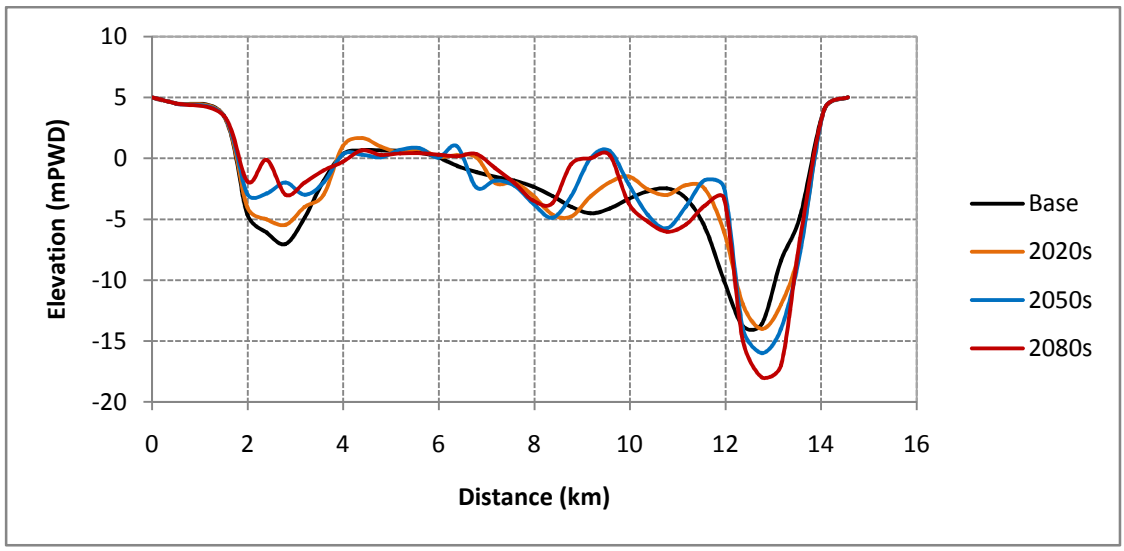

(c) Section 3

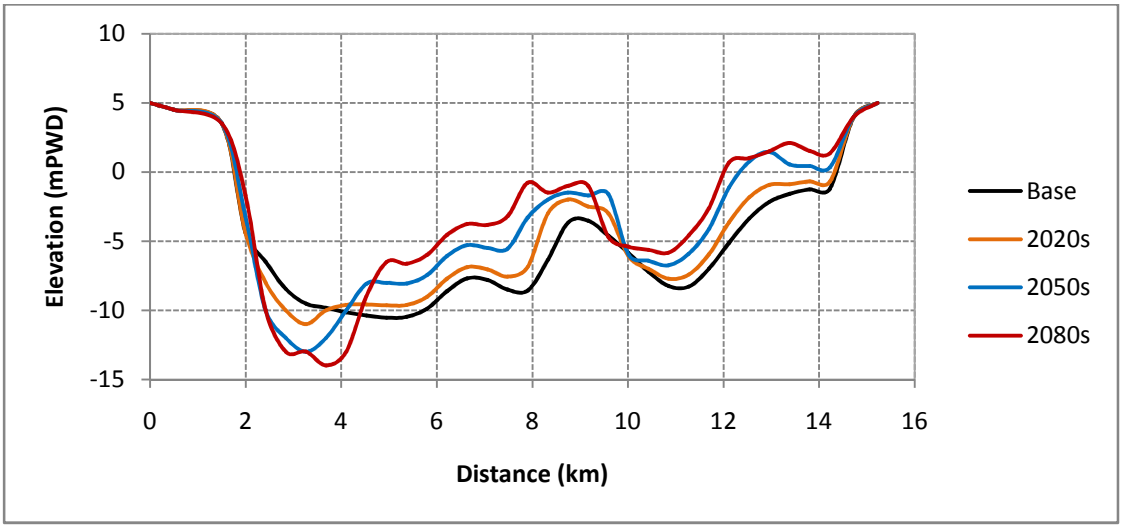

(d) Section 4

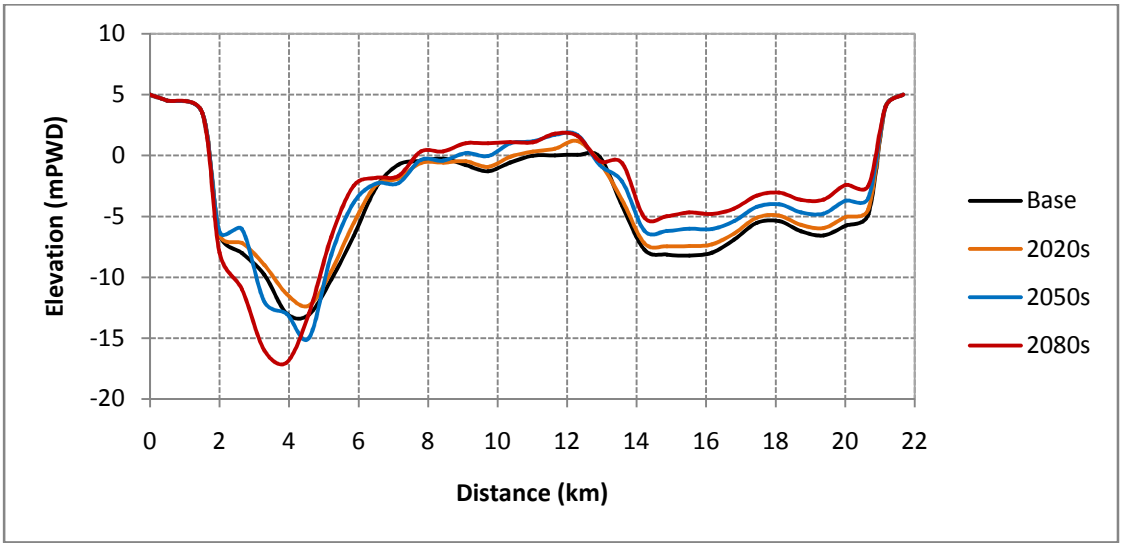

(e) Section 5

Figure 6.13: Cross sectional changes under scenario A1B for different periods

Gradual deposition occurs under scenario B1 for different periods. The deposition-erosion pattern and resulting bed level changes are more moderate for this scenario due to less discharge and sediment transport capacities of the river compared to scenarios A1FI and A1B. From Figure 6.14 it is seen that overall deposition occurs around the char areas of Haimchar, Bhola and Char Gazaria and along the lower portion of the river. Figure 6.15 depicts the anticipated bed level changes of the selected sections for different periods. At Haimchar (Section 1) the right channel remains stable while the left channel undergoes deposition and erosion of about 4 m and 3 m respectively for 2080s. Near Lahshmipur (Section 2), 3 m erosion at middle and 2 m deposition at the left channel has been observed. For sections 3, 4 and 5, an overall maximum deposition of 2 to 4 m with erosion upto 2 m can be found for different periods compared to base period.

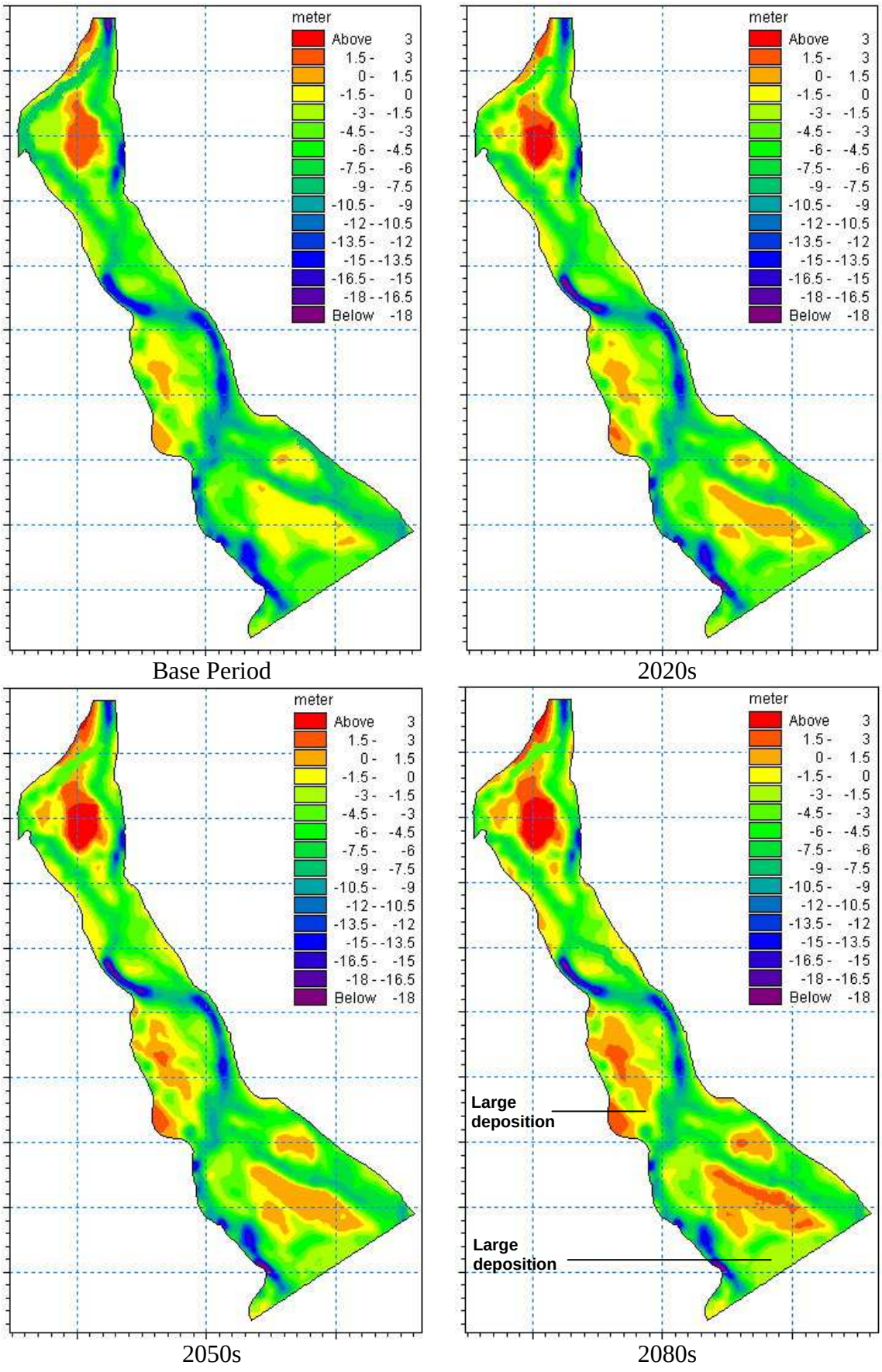

Figure 6.14: Bed level changes under scenario B1 for different periods

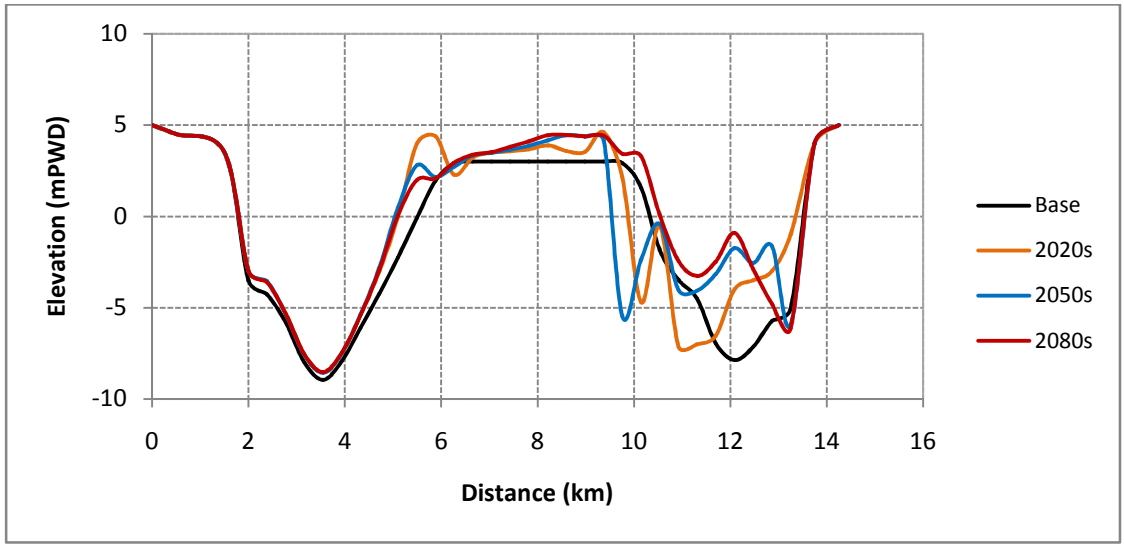

(a) Section 1

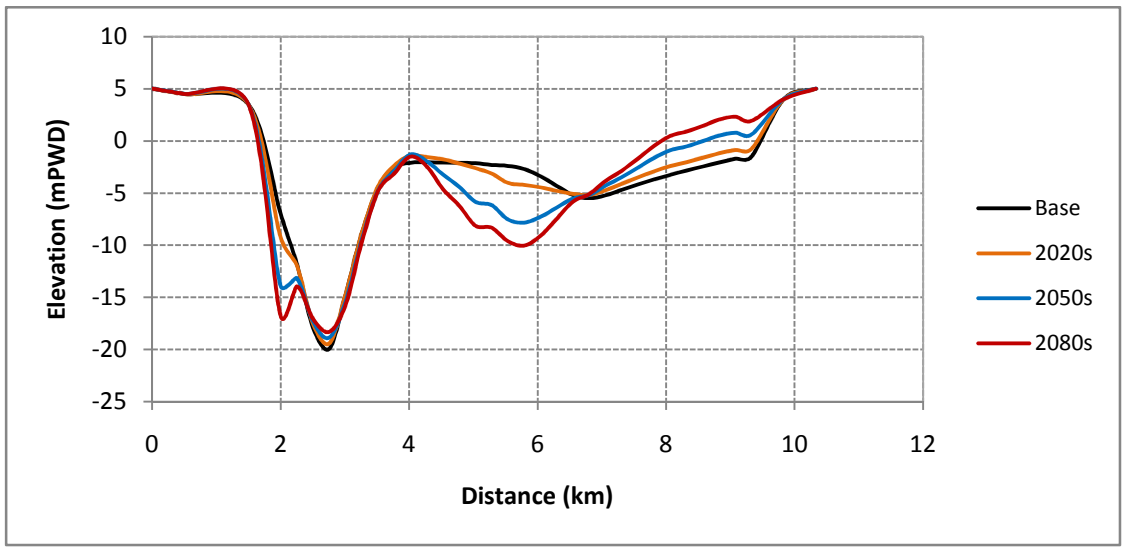

(b) Section 2

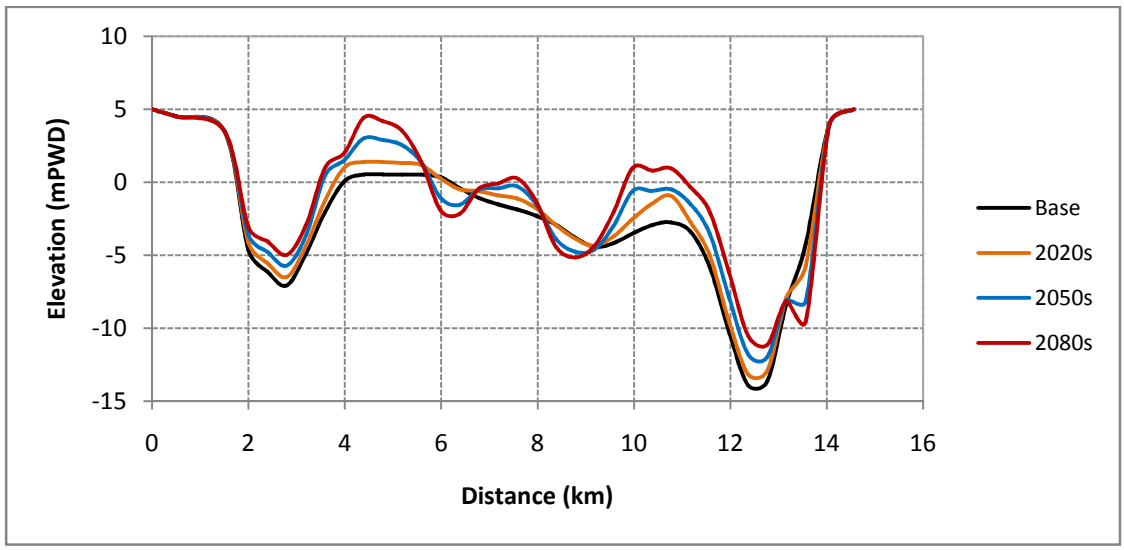

(c) Section 3

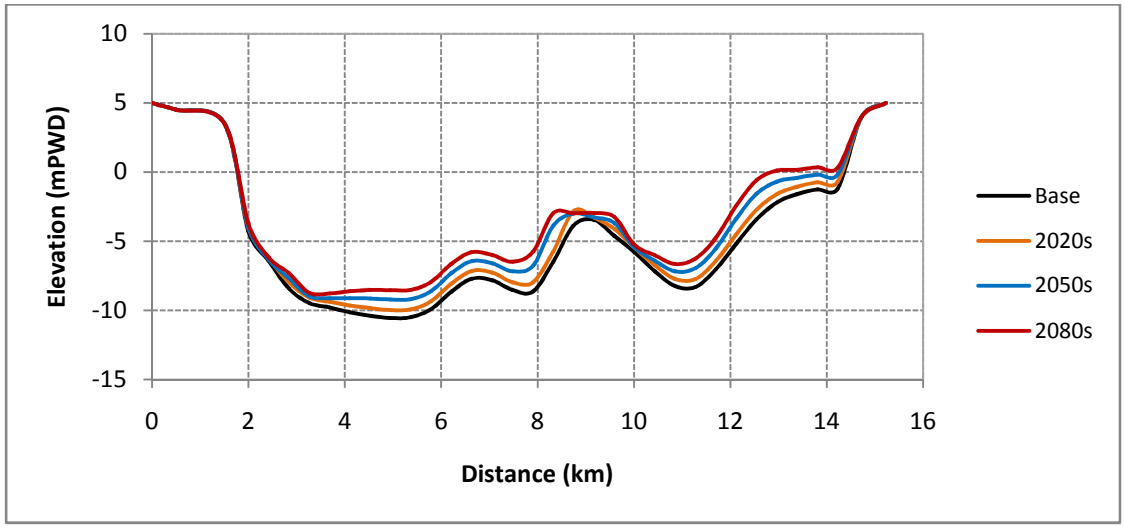

(d) Section 4

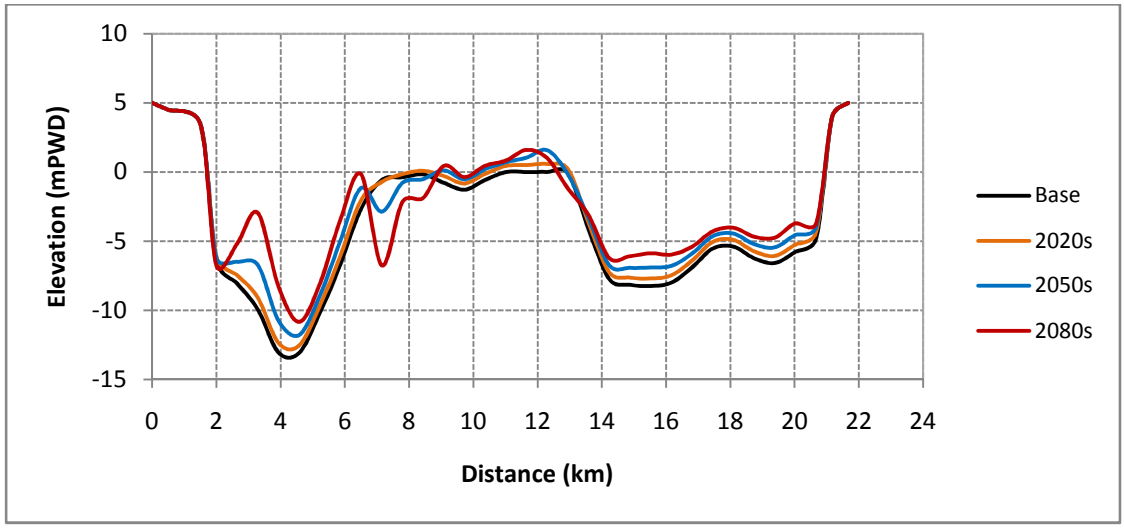

(e) Section 5

Figure 6.15: Cross sectional changes under scenario B1 for different periods

Beside the local erosion-deposition of different points in each individual cross section, the net erosion or deposition for any section can also be determined by comparing the net changes of area between the base period and the concerned periods for various climate change scenarios. Table 6.5 elaborates the net deposition or erosion of the selected cross sections for the periods of 2020s, 2050s and 2080s under scenarios A1FI, A1B and B1. From the table it is found that net deposition occurs in all the sections except Section 2 where gradual erosion takes place for different periods. For A1FI, the net deposition compared to base period is about 0.91 m, 1.67 m and 2.44 m for the periods of 2020s, 2050s and 2080s respectively. Similarly, net depositions of about 0.71 m, 1.85 m and 2.71 m for scenario A1B and 0.60 m, 0.94 m and 1.40 m for scenario B1 have been found during the stated periods respectively. Hence an overall net deposition occurs along the Lower Meghna River for various climate change scenarios. The whole process

can be rationalized as a deposition dominated morphologic change due to climate change and sea level rise.

Table 6.5: Bed level changes for the selected sections under various scenarios

Scenario	Section	Maximum Deposition (m)			Maximum Erosion (m)			Net Deposition/ Erosion (m)		
		2020s	2050s	2080s	2020s	2050s	2080s	2020s	2050s	2080s
A1FI	1	2.14	4.40	4.92	-1.72	-3.48	-5.65	0.91	1.25	1.39
	2	1.49	3.21	2.70	-3.20	-5.68	-4.75	-0.65	-1.10	-2.06
	3	3.41	4.40	5.51	-1.66	-2.92	-2.11	0.51	1.06	0.90
	4	3.07	4.05	4.64	-0.35	-3.88	-1.01	0.65	1.67	2.44
	5	2.29	2.78	3.11	-0.89	-2.28	-1.41	0.45	1.30	1.79
A1B	1	2.28	4.74	6.81	-2.48	-3.19	-3.64	0.64	1.42	1.81
	2	2.24	3.40	4.92	-1.96	-3.37	-5.00	-0.53	-0.79	-0.40
	3	2.76	3.64	3.99	-2.10	-2.62	-2.74	0.22	0.46	0.73
	4	2.52	3.56	5.28	-0.12	-0.23	-3.10	0.71	1.85	2.71
	5	2.20	3.36	4.56	-0.39	-1.12	-1.51	0.45	1.37	2.19
B1	1	1.88	2.36	3.08	-2.28	-2.59	-3.17	0.60	0.68	1.08
	2	0.89	1.68	1.55	-2.25	-2.84	-3.70	0.04	-0.43	-0.62
	3	1.70	2.93	3.49	-1.38	-1.49	-2.43	0.45	0.85	1.31
	4	1.02	2.63	3.52	-0.17	-0.57	-0.88	0.44	0.94	1.40
	5	0.86	2.37	3.77	-0.12	-2.15	-3.89	0.43	0.84	1.19

The model results and above discussion indicates an average deposition and consequent bed level rise of the Lower Meghna River due to climate change and sea level rise. Due to continuous deposition the bed level of the river will raise upto 0.63 m, 1.32 m and 1.63 m during the periods of 2020s, 2050s and 2080s respectively for scenario A1FI. Likewise, the bed level rise compared to base period are 0.50 m, 1.27 m and 1.86 m for scenario A1B and 0.48 m, 0.83 m and 1.24 m for scenario B1 during the stated periods.

The rise of river beds depends on the siltation rate of a particular river. The siltation rate may vary over different part of the river depending on the local hydraulic and morphologic conditions. However in the long term, the rate of siltation is greatly influenced by the discharge and sediment transport capacities of the channel. Due to climate change and sea level rise, the changed water and sediment discharge as well as the higher water levels resulting from backwater effect have a profound impact on the

siltation rate of Lower Meghna River. The siltation rates of the river for various climate change scenarios have been given in Table 6.6.

Table 6.6: Siltation rate at the selected cross sections of the river for various scenarios

Section	Siltation Rate (cm/year)								
	A1FI			A1B			B1		
	2020s	2050s	2080s	2020s	2050s	2080s	2020s	2050s	2080s
1	2.37	1.12	0.47	1.47	2.60	1.31	1.34	0.24	1.36
2	-	-	-	-	-	-	-	-	-
3	1.03	1.85	0.53	1.07	1.80	2.89	0.84	1.33	1.52
4	1.52	3.39	2.56	1.69	2.87	3.81	0.80	1.55	1.65
5	0.84	2.82	1.64	0.83	2.76	3.06	0.77	1.38	1.15

From the table it is found that siltation rate for scenario A1FI varies between 0.84 and 3.39 cm/year for different periods. It is also evident that for this scenario, the siltation rate increases considerably upto 2050s followed by a reduction in 2080s. But for scenarios A1B and B1 the rate of siltation increases upto 2080s. The rate of siltation for scenario A1B is 0.83 – 3.81 cm/year and for scenario B1 is 0.77 – 1.65 cm/year during different periods. However the overall siltation rate of the river differs from those given in the table. The average siltation rate of Lower Meghna River for different climate change scenarios have been shown in Figure 6.16.

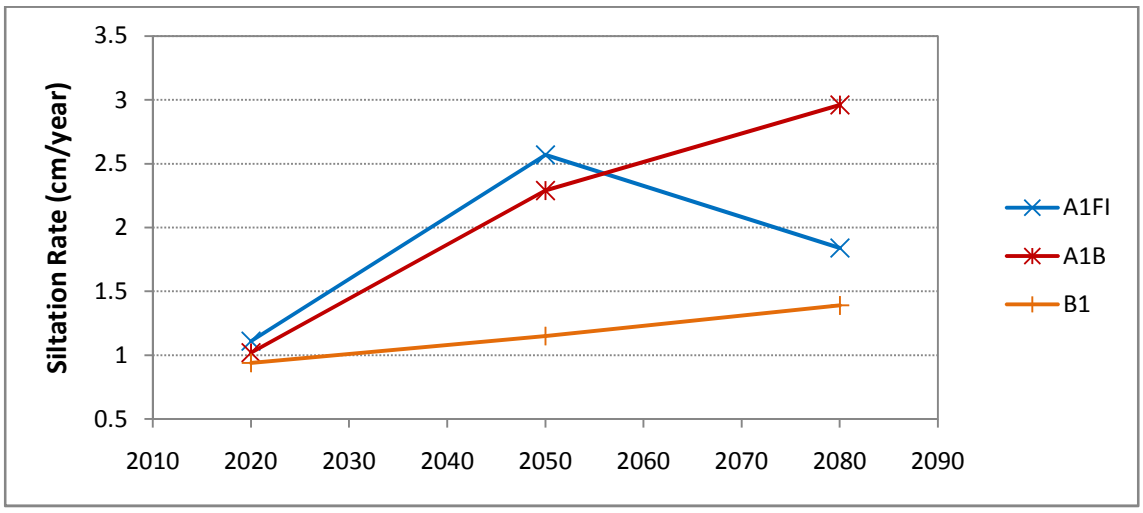

Figure 6.16: Estimated siltation rate for various climate change scenarios

From the figure it is seen that the rate of siltation at 2020s is almost same for various climate change scenarios. For scenario A1FI, this rate is 1.11 cm/year at the period of

2020s. During 2050s, the rate is maximum of about 2.57 cm/year as a result of higher discharge and sediment transport associated with strong backwater effect due to sea level rise. After that the sediment transport capacity of the river decreases due to reduced discharge but the backwater effect becomes more prominent due to rising sea level and hence the siltation rate drops 1.84 cm/year during 2080s. For scenario A1B, the discharge as well as the sediment transport of the river increases continuously upto 2080s. The large amounts of sediments carried by higher discharge are enforced to deposit by the rising levels of sea. Therefore the siltation increases progressively at a rate of 1.02, 2.29 and 2.96 cm/year for the periods of 2020s, 2050s and 2080s respectively. For scenario B1, this rate has been found as 0.94, 1.15 and 1.39 cm/year respectively.

6.5 Evaluation of Delta Progradation

Deltas are generally known as areas of a net deposition of sediment either carried by the river or supplied from the sea. The growth of the delta and the accretion of land is a continuous and generally a very gradual natural process impacted by the ever-changing dynamics of the channel. The Meghna Estuary is an active delta building estuary dominated by the Lower Meghna River. Although various coastal and estuarine processes contribute to the delta development, the role of riverine deposition becomes most significant for shallow water environment like the Lower Meghna River.

Climate change and associated sea level rise will accelerate the process of delta development along the downward part of Lower Meghna River. As mentioned earlier, the higher discharge during monsoon increases the sediment transport capacity of the river and the excess sediments carried by the river are deposited in the deltaic zone. The rising levels of sea will amplify the rate of deposition. As a result of this continuous deposition, new lands will be formed and the delta front will move seaward. Such processes can be evaluated and quantified using numerical model based on modified Exner’s equation by incorporating various conditions of discharge, sediment transport and sea level rise due to climate change. Figure 6.17 shows the bed profile of Lower Meghna River with associated seaward delta front movement for various climate change scenarios.

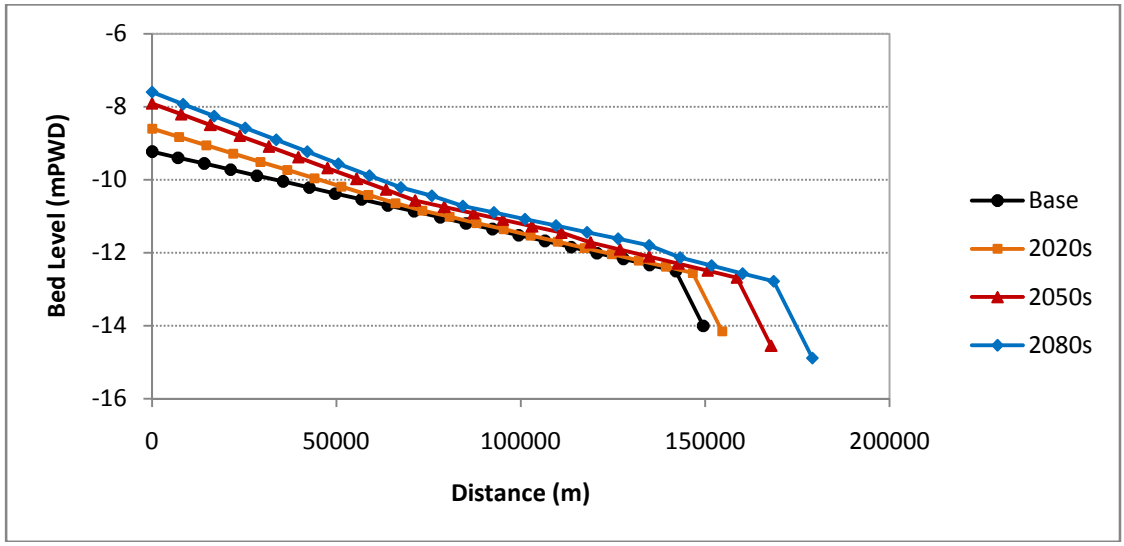

(a) Scenario A1FI

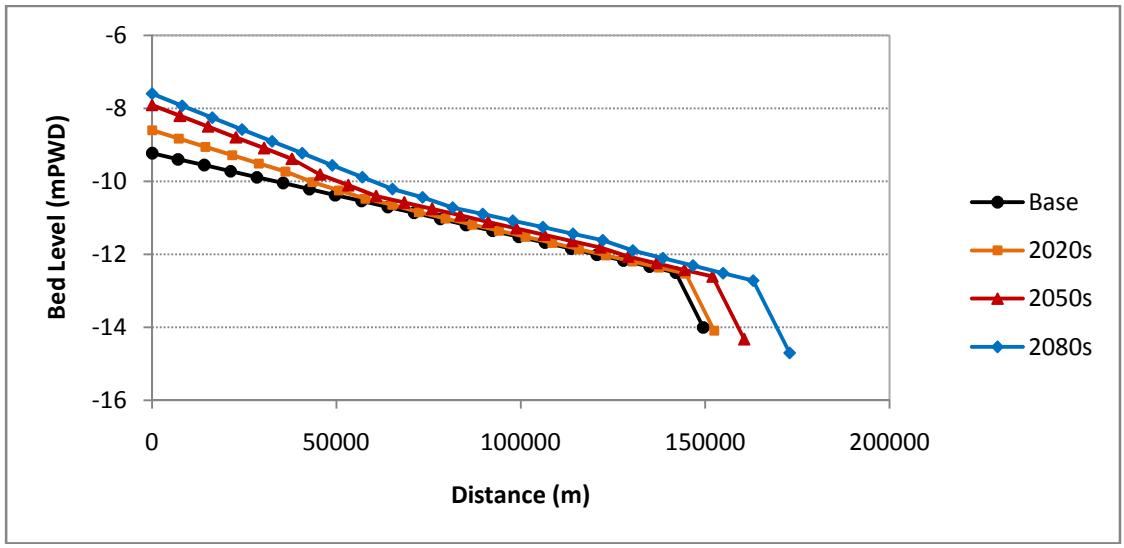

(b) Scenario A1B

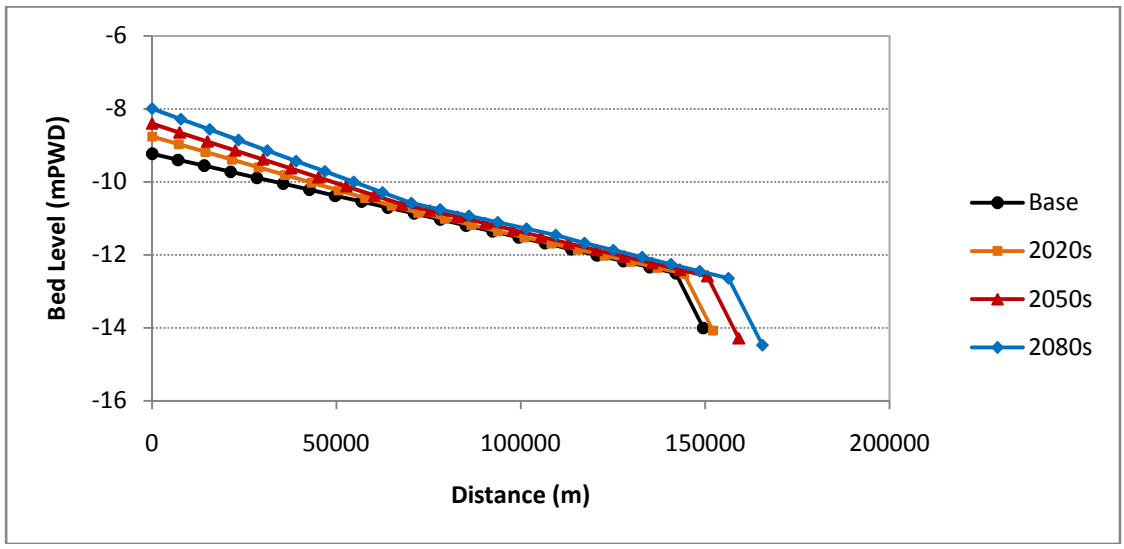

(c) Scenario B1

Figure 6.17: Progradation of delta for various climate change scenarios

During 2020s, the delta line moves slightly towards sea. After that, the delta building process accelerates and considerable progradation of delta occurs during 2050s and 2080s as a result of greater deposition and increasing levels of sea. Also the progradation is maximum for scenario A1FI because of increased discharge during monsoon and higher levels of sea for various periods.

From the figure it is found that the delta progrades 4.63, 16.59 and 26.56 km seaward for scenario A1FI during the periods of 2020s, 2050s and 2080s. The migration of delta front towards sea has been found as 2.67, 9.98 and 21.03 km for scenario A1B and 2.30, 8.64 and 14.33 km for scenario B1 for the above periods respectively. The progradation for scenario B1 is less compared A1FI and A1B due to lower discharge and smaller rise in sea levels.

CHAPTER 7
CONCLUSIONS AND RECOMMENDATIONS

7.1 General

The anticipated change in climate and sea level rise is likely to have a profound impact on the hydraulic and morphologic conditions of Lower Meghna River. Altered basin water balance due to precipitation changes and rising levels of sea will affect the discharge and water level of the river. Such changes will disrupt the existing equilibrium of water and sediment transport through the channel and will trigger new hydraulic and morphologic state of the river. The backwater effect will be more pronounced and the siltation rate will increase leading to greater deposition and consequent bed level rise of the river. Excess deposition and higher sediment transport capacity causes the river delta front to move seaward and initiates delta progradation. Such changes are observed for the all climate change scenarios selected for the present study.

7.2 Conclusions

The following conclusions can be drawn after summarizing the present study –

i. Due to climate change, a potential increase in precipitation over GBM basin is likely to increase basin runoff, which in turn affects the discharge of Lower Meghna River. The projected discharges for various scenarios indicate a higher discharge during wet season and less discharge in the dry season. For scenario A1FI, maximum monthly discharge has been found as 95539 m^3/s, 132835 m^3/s and 111730 m^3/s for the periods of 2020s, 2050s and 2080s respectively which are 7.7%, 39.7% and 32% higher than the base condition. During monsoon, the discharge may be as high as 89586 m^3/s, 99009 m^3/s and 121271 m^3/s for scenario A1B and 85611 m^3/s, 90830 m^3/s and 96274 m^3/s for scenario B1 during the respective periods.

ii. Coastal rivers like the Lower Meghna River will be significantly affected by the global warming induced sea level rise and associated backwater effect. The cumulative impact of changed discharge and sea level rise creates greater backwater effect and elevates water levels along different parts of the river. This effect will be more pronounced during dry seasons. The water level will raise upto 20.4 cm, 16.9 cm and 13.5 cm for scenarios A1FI, A1B and B1 respectively at the end of 2080s. Such effect will be felt further upstream of the river.

iii. The morphology of the Lower Meghna River reacts to changes in the upstream input of water and sediment as well as water level variations resulting from backwater effect. The whole process can be rationalized as a deposition dominated morphologic change due to climate change and sea level rise. The model results also indicate an overall net deposition along the river for various climate change scenarios. Due to continuous deposition the bed level of the river will raise upto 0.63 m, 1.32 m and 1.63 m during the periods of 2020s, 2050s and 2080s respectively for scenario A1FI. Likewise, the bed level rise compared to base period are 0.50 m, 1.27 m and 1.86 m for scenario A1B and 0.48 m, 0.83 m and 1.24 m for scenario B1 during the stated periods respectively.

iv. The bed level changes or the rise of river beds depend on the siltation rate of a particular river. The siltation rate of Lower Meghna River increases as a result of increased discharge and sediment transport capacities of the channel and rising sea level for various climate change scenarios. For scenario A1FI, the average rate of siltation increases considerably upto 2050s followed by a reduction in 2080s. Siltation increases progressively at a rate of 1.02 cm/year, 2.29 cm/year and 2.96 cm/year for scenario A1B and 0.94 cm/year, 1.15 cm/year and 1.39 cm/year for scenario B1 during the periods of 2020s, 2050s and 2080s respectively.

v. Climate change and associated sea level rise will accelerate the process of delta progradation along the downward part of Lower Meghna River where the delta building process is dominated by riverine deposition. Various scenarios indicate an overall seaward movement of delta front. For scenario A1FI, the migration of delta front towards sea can be found as 4.63 km, 16.59 km and 26.56 km during the periods of 2020s, 2050s and 2080s. Similarly, the delta progrades seaward upto 2.67 km, 9.98 km and 21.03 km for scenario A1B and 2.30 km, 8.64 km and 14.33 km for scenario B1 for the above periods respectively.

7.3 Recommendations

Based on the present study, following recommendations can be made for future study –

i. The limitations of various projections of the climate models are the primary sources of uncertainty for the present study. Improvements to these models and more accurate regional predictions would greatly improve the kinds of analyses reported here, and would facilitate the exploration of climate change impacts for legitimate

hydrologic and morphologic predictions of rivers and associated water resource system.

ii. The change of sediment yield of the basin due to climate change was not considered in the present study. Studies can be carried out to assess the impact of such changes on the morphology of a river.

iii. The discharge of Lower Meghna River has been assessed from the precipitation projections generated by the HadCM3 GCM model. Other GCM model projections can also be incorporated for similar type of studies. Multi-model ensemble mean of various climate models can be used for more accurate and confident predictions of climate change impacts on a river.

iv. For the present study, the ANN model has been developed using the monthly precipitation data of coarse resolution ($3.75^0 \times 2.5^0$). For more accuracy and better understanding of the process, daily data of finer grid resolution can be used.

v. Due to the computational time barrier and numerical stability, it was not possible to simulate the MIKE 21 Flow Model FM for longer period of time continuously upto 2080. Therefore the simulations were performed only for the projection periods of 2020s, 2050s and 2080s.

vi. MIKE 21 Flow Model FM gives erosion/deposition for the nodes to produce the bed level lowering or rising, however, it cannot automatically shift the bank line when a bank node gets erosion/deposition for itself. So any lowering of nodes at the bank, indicate the bank at that location is vulnerable, which is supposed to produce bank erosion and subsequent bank line shifting. A study on bank line shifting due to erosion can be undertaken, using manual procedure of shifting the bank line, by lowering the ground elevations in the prospective bank line nodes of the model.

vii. Similar type of studies can be carried out for other major rivers of Bangladesh such as the Ganges, the Jamuna, the Upper Meghna etc. by considering the Ganges basin, Brahmaputra basin and Meghna basin separately.

REFERENCES

Agrawala, S., Ota, T., Ahmed, A.U., Smith, J. and Aalst, M. (2003), "Development and Climate Change in Bangladesh: Focus on Coastal Flooding and the Sunderbans", Organization for Economic Co-operation and Development (OECD), Paris.

Ahmed, A. U. (2006), "Bangladesh Climate Change Impacts and Vulnerability: A Synthesis", Climate Change Cell, Dhaka.

Ahmed, A. U. and Mirza, M. M. Q. (1998), "Review of Causes and Dimensions of Flood with Particular Reference to Flood'98: National Perspectives", Paper presented to the national seminar on Flood'98 and Management of Floods in Future, organized by Jatiyo Tran Committee, Dhaka University and others, 8 December.

Akamatsu, Y., Parker, G. and Muto, T. (2005), "Effect of Sea Level Rise on Rivers Flowing into the Ocean: Application to the Fly-Strickland River System, Papua New Guinea", Proc. Of River, Coastal and Estuarine Morphodynamics, pp685-695.

Ali, A. (1999), "Climate Change Impacts and Adaptation Assessment in Bangladesh", Climate Research, Vol. 12, pp. 109–116.

Ali, A., Mynett, A. E. and Azam, M.H. (2007), "Sediment Dynamics in the Meghna Estuary, Bangladesh: A Model Study", Journal of Waterway, Port, Coastal, and Ocean Engineering, Vol. 133, No. 4, July 1, 2007 pp 255-263

ASCE Task Committee on Artificial Neural Networks in Hydrology (2000a), "Artificial Neural Networks in Hydrology. I: Preliminary Concepts", Journal of Hydrologic Engineering, Vol. 5(2), pp 115-123.

ASCE Task Committee on Artificial Neural Networks in Hydrology (2000a), "Artificial Neural Networks in Hydrology. II: Hydrologic Applications", Journal of Hydrologic Engineering, Vol. 5(2), pp 124-137.

Bates, B.C., Kundzewicz, Z.W., Wu, S. and Palutikof, J.P. (Eds.) (2008), "Climate Change and Water", Technical Paper of the Intergovernmental Panel on Climate Change, IPCC Secretariat, Geneva, 210 pp.

Besaw, L.E., Rizzo, D.M., Bierman, P.R. and Hackett, W.R. (2010), "Advances in ungauged streamflow prediction using artificial neural networks", Journal of Hydrology, Vol. 386, pp 27–37.

Blum, M. D. and Tornqvist, T. E. (2000), "Fluvial Response to Climate and Sea Level Change: A Review and Look Forward", Sedimentology, Vol. 47, Suppl. 1, pp 2-48.

Bronstert, A., Niehoff, D. and Burger, G., (2002), “Effects of Climate and Land-Use Change on Storm Runoff Generation: Present Knowledge and Modelling Capabilities”, Journal of Hydrological Process, Vol 16, pp 509–529.

CCC (2009a), “Characterizing Country Settings: Development of a Base Document in the Backdrop of Climate Change Impacts”, Climate Change Cell, DoE, MoEF; Component 4b, CDMP, MoFDM, Dhaka.

CCC (2009b), “Impact Assessment of Climate Change and Sea Level Rise on Monsoon Flooding”, Climate Change Cell, DoE, MoEF; Component 4b, CDMP, MoFDM, Dhaka.

CEGIS (2010), “Impacts of Climate Change on Bangladesh Rivers”, Paper presented at the wokshop on Impact of Climate Change on River and Estuary Morpholgy, Dhaka.

Chen, X., Wu, J. and Hu, Q. (2008), “Simulation of Climate Change Impacts on Streamflow in the Bosten Lake Basin Using an Artificial Neural Network Model”, Journal of Hydrologic Engineering, Technical notes, pp 180-183.

Christensen, N. and Lettenmaier, D.P. (2006), “A multimodel ensemble approach to assessment of climate change impacts on the hydrology and water resources of the Colorado River basin”, Hydrol. Earth Syst. Sci. Discuss., Vol. 3, pp 3727–3770.

Dawson, C. W. and Wilby, R. (1998), “An artificial neural network approach to rainfall-runoff modeling”, Journal of Hydrological Sciences, Vol 43, pp 47-66.

DHI (2007), “MIKE 21 and MIKE 3 Flow Model FM”, Scientific Documentation prepared by Denish Hydraulic Institute, Denmark.

Ericson, J.P., Vorosmarty, C.J., Dingman, S.L., Ward, L.G. and Meybeck, M. (2006), “Effective sea-level rise and deltas: causes of change and human dimension implications”, Global Planet. Change, Vol. 50, pp 63–82.

Gain, A.K., Immerzeel, W.W., Sperna-Weiland, F.C. and Bierkens, M.F.P. (2011), “Impact of Climate Change on the Stream Flow of Lower Brahmaputra: Trends in High and Low Flows Based on Discharge Weighted Ensemble Modeling”, Hydrol. Earth Syst. Sci. Discuss., Vol. 8, pp 365–390.

GOB (2005), “National Adaptation Programme of Action (NAPA)”, Final report, Ministry of Environment and Forest, Government of the People’s Republic of Bangladesh (GOB), Dhaka, 48 p.

Hamlet, A. F. and Lettenmaier, D. P. (1999), “Effects of Climate Change on Hydrology and Water Resources in the Columbia River Basin”, Journal of the American Water Resources Association, Vol. 35, No.6, pp1597-1623.

Hanh, P.T.T. and Furukawa, M. (2007), “Impact of sea level rise on coastal zone of Vietnam”, Faculty of Science, University of the Ryukyus, Bull. No. 84, pp 45 – 59.

Huang, Z., Zong, Y. and Zhang, W. (2004), “Coastal inundation due to sea level rise in the Pearl River Delta, China”, Natural hazards., 33 (2). pp. 247-264.

Huntington, T.G. (2006), “Evidence for intensification of the global water cycle: review and synthesis”, Journal of Hydrology, Vol. 319, pp 83–95.

IPCC (1997), “An introduction to simple climate models used in the IPCC Second Assessment Report”, IPCC Technical Paper II [Harvey, D., J. Gregory, M. Hoffert, A. Jain, M. Lal, R. Leemans, S. Raper, T. Wigley, and J. de Wolde, (eds.)], Intergovernmental Panel on Climate Change, Geneva, 47 pp.

IPCC (2001a), “Climate Change 2001: The Scientific Basis”, Contribution of Working Group I to the Third Assessment Report of the Intergovernmental Panel on Climate Change [Houghton, J.T., Y. Ding, D.J. Griggs, M. Noguer, P.J. van der Linden, X. Dai, K. Maskell, and C.A. Johnson (eds.)]. Cambridge University Press, Cambridge and New York, 881 pp.

IPCC (2001b), “Climate Change 2001: Impacts, Adaptation, and Vulnerability”, Contribution of Working Group II to the Third Assessment Report of the Intergovernmental Panel on Climate Change [McCarthy, J.J., O.F. Canziani, N.A. Leary, D.J. Dokken, and K.S. White (eds)]. Cambridge University Press, Cambridge and New York, 1032 pp.

IPCC (2001c) “Climate Change 2001: Mitigation”, Contribution of Working Group III to the Third Assessment Report of the Intergovernmental Panel on Climate Change [O. Davidson, R. Swart, (eds)]. Cambridge University Press, Cambridge and New York.

IPCC, (2007a), “Climate Change 2007: The Physical Science Basis”, Contribution of Working Group I to the Fourth Assessment Report of the Intergovernmental Panel on Climate Change [Solomon, S., D. Qin, M. Manning, Z. Chen, M. Marquis, K.B. Averyt, M. Tignor and H.L. Miller (eds.)]. Cambridge University Press, Cambridge, United Kingdom and New York, NY, USA, 996 pp.

IPCC, (2007b), “Climate Change 2007: Impacts, Adaptation and Vulnerability”, Contribution of Working Group II to the Fourth Assessment Report of the Intergovernmental Panel on Climate Change, M.L. Parry, O.F. Canziani, J.P. Palutikof, P.J. van der Linden and C.E. Hanson, Eds., Cambridge University Press, Cambridge, UK, 976pp.

IPCC, (2007c), “Climate Change 2007: Mitigation”, Contribution of Working Group III to the Fourth Assessment Report of the Intergovernmental Panel on Climate Change [B. Metz, O.R. Davidson, P.R. Bosch, R. Dave, L.A. Meyer (eds)], Cambridge University Press, Cambridge, United Kingdom and New York, NY, USA.

IPCC-TGICA (2007), “General Guidelines on the Use of Scenario Data for Climate Impact and Adaptation Assessment. Version 2”. Prepared by T.R. Carter on behalf of the

Intergovernmental Panel on Climate Change, Task Group on Data and Scenario Support for Impact and Climate Assessment, 66pp.

Islam, A.K.M.S., Siddiquee, S.A., Islam, M.N. and Mondal, M.S. (2008), "Improving Flood Forecasting of Bangladesh using Artificial Neural Network (Ann) and Remotely Sensed Rainfall Data", Final Report, Institute Of Water And Flood Management, BUET.

IWM and CEGIS (2007), "Investigating the Impact of Relative Sea-Level Rise on Coastal Communities and their Livelihoods in Bangladesh", Final Report, Prepared for UK Department for Environment Food and Rural Affairs.

Jeong, D. and Kim, Y. (2005), "Rainfall-runoff models using artificial neural networks for ensemble streamflow prediction", Hydrological Process, Vol 19, pp. 3819–3835.

Lai, S. Y. J. and Capart, H. (2007), "Response of Hyperpycnal Deltas to a Steady Rise in Base Level", Proc. of 5th IAHR Symposium on River, Coastal and Estuarine Morphodynamics, London, pp 558-570.

Li et al. (2008), "Impact of Future Climate Change on Runoff in the Head Region of the Yellow River", Journal of Hydrologic Engineering, Vol 13(5), pp 347-354.

Matin, M.A. and Kamal, R. (2010), "Impact of Climate Change on River System", Proceedings of the International Symposium on Environmental Degradation and Sustainable Development, April.

McCabe, G. J. and Wolock, D. M. (1997), "Climate Change and the Detection of Trends in Annual Runoff", Journal of Climate Research, Vol 8, pp 129-134.

Ministry of Water Resources (MWR), (1998), "Morphological processes, Meghna estuary study, draft master plan." Rep. Prepared by DHV Consultants, Vol. 2, Bangladesh Water Development Board, Bangladesh.

Ministry of Water Resources (MWR), (2001), "Hydro-morphological dynamics of the Meghna estuary." Rep. Prepared by DHV Consultants, Bangladesh Water Development Board, Bangladesh.

Mirza, M.M.Q. (2002), "Global warming and changes in the probability of occurrence of floods in Bangladesh and implications", Global Environment Change, Vol. 12, pp 127–138.

Mirza, M.M.Q. and Dixit, A. (1997), "Climate Change and Water Resources in the GBM Basins", Water Nepal, Vol. 5(1), pp. 71-100.

Mirza, M.M.Q., Warrick, R.A. and Ericksen, N.J. (2003), "The implications of climate change on floods of the Ganges, Brahmaputra and Meghna Rivers in Bangladesh", Climatic Change, Vol. 57, pp 287–318.

Muto, T. (2001), “Shoreline autoretreat substantiated in flume experiment”, Journal of Sedimentary Research, 71(2), 246-254.

Nakicenovic, N., J. et al (2000), “Emissions Scenarios”, A Special Report of Working Group III of the Intergovernmental Panel on Climate Change. Cambridge University Press, Cambridge, UK and New York, NY, USA, 599 pp.

Nohara, D., Kitoh, A., Hosaka, M. And Oki, T. (2006), “Impact of Climate Change on River Discharge Projected by Multimodel Ensemble”, Journal of Hydrometeorology, Vol. 7, pp1076-1089.

Parker, G., Akamatsu, Y., Muto, T. and Dietrich, W. (2004), “Modeling The Effect of Rising Sea Level on River Deltas and Long Profiles of Rivers”, Proceedings, International Conference on Civil and Environmental Engineering (ICCEE-2004), Hiroshima University, Japan, July.

Parker, G. and Y., Muto, T. (2003), “1D Numerical Model of Delta Response to Rising Sea Level”, Proceedings of the 3rd IAHR Symposium, River, Coastal and Estuarine Morphodynamics, Barcelona, Spain, 1-5 September.

Promny, I.M. (2011), “Climate projections for sediment budgeting and river morphology of German waterways”, Federal Institute of Hydrology, Koblenz, Berlin.

Rahman, A. and Alam, M. (2003), “Mainstreaming Adaptation to Climate Change in Least Developed Countries (LDCs)”, Working Paper 2: Bangladesh Country Case Study.

Scott, S.H. and Jia, Y. (2010), “Simulation of Sediment Transport and Channel Morphology Change in Large River Systems”, US-China Workshop on Advanced Computational Modelling in Hydroscience & Engineering, September 19-21, Oxford, Mississippi, USA.

Springer, G.S., H.D. Rowe, B. Hardt, F.G. Cocina, R.L. Edwards, and H. Cheng – Climate driven changes in river channel morphology and base level during the Holocene and Late Pleistocene of southeasternWest Virginia. Journal of Cave and Karst Studies, v. 71, no. 2, p. 121–129 2009.

UNFCCC (2007), “Climate Change: Impacts, Vulnerabilities and Adaptation in Developing Countries”, Background paper for the expert meeting on adaptation for developing States. UNFCCC Secretariat. Bonn, Germany.

Vastila, K., Kummu, M., Sangmanee, C. and Chinvanno, S. (2010), “Modelling climate change impacts on the flood pulse in the Lower Mekong floodplains”, Journal of Water and Climate Change, Vol. 01.1, pp 67-86.

Verhoog, F. H. (1987), “Impact Of Climate Change on the Morphology of River Basins”, Proceedings of the Vancouver Symposium, IAHS, Publ. no. 168.

Zhu, Y. M., Lu, X. X. and Zhou, Y., (2008), “Sediment Flux Sensitivity to Climate Change: A Case Study in the Longchuanjiang Catchment of The Upper Yangtze River”, China, Global and Planetary change, vol 60, 3-4, p. 429-442.

APPENDIX A

PRECIPITATION DATA

Table A1: CRU Observed Precipitation over GBM Basin

Time / Nodes	Precipitation (mm/day)																								
	1	2	3	4	5	6	7	8	9	10	11	12	13	14	15	16	17	18	19	20	21	22	23	24	25	26
Jan-75	0.6	4.4	0	0.1	0	0.2	0.2	0.3	0.7	0.2	0	0	0.4	0.4	1.4	0.1	0.2	0.4	0	0	0.5	0	0	0.1	0	0.5
Feb-75	0.9	1.9	0.2	0.1	0	0	0	0.3	1.6	0.7	0	0	0.8	0.3	0.2	0.3	0.9	1.2	0	0	1	0.2	0	0.6	0	0
Mar-75	1.1	2	0	0.2	0.1	0.2	0.1	0.4	2.2	0.8	0	0	0	0.7	0.3	0.5	1.1	0.8	0	0	1	0.6	0.6	0	0	0.1
Apr-75	0	0.5	0	1.2	0	0	0	0.5	6.2	5.8	0	0	0	0.2	0.5	8.2	8.5	1.8	0	0	0	0.7	0.7	1.4	0.4	0.6
May-75	0	0.6	0.3	0.5	0.3	0.1	0	6.5	12	2.3	0	0.7	0	0.1	2.7	14	12.8	8	0	0.2	0	1.4	2.5	6.4	8.5	5.8
Jun-75	2	8.3	0.8	1.7	5.4	1.3	3.3	20.3	10	1.1	3.1	1.7	5.8	4.6	3.2	11.9	12.1	3.9	3	6.2	8.4	9.6	7.5	8.9	9.6	7.1
Jul-75	2.7	14.6	4.2	4.2	11.9	3.3	10.3	27.5	13.8	4	5.8	3.7	9.5	13	10.4	30.1	22.8	10.2	2.6	8.1	7.6	11.7	12.3	18.6	15.4	15.6
Aug-75	8.8	9.3	1.8	1.4	6.7	2.9	6.1	5.2	21.2	3.1	7.4	15.1	14.7	5.5	6.1	9.6	11.3	7.9	7.3	13.2	15.2	12.6	11.2	9.3	9.3	9.7
Sep-75	3	11	3.6	2.1	12.3	2.8	6.3	23.4	7.6	1.6	4.7	4.9	8.3	5	7.5	11.3	11.4	6.2	6.2	7.6	10.4	9.8	8.3	8.3	22.2	7.2
Oct-75	0.1	0.7	0.2	0.9	2.1	0	1	5.4	4.3	2	2.4	2.2	1.4	1.6	3.1	9.4	10.2	4.9	5	2.9	2.6	3.8	4.6	7.2	10	8.2
Nov-75	0	0	0	0	0	0	0	0.2	0.5	0.1	0	0	0	0	0	0.6	0.8	5.2	0	0	0	0.1	0.1	2.1	0.8	4.6
Dec-75	0	0	0	0	0	0.1	0	0	0.6	0.1	0	0	0	0	0	0	0.1	0.1	0	0	0	0	0	0	1.3	0
Jan-76	1.2	0.1	0	0	0.2	0.4	0	0.5	0.1	0	0.3	0	0.6	0.8	0.1	0	0.4	0.9	0.1	0.1	0.1	0	0	0	0	0
Feb-76	3.2	4	0	0	0.5	0	0.2	1.7	3.2	0.5	0.2	0	0	0.1	0.7	0.3	1.8	2.1	0	0	0	0.1	0.5	1.2	0	0
Mar-76	0.7	1	0	0.4	0	0	0.1	0	5.7	2.7	0	0	0.4	0	0	4.5	6.1	1.2	0.1	0.1	0.5	0.3	0.4	0.4	0	0
Apr-76	0.1	1.9	0.4	0.8	0.1	0.3	0.1	3	8.1	2.1	0	0	0.1	0.5	0.4	4.7	7.8	3.3	0	0	1.1	1.1	1.1	2.7	2.9	0.8
May-76	0.6	1.2	0.8	0.9	0	0.4	0.4	4.7	6.3	0.6	0	0.2	0.2	0.2	4.8	8.9	10.4	2.9	0	0	0.7	2.2	4.1	7.3	8.1	5.5
Jun-76	3.2	3.5	3.6	4.1	0.4	1.8	3.8	14.7	16.6	2.5	1.5	3.5	3.5	0.8	3.8	26.9	18	8.8	5.8	7.9	3.7	3.4	5.7	13.4	14.8	10.7
Jul-76	6.5	7.4	2.8	2.5	2.6	3.5	6.1	14.8	23.7	2.1	4.8	7.3	11.7	8.7	9.7	19.2	16.6	10.8	7	10.1	11.6	12.8	13.6	19.4	22.4	14.1
Aug-76	7.8	18	3.2	2.6	6.4	3.2	9.7	22.6	10	1.4	6.1	10.8	15.5	4.5	8.3	19.8	14.1	6.5	7.6	11.5	13.2	11.5	13.9	12.6	1.6	10.7
Sep-76	0.4	2.7	0.5	2.7	6.3	5.8	2.7	7.8	3.8	2	2.2	4	6.5	13.9	10.2	8.8	6.2	4.2	3.1	4.6	8.5	9.9	7.7	6.8	7.8	3.5
Oct-76	0	0.3	0.2	0.6	0	0	0	2.8	1.4	0.8	0	0	0	0	0.9	3.1	2.8	2.8	0.1	0	0	0.4	1.9	3.8	9.2	5
Nov-76	0	0	0	0	2	0.5	0.4	0	0.7	1	0.7	1.3	1.8	0.1	0.5	0.2	0.6	3	1.8	3	1.7	0.3	0.2	1.7	0	3.2
Dec-76	0	0.1	0	0.1	0	0	0	0	0.2	0	0	0	0.1	0	0	0	0	0.1	0	0.1	0.1	0	0	0.2	1.2	0

Table A1 (continued)

Time / Nodes	Precipitation (mm/day)																								
	1	2	3	4	5	6	7	8	9	10	11	12	13	14	15	16	17	18	19	20	21	22	23	24	25	26
Jan-77	1.2	1.7	0	0.1	0.3	0.4	0.9	0.2	0.6	0.5	0.5	0.1	0	0.9	0.1	0.1	0.2	1.2	0.1	0.1	0	0	0	0.1	0	0
Feb-77	0.1	0.3	0	0.7	0	0	0	0.5	2.4	0.9	0	0.3	0.3	0.6	0.5	0.9	1.4	1.6	0	0.1	0.1	0.1	0.2	1.5	0.7	0
Mar-77	0	0.2	0.3	0.3	0	0	0	1.7	3.8	1.7	0	0.1	0.5	0	0.2	3.3	6	0.8	0	0.1	0.9	0.2	0.1	0.1	0	0
Apr-77	1.7	1.9	0.9	0.8	0.3	0.1	0.9	7.7	13.7	2.9	0.1	0.3	0	0.7	0.6	13.4	20.6	5.2	0	0.1	0.1	1.7	1.8	8.5	18.9	7.4
May-77	1.6	5.4	1.7	1.3	0.1	0.2	0.5	8.6	10.5	2.5	0.8	0.8	0.2	1.2	6.9	16.6	20.9	4.9	0.5	0.5	0.7	2	4	7.7	11.8	5.6
Jun-77	5.1	4.9	3.5	2.2	4.1	4.7	0.7	11	16.2	1.7	5.6	5.8	14.6	4	7.2	21	19.4	8.1	4.1	6.3	10.7	8.1	10.6	17.3	15.5	10.8
Jul-77	8.8	10.8	4.4	2.8	4.3	7.5	12.7	20.3	20.5	3.7	16.5	1.1	10.4	14.8	16.9	20	20.8	8.3	9.7	11.4	7.5	13	14.9	15.7	21.6	12.9
Aug-77	9	6	3.2	5.2	2.5	1.1	6	17.3	22.5	6.2	2.6	6.9	16	7.8	5.2	17.9	18.2	9.8	4.5	7.6	10.9	11.8	9.9	8.1	8	10.7
Sep-77	3.9	5.2	1.8	2	0.9	6.6	7.4	13.2	7.4	3.6	2.2	4	5.4	5.8	3.8	5.6	8.5	6.2	5.7	6.3	7.4	6	6.7	6.2	0.8	7.8
Oct-77	0.2	0.4	1.1	1.5	0	0	1.4	5.7	5.8	0.8	0	0.2	0.6	2.5	3.6	7.9	8.6	2.2	0	0.2	2.6	2.3	2.7	2.7	1.8	3.8
Nov-77	0	0	0	0.1	0	0.1	0	2.1	1.4	1.1	0	0.3	1.5	0.7	0.1	1.3	2.3	0.4	0.2	1.6	7.1	2.9	1.1	1	1	1.4
Dec-77	1.1	1.3	0	0.2	0	0	0.1	0	1.8	0.4	0	0	0	0.3	0.8	0.6	1.3	0.8	0	0	0.8	0.6	0.3	0.5	1.3	0.5
Jan-78	0.2	0.4	0.1	0	0	0	0	0.6	0.4	0.2	0	0	0.2	0.8	0.2	0	0.1	0.1	0	0.1	0.4	0	0	0	0	0.1
Feb-78	1	0.9	0	0	0.2	0.5	0.6	0.4	2.6	0.5	0.1	0.4	3.5	2.6	1.4	0.2	1.1	0.2	0	0.3	2.1	1.4	0.5	0.2	0	0
Mar-78	2	4.3	0	0	0	0.4	1.3	2	1.9	0.9	0	0.4	1.6	1.6	1	0.9	3.3	0.1	0	0.1	2.3	0	0	0.8	0	0
Apr-78	0.4	0.7	0	0.8	0.4	0.8	0.1	3.9	5.5	0.9	0	0	0.8	0.7	1.1	4.7	7	1.6	0.1	0.2	0.7	0	0	3.8	9	0
May-78	0.1	0.4	2.5	2.2	0	0	0	6	5.6	2.4	0	0	0	0	4	14.7	13.5	9.1	0	0	0.2	0	0	10	17.1	0
Jun-78	2.4	4.8	1.8	3.8	1.5	1.6	4	19.9	15.1	5.1	2.9	5.5	8	8.3	6.3	24.6	18.2	8	7.1	6	5.6	0	0	16.3	20.7	0
Jul-78	6.3	6.2	2.4	3.1	6.1	8.5	6.8	15.7	17.4	5.6	7.1	8.3	11.1	5.1	10.8	19.1	15.8	9.2	4.2	7.7	10.6	0	0	12.4	17.8	0
Aug-78	5.3	11.3	5.5	2.6	5.7	1.3	6.3	14.2	4.7	2.8	5.7	15.4	25.9	8.5	9.3	9.9	9.3	7	6.9	13	12.5	0	0	12.1	19	0
Sep-78	2.1	7.9	1.9	2.7	0.2	1.3	5.9	12.4	8.2	3.6	0.3	0.9	6.4	12.1	11.7	9.9	13.5	8	0.5	1.6	2.3	0	0	17	16	0
Oct-78	0.1	0.4	0.1	0.4	0	0	0	1.8	3.2	0.3	0	0	0	0.8	5.9	2.1	3.8	1.5	0.3	0.6	0.4	0	0	4.7	6.2	0
Nov-78	0.2	0.2	0.7	0.7	0.5	0	0	0.5	3.4	1.2	1.1	0	0.1	0	0.1	0.4	1.9	0.4	0.7	1.2	0.9	0	0	0.4	0	0
Dec-78	0.1	0.6	0	0	0	0	0.2	0.3	0	0	0	1.4	2.7	0.4	0.2	0	0.1	0.2	0.2	0.8	1.4	0	0	0	0	0

Table A1 (continued)

Time / Nodes	Precipitation (mm/day)																								
	1	**2**	**3**	**4**	**5**	**6**	**7**	**8**	**9**	**10**	**11**	**12**	**13**	**14**	**15**	**16**	**17**	**18**	**19**	**20**	**21**	**22**	**23**	**24**	**25**	**26**
Jan-79	1	1.5	0	0	0	0.3	0.3	0.3	0.7	0.2	0	0.3	2.5	0.7	1	0.1	0.3	0.1	0	0.4	3	0.6	0	0.5	0	0
Feb-79	2.9	2.5	0.1	0.5	0.7	1.3	2.1	0.9	0.2	0.1	0.4	0.5	1.1	0.7	0.7	0.4	1.1	0.4	0.1	0.3	1.8	0	0	0.3	0	0
Mar-79	2	2.6	0	0	0	0.3	0.2	0	0.9	1.6	0	0	0.2	0	0.2	0.7	1.4	1.9	0	0.1	0	0.1	0.3	0.8	0	0
Apr-79	0.7	1	0.3	0.2	0	0	0.1	4.7	2.3	0.9	0	0.1	0	0.3	1.7	3.4	7.2	1.1	0	0	0	0.6	1.5	1.1	0.1	0.4
May-79	0.9	3.7	0	0.9	0.8	0.9	0.8	2.5	4.8	0.4	0.2	0.8	1	0.1	0.3	10.3	7.9	1.7	0.1	0	0.4	0.5	1	2	0.7	1.8
Jun-79	1.4	2.4	1.7	2.6	2.3	0.1	1	13.9	9	3.3	0.6	2.4	2	4.7	2.2	12.7	12	7.8	6.1	4.2	4.5	5.6	5.4	13	0	10.8
Jul-79	6.2	6.6	4.7	3	10.1	1.1	4.4	30.9	18.6	2.6	2.2	8.3	14.2	8.7	13.2	33	21.7	7	1.8	5.3	9.7	11	11.7	14.4	6.5	5.1
Aug-79	1.5	6	5.2	3.3	7.9	0.8	1.7	12.3	11.3	3.4	4.9	8.2	7.9	4.5	6.8	19.2	9.3	8	19.9	13.2	17.2	11.5	11.2	17.6	12.7	7.9
Sep-79	1.1	0.6	1.8	3.3	0.1	1.6	0.3	11.4	12.1	2.8	0.3	0.6	0.4	3.2	4.9	17.2	13.8	6.4	1.5	1.4	3.6	5.7	6.9	8.7	3.4	5.3
Oct-79	0	0	1.2	1.6	0.7	0.5	0	5.4	8.9	3.8	0.7	0.4	0	0.1	4.3	8.6	10.9	6	0.4	0.8	1.2	1.9	3	3.1	0.6	2.2
Nov-79	0.5	0.8	0	0	0	0.1	0.5	1.4	0.5	0	2	1.4	7	2.3	1.4	0.8	0.9	0.7	3.5	3.1	2	1.3	0.8	0.8	0	0
Dec-79	0.2	0.6	0.3	0.1	0	0.1	0.2	2.8	1.9	1.1	0	0.2	0	0.2	0.5	1.3	3.6	3.3	0	0.2	0.1	0.3	0.5	1.3	0.3	0
Jan-80	0.3	0.5	0	0.1	0	0	0	0.3	0.7	0.5	0	0	0	0.1	0.4	0.1	0.2	0.3	0.1	0	0.1	0.2	0.6	0.2	0	0
Feb-80	0.3	1.4	0	0.3	0	0	0.2	0.9	1.9	0.3	0	0	0.1	0.5	0.2	0.7	2.4	0.9	0	0	0.2	0.2	0.7	2.6	0.1	0
Mar-80	1.3	3.6	0.1	0.4	0	0.6	0.9	2.5	5.3	1.8	0	0.1	0	0.2	0.6	1	5	2.1	0	0	0.1	0.3	0.8	2.5	0.9	0.2
Apr-80	0.2	0.4	0.2	0.2	0	0	0	1.3	13.4	3.1	0	0	0	0	0.4	2.7	6	1.7	0	0	0.1	0.6	1	1.1	0	0
May-80	0.2	0.5	2.2	1.7	0.3	0.3	0.2	5.4	7.3	1.8	0	0.1	0	0.1	1.7	10.4	10.3	2.5	0	0	0	1.1	3.2	9.3	3.9	3.9
Jun-80	1.6	8	3.3	2.1	2	0.6	2.1	13.5	9.3	2.1	3.5	1.1	8.9	6.1	8.6	10.7	13.9	9.9	9.3	10.8	5.8	9.9	10	10.6	8.6	7.9
Jul-80	18	21.7	2.7	2.8	3.9	3	7.1	29.2	18	3.4	3.2	5.1	11.6	15.4	10	10.6	13	5.8	9.4	7.4	5.8	13.5	12.7	15	6.2	6.1
Aug-80	5.2	13.6	5.4	5	0.2	0.6	8.8	19.9	20.8	3.4	3.1	7.5	12.6	16.6	11.3	10.1	13.6	6.5	4.4	10.3	14.1	13.7	12	12.6	8.9	6.3
Sep-80	0.9	13.8	1.8	2	0.7	0.9	0.7	7.7	10.9	1.5	0.2	2	1.1	5.6	4.9	7.4	7.7	6.8	0.7	1.2	1.9	6.9	8.6	5.9	9.1	6.3
Oct-80	0.8	1.6	0.5	0.2	0	0.1	0.6	5.8	5.7	4.4	0	0	0	0.4	1.8	3.9	5.9	8.5	0	0	0.1	1.1	2.8	6.7	10	6.3
Nov-80	0.5	0.1	0	0	0	0.4	0.1	0.1	0	0	0	0	0	0	0	0	0	0	0.1	0.1	0	0	0	0.1	0.1	0.3
Dec-80	3.3	0.4	0	0.1	1	0.1	0.7	0	0	0	0.7	0.2	0.9	0.4	0	0	0.1	0	0.3	0.9	1.4	0.7	0.2	0	0	0.6

Table A1 (continued)

Time / Nodes	Precipitation (mm/day)																								
	1	2	3	4	5	6	7	8	9	10	11	12	13	14	15	16	17	18	19	20	21	22	23	24	25	26
Jan-81	1.8	2.6	0	0	0	0	0.4	1	1.4	0.7	0	0.2	0.1	0.7	0.7	0.9	0.8	0.6	0.1	0.1	0.3	0.5	0.6	1	1	0
Feb-81	0.8	1	0	0.2	0	0.1	0.1	0.6	2.4	1.1	0	0	0.1	0.2	0.6	0.8	1.4	0.8	0	0	0	0	0	1.1	0	0
Mar-81	2.6	5	0	0.5	0.5	1.1	1.1	2.3	4.2	1.7	0.2	0.2	0.3	0.5	0.4	2.4	5.2	1.6	0	0.1	1.1	1.2	1.9	4	1	0.3
Apr-81	0.1	0.2	0.1	0.4	0	0	0	5	4.8	0.8	0	0	0	0.1	1.9	8.5	11.8	1.1	0	0	0.1	1.7	3.4	10.2	7.3	2.5
May-81	0.5	1.8	1.4	1.7	0.1	1.1	1	6.8	9.4	0.9	0.2	0.3	0.3	0.4	3.1	12.4	13.9	3.6	0.1	0.2	0.8	1.6	3.7	9.7	8	6
Jun-81	2.2	4.2	2	1.7	0	0.8	7.8	5.3	14.1	2.4	0.4	3.1	0.7	3.3	2.9	5.5	7.1	12.5	2.1	4.1	5.5	3.9	4.7	8.5	23.5	11
Jul-81	13.4	16.9	3.4	3.8	1.8	7.3	9.4	25.1	19.9	3.5	4.5	8.1	3.2	14.2	13.1	13.1	15.1	7.2	8.7	9.5	11.9	13.4	15.3	19.2	14	11.4
Aug-81	4.7	3.7	2.4	1.8	1.8	1.4	4.9	15.1	20.8	2.2	6.1	10	7.6	11.3	8	13.6	14.3	7	7.9	16	10	10.6	9.5	11.5	14.6	15.1
Sep-81	1.2	3.7	1.2	1.7	3	0.5	2.2	10.1	7.5	0.9	2.5	3.2	3	5	6.4	11.6	10.1	3.7	3.5	4.2	10.6	8.8	8.8	7.3	2	6.6
Oct-81	0.5	0	0	0.2	0	0	0	0.3	3.2	0.1	0	0.1	0	0.1	0.2	0.6	1	0.7	1.2	0.8	1	0.7	0.7	0.9	0.2	1.7
Nov-81	1.3	2.5	0	0.4	1.5	1.4	0.3	0.2	0	0.1	1.3	1.3	0	0.6	0.3	0.1	0.1	2.5	2	1	0.1	0.2	0.2	0	1	3.5
Dec-81	0.2	0.2	0.4	0.6	0	0	0.1	2.9	0.9	0.3	0	0.1	0.9	0.2	1.3	2.1	5	0.5	0	0	0.9	0.2	1.2	2.1	1.3	0.6
Jan-82	1.1	2	0	0	0.4	0.5	0.7	0.6	0.1	0	0	0.5	5.4	2.1	0.9	0	0.1	0	0.1	0.5	1.5	0.8	0	0	0	0
Feb-82	1	1.6	0.1	0.1	0	0.1	0.3	0.5	2.6	0.3	0	0.1	0.3	0.7	0.3	1.4	1.1	2.5	0	0.2	0.6	0	0	1.1	0.7	0
Mar-82	3.4	7	0.2	0	0.3	1.3	1.1	3.1	2.4	1.1	0	0.2	0	2.7	1.2	1.2	3.4	0.4	0	0.1	0.3	1.2	1	0.9	0.4	0
Apr-82	1.4	2.1	0.3	0.9	5	1	0.5	5.6	9.6	0.9	0.1	0.8	0.1	0.2	1.4	6.8	15.6	4.2	0.2	0.1	0	1.2	2.4	5.3	4.1	2.8
May-82	1.6	3.4	0.1	0.3	3.9	3	1.1	5.7	5.8	0.4	2.4	2.1	0	1	3.1	7.1	8	1.1	2	0.7	0.5	1.3	2	3	2.6	2.3
Jun-82	1.6	1.5	1.7	4.5	0.2	1.3	0.9	14	11.2	4.2	0.4	1.6	1.6	3.4	5.2	21.3	16.1	9	0.3	3	5.8	6.2	7.8	13.8	28.9	12.6
Jul-82	6.6	7	4.4	3.1	5.2	12.4	4.5	19.5	13.5	1.5	6.4	8.5	7.6	7.3	8.4	22.2	15.6	6.3	5.7	6.6	10.2	10.1	9.4	9.5	28.3	10
Aug-82	9.5	15	2.5	1.6	2.6	5.1	13.6	24.5	16	1.7	2.7	9	5	11.9	13.8	17.2	18.7	7.7	4.4	4.7	11.4	14.7	15.4	18.9	16.1	10.2
Sep-82	0.9	3.1	0.6	2.4	0	0	0.7	14.3	10.2	2.5	0	1	0.2	13.5	9.3	13.7	12.3	6.4	0.7	2.4	4.2	8	7.1	7.9	0.1	9.5
Oct-82	0.7	0.6	0.5	0.4	0.5	0.5	0.2	1	0.4	0.9	0	0.3	2.7	0.2	0.7	1.9	1.7	2.3	0.1	1	1.6	1	1.8	0.5	4	1.4
Nov-82	0.6	0.1	0.1	0.1	0	0	1	1.6	3.1	0.5	1.7	1.4	0.1	1.4	1.5	0.7	3.6	3	5	3.2	0.8	1.1	1.2	1.2	0	1.9
Dec-82	0.7	1.1	0	0.1	0	0.1	0.3	0	1.3	0.3	0	0	0.6	0.2	0	0.1	0.1	0.4	0.2	0	0	0.1	0	0.1	1.2	0

Table A1 (continued)

Time / Nodes	Precipitation (mm/day)																								
	1	2	3	4	5	6	7	8	9	10	11	12	13	14	15	16	17	18	19	20	21	22	23	24	25	26
Jan-83	1.5	4.3	0	0.1	0	0.1	0.7	0.4	1.3	0.3	0	0.1	0.5	0.4	0.2	0.3	0.3	1.6	0	0	0.1	0	0	0.6	0.3	0.1
Feb-83	1	0.8	0.1	0.2	0	0	0.3	1.7	3.8	0.5	0	0	0	0.2	1	0.9	3.7	2.5	0	0	0.3	0.6	1	1.6	1.6	0.9
Mar-83	1.7	1.9	0.3	0.6	0	0.4	0.1	2.1	1.3	1	0	0	0	0.1	0.5	3.2	4.5	3.1	0	0	0.1	0.4	1	2.4	0.6	0
Apr-83	3.8	5.1	0.1	0.4	1.2	1.7	2.4	4	6.4	2.1	0.6	1.1	0	0.6	1.1	5.8	9.2	3.7	0.2	0.5	0.1	0.6	1.4	5.3	4.1	0.9
May-83	2.4	8.7	1.3	0.7	0.8	3.1	1.7	8.8	9.6	0.6	0.1	0.5	0.2	1.2	4.5	12.3	13.6	1	0	0.1	0.1	2	3.9	8.8	8.7	3.9
Jun-83	2	6.8	0.2	3	0.9	1.9	2.3	12.9	15.2	0.3	0.6	2.1	3.7	3	5.3	12.5	14.6	10.3	8.5	4.5	3.5	5.1	7.8	10.6	11.4	9
Jul-83	7.2	8.9	1.4	2	8.7	5.8	1.8	23.8	25.6	1.2	3.6	10.3	17.9	8.7	10.5	22.7	19.7	6.6	9.7	11.3	9	10.8	11.9	15.8	29.2	11.7
Aug-83	12	4.6	2.2	1.4	6.5	5.9	13.6	19.4	10.8	3.6	4.6	11	15.3	6.7	10.2	17.3	15.9	14.2	8.5	10.8	15.6	11.8	14.8	22.7	11.6	13.8
Sep-83	5.3	16.7	1.8	1.6	0.4	1.3	4.5	16.6	14.2	0.9	1.9	4.9	18.6	6.2	8.7	16	16.1	4.7	2.2	6.3	11.3	8.9	8	7.2	12.5	6.9
Oct-83	1.3	1.4	0.2	0	1	0.1	0.9	5.2	3.6	0.3	1	1.2	3.2	2.1	4.5	10	7.7	5.9	0.9	2.3	1.9	2.2	5.4	9.1	8.9	6.7
Nov-83	0	0	0	0.2	0	0	0	0	0.2	0.9	0	0	0	0	0	0.1	0.1	2.8	0	0	0	0.1	0.2	0.5	8.4	5.6
Dec-83	0.2	0.8	0	0	0	0	0.1	0.6	1.3	0.8	0	0	0	0.1	0.2	0.9	1.2	2.8	0	0	0.3	0.1	0	0.7	1.4	1.9
Jan-84	0.2	0.8	0.1	0	0	0	0	1.3	0.5	0.1	0	0.1	3	1.5	1.2	0.5	0.6	1.1	0	0	1.6	0.6	0.4	0.7	0.1	0
Feb-84	1.8	6.6	0	0	0	0.2	0	0.4	0.6	0	0	0.2	1.3	1.2	0.4	0.3	0.2	0.2	0	0.1	1.6	0.9	0.2	0	0	0
Mar-84	0.4	0.6	0	0.7	0	0	0	0.5	2.6	0.8	0	0.5	0	0	0.1	0.8	2.1	0	0	0	0	0.1	0.1	0.2	0	0
Apr-84	1.1	1.7	0	0.8	0.1	0.1	1.9	4.9	10.6	3.9	0	0.2	0	0.5	1.3	6.4	13.8	2.8	0	0	0	0.9	1.4	3	2.2	1.1
May-84	0.1	0.1	1	1.8	0	0	0.1	6.9	11.3	2	0	0	0.2	0.1	2	32.6	22.5	6.5	0	0	0	1.7	3.6	10.4	11	6
Jun-84	1.1	7	3.1	2.2	0.2	0	2.1	14.1	10.5	2.9	0.3	1.2	3.9	5.5	12.5	28	27.5	15.9	1.7	1	3.6	9.7	16.8	26.6	24.4	16.2
Jul-84	7.3	6.6	7	2.7	2.4	0.9	4.5	15.1	18	4	3	6.4	3	6.9	13.5	13.3	27.4	8.9	4.4	7.9	9.8	11.7	14.5	16.7	27.2	10.8
Aug-84	8.5	5.4	1	0.9	4	2.1	9.3	18.1	9.3	4	10.5	13.1	15.5	7.5	9.4	24.6	11.3	7.9	6.5	17.2	21.3	14.2	13.6	15.3	9.3	11.4
Sep-84	4.2	1.8	1.6	2.4	3.2	1.3	3.7	2.8	15	4.1	0.9	2.4	1.6	6.4	8.4	5.5	20	4.6	4.7	1.2	1.1	4.4	6.1	6.9	4.2	5.5
Oct-84	0	0.1	0.1	1.1	0	0	0	0.2	4.6	2	0	0.1	0	1.1	2.4	0.1	5.2	6.6	0	1.1	1.9	0.9	2.3	3.8	0	5.5
Nov-84	0.1	0	0	0	0	0	0	1	0	0.1	0.1	0	0	0	0.1	0.5	0.7	0	0	0	0	0	0.1	0.1	0.1	0
Dec-84	0.4	0.6	0	0	0	0	0	1.1	2	0.1	0	0	0	0	0.3	1.5	2.4	0.5	0	0.1	0	0	0	0	1.2	0

Table A1 (continued)

Time / Nodes	Precipitation (mm/day)																								
	1	2	3	4	5	6	7	8	9	10	11	12	13	14	15	16	17	18	19	20	21	22	23	24	25	26
Jan-85	0.3	0.8	0.1	0	0	0	0.2	0.3	0.6	0.1	0	0	0.8	1	0.4	0.1	0.2	0.1	0	0	0.9	0.9	1.2	0.2	0.2	0
Feb-85	0.1	0.1	0.1	0.1	0	0	0	0.7	0.8	0.2	0	0	0	0	0.4	0.7	1.4	1.4	0	0	0.1	0.1	0.2	0.2	0	0
Mar-85	0.3	0.1	0	0.6	0	0	0.2	2.5	5.4	2.5	0	0.3	0	0	0.4	5.1	9.4	1.5	0	0	0.1	0.2	0.6	1.7	0.4	0
Apr-85	0.6	1.3	0.1	1.5	0.1	0.2	0.5	4.2	11.3	0.9	0	0.1	0.2	0.4	1	7.8	13.5	3.9	0	0.3	0.5	0.5	1.1	2.9	2.3	2.4
May-85	0.4	2.9	0.5	1.3	2.8	0.7	0.1	5.6	5.1	1.8	0.2	0.1	0.5	0.1	3.1	13.2	9.5	6.9	0.3	0.1	0.5	1.1	2.4	7.9	15.8	7.6
Jun-85	1.5	5.3	3.3	4.9	0	0.6	1.3	13.6	18.3	2.2	1.4	0.8	3.5	2.1	5.1	24.3	18.2	15.4	0.7	1.6	6	7.4	8.4	11.2	21.9	11
Jul-85	9.2	9.8	4.7	3.1	1.6	2.4	14.8	15	19.2	4.9	3.6	5.6	13.4	10.1	15.6	26.2	25.3	7.7	5.3	7.5	13	12.9	14.8	13.9	27	10.8
Aug-85	7	9.6	3.7	2.7	1.6	2.5	8.8	12.1	11.8	2.4	4.3	10.1	16.3	10.3	8.8	13.5	12.1	6.4	6.1	8.4	11.6	12.2	11.2	11.9	17.7	9.2
Sep-85	3.1	7.2	4.5	2.7	0.2	0	4.7	8.9	8.5	2.3	0.3	1.4	6.8	6.7	7	13.3	10.6	6.6	0.7	2.2	3.5	7.2	7.1	7.1	8.6	7.1
Oct-85	6.2	10.3	0.5	0.7	0.2	0	3.6	0	2.6	0.2	2.4	3.9	5.5	3.7	5.8	3.1	4	3.4	6.5	8.6	7.4	5.7	5.2	3.8	2	2.1
Nov-85	0	0	0	0.2	0	0	0	0.7	0.5	0.4	0	0	0	0	0	0	0.2	0.6	0	0.1	0	0.1	0.4	1.1	11.7	5.9
Dec-85	1.4	3.1	0	0	0	0	0.6	1	0.5	0.1	0	0.1	0	0	0.4	0.4	0.9	0.4	0	0	0.1	0.1	0.1	0	0	0
Jan-86	0.4	0.3	0	0.1	0	0.1	0.5	0.2	0.4	0	0	0.1	0.4	0.4	0.1	0.2	0.2	0.2	0	0	0.9	0.9	1.1	0.3	0	0
Feb-86	2	2.1	0	0	0.1	0.6	0.9	0.3	1.4	0.1	0	0.2	1.5	1.4	0.3	0.1	0.4	0.3	0	0.1	1.7	0.9	0.2	0	0	0
Mar-86	1	1.2	0.1	0.2	0	0.1	0.4	0.7	2.1	0.8	0	0.1	0.7	0	0	0.4	1.2	0.8	0	0	0.2	0.1	0.1	0.2	0	0
Apr-86	0.4	2.1	0.1	1.3	0	0	0	2.6	9.5	2.5	0.1	0	0	0.1	0.9	11.6	15.8	3.5	0	0	0.1	0.9	1.6	3.9	1.5	2.3
May-86	0.8	4.8	0.6	0.1	1.7	0.7	1.1	5.4	2.9	0.5	0.1	0.5	0.4	1.8	3.9	6.7	7.4	0.6	0.1	0.1	0.6	1.7	3.5	6.6	4.6	2.1
Jun-86	2.8	2.6	0.5	1.6	0.1	3	2.8	15.4	7.6	1.1	2.8	3.6	5	2.5	5.2	13.8	12.5	6.4	8.5	6.8	6.2	6.4	7.7	11.8	30.3	10.2
Jul-86	7.3	15.2	1.9	1.8	5.2	5.3	4.3	23.8	16.9	4.4	1.8	7.3	10.4	8.2	13.3	19.7	16.5	12.3	1.2	8	10	11.2	13.2	16.4	25.9	12.8
Aug-86	5.3	6	2.5	3.3	2.1	1.6	3.5	11.9	12.4	1.6	3.2	6.9	4.8	11.9	6.5	12.5	11.7	6.1	3.4	9.8	11.4	13.1	11.9	8.2	10.9	6.9
Sep-86	3	7.1	2.7	3.1	0	0.4	2.2	17.7	13.3	1.4	0	1	1.5	5.9	11	17.9	16.3	2.6	0.1	1.6	3.4	5.5	11.4	18.4	10.4	5.8
Oct-86	0.6	1	1.1	1.6	0.1	0	1.5	5.3	5.6	4.2	0	0.2	0.8	0.2	3.7	12.2	10.5	9.6	0	0.4	0.3	1.1	2.6	5.3	7.8	6.2
Nov-86	0.1	0.4	0	0.1	0	0	0	0.9	0.9	1.3	0	0	0	0.1	0.2	2.6	3.4	2.5	0	0.1	0.6	1.4	2.7	6.2	3.8	2
Dec-86	0.4	1.6	0	0	0	0	0.4	0.4	0.4	0.3	0	0	1	0.6	0.2	0.5	0.5	0.4	0	0	1.6	0.6	0	0	0	0.1

Table A1 (continued)

Time / Nodes	Precipitation (mm/day)																								
	1	2	3	4	5	6	7	8	9	10	11	12	13	14	15	16	17	18	19	20	21	22	23	24	25	26
Jan-87	2.2	1	0	0.3	0.2	1.6	0.8	0.3	0.1	0.2	0	5.9	0.9	0.5	0	0.1	0.2	0.6	0	0.1	0.5	0.3	0	0.1	0	0
Feb-87	1.8	2.3	0	0	0	0.7	0.3	0.6	1.6	0.6	0	0	1.7	0.5	0.2	0.3	1	1.6	0	0.1	0.6	0.3	0.2	0.2	2	0.1
Mar-87	1.3	0.5	0	0.5	2.8	0.5	0.2	2	5.2	0.3	0.3	0	0	0.3	0.3	2.8	6.2	1.1	0	0.1	0.8	0.5	0.5	1.2	0.3	0
Apr-87	0.5	11.4	0.5	0.7	0	0	0	5.9	7.7	1.4	0	0	0	0	1.4	9.7	16	3	0	0	0	0.7	2.1	5.8	6.5	3.4
May-87	2.2	4.8	0	0.8	1	0.9	2	2.8	8.5	0.5	0.2	0.9	0.5	0.3	0.6	7.2	8.1	0.3	0.1	0.4	0.7	1.6	1.9	3.4	1.7	1
Jun-87	2.4	2.2	1.2	1.9	1.4	0.5	0.9	12.8	8	1.3	0.3	2.8	2.1	0.3	6.1	15.7	11.8	7.4	0.6	3.3	4.3	4	5.1	8.1	7.5	7
Jul-87	3.3	3.6	3.7	5.2	0.6	0.3	2.4	28.5	17.7	4.2	0.6	3.2	7.1	5	8.9	23.3	22.8	9.9	0.9	4.5	7.8	9.4	12.9	21.2	13.7	17.4
Aug-87	2.8	7.2	4.7	4.9	0.8	0.8	4.8	15.9	12.8	3.1	2.5	4.9	15.2	8.5	4.3	14.1	13.6	7	3.7	10.9	11.4	11.3	11	19	2.9	16.7
Sep-87	0.9	3.2	2.5	5.2	0	0	1.1	19.2	16.5	3	0	0	6.2	6.8	6.3	3.7	16.8	8.5	0.1	0.3	2.1	5.4	7.1	11.3	3.4	9.5
Oct-87	2.2	2.7	0.3	1.6	0	0.3	0.2	2.4	2.4	0.3	0	2.2	0.4	2.7	0.6	0.6	4.2	1.1	0	1.3	1.7	1.9	2.1	2.3	0.2	1.1
Nov-87	0	0	0	0	0	0	0	0	0.4	1	0	0	0	0.3	0.6	0.3	1	1.5	0	0.4	3.1	0.1	0.8	1.2	1.5	2.5
Dec-87	0.5	0.6	0	0.3	0.2	0	0.3	0.2	0.8	0.5	0.6	0.8	0.9	0.1	0.2	1.2	0.3	0.5	0.3	0.9	0.5	0.2	0.2	0.3	0	0
Jan-88	0.4	0.5	0	0.1	0.2	0	0.1	0.3	0.6	0.4	0	0.4	0	0.3	0.2	0.1	0.3	0.2	0	0	0	0.1	0.1	0	0	0
Feb-88	0.8	2.4	0	0.2	0	0	0.2	1.2	1.2	1.1	0	0	0.1	0.3	0.7	1.3	2.3	1.3	0	0	0.4	0.8	0.8	0.9	0	0
Mar-88	2.6	1.3	0	0.7	0.3	1.2	0.8	3.7	4.7	2.4	0	0.1	0	0.8	2.1	2.5	7	0.6	0	0	0.2	0.6	1.4	1.5	0.4	0
Apr-88	0.4	2	0.2	0.9	0.7	0	0.7	4.2	7.1	3	0.1	0	0.1	0.1	1	6	7.9	2	0.1	0.3	0.7	1.2	1.6	3	5.6	2.6
May-88	0.1	1.6	0.2	3.4	0	0	0.1	6.4	13.9	3.7	0	0	0	0.4	0.6	18.4	18.2	8.8	0	0	0.1	1.9	3.1	11	11.2	7.9
Jun-88	2.5	4.2	0.7	1.2	1	1.5	2.6	17.6	7	0.9	0.5	4.8	6.8	5.9	4.5	25.4	19	8	1	3.5	5.5	7.4	9.9	19.6	25.9	15.4
Jul-88	9.6	11.9	3.6	3	5.8	1.7	7.4	24.2	23.4	4.3	8.6	9.7	6.9	7.7	7.2	28	22.7	8.8	12.4	12.1	10.8	11.5	11.7	13.2	30.6	14
Aug-88	9	13	7.2	3.7	4	1.6	10.1	27.9	25.1	4.8	4.9	5.6	6.8	7.5	13.2	28.9	28.5	9.4	4.8	9.2	11.4	10.8	11.6	13.3	17.2	12.4
Sep-88	5.6	4.6	2	3.7	3.1	1.4	2.1	5.9	12.3	0.8	1.7	5	2.7	3.5	4.8	16.4	12.7	7.2	3.2	6.4	9.5	6.6	7.9	7.8	6.1	8.1
Oct-88	2	2	0	0.4	0	0.9	0.8	0	8.3	2.1	0	0.1	0	1	1.8	6	9.1	4.7	0.1	2.2	1.6	1.4	2.1	5	2.8	4.7
Nov-88	0	0	0	0.3	0	0	0	1.4	0.8	1.6	0	0	0	0	0.5	3.5	5.5	2.3	0	0	0.9	0.5	0.9	3.2	2.6	2.4
Dec-88	0.8	1.3	0	0	0	0	0	1.1	0.5	0	0	0	0.1	0.5	0.2	0.6	2.5	0.1	0	0	0.1	0.2	0.1	0	1.5	0.3

Table A1 (continued)

Time / Nodes	Precipitation (mm/day)																								
	1	2	3	4	5	6	7	8	9	10	11	12	13	14	15	16	17	18	19	20	21	22	23	24	25	26
Jan-89	1.9	3.6	0	0	0.2	0.9	0.8	0.3	0.6	0.1	0.1	0.4	0.1	0	0.3	0.2	0.3	0.1	0.1	0.1	0	0	0.1	0	0	0
Feb-89	0.4	0.9	0	0.1	0	0	0	1.6	3.9	2.9	0	0	0	0	0.3	1.5	4.2	0.5	0	0	0	0	0.2	0.3	0.2	0
Mar-89	1.3	1.8	0	0	0.2	0	0.8	0.5	1.3	0.2	0	0	0.9	0.2	0.2	0.3	0.9	1.9	0	0.4	2.6	1.1	0.4	0.2	0	0
Apr-89	0.1	0.1	0.2	1.3	0	0	0	2.9	6.7	3	0	0	0	0	0	8.8	14	1.4	0	0	0	0.3	0.8	2.9	5.4	1.2
May-89	0.3	1.8	0.5	2.7	0	0	0	4.3	6	0.4	0	0	0	0.4	0.6	10.6	7.3	1.4	0	0.2	0.2	1.7	3	6.3	2.7	4.2
Jun-89	1	6.2	1.4	3	0.3	0.2	0.1	16.6	11.9	1.1	1.1	0.6	3.5	4.6	6	18.5	18.4	6.2	3.9	6.2	5.3	6.4	8.2	8.4	8.6	6.8
Jul-89	8.6	9.1	3.3	3.3	2.4	3.8	5.2	27.9	16.8	5.4	4.4	2.6	6.9	10.5	8.3	8.7	23.8	12.1	7.4	5.1	8.5	11.2	13.9	16.9	9.1	14.3
Aug-89	6	8.3	4.7	3.4	5.5	3.7	8.9	13	12.5	1.4	5.4	9.6	14.4	5.3	6.7	16.2	11.7	7.1	6.8	9.7	10.1	9.7	7.4	5.3	13.4	6.9
Sep-89	4.1	4.5	1.6	2.3	0.8	0.5	2.9	16.2	15.2	4	0.3	0.4	1.4	3.9	7.5	9	17.4	4.4	0.4	4	4.1	6.2	8.6	10.4	18.1	6.9
Oct-89	0.3	0.4	0.2	2.1	0	0	0.1	4.4	9.7	5	0	0	0	0.9	1.4	0.3	11	14.2	0	0	0.3	1.2	3.3	11.5	0	10.9
Nov-89	0.3	0.3	0	0.6	0	0	0.1	0.2	1	0.6	0	0	0	0.4	0	0.1	0.7	0.3	0	0	0	0.1	0	0.1	0	0
Dec-89	0.2	1	0	0.1	0	0	0.2	0.3	0.6	0.3	0	0	0.4	0.8	0.1	1.1	0.3	1.1	0	0.1	0.9	0.5	0.1	0	1	0
Jan-90	0.3	0	0	0.1	0	0	0	0.1	0.7	0.5	0	0	0	0	0	0.1	0.2	0	0	0	0	0	0	0	0	0
Feb-90	4	3.9	0	0.1	1.1	0.7	1.5	1	2.6	0.8	0.2	0.5	1	1.2	0.3	1.7	1.9	1.4	0.2	0.2	0.6	0.3	0	1.9	2.3	1.6
Mar-90	1.7	3	0.2	0	0	0	0	2.5	2.3	1.3	0	0	0.1	0.2	0.8	3.2	5.7	3.3	0	0	0.5	1.2	2.2	4.1	0.8	1.8
Apr-90	0.3	0.7	0.5	0.4	0	0	0.1	4	8.5	1.4	0	0	0	0.4	0.4	10	15.4	2	0	0	0	0.6	1.4	4.2	3.6	0.9
May-90	1	3.8	2.2	1.5	0.1	3.2	1	12	7.2	1.7	0.3	0.7	0.7	1	6.1	12.8	9.2	7.5	0.6	1.2	2.5	5.6	8	9.9	8.8	7.3
Jun-90	1.2	5.8	3.6	4.8	0.1	0.4	2.7	16.3	23.4	3.9	0.2	2.6	16.1	8.5	5.9	18.9	20.2	9.1	0.9	3.2	9.9	10.5	9.9	12.9	9.2	12.7
Jul-90	6	15	6.2	4.1	2.7	1.6	7.8	10.8	21.4	4.2	3.2	9.1	22	14.3	10.7	29.8	31	11.1	4.1	8.1	11.5	13.7	15.9	22.5	8.6	14.7
Aug-90	10.9	12.8	4	2.7	7.3	2	11.9	14.3	11.5	2.6	8.3	4.3	21.7	10.3	7.7	11.4	8.1	2.2	13.4	19.6	16.1	14.4	11.3	7.2	7.9	4
Sep-90	7.2	4.2	3	4.7	2.9	0.4	9.4	6.2	22.3	3.7	3.5	3.2	11.7	7.9	7.1	13.8	16.4	5.2	3.4	5.9	4.7	7.6	8.1	7.8	28.2	5.7
Oct-90	0.7	0.8	0.2	2.3	0	0	0	0.1	3.1	0.7	0.1	0.2	0.3	0.6	8.4	9.2	9.6	1.4	0.3	0.5	2.1	4.7	7.3	6.2	0.6	3.8
Nov-90	0.9	0.5	0	0.1	0	0.1	0.2	0	0.1	0	0	0.6	0	0	0	1.1	0.5	0.8	0	0.2	0.1	0.1	0	2.4	1.5	8.6
Dec-90	1.4	3.3	0	0	0.1	0	0.3	1.1	0.5	0.5	0.6	0	0	0.1	0	0.2	0.1	0.7	0.4	0.8	0.8	0.3	0.1	0.5	0	0

Table A1 (continued)

Time / Nodes	Precipitation (mm/day)																								
	1	2	3	4	5	6	7	8	9	10	11	12	13	14	15	16	17	18	19	20	21	22	23	24	25	26
Jan-91	0.1	0.4	0.1	0.1	0	0	0.1	0.6	3	0.7	0	0	0	0.7	0.3	0.6	0.4	2.8	0	0	0.5	0.5	0.5	0.6	0.2	0
Feb-91	1.6	1.9	0.1	0.1	0	0.2	0.9	0.2	1.6	0.2	0	0.1	0.2	0.4	0	0.4	0.5	0.6	0	0	0.2	0.2	0.2	0.3	0	0
Mar-91	0.7	2.1	0.1	0.4	0	0	0.1	2.2	3.4	0.9	0	0	0.7	0.6	0.4	1.8	4.6	0.8	0	0	0.2	0.5	0.8	1.6	1.2	0.1
Apr-91	0.6	1.9	0.3	0.4	0	0	0.1	3.1	5.3	2.2	0	0	0.3	0.4	0.8	3.7	7.4	3.4	0	0	0.5	0.8	0.8	1.6	9.2	3.7
May-91	0.9	3.6	0.4	0.9	0	0.9	1.3	5.4	12.1	3.2	0	0	0	0.3	0.9	14.5	18.7	4.8	0	0	0	1.5	1.7	4.1	5.5	3.6
Jun-91	2.1	4	2.7	3.2	0.5	0.9	0.3	13.8	19.9	2.6	0.3	2	3.9	4.6	4	21.4	18.5	9.2	0.8	5.6	5.9	9.1	10.5	15.3	30.8	10.9
Jul-91	3.4	6.5	5.1	6.6	4.8	1.5	4.8	17.9	19.6	3.5	5.5	9.7	4.2	7.5	7.2	20.5	15.8	9	9	12.9	11.4	11.3	10.5	15.2	31.8	12.2
Aug-91	6	8	4.8	6.4	1.1	0	8.6	23.9	15.5	3.9	1.4	8	17.6	6	12.4	22	19	8.5	2.3	4.4	11	10.7	13.1	16.1	0	13.6
Sep-91	2.1	2.8	2.2	2.4	0.4	1.1	3.6	12.5	15.3	3.1	0.4	0.9	1	4.4	6.8	13.2	13.1	8.4	0.3	0.6	0.8	5.5	9.5	10.5	13.1	8.2
Oct-91	0.3	0.3	0	0.3	0	0	0	5.9	6.3	1.3	0	0	0	0.3	2.3	11.3	14.3	4.1	0	0.1	0.1	0	2.6	6.8	9.9	5.1
Nov-91	0.3	0.2	0	0.1	0	0	0.3	0	0.6	0.7	0	0.1	0.1	0	0	0	0.3	3.1	0	0.1	0	0	0	0.1	0	2.7
Dec-91	0.7	0.6	0.1	0	0	0.2	0.7	1.2	1.8	0.2	0	0.4	0	1	0.3	1	2.6	0.7	0	0	0	0.3	0.2	1.1	2.1	0.6
Jan-92	1.6	2.4	0	0.1	0.1	0.5	0.5	0.5	1.7	0.4	0	0	0	0.1	0.3	0.3	0.5	0.7	0	0	0	0.1	0.2	0.3	0.3	0
Feb-92	1.5	2.4	0	0.2	0.5	0.9	0.5	1.3	4.9	1.5	0.5	0	0.2	0.6	0.9	1.2	2.7	2.2	0	0	0	0.5	0.6	1	0	0.7
Mar-92	0.9	1.2	0.1	0.4	0.1	0.2	0.6	0.4	4.7	1.5	0	0	0	0	0	0.2	2.1	1.6	0	0	0	0	0	0	0	0
Apr-92	0.3	0.7	0.1	0.4	0	0	0.1	1.8	8.2	2.3	0	0	0	0.1	0.3	2.2	6.8	2.5	0	0	0.1	0.3	0.3	0.6	0.6	0
May-92	0.6	1.8	1	1.2	0.2	0.7	0.6	4.9	7.7	1.3	0	0.3	1	0.4	2.2	13	14.2	2.1	0	0.4	0.7	1.5	2.7	6.3	8.4	2.5
Jun-92	0.8	3.7	2.2	1.6	0	0.2	0.6	14.4	14.6	1.2	0.4	0.9	0.2	1.3	3.2	17	22.8	2.3	1	2.8	2.4	4.3	6.8	11.7	13.6	6.9
Jul-92	3.8	4.7	2.2	1.5	4	1.9	2.9	24.3	15.8	3.6	5.3	5.1	1.3	4.4	9.7	29.8	20	11.3	8.8	5.9	6.2	9.7	13.6	21	13.3	16.1
Aug-92	8	8.8	3	2	3.5	5.5	7.9	13.1	7.5	3.3	3.1	7.1	8.8	6.8	3.9	13.6	13.4	9.2	3.7	7.2	14.2	10.5	8.2	7.1	8.8	7.7
Sep-92	8.1	7.9	1.4	2.4	2.3	5	4.7	8.9	14.8	1.5	2.7	5	10.7	5.4	2.9	10.2	11.5	6.2	4.8	7.7	11.8	6.4	5.6	7	3.8	6.6
Oct-92	1.4	0.8	0.1	0.3	0	0.9	2	2.2	4.5	2	0	3.7	0	2.1	1.5	3.1	4.4	8.4	0.1	1.1	0.9	1	1.2	2.6	3.4	5.2
Nov-92	0.7	0.5	0	0	0	0	0.3	0.1	0.3	0.3	0	0	0	0.1	0	0.2	0.4	0.9	0.1	0.1	0.3	0.1	0	0.3	0	1.6
Dec-92	0.1	0.1	0	0	0	0	0	0.2	0.1	0.1	0	0	0	0	0	0.2	0.4	0.2	0	0	0	0	0	0	0	0

Table A1 (continued)

Time / Nodes	Precipitation (mm/day)																								
	1	2	3	4	5	6	7	8	9	10	11	12	13	14	15	16	17	18	19	20	21	22	23	24	25	26
Jan-93	0.4	0.7	0.1	0.1	0	0	0.2	1.8	1.9	0.7	0	0	0	0	0.6	1.5	1.7	1.5	0	0	0	0	0	0.3	1.1	0.1
Feb-93	0.7	1.3	0	0.2	0.8	1.2	0.3	1	3.3	2.2	0.9	0	0.5	0.3	0.3	0.7	2.7	3.7	0.1	0	0.7	0.3	0.1	0	0	0
Mar-93	0.8	2.3	0.3	0.1	0	0.1	0.4	2.4	5.4	0.5	0	0.1	0.1	0.7	0.5	4.5	7.2	0.8	0	0.1	2.8	1.3	1.3	3.4	1.6	0
Apr-93	0.4	0.9	0.6	0	0	0	0.1	3.8	20	0	0	0	0	0	0.7	15.9	15	0	0	0	0.1	0.8	2.6	8.5	8	2.4
May-93	0.2	1.8	1.2	2.3	0.2	0.2	0.4	7.8	12.3	2.9	0	0.2	0.3	0.6	3.1	10.5	18.2	7.2	0	0.1	0.6	2.3	4.2	12.9	21.4	9.4
Jun-93	1.6	6.8	3.9	3.2	2.1	1	3.5	14.6	18.4	2.6	0.4	2.8	2.9	1.5	3.3	29.1	23.9	9.9	0.6	3.6	4.9	5.4	6.4	11.2	43.6	10.3
Jul-93	9.5	13.5	5	2.8	6.3	4.6	9.6	21.4	19	4.8	9.3	10.7	4.6	10.5	6.3	21.5	19.8	9.3	11.3	13.9	13	12.1	12.4	20.8	30.4	13.9
Aug-93	2.4	4.6	6.3	3.4	1	0.6	5.1	17.6	22	3.4	0.9	6	5.2	5.8	5.2	18	19.9	7.4	1.3	5.9	8.7	9	10.8	16.2	17.9	12.2
Sep-93	5.3	8.4	2.7	2.4	1.3	1.4	5.9	18.2	15.5	3.2	1.4	3.7	2.4	7.9	10.6	6.2	16.8	8.9	2.2	6	8.9	10.8	12.5	14.3	11	9.8
Oct-93	0.3	0.9	0.2	0.4	0.4	0.1	0.4	2.2	3.2	1.2	0.1	0.3	0.8	1.8	1.7	0.6	4.1	3.4	0.4	0.5	1.9	3.5	5	7.5	3.2	5.1
Nov-93	0	0	0	0.1	0.3	0.2	0	0.1	0.2	0.1	0.4	0.1	0	0	0.1	0	0.3	0.1	0.5	0.2	0	0.1	0.4	1.2	0	0
Dec-93	0	0	0	0	0	0	0	0	0	0	0	0	0.1	0	0	1.5	0	0	0	0.1	0.3	0.4	0	0	0	0
Jan-94	1.4	2.6	0	0	0.8	0.6	0.8	1.4	1.3	0	0.2	1.3	0.6	1.1	1.7	0.2	0.7	0	0.2	0.8	1.1	0.2	0.2	0.1	0.1	0
Feb-94	1.1	1.9	0	0.1	0	0	0.7	1.3	2	0.9	0	0	0.7	0.7	1	1.4	1.8	2.2	0	0	1.6	0.7	0.8	1.5	0.9	0.1
Mar-94	0.3	0.5	0	0.4	0	0	0.1	0	6.4	2	0	0	0	0	0	0	0	2.8	0	0	0	1	1.4	0	0	2.2
Apr-94	0.9	6.2	0.3	0.4	1.2	1	1.5	3.3	8.2	1.1	0	0	2.9	1.5	0.6	7.3	8.1	1.4	0	0.1	2.5	1.4	1.8	4.2	4	1.4
May-94	0.8	2.6	1.1	1.2	0.1	0.8	0.5	3.7	9.1	0.9	0	0.2	0.6	0.1	1	15.9	12.1	1	0	0.1	0.3	2.1	3	9.8	13.2	5.5
Jun-94	1.8	5.2	1.7	2.6	0.3	0.7	2.4	16	11.8	2.7	1	5	10.6	7.7	4	20.4	18.8	8.3	2.3	7.3	6.3	8.4	8.4	11.4	13.7	10
Jul-94	10.4	11.4	3.3	3.4	6.3	2.2	16.6	19.5	9.8	4.3	8	10.2	23.8	10.4	8.3	23.1	15.3	7.6	9.7	9.8	20.1	15.8	15.1	18.1	26.3	13
Aug-94	6.5	9.1	3.2	1.2	7.8	3.7	10.1	18.2	9.2	2.9	6.1	12.6	12.8	10.5	8.8	18.3	14.7	7.4	7.2	12.8	12.7	12.7	12.1	14.1	6.6	13.1
Sep-94	4.9	2.5	0.9	0.8	1.4	1.2	0.7	6.7	12.2	1.5	9.7	4.9	2.5	4.6	4.5	5.5	11.8	4.9	11.8	11.4	9	6.3	4.9	5.4	0	7
Oct-94	0.7	0	0.3	0.9	0	0	0	3.5	11.9	1.2	0	0	0.6	1.4	2.1	4	5.1	0.9	0	0.1	3.3	2.8	4.9	6.7	0.8	2.6
Nov-94	0	0	0	0.3	0	0	0	0.1	0.6	0.8	0	0	0	0	0	0.3	0.2	2	0	0	0.2	0	0	0.3	0	1.7
Dec-94	0.5	0.2	0	0.1	0	0	0	0	0	0.4	0	0	0	0	0	0	0	0.7	0	0	0	0	0	0	0	0.6

Table A2: HadCM3 GCM Projected Precipitation for Scenario A1FI

Time / Nodes	Precipitation (mm/day)																								
	1	2	3	4	5	6	7	8	9	10	11	12	13	14	15	16	17	18	19	20	21	22	23	24	25	26
Jan-20	1	1.8	0	0.1	0.1	0.3	0.4	0.5	0.7	0.3	0.1	0.5	1.1	0.8	0.7	0.2	0.3	0.4	0	0.1	1	0.4	0.3	0.3	0.1	0
Feb-20	1.3	2.3	0	0.1	0.2	0.2	0.4	0.8	2.2	0.8	0.1	0.1	0.7	0.6	0.6	0.9	2	1.3	0	0.1	0.7	0.4	0.4	1.2	0.6	0.1
Mar-20	1.7	2.1	0.1	0.4	0.3	0.4	0.4	1.5	3.2	1.3	0	0.1	0.2	0.4	0.4	1.5	3.4	1.1	0	0	0.5	0.4	0.5	0.9	0.2	0.1
Apr-20	0.6	1.6	0.3	1.1	0.4	0.2	0.3	4.2	8.8	3.1	0.1	0.2	0.1	0.3	0.8	6.3	10.7	2.8	0	0.1	0.2	0.7	1.1	3.5	4.9	1.7
May-20	0.5	2.6	0.9	1.4	0.3	0.6	0.5	5	6.3	1.1	0.4	0.3	0.2	0.4	2	8.9	9.1	3.8	0.3	0.1	0.5	1.2	1.8	3.3	6.4	4
Jun-20	2.4	6.1	2.1	3.5	1.2	1.4	2	20.2	19.7	3.2	1.8	3.2	6.4	4.7	7.2	25.9	19.8	10.8	3.5	5.8	6.7	5.1	9.7	19.6	20.4	12.2
Jul-20	8.3	9	4.4	3.9	5.5	4.4	5.4	24.5	22.6	4.1	3.4	7.2	9.6	7.7	14.2	26.1	23.7	9.2	2.7	9.1	8.4	9.7	16.2	20.3	21.1	10.8
Aug-20	6.9	10.9	3.3	3.4	5.2	2.5	10.1	20.3	16.8	3.4	5.8	10.5	15	9.9	9.8	17.9	15.3	9.1	7.5	14.2	15	11.5	10.1	17.8	12.6	10.2
Sep-20	4.6	11.1	1.7	3.9	3.8	2	5.4	13	14.2	3.4	1.9	3.4	6.7	10	8.5	10.7	14.4	6.1	2.9	5.1	8.6	7.6	6.5	6.5	12.5	5.5
Oct-20	1	1.4	0.5	1.1	0.4	0.2	0.8	3.5	6.6	2.3	0.5	0.7	1.1	1.2	3.4	6.5	9.4	6	0.7	1.3	1.8	2.1	3.8	6.5	5.5	5.9
Nov-20	0.5	0.4	0.1	0.2	0.4	0.3	0.2	0.6	0.9	0.7	0.6	0.6	0.8	0.4	0.4	0.8	1.2	1.7	1.1	1	1.4	0.6	0.6	1.1	1.8	2.5
Dec-20	0.8	1	0.1	0.1	0.1	0	0.3	0.9	1.1	0.3	0.1	0.2	0.6	0.3	0.3	0.7	1.2	0.8	0.1	0.3	0.6	0.3	0.2	0.4	0.9	0.3
Jan-50	1.2	2.4	0	0.1	0.1	0.4	0.6	0.5	0.7	0.2	0.1	0.6	1.4	0.9	0.7	0.2	0.2	0.4	0	0.1	0.8	0.5	0.3	0.2	0.1	0.1
Feb-50	0.9	1.3	0	0.2	0.2	0.2	0.3	0.8	2	0.6	0	0.1	0.5	0.7	0.4	0.6	1.2	0.9	0	0.1	0.6	0.4	0.3	0.7	0.4	0.1
Mar-50	1.4	2.8	0.1	0.4	0.3	0.3	0.5	1.5	3.3	1.6	0	0.1	0.3	0.5	0.4	1.6	3.3	1.3	0	0	0.6	0.5	0.5	0.9	0.2	0.1
Apr-50	0.4	1.7	0.4	1.2	0.3	0.1	0.4	5	12.4	4.8	0.1	0.2	0.1	0.3	1.1	8.9	12.5	3.3	0.1	0.1	0.2	0.8	1.4	4.1	4.3	1.4
May-50	0.8	2.5	0.6	1.1	0.5	1	0.5	3.6	3.8	0.6	0.3	0.5	0.3	0.3	1.6	7.9	6.6	3.4	0.3	0.2	0.6	1.2	1.8	3.1	6.5	3.7
Jun-50	2.8	6.7	1.8	3.2	1.1	1.6	1.9	17.4	15.8	2.7	2.1	3.1	6.6	5.9	7.5	21.4	19.5	11.8	3.5	5.6	6.7	4.4	11.9	15.9	18.7	13.6
Jul-50	6.6	5.4	5.9	3.8	5.3	3.6	3	33.8	24.2	4.2	1.6	8.2	7.1	5.8	17.1	33.7	29	9.2	2.5	9.5	7.6	7.3	19.8	30.5	23.8	8
Aug-50	6.5	13.4	3	3.7	4.6	2.5	11.5	24.3	19.1	3.6	7.8	10.5	18.2	13.3	12.3	23.8	17.3	8.5	5	14.6	16.6	7.1	5.4	23.2	13.4	6.7
Sep-50	5.1	9.8	1.8	4.7	3.5	2.4	4.9	13.1	14.6	3.4	2	3.5	6.5	7.7	9.1	9.4	16.2	5.9	2.7	5.5	7.8	9.2	4.9	3.9	13	4.1
Oct-50	1.2	1.5	0.7	1.5	0.4	0.1	0.8	4.8	8.3	2.6	0.5	0.7	1.2	1.6	4.3	7.1	9.8	6.9	0.8	1.4	1.9	2.3	3.8	5.2	5.1	4.7
Nov-50	0.4	0.4	0.1	0.2	0.3	0.2	0.2	0.7	0.9	0.7	0.4	0.3	0.8	0.4	0.4	0.7	1.4	1.4	0.8	0.6	1.3	0.5	0.6	1.5	2.2	2.5
Dec-50	0.6	0.9	0.1	0.1	0.1	0	0.3	0.7	0.9	0.3	0.2	0.2	0.7	0.3	0.3	0.6	1.1	0.8	0.2	0.4	0.7	0.3	0.2	0.4	0.9	0.3

Table A2 (continued)

Time / Nodes	Precipitation (mm/day)																								
	1	2	3	4	5	6	7	8	9	10	11	12	13	14	15	16	17	18	19	20	21	22	23	24	25	26
Jan-80	0.6	1.6	0	0.1	0.1	0.2	0.5	0.5	0.6	0.3	0	0.4	1.4	0.8	0.6	0.2	0.2	0.4	0	0.1	0.7	0.4	0.3	0.2	0.1	0
Feb-80	0.6	1.9	0	0.2	0.1	0.1	0.4	0.8	2.2	0.7	0	0.1	0.5	0.6	0.5	0.6	1.5	0.8	0	0	0.5	0.4	0.3	0.7	0.4	0.1
Mar-80	0.6	2.7	0.1	0.4	0.2	0.2	0.5	1.4	3.1	1.4	0	0.1	0.3	0.5	0.5	2.1	4.4	1.4	0	0	0.6	0.5	0.6	1.1	0.3	0.1
Apr-80	0.5	1.8	0.3	1	0.2	0.1	0.5	3.9	8.4	3.1	0.1	0.1	0.1	0.2	0.9	7	12.2	3.2	0.1	0	0.3	0.7	1.3	3.1	4.5	1.4
May-80	0.5	1.8	0.6	1.3	0.1	0.5	0.3	3.7	5.4	1.1	0.3	0.3	0.2	0.2	1.2	7.4	7.1	3.4	0.3	0.1	0.5	0.8	0.8	1.3	5.5	2.2
Jun-80	2.8	5.6	1.3	3.3	0.9	1.5	2.5	23.4	18.6	3.2	1.9	3	7.6	6.1	9.9	32.7	26.6	15.1	3.7	6.5	7.8	3.7	15.7	28.1	26.2	19.3
Jul-80	8.4	10.3	5.9	3.6	5.5	4.3	5	35.2	27.9	5.1	2	8.2	8	4	20.6	38	31.3	6.5	1.7	9.8	7.7	3.9	24.5	32.9	29.1	4.5
Aug-80	6.5	14.7	2.8	3.4	5.1	2.3	12.7	26.8	22.3	4.1	8.9	11.3	20.2	15.1	14.4	25.5	18.9	10.5	2.7	15.4	19.5	4.2	3.7	24.6	15.1	3.6
Sep-80	6.5	10.8	1.8	4.2	3.8	2.9	4.7	11.4	15.8	2.9	1.5	3.7	6.1	8.2	10.1	8.6	18.3	4.7	3.5	6.1	7.9	9.8	3.8	2.1	15.6	2.3
Oct-80	1.5	1.8	0.7	1.9	0.5	0.2	1	5.7	10.9	3.3	0.6	0.9	1.5	1.6	4.8	8.2	10.6	8.2	1	2.1	2.3	2.5	4.4	5.3	4.6	4.3
Nov-80	0.4	0.4	0.1	0.1	0.3	0.2	0.3	0.7	0.7	1	0.7	0.5	1.3	0.6	0.5	0.7	1.1	0.6	1.1	1.1	2	0.8	0.7	1.4	2.2	2.3
Dec-80	0.6	1.1	0.1	0.1	0.1	0	0.3	0.7	0.9	0.3	0.1	0.2	0.7	0.3	0.3	0.6	1.1	0.8	0.1	0.2	0.6	0.3	0.2	0.3	0.8	0.3

Table A3: HadCM3 GCM Projected Precipitation for Scenario A1B

Time / Nodes	Precipitation (mm/day)																								
	1	2	3	4	5	6	7	8	9	10	11	12	13	14	15	16	17	18	19	20	21	22	23	24	25	26
Jan-20	1	1.7	0	0.1	0.1	0.3	0.4	0.5	0.6	0.3	0.1	0.5	1	0.7	0.5	0.2	0.3	0.5	0	0.1	0.6	0.3	0.3	0.3	0.1	0.1
Feb-20	1.4	2	0	0.2	0.2	0.2	0.5	1.1	2.7	0.9	0	0.1	0.7	0.8	0.5	0.8	2	1.5	0	0.1	0.5	0.5	0.3	0.8	0.6	0.2
Mar-20	1.3	2.2	0.1	0.3	0.3	0.4	0.4	1.6	3.2	1.3	0	0.1	0.3	0.5	0.5	1.7	3.3	1.1	0	0	0.7	0.5	0.7	1.3	0.3	0.2
Apr-20	0.4	1.7	0.3	0.9	0.5	0.1	0.4	3.6	9.3	2.8	0.1	0.1	0.1	0.3	0.8	6.9	14.9	4.9	0.1	0.1	0.2	0.8	1.6	4.3	6.5	3.9
May-20	0.6	2.6	1.2	1.5	0.3	0.7	0.6	7.4	11.7	1.3	0.3	0.4	0.2	0.5	2	12.9	16	4.4	0.3	0.1	0.4	1.4	1.7	3.5	9.3	5
Jun-20	2.2	4.3	2.3	2.9	1.4	1.3	2.1	18.3	16.8	2.5	1.8	2.8	5.1	5.2	10.2	22.5	16.3	9	4.4	4.9	5.9	8.9	11.9	14.4	18.3	9.1
Jul-20	8.5	10	4.7	3.3	5.8	4.3	6.8	25.9	17	3.9	3.6	7	10.6	10.2	12.2	26.8	24.3	9.4	3.7	8.5	10.2	10.2	17.6	24.6	22.1	10
Aug-20	7.1	10.4	3.8	2.7	5.1	2.4	11.4	18.8	13.6	2.8	5.1	10.8	16.2	13.3	11.2	18.5	15	8.8	7.6	13.6	16.9	15.8	10.9	9.7	12.8	9.6
Sep-20	3.2	5.5	2.7	4.1	2.8	1.6	3.3	14.5	15.3	2.8	1.7	2.2	4.8	6.8	7.1	12	14.1	6	2.3	3.2	5.8	6.5	6.6	7.9	9.2	5.8
Oct-20	1.5	1.8	0.5	1.4	0.4	0.2	0.7	3.8	6.4	2.2	0.5	0.6	0.8	1	3.1	4.9	7.9	5.6	1.1	1.5	1.6	2.1	3.1	4.7	4.6	4.3
Nov-20	0.3	0.4	0.1	0.2	0.2	0.2	0.2	0.7	0.7	0.5	0.4	0.5	0.7	0.6	0.4	0.7	1.3	1.5	0.6	1	1.1	0.7	0.6	1.3	2.4	3
Dec-20	0.7	0.9	0	0.1	0.1	0	0.2	0.8	0.9	0.3	0.1	0.2	0.6	0.3	0.3	0.6	1.1	0.8	0.1	0.3	0.6	0.3	0.2	0.3	0.8	0.3
Jan-50	0.8	1.8	0	0.1	0.1	0.3	0.4	0.5	0.7	0.3	0.1	0.5	0.8	0.7	0.6	0.2	0.3	0.6	0	0.1	0.6	0.4	0.3	0.3	0.2	0.1
Feb-50	1	2.2	0	0.2	0.2	0.2	0.6	0.9	2.6	0.8	0.1	0.1	0.9	0.8	0.6	0.8	1.9	1.6	0	0.1	0.6	0.5	0.4	1	0.7	0.2
Mar-50	1.3	2.4	0.1	0.4	0.2	0.3	0.5	1.6	3.1	1.4	0	0.1	0.3	0.5	0.5	1.9	3.4	1.3	0	0	0.7	0.5	0.7	1.1	0.3	0.1
Apr-50	0.7	2.4	0.3	0.8	0.4	0.2	0.5	4.2	7.1	1.8	0.1	0.1	0.1	0.3	0.9	7.4	13.3	3.2	0.1	0.1	0.2	0.8	1.5	3.2	5.4	2
May-50	0.5	2.9	1	2	0.3	0.6	0.6	6.6	14.2	2.3	0.3	0.4	0.3	0.5	2.8	13.3	16	5.7	0.3	0.2	0.5	1.6	2.5	3.8	8.6	5.3
Jun-50	2	4.2	2.5	2.7	1.4	1.2	2	21.3	18.4	2.5	2.1	2.9	5.6	3.8	6.3	31.9	18.1	11.2	4.2	4.6	6.8	6.9	9.5	18	18.5	10
Jul-50	8.2	10	4.6	3.4	4.6	4.3	6.2	32.3	14.3	3.5	1.7	6.6	8.8	5.7	18	44.3	30.6	8.6	1.1	8.6	9.1	5.7	21.3	31.1	24.4	7.1
Aug-50	8.4	9.6	4.6	3.1	5.1	2.7	10	21	12.5	3	3.9	11.4	15.7	9.4	10.6	25.2	15.7	8.5	4.9	14.6	16.4	9.7	17.7	22.2	12.2	7.2
Sep-50	4	7.8	2.3	4.2	2.9	2	4.2	15	13.9	3.1	1.5	2.7	5.1	5.8	9.7	12.2	14.8	6.3	2.3	4	6.1	5.2	10	12.1	11.3	4.8
Oct-50	0.7	1.2	0.5	1.5	0.4	0.1	0.5	4.5	7.1	2.5	0.5	0.4	0.7	1	3.5	6.2	8.9	6.2	0.7	1	1.5	2	3.5	6.2	5	4.2
Nov-50	0.3	0.5	0.1	0.2	0.3	0.2	0.2	0.7	0.8	0.6	0.5	0.5	0.8	0.5	0.3	0.7	1.2	1.7	0.9	1.1	1.3	0.7	0.6	1.2	2.2	2.5
Dec-50	0.6	1	0	0.1	0.1	0	0.3	0.8	0.9	0.3	0.1	0.2	0.5	0.3	0.4	0.7	1.2	0.9	0.1	0.2	0.5	0.3	0.3	0.5	1.1	0.3

Table A3 (continued)

Time / Nodes	Precipitation (mm/day)																								
	1	2	3	4	5	6	7	8	9	10	11	12	13	14	15	16	17	18	19	20	21	22	23	24	25	26
Jan-80	0.9	1.8	0	0.1	0.1	0.2	0.4	0.5	0.6	0.3	0	0.3	0.6	0.6	0.5	0.2	0.3	0.6	0	0.1	0.4	0.3	0.3	0.2	0.1	0.1
Feb-80	0.8	1.6	0	0.2	0.1	0.2	0.5	0.9	2.6	0.8	0	0.1	0.6	0.8	0.4	0.7	1.6	1.1	0	0	0.3	0.5	0.3	0.7	0.5	0.1
Mar-80	1.6	2.4	0.1	0.4	0.2	0.4	0.5	1.4	2.9	1.3	0	0.1	0.3	0.5	0.4	1.5	2.6	0.8	0	0	0.6	0.4	0.5	0.8	0.2	0.1
Apr-80	0.3	1.4	0.2	0.9	0.3	0.1	0.4	3.1	5.6	1.5	0.1	0.1	0.1	0.2	0.6	5	9.6	3	0.1	0.1	0.2	0.5	0.9	2	4.4	2.5
May-80	0.3	2	1	1.8	0.4	0.4	0.4	7	10.9	1.2	0.3	0.3	0.2	0.3	2.3	14.4	12	3.3	0.3	0.1	0.3	1	1.9	3.9	7.7	2.5
Jun-80	2.4	3.8	3.1	2.8	1.1	1.2	1.8	20.6	10.3	1.6	1.6	2.4	5.3	2.5	6.9	10.1	25.6	5.4	4.4	2.8	7.1	3.8	13.9	26.2	24.7	3.3
Jul-80	10.1	8.7	5.8	3.4	5.3	4.4	4.7	35.2	11	2.9	1.5	6.3	9.1	3.7	19.4	9.5	31.8	6.1	1	7.5	9.1	3	25.3	33.2	29.5	4.4
Aug-80	7.9	8.5	4.8	3.3	5.2	2.6	7.5	24.8	10.7	2.8	1.8	10.6	13.1	7.2	13	9.9	18.2	6.9	2.7	14.9	13.3	7.2	20.2	25	15.4	4.7
Sep-80	5.3	9.3	2.5	4.4	3.1	2.6	4.2	10.8	13	2.9	1.1	3.3	5.8	6.1	6.1	9.8	12.7	5.5	1.5	4.7	7.4	5.1	4.4	3.7	6.9	3.6
Oct-80	1.2	1.6	0.5	1.7	0.5	0.2	0.6	3.6	7.5	2.6	0.6	0.8	0.8	1.3	3.2	5.1	7.3	5.7	1.1	1.8	1.9	2.4	3.2	4	3.5	3.3
Nov-80	0.3	0.4	0.1	0.2	0.2	0.2	0.2	0.7	0.9	0.7	0.5	0.5	1.1	0.6	0.4	0.8	1.3	2.1	1	1.2	1.8	0.7	0.7	1.2	1.9	2.9
Dec-80	0.7	1.1	0.1	0.1	0.1	0	0.3	0.9	1.1	0.4	0.1	0.2	0.6	0.4	0.4	0.7	1.2	0.9	0.1	0.2	0.5	0.3	0.2	0.4	0.9	0.3

Table A4: HadCM3 GCM Projected Precipitation for Scenario B1

Time / Nodes	Precipitation (mm/day)																								
	1	2	3	4	5	6	7	8	9	10	11	12	13	14	15	16	17	18	19	20	21	22	23	24	25	26
Jan-20	0.8	1.3	0	0.1	0.1	0.2	0.3	0.5	0.7	0.3	0	0.4	1	0.7	0.6	0.2	0.3	0.6	0	0.1	0.7	0.4	0.3	0.3	0.1	0.1
Feb-20	1.5	1.8	0	0.1	0.2	0.3	0.3	0.7	1.9	0.7	0.1	0.1	0.6	0.5	0.4	0.6	1.6	1.3	0	0.1	0.6	0.4	0.3	1	0.5	0.2
Mar-20	1.6	3.2	0.1	0.4	0.3	0.4	0.6	1.9	3.5	1.5	0	0.2	0.3	0.5	0.6	2	4.5	1.8	0	0.1	0.7	0.5	0.6	1	0.3	0.1
Apr-20	1.1	2.1	0.3	0.9	0.5	0.3	0.6	4.5	11.6	4.3	0.1	0.2	0.1	0.3	1.3	9.7	18.1	5.9	0	0.1	0.3	0.9	1.9	5.3	5.8	1.8
May-20	0.5	2.5	1.2	1.1	0.3	0.6	0.6	8.4	4.6	0.9	0.3	0.3	0.2	0.4	3.7	16.5	17.3	3	0.2	0.2	0.4	1.5	3.8	11.3	9.6	3.9
Jun-20	1.5	3.2	2.1	2.6	1.2	1.1	1.7	8.2	14.8	2	2	2.8	5.4	3.9	6.6	26.3	18	7.1	4.3	4.9	6	6.2	7.9	14	20	9.7
Jul-20	6.2	6.1	4.6	3.2	4.3	3.3	3.2	27.1	16.4	3.5	1.8	5.4	6.3	7.4	14	27	23.8	8.8	2	7.8	6.6	9.5	14.2	32.6	20.7	10.5
Aug-20	5.9	5.8	4.7	2.9	4.3	2.2	5.7	20	13.2	3.2	4.5	9.9	11.4	7.9	9.5	18.4	14.1	8.8	6.6	13	12.9	9.4	13.6	17.8	11.7	10.1
Sep-20	3.4	8.2	2.1	3.6	2.4	1.6	4.4	12.6	12.6	3	1.3	2.7	5.7	7.9	7.7	12	13.4	5.5	2.3	4.7	6.8	6.5	7.8	11.4	10.1	5.2
Oct-20	1.2	1.2	0.5	1.1	0.3	0.2	0.6	4.2	7	2.2	0.3	0.5	0.8	1.1	3.8	7.4	10.1	6.1	0.6	0.9	1.4	2.1	4	6.7	5.6	5
Nov-20	0.3	0.4	0	0.2	0.3	0.2	0.2	0.6	0.8	0.7	0.5	0.5	0.8	0.4	0.4	0.8	1.3	2.1	1.2	0.9	1.3	0.5	0.6	1.3	2.1	3.3
Dec-20	0.7	0.9	0	0.1	0.1	0	0.2	0.6	0.8	0.3	0.1	0.2	0.6	0.2	0.3	0.6	1	0.7	0.1	0.2	0.6	0.2	0.2	0.3	0.8	0.3
Jan-50	0.9	1.7	0	0.1	0.1	0.3	0.4	0.4	0.5	0.2	0.1	0.4	0.8	0.7	0.6	0.2	0.2	0.4	0	0.1	0.5	0.4	0.3	0.2	0.1	0.1
Feb-50	1	1.5	0	0.1	0.1	0.2	0.4	0.7	1.7	0.6	0	0.1	0.5	0.6	0.5	0.7	1.5	1.1	0	0.1	0.6	0.4	0.3	0.9	0.5	0.1
Mar-50	1.2	2.6	0.1	0.3	0.2	0.3	0.5	1.5	2.9	1.3	0	0.1	0.3	0.5	0.5	1.8	3.9	1.6	0	0	0.7	0.5	0.6	1.2	0.3	0.2
Apr-50	0.5	1.9	0.3	1	0.4	0.2	0.5	4.6	8.3	3.3	0.1	0.1	0.1	0.3	1	8.2	12.7	3.9	0	0	0.2	0.7	1.4	3.9	4.8	1.7
May-50	0.7	2.5	1.2	1.3	0.6	0.8	0.5	7.8	6	1.4	0.3	0.4	0.2	0.3	3.4	13.6	15.3	5.3	0.3	0.1	0.5	1.1	3.5	7.5	7.8	5.4
Jun-50	1.8	4.2	2.4	3	1.2	1.1	2	16.1	12.5	2.3	1.7	2.7	5.6	3.5	6	24.8	16.9	8.5	3.4	5.3	6.1	5	9	15.6	17.8	9.3
Jul-50	7.1	6.8	4.5	3.4	4.8	3.7	3.9	29.8	14.9	3.3	3.6	5.8	7.2	5.6	16.4	32.1	27.3	8.2	3.2	7.5	6.8	5.1	19.5	27.4	24	7.7
Aug-50	6.9	6.4	4.7	3.1	4.5	2.4	5.6	21.9	12.7	2.9	4.1	10.2	10.3	5.1	11.3	20.9	16.1	8.5	5.2	13.8	12.6	6.2	16.9	21.3	12.9	8
Sep-50	3.6	8	2.6	4	2.8	2	4.2	13.4	13.5	2.8	1.5	2.8	5.6	7.2	7.7	11.8	13.7	5.3	2.3	4.7	6.4	5	9	13.2	11.8	4.3
Oct-50	1	1.3	0.6	1.2	0.3	0.1	0.6	3.7	6.9	2.1	0.4	0.6	1.1	1.4	3.3	5.3	7.5	5.6	0.7	1.5	1.9	2	3.3	4.9	4.2	5.1
Nov-50	0.3	0.3	0	0.2	0.2	0.2	0.1	0.5	0.8	0.6	0.4	0.4	0.6	0.3	0.3	0.6	1.2	1.8	0.8	0.7	0.9	0.5	0.5	1.1	2	3.1
Dec-50	0.7	1.1	0	0.1	0.1	0	0.2	0.7	0.8	0.3	0.1	0.2	0.5	0.2	0.3	0.6	1	0.6	0.1	0.2	0.5	0.2	0.2	0.3	0.8	0.2

Table A4 (continued)

Time / Nodes	Precipitation (mm/day)																								
	1	2	3	4	5	6	7	8	9	10	11	12	13	14	15	16	17	18	19	20	21	22	23	24	25	26
Jan-80	0.8	1.3	0	0.1	0.1	0.2	0.3	0.5	0.6	0.3	0	0.3	0.7	0.5	0.5	0.2	0.2	0.4	0	0.1	0.6	0.3	0.3	0.2	0.1	0
Feb-80	0.9	1.7	0	0.2	0.1	0.2	0.4	0.8	2	0.7	0.1	0.1	0.7	0.6	0.4	0.5	1.2	0.8	0	0	0.5	0.3	0.3	0.7	0.4	0.1
Mar-80	0.9	2.5	0.1	0.4	0.2	0.2	0.5	1.8	3.7	1.6	0	0.1	0.3	0.5	0.5	1.9	3.6	1	0	0	0.6	0.6	0.5	0.8	0.2	0.1
Apr-80	0.4	1.9	0.3	0.9	0.3	0.1	0.4	3.4	6.7	2.5	0.1	0.1	0.1	0.2	0.7	4.5	6.8	2.5	0.1	0.1	0.2	0.6	1.2	2.5	3.2	1.3
May-80	0.5	2.8	1.1	1.5	0.5	0.7	0.4	8	5.7	1	0.3	0.3	0.2	0.3	4.1	16.6	17.2	3.6	0.2	0.1	0.4	1	4.5	10.8	9.3	3.2
Jun-80	1.8	4.6	2.3	2.9	1.2	1.1	2.4	20.3	15.2	2.4	1.8	3	6.7	4.1	5.9	20.1	16.3	8.5	3.4	5.7	7	4.6	10.8	17.6	17.5	7.6
Jul-80	7.4	7.8	4.6	3.3	4.2	3.9	4.4	30	14.2	3.4	2.5	5.6	7.5	7	15.6	31.6	30.2	9.2	2.3	8	7.5	7.2	19.3	28.5	19.4	8.5
Aug-80	6.8	7.3	4.3	3.4	3.9	2.3	5.8	22.3	11.9	2.9	3.7	8.8	10	4.7	12.3	21.5	19.3	7.7	5.8	13	11.5	5.2	17.3	34	13.2	6.2
Sep-80	3.8	9	2.3	3.9	2.7	1.9	4.3	14	12.1	2.7	1.5	2.7	5.3	7.2	8.4	13.9	15.1	5	2.1	4.5	7.2	5.5	10.2	14.8	11.9	3.9
Oct-80	0.7	1	0.5	1.1	0.3	0.2	0.6	4.8	8.1	2.5	0.4	0.6	0.8	0.7	3.3	7.3	10.2	7.2	0.7	0.9	1.3	1.5	3.7	6.3	5.6	5.5
Nov-80	0.4	0.4	0.1	0.2	0.2	0.2	0.2	0.6	0.9	0.7	0.3	0.4	0.6	0.4	0.3	0.7	1.3	2.3	0.8	0.8	1.2	0.5	0.5	1.1	2.3	4.1
Dec-80	0.5	0.8	0	0.1	0.1	0	0.2	0.7	0.8	0.3	0.1	0.2	0.4	0.2	0.3	0.6	1.1	0.7	0.1	0.2	0.4	0.2	0.2	0.3	0.8	0.3

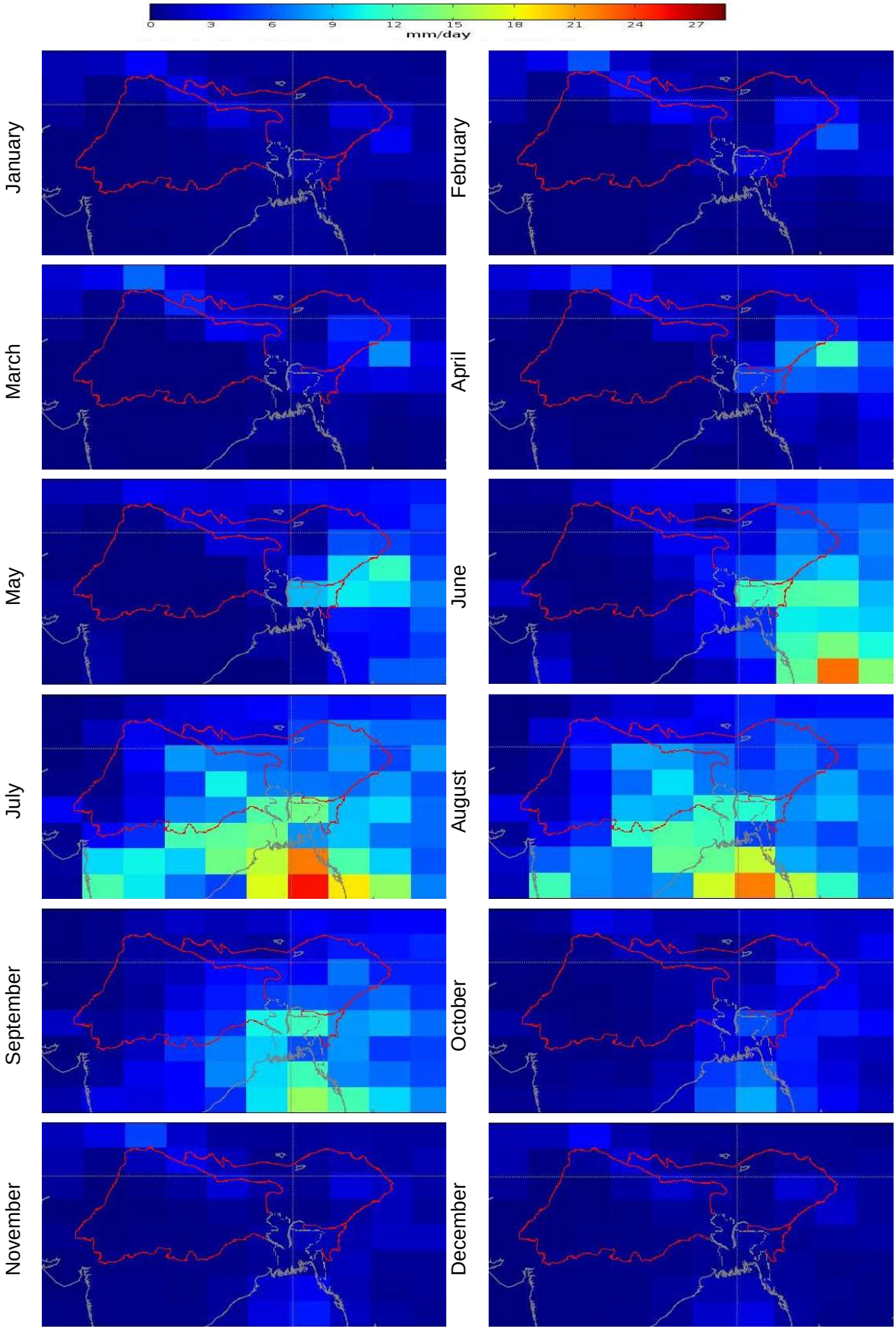

Figure A1a: Projected Precipitation over GBM basin for scenario A1FI during 2020s

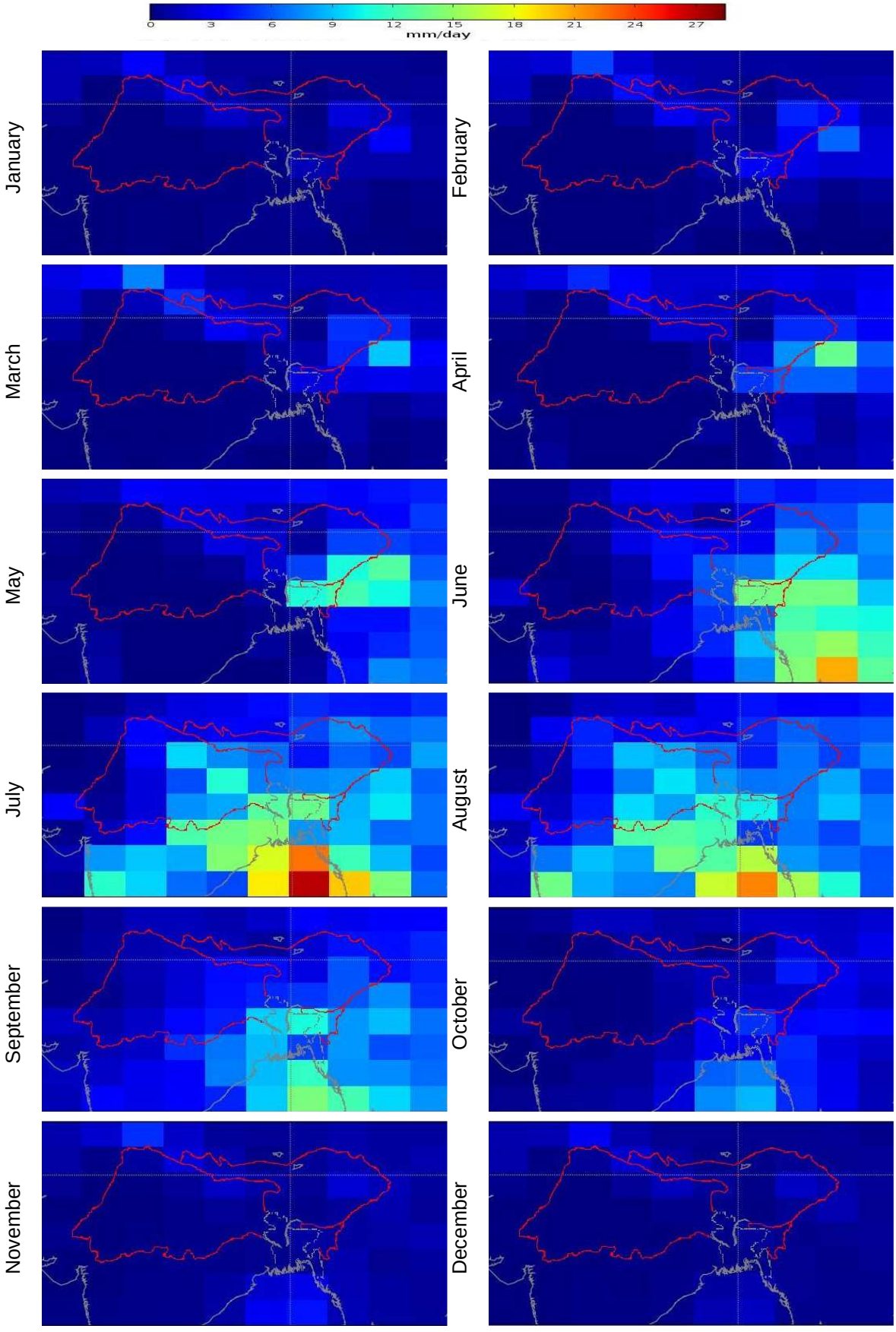

Figure A1b: Projected Precipitation over GBM basin for scenario A1FI during 2050s

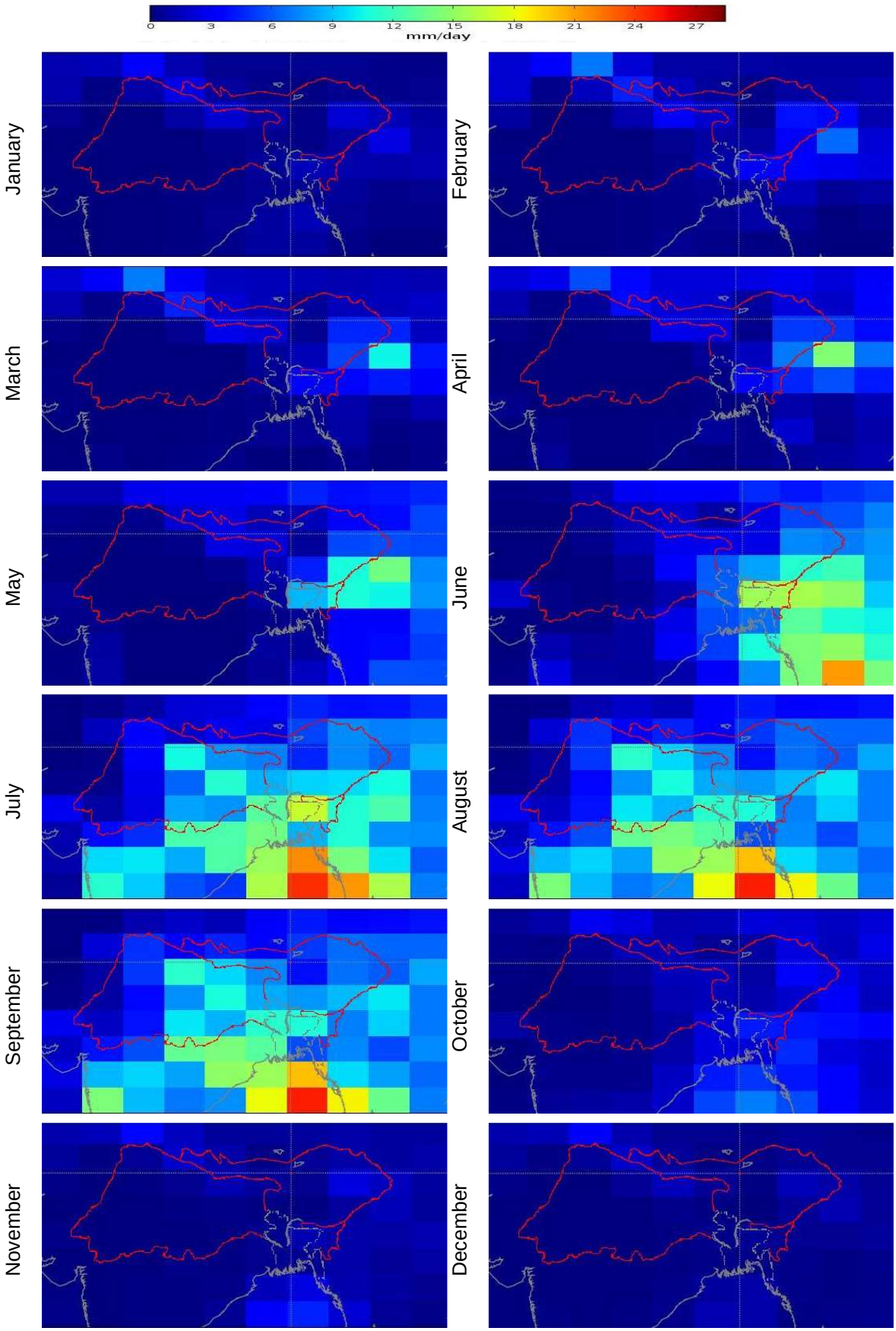

Figure A1c: Projected Precipitation over GBM basin for scenario A1FI during 2080s

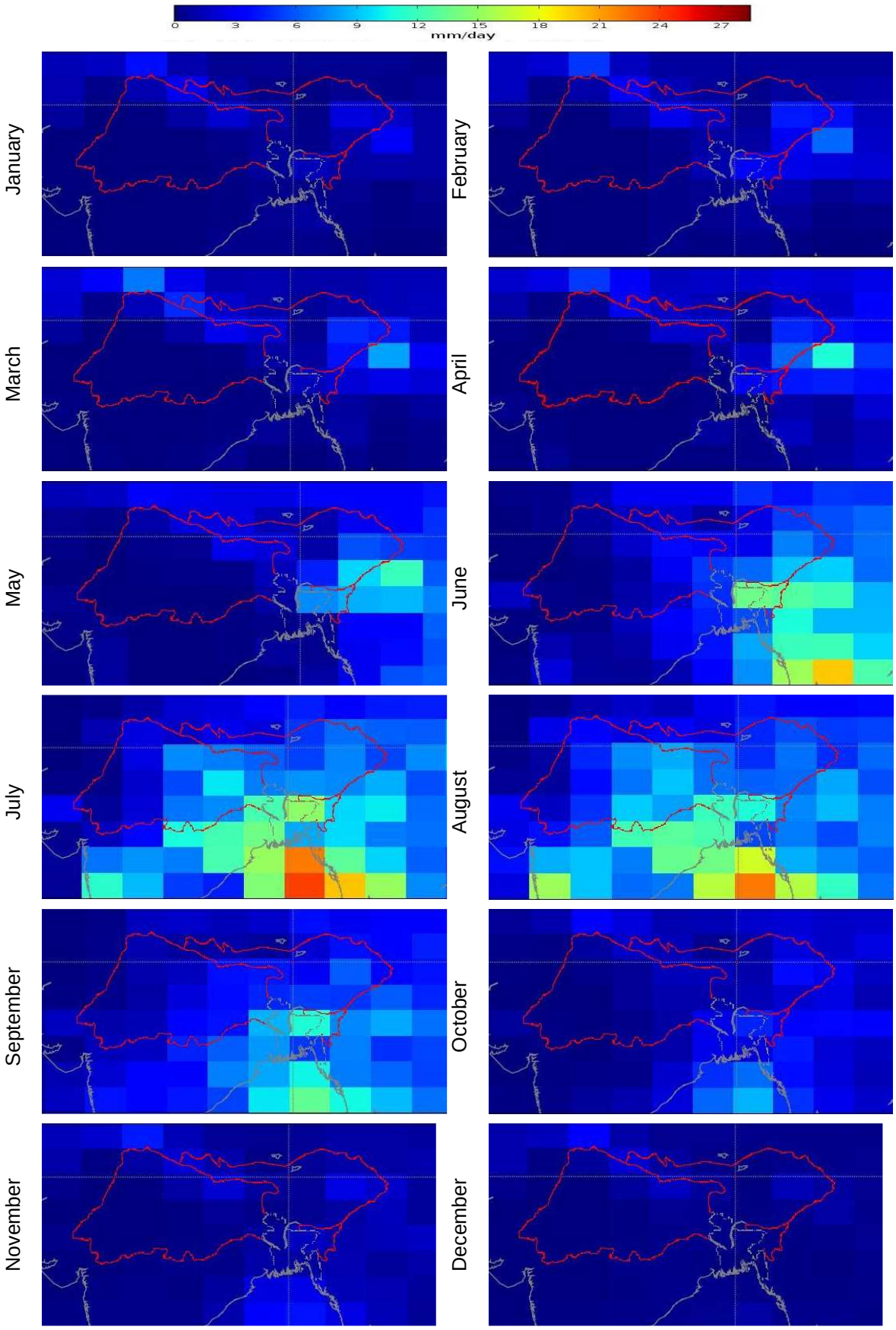

Figure A2a: Projected Precipitation over GBM basin for scenario A1B during 2020s

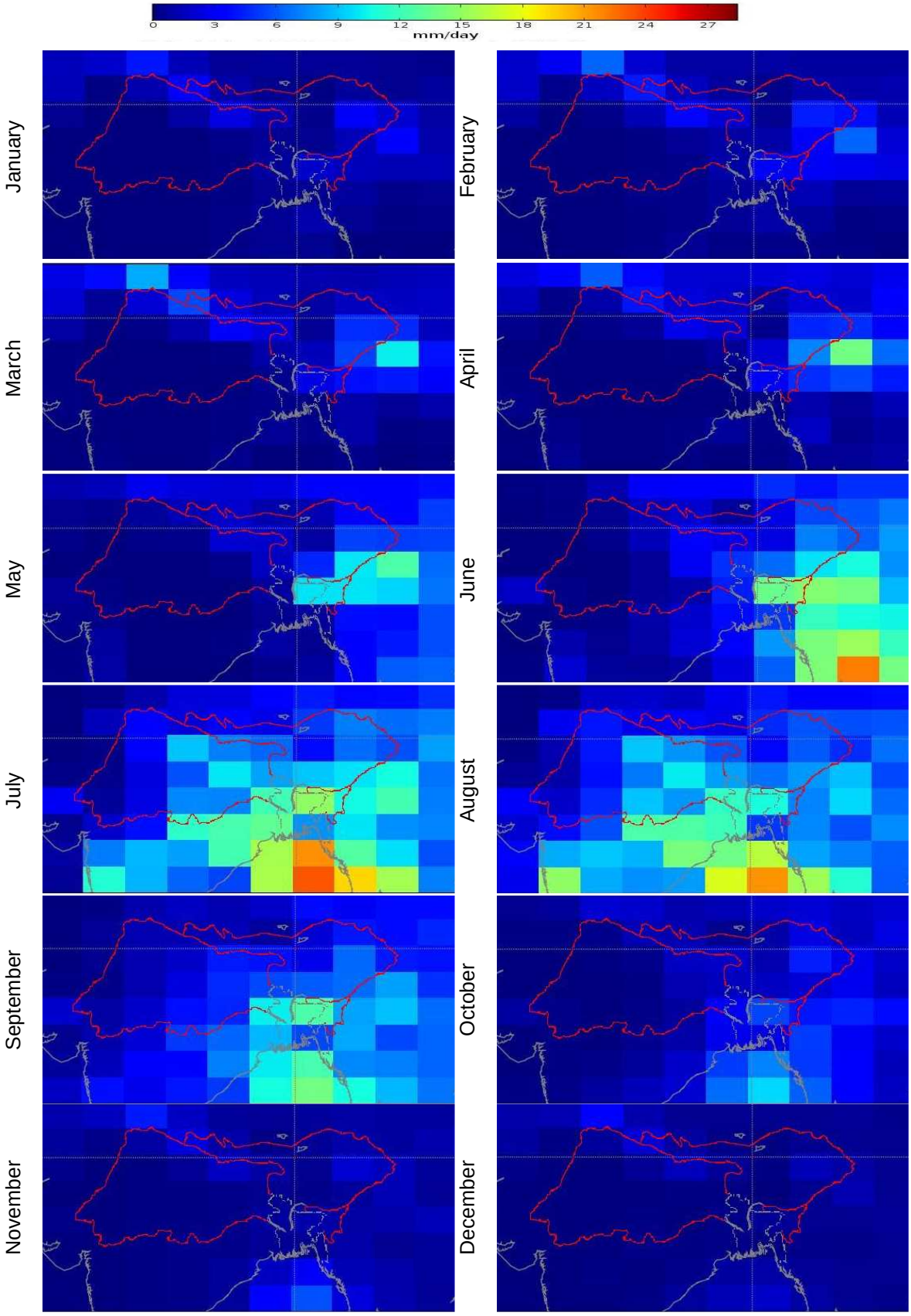

Figure A2b: Projected Precipitation over GBM basin for scenario A1B during 2050s

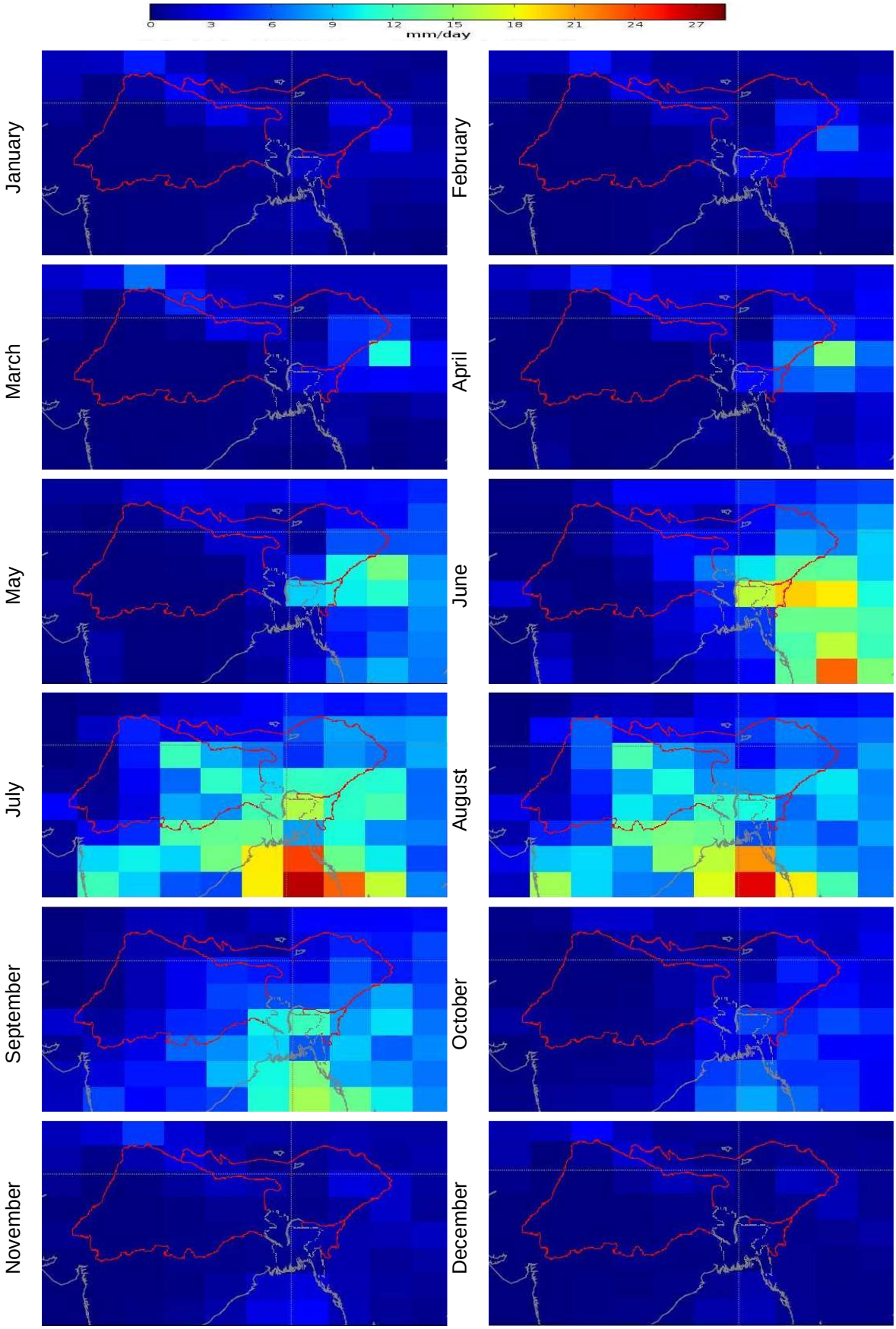

Figure A2c: Projected Precipitation over GBM basin for scenario A1B during 2080s

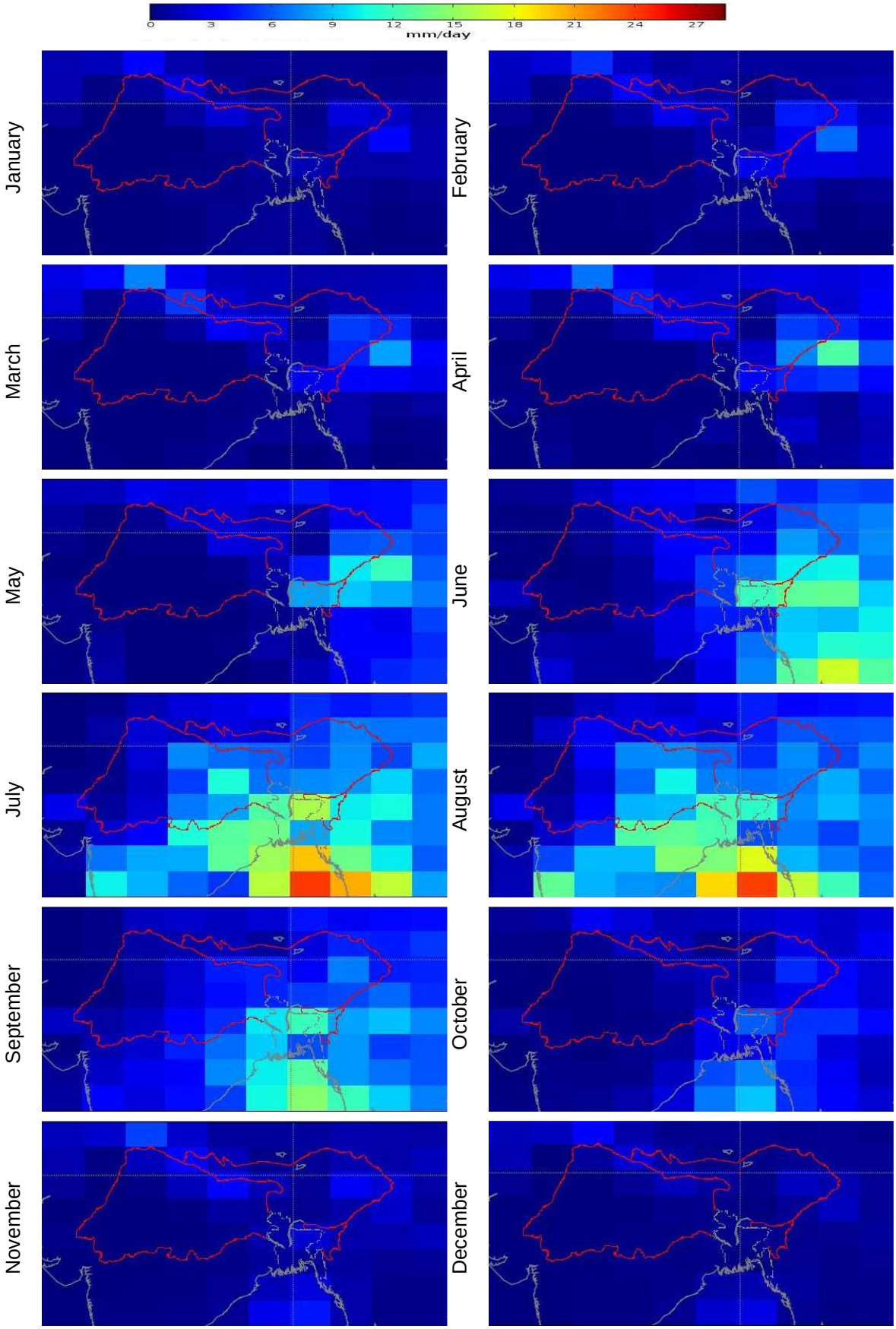

Figure A3a: Projected Precipitation over GBM basin for scenario B1 during 2020s

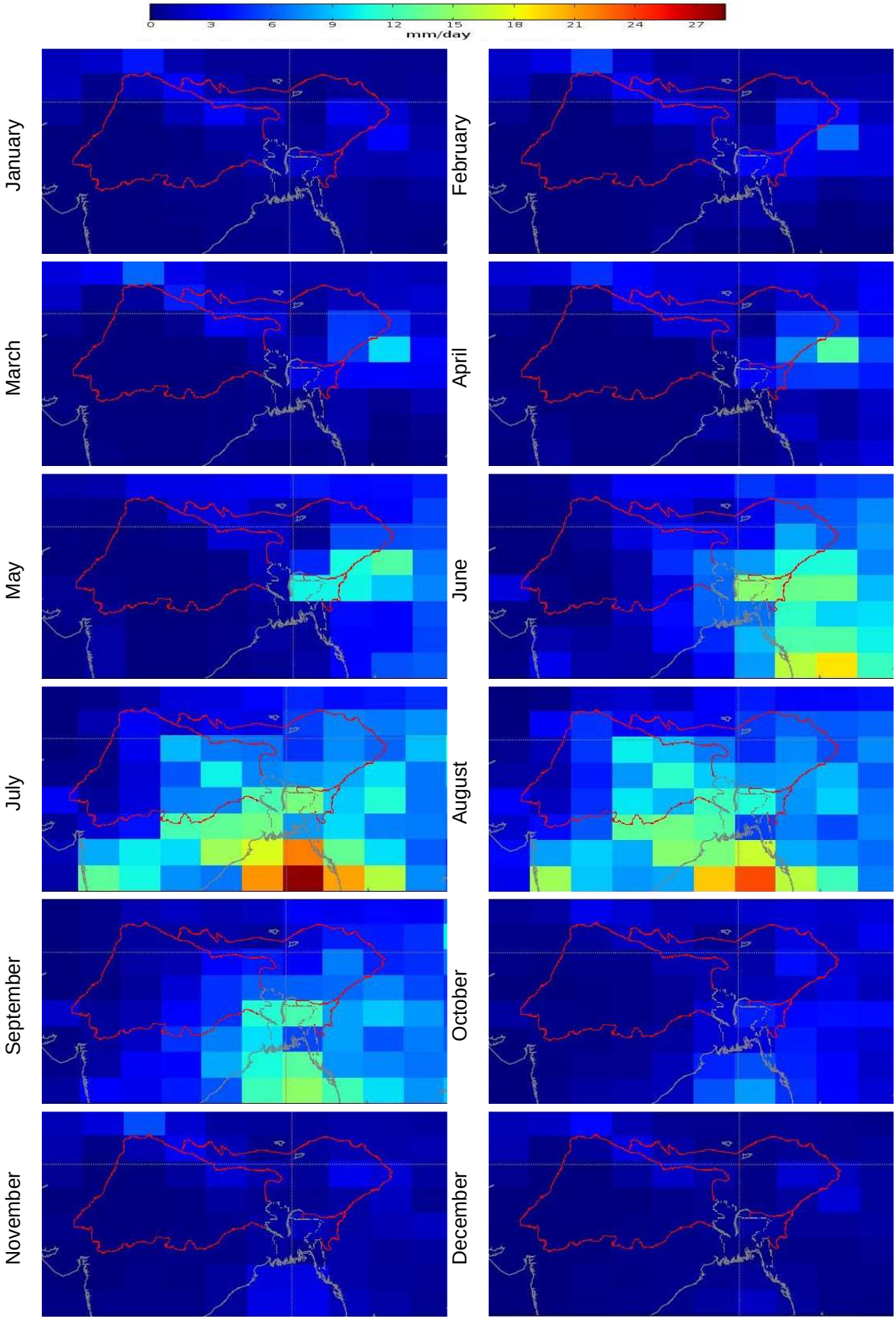

Figure A3b: Projected Precipitation over GBM basin for scenario B1 during 2050s

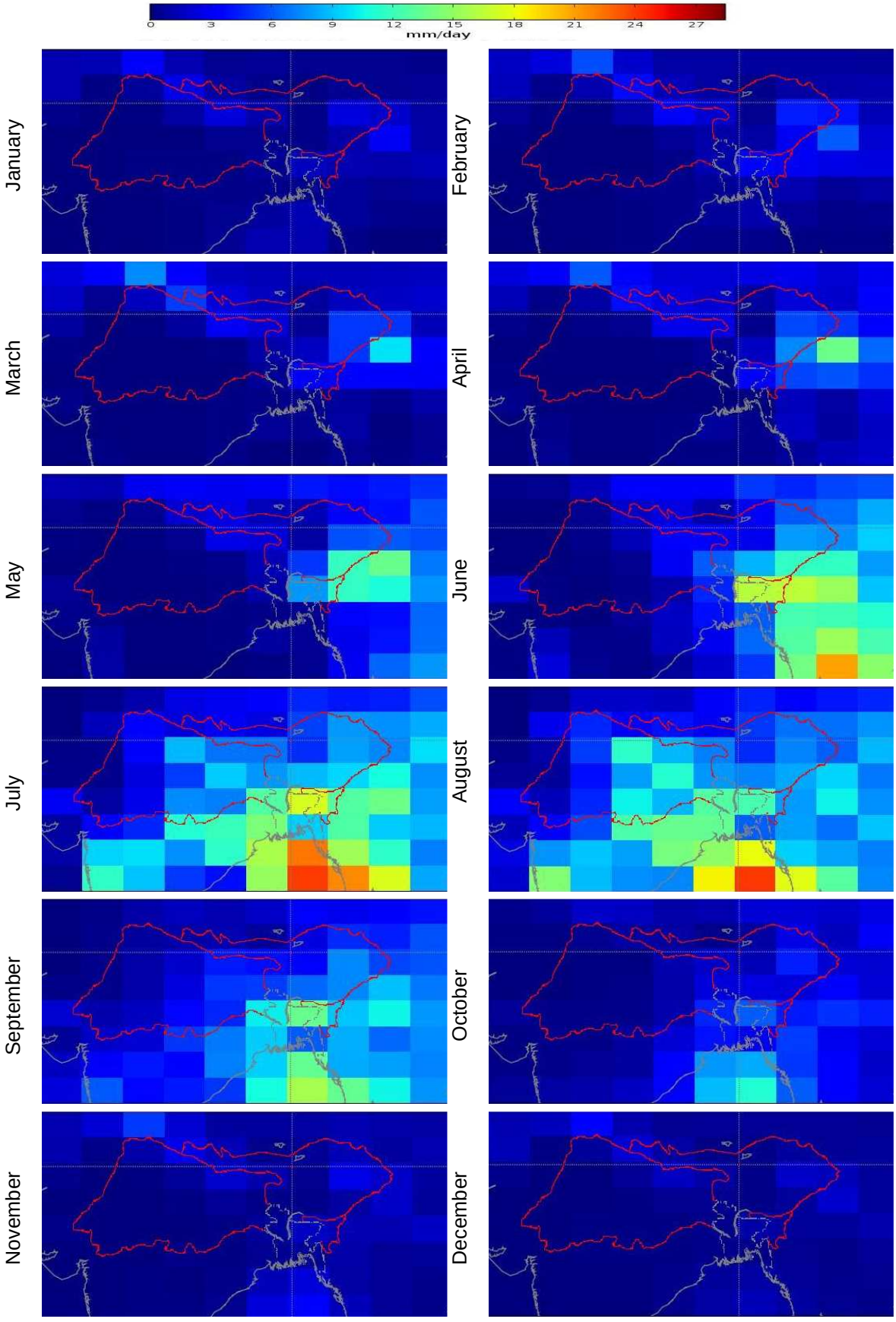

Figure A3c: Projected Precipitation over GBM basin for scenario B1 during 2080s

APPENDIX B

CALIBRATION AND VALIDATION OF ANN MODEL

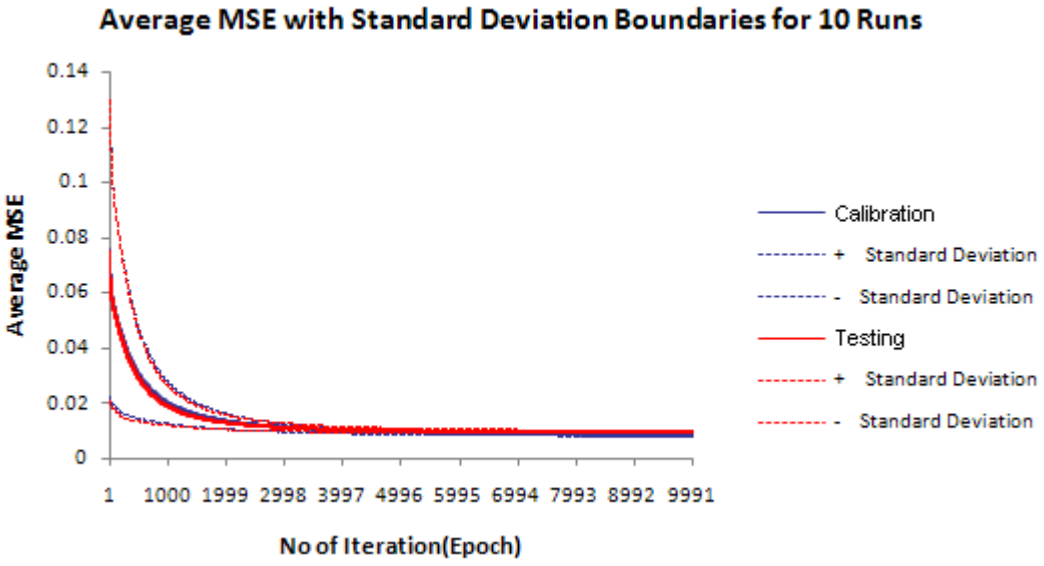
Average MSE with Standard Deviation Boundaries for 10 Runs
Average MSE
0.14
0.12
0.1
0.08
0.06
0.04
0.02
0
1 1000 1999 2998 3997 4996 5995 6994 7993 8992 9991
No of Iteration(Epoch)
Calibration
+ Standard Deviation
- Standard Deviation
Testing
+ Standard Deviation
- Standard Deviation

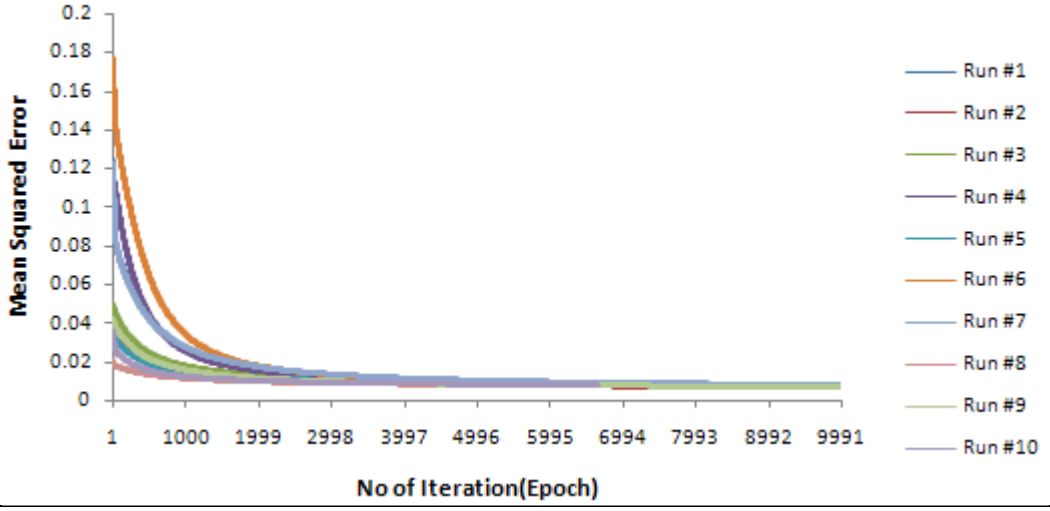
Calibration
Mean Squared Error
0.2
0.18
0.16
0.14
0.12
0.1
0.08
0.06
0.04
0.02
0
1 1000 1999 2998 3997 4996 5995 6994 7993 8992 9991
No of Iteration(Epoch)
Run #1
Run #2
Run #3
Run #4
Run #5
Run #6
Run #7
Run #8
Run #9
Run #10

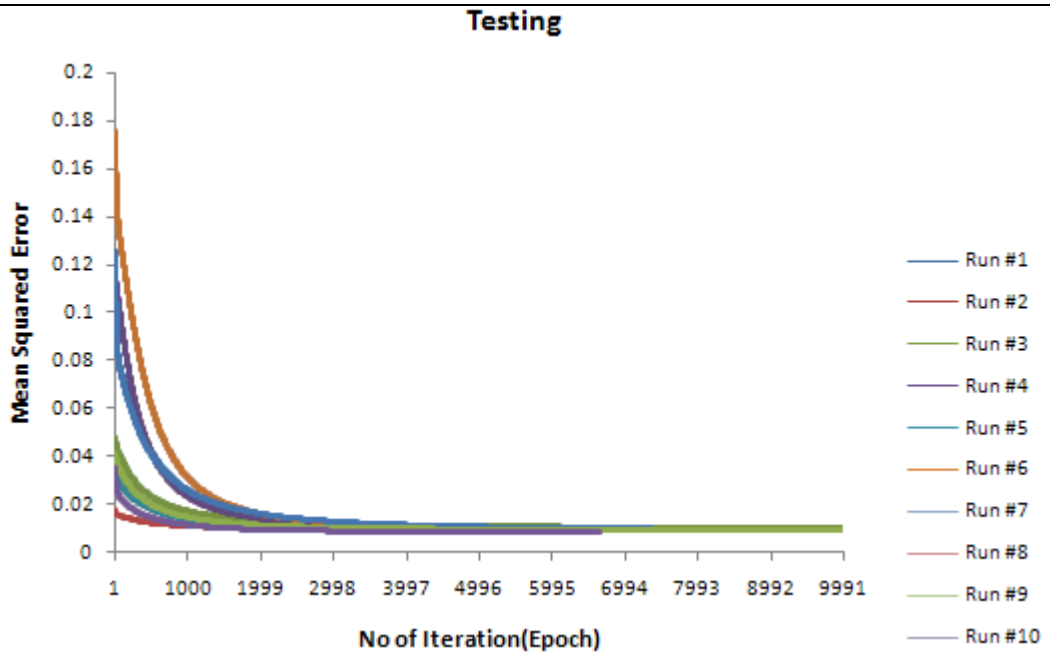
Testing
Mean Squared Error
0.2
0.18
0.16
0.14
0.12
0.1
0.08
0.06
0.04
0.02
0
1 1000 1999 2998 3997 4996 5995 6994 7993 8992 9991
No of Iteration(Epoch)
Run #1
Run #2
Run #3
Run #4
Run #5
Run #6
Run #7
Run #8
Run #9
Run #10

Figure B1a: Performance of the ANN model during calibration for trial 1

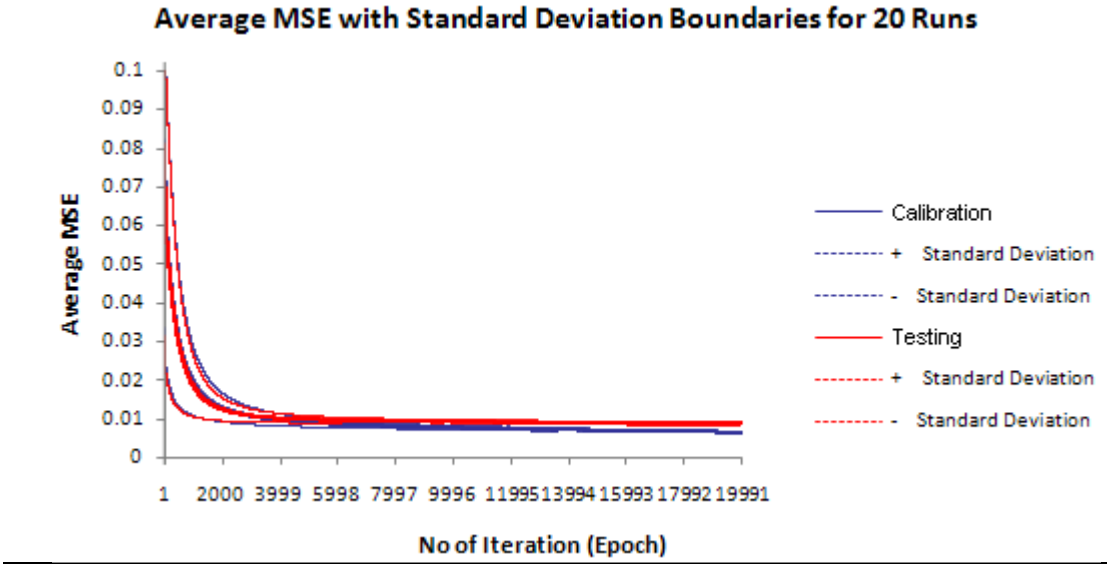

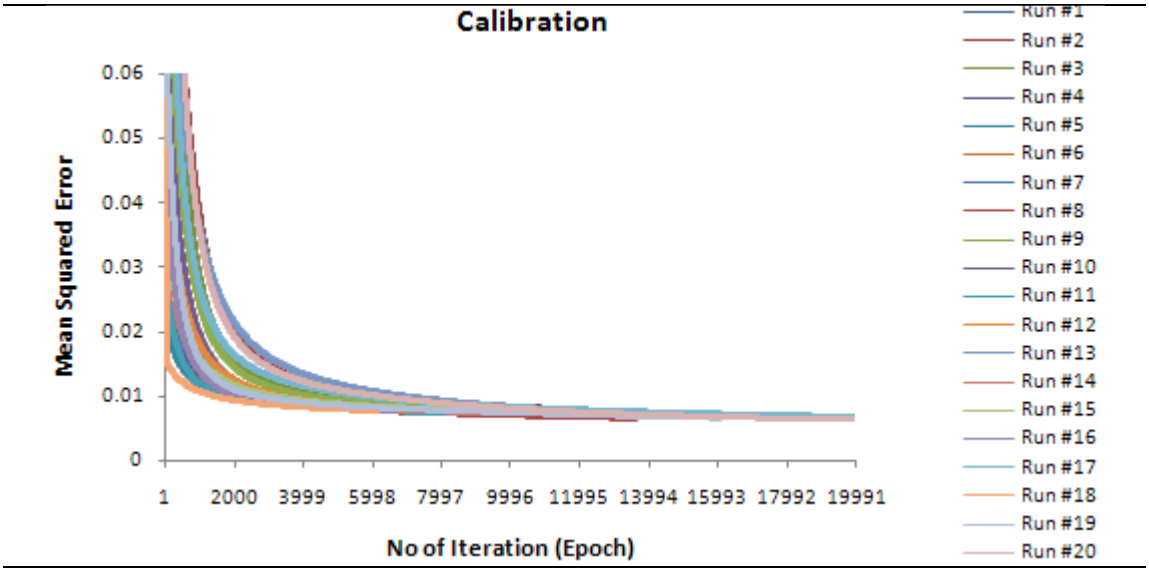

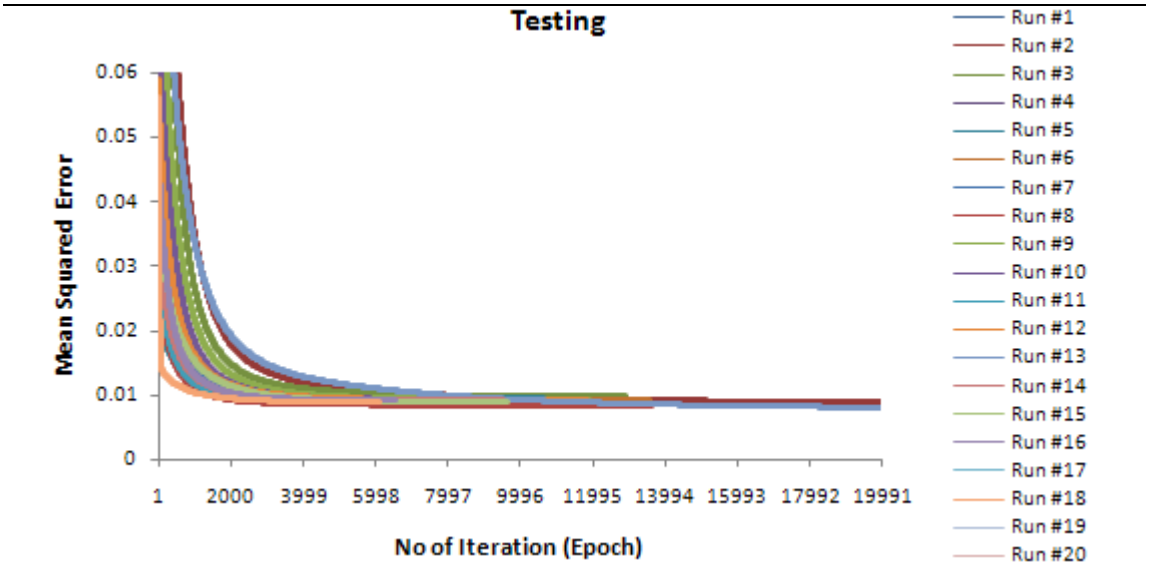

Figure B1b: Performance of the ANN model during calibration for trial 2

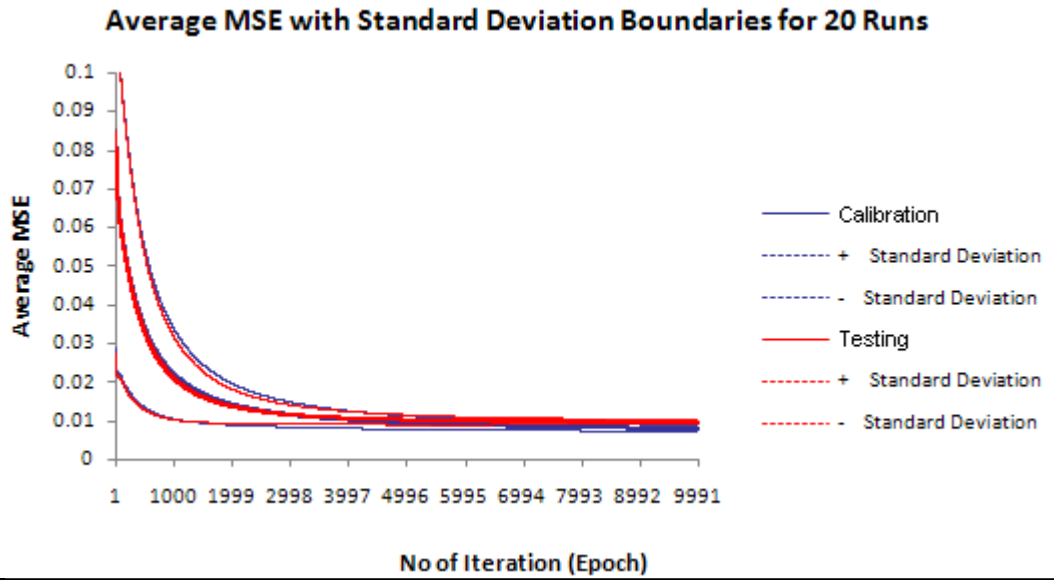

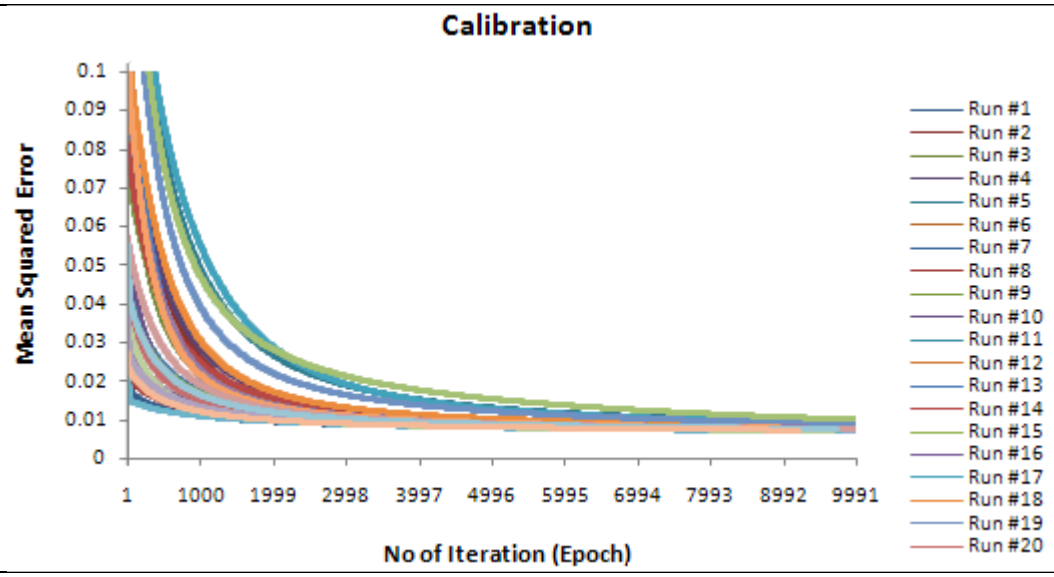

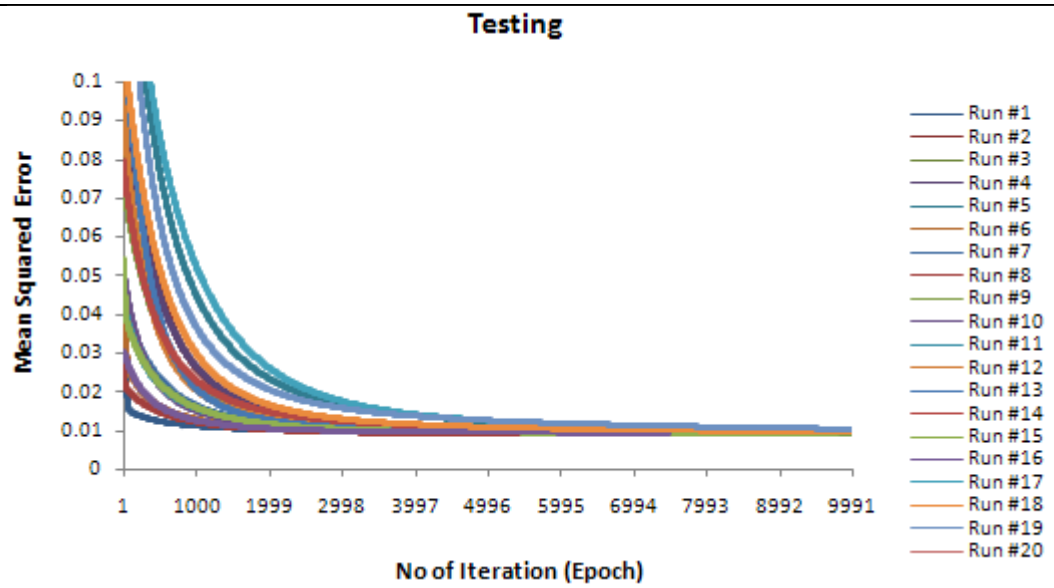

Figure B1c: Performance of the ANN model during calibration for trial 3

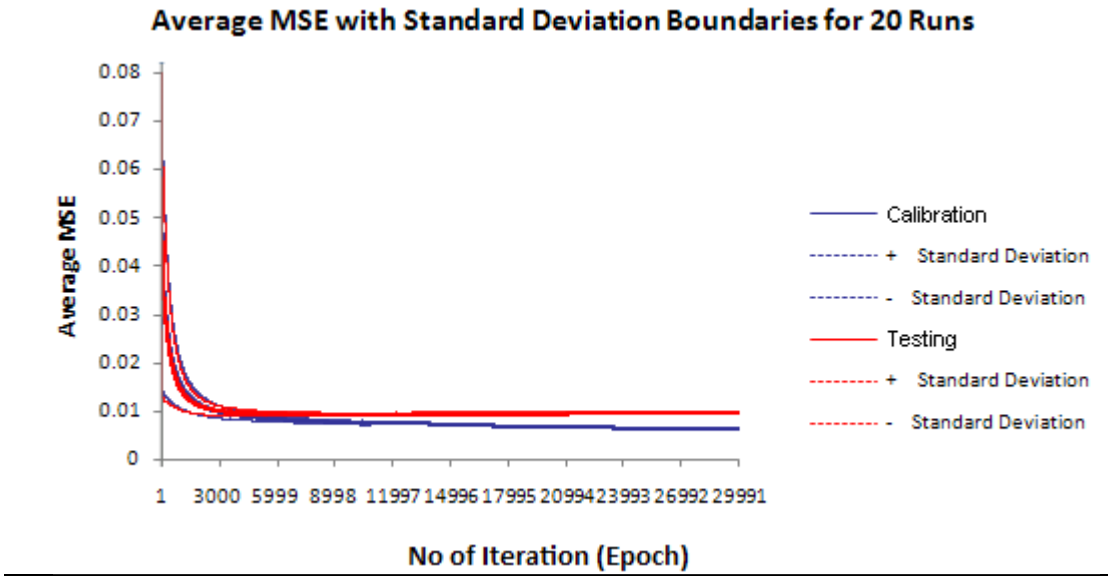

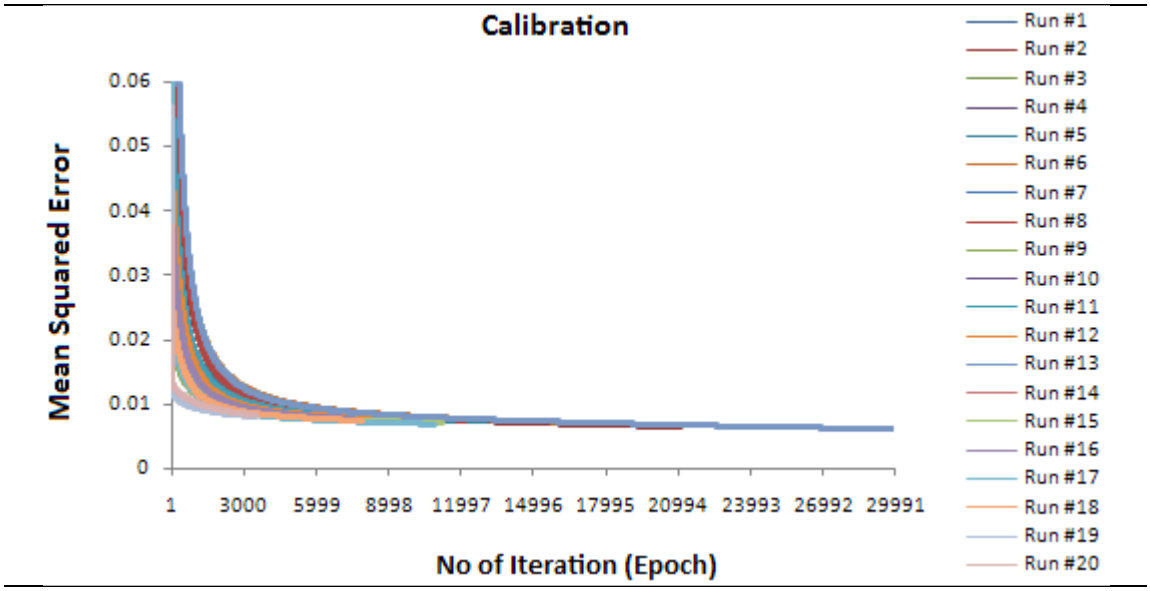

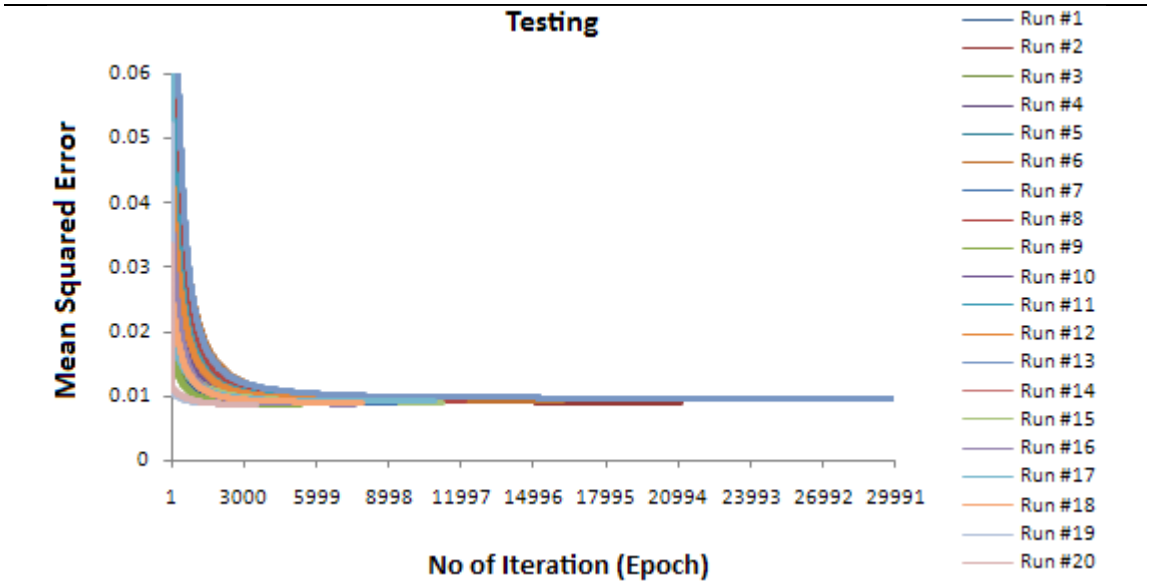

Figure B1d: Performance of the ANN model during calibration for trial 4

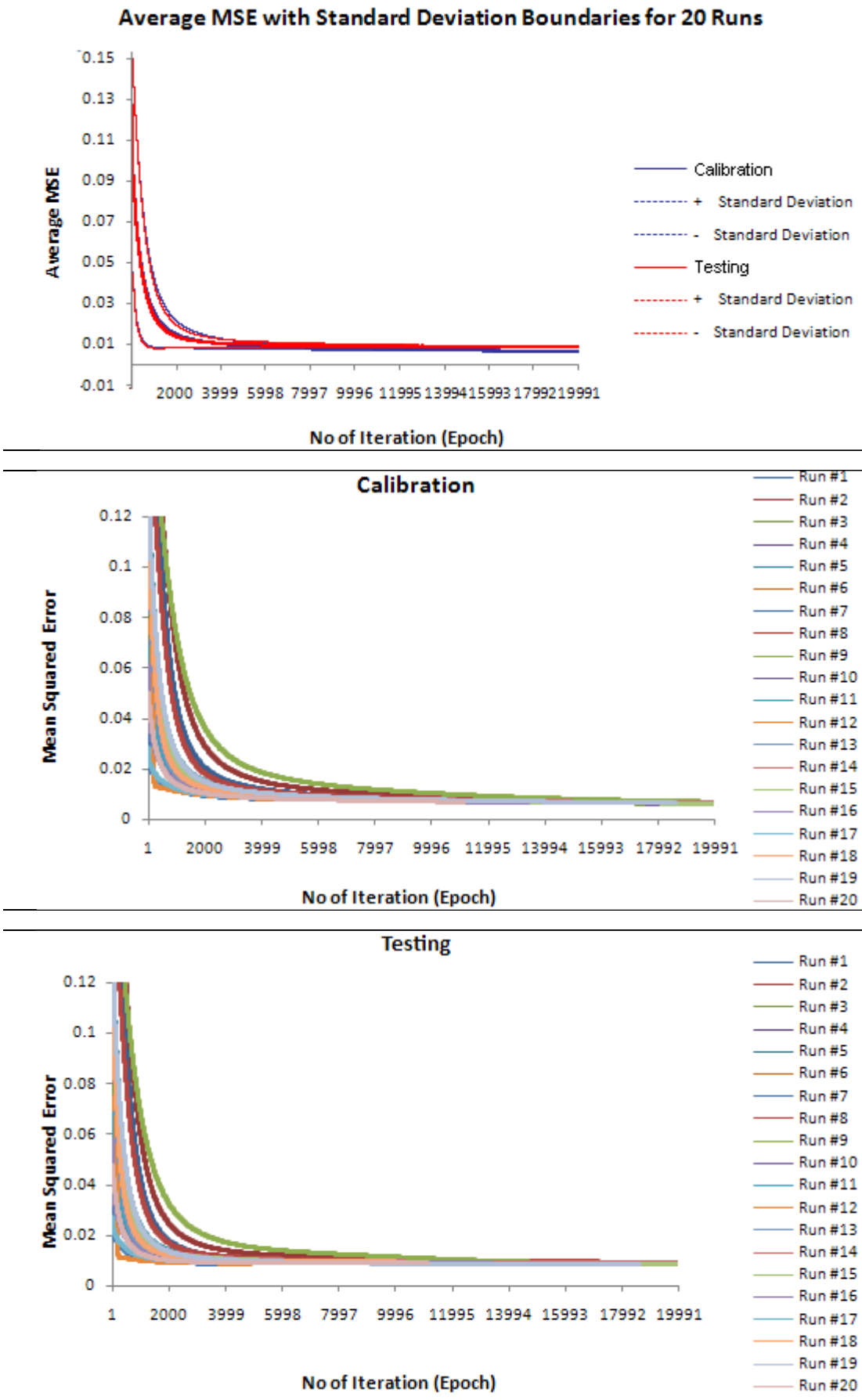

Figure B1e: Performance of the ANN model during calibration for trial 5

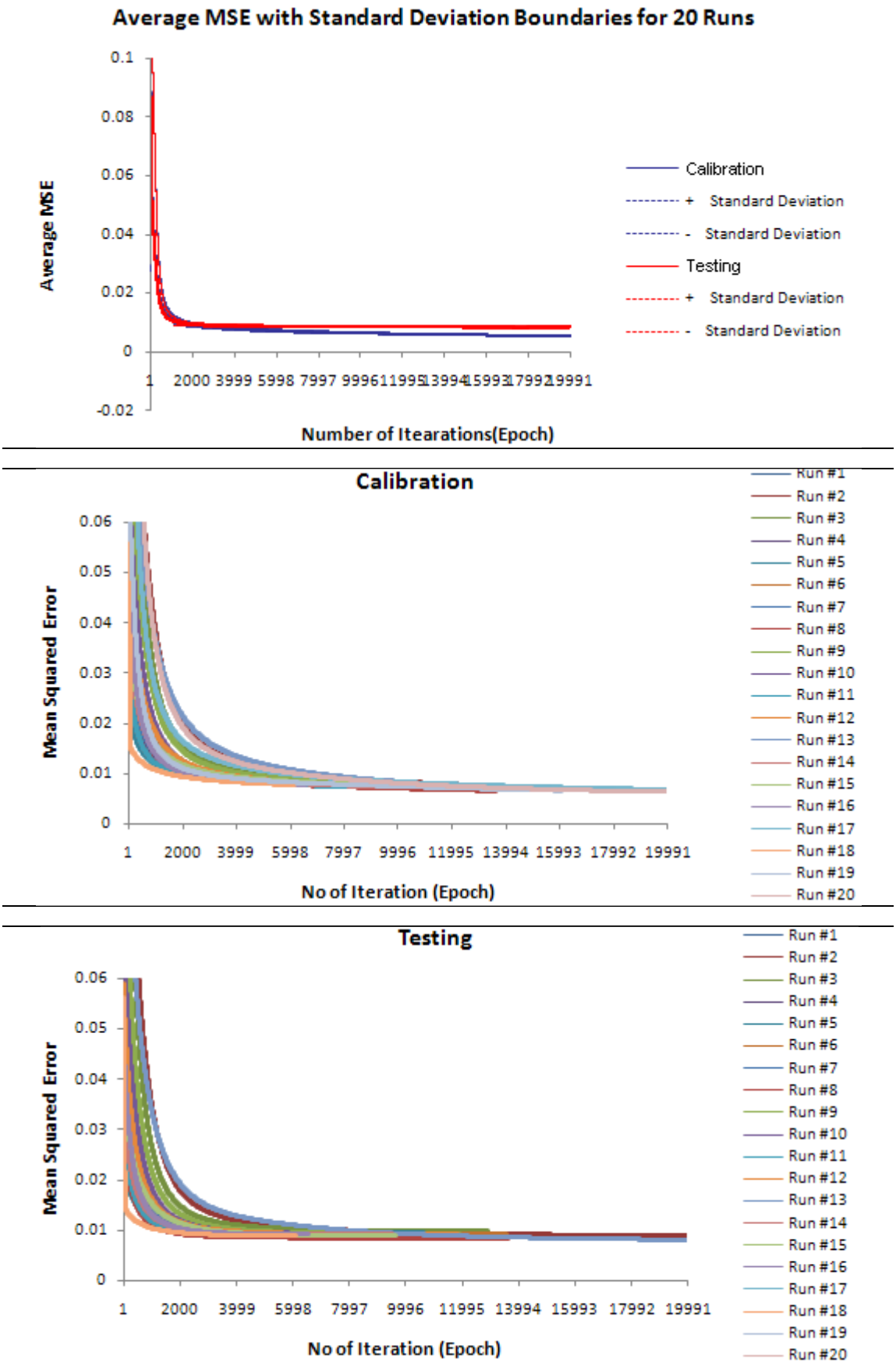

Figure B1f: Performance of the ANN model during calibration for trial 6

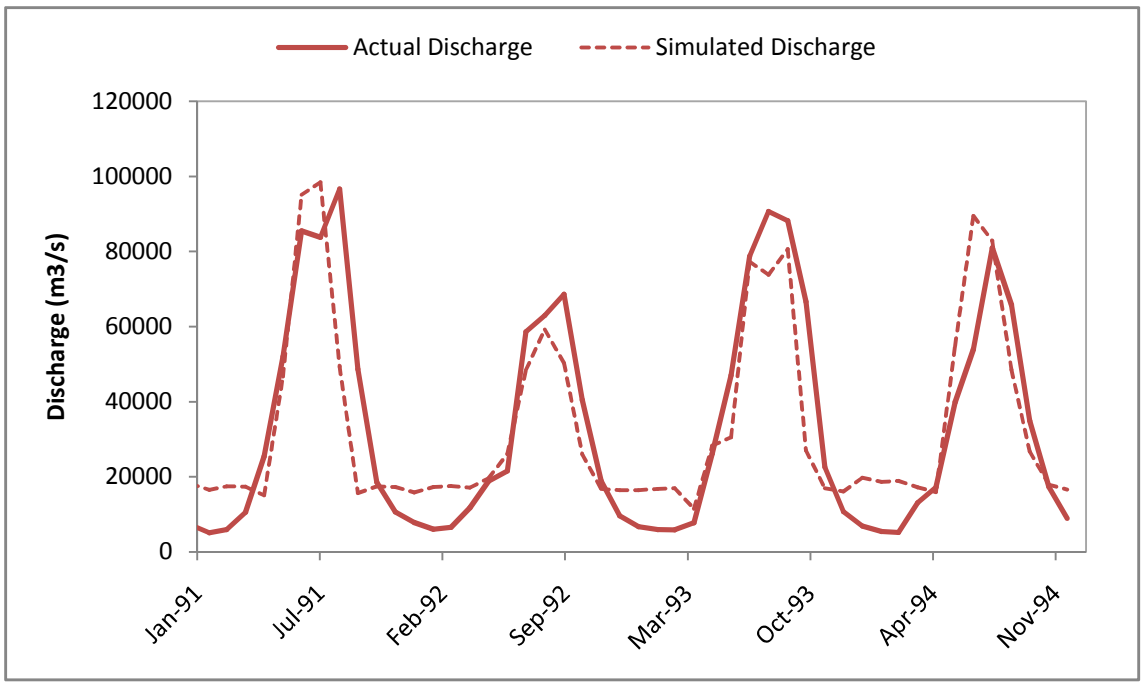

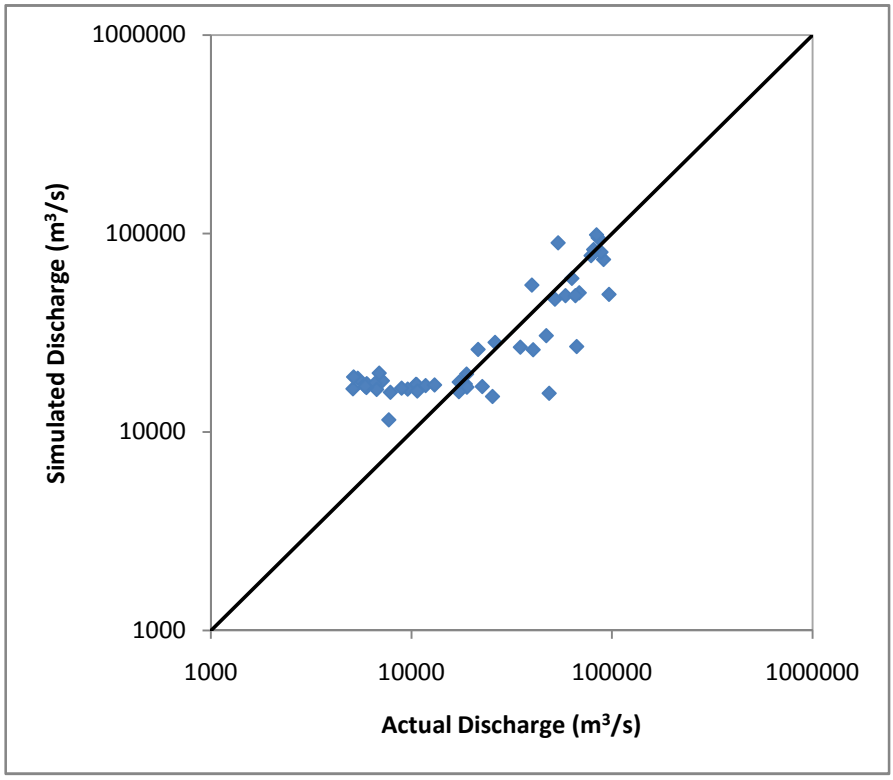

Figure B2a: Validation of the ANN model for trial 1

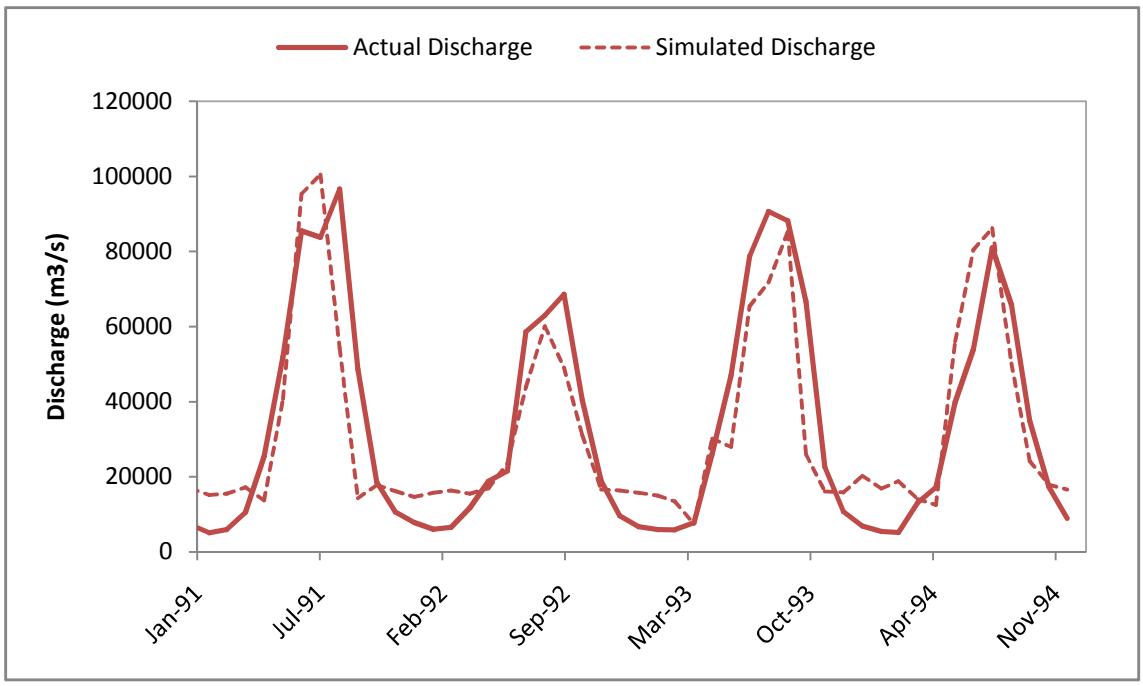

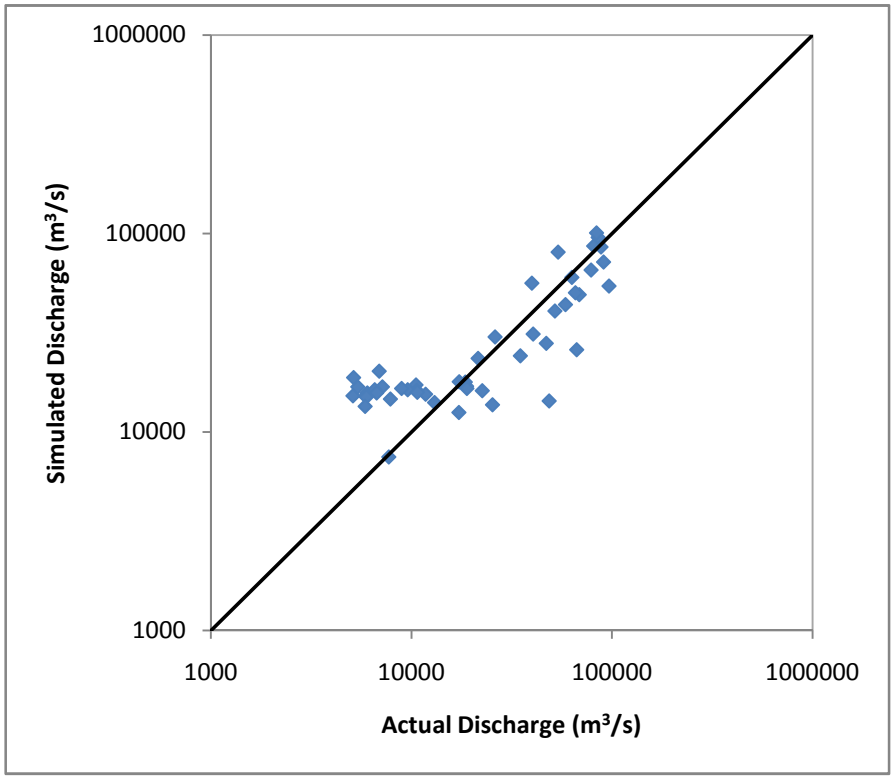

Figure B2b: Validation of the ANN model for trial 2

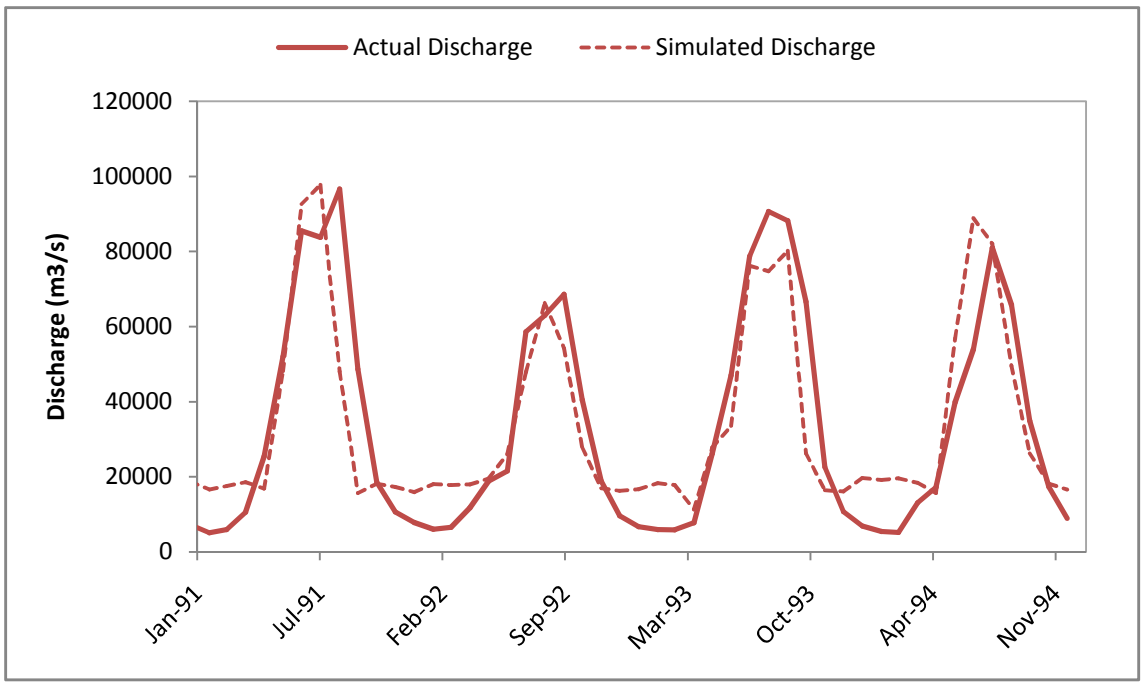

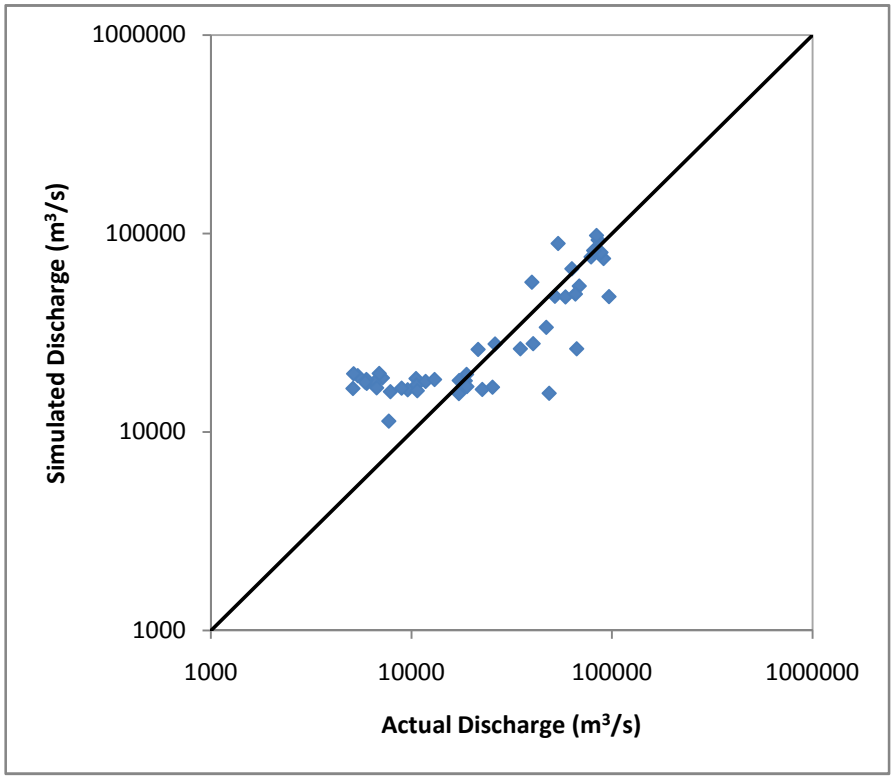

Figure B2c: Validation of the ANN model for trial 3

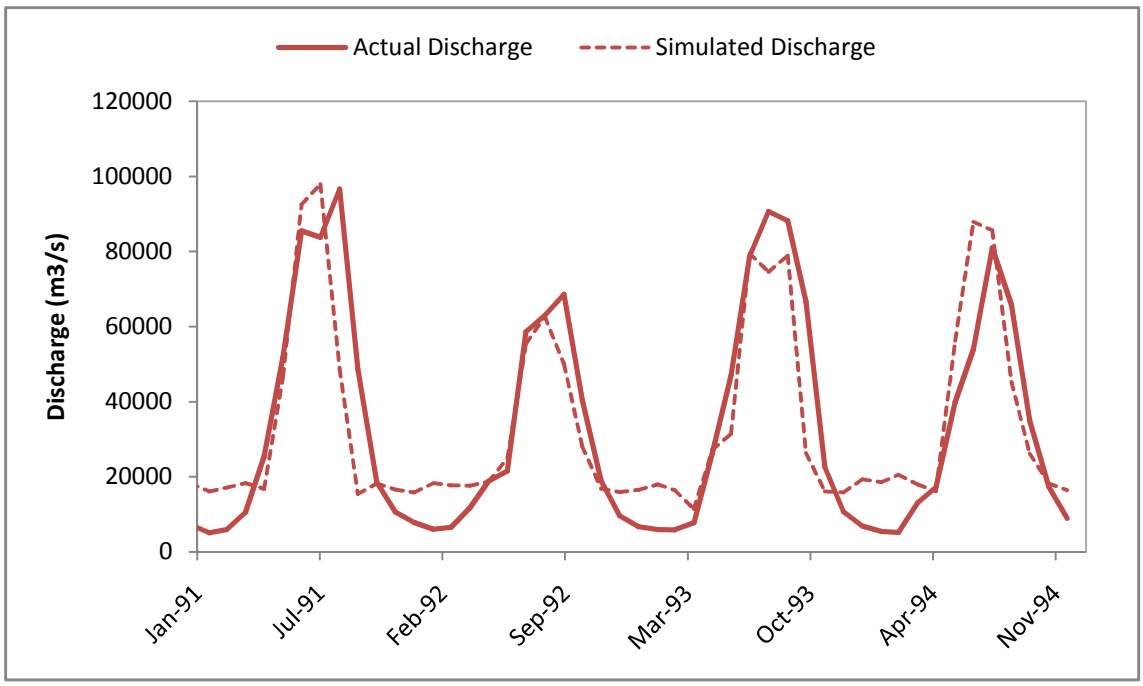

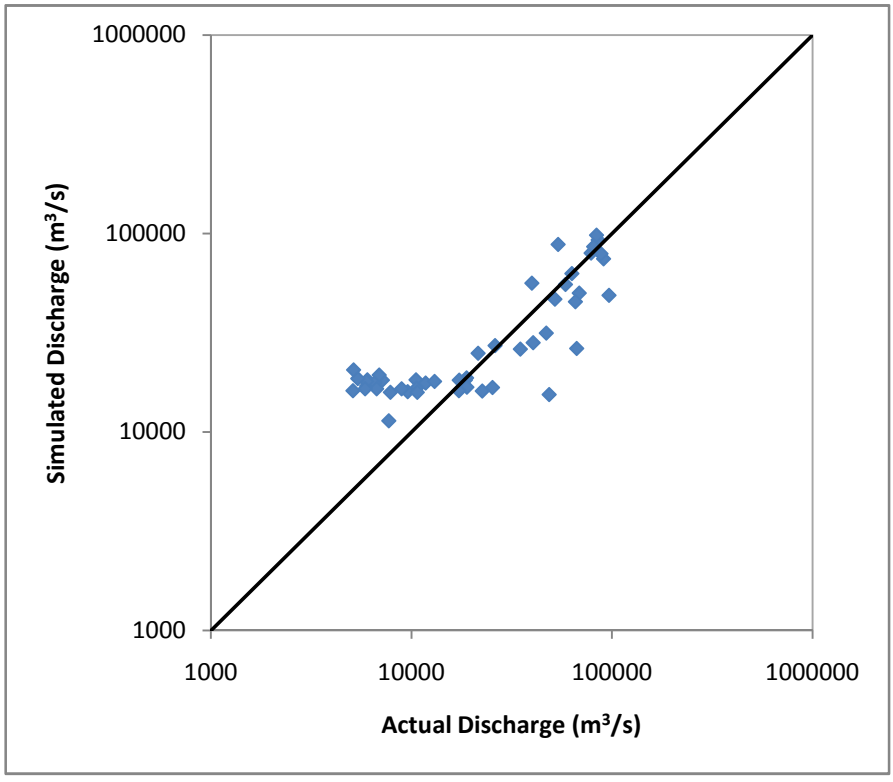

Figure B2d: Validation of the ANN model for trial 4

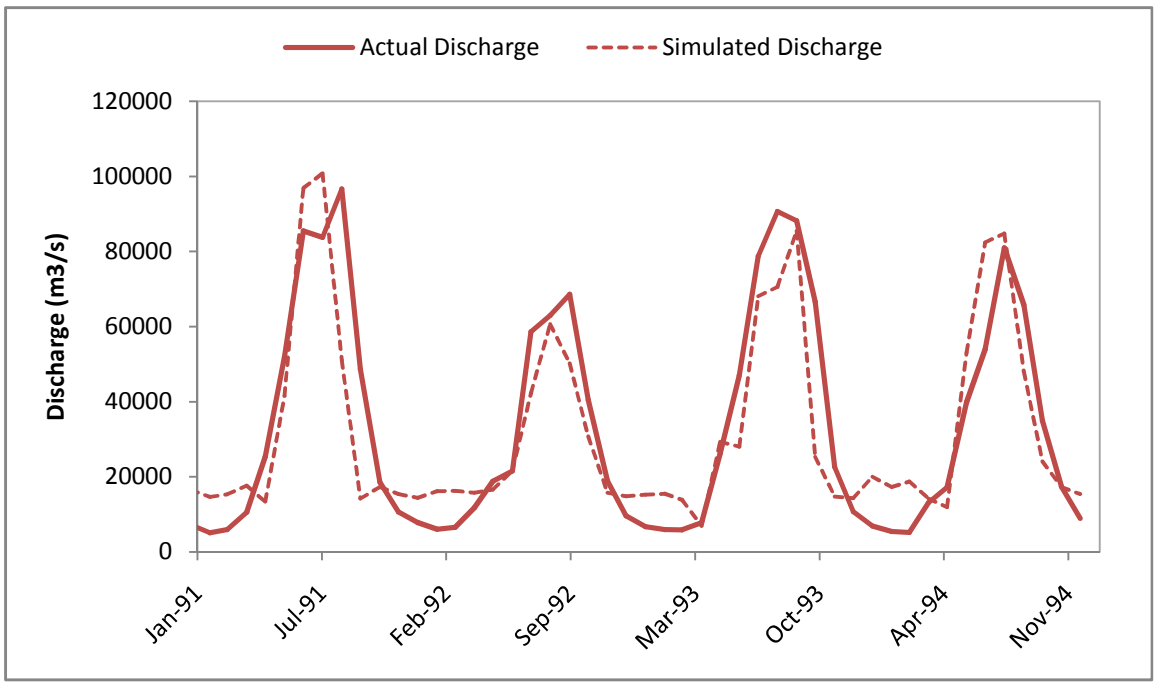

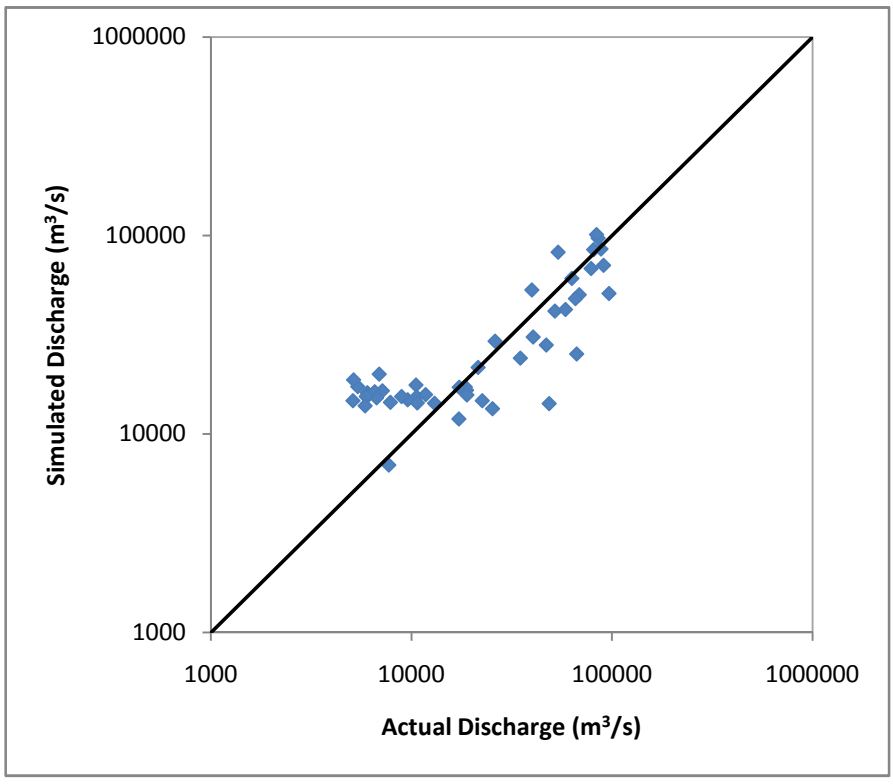

Figure B2e: Validation of the ANN model for trial 5

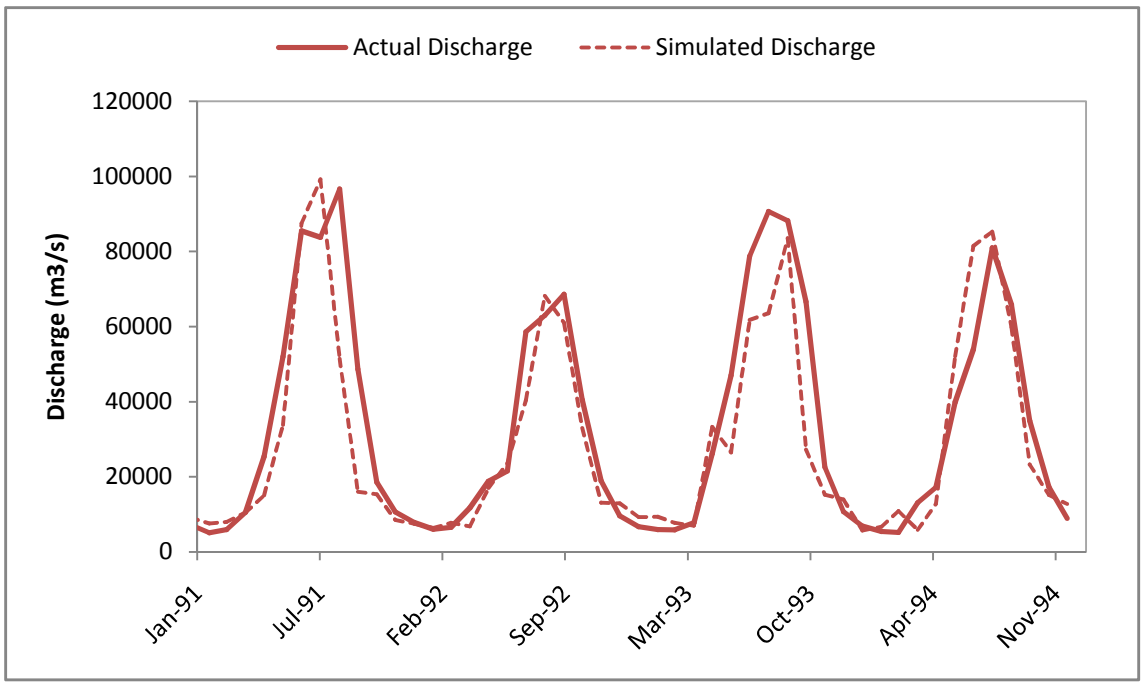

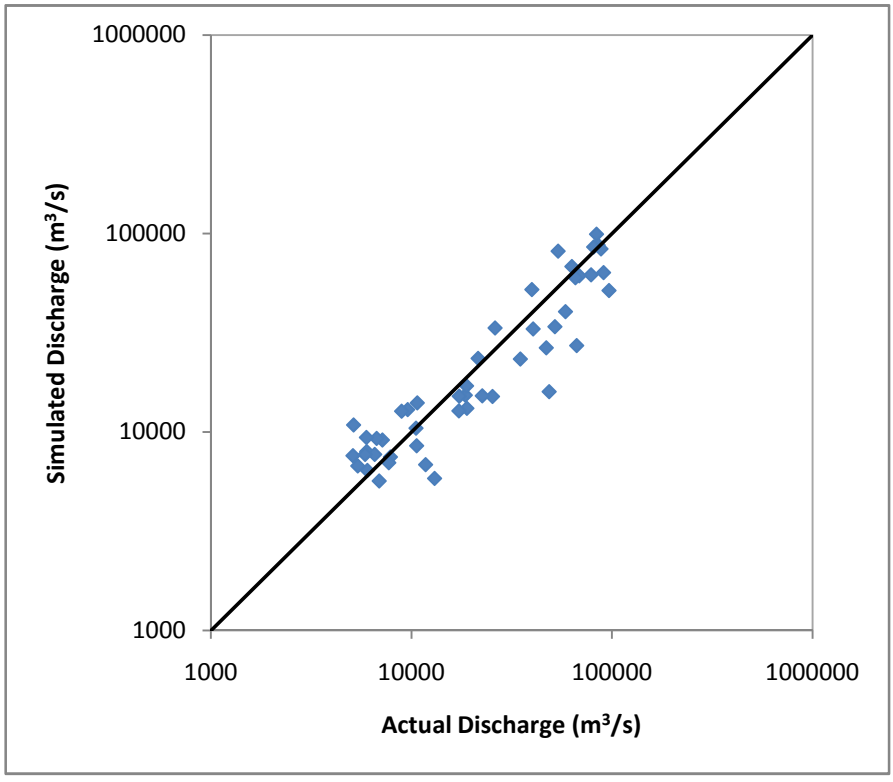

Figure B2f: Validation of the ANN model for trial 6

APPENDIX C

STABILITY CHECK AND WATER LEVEL RESULTS OF MIKE 21 FM

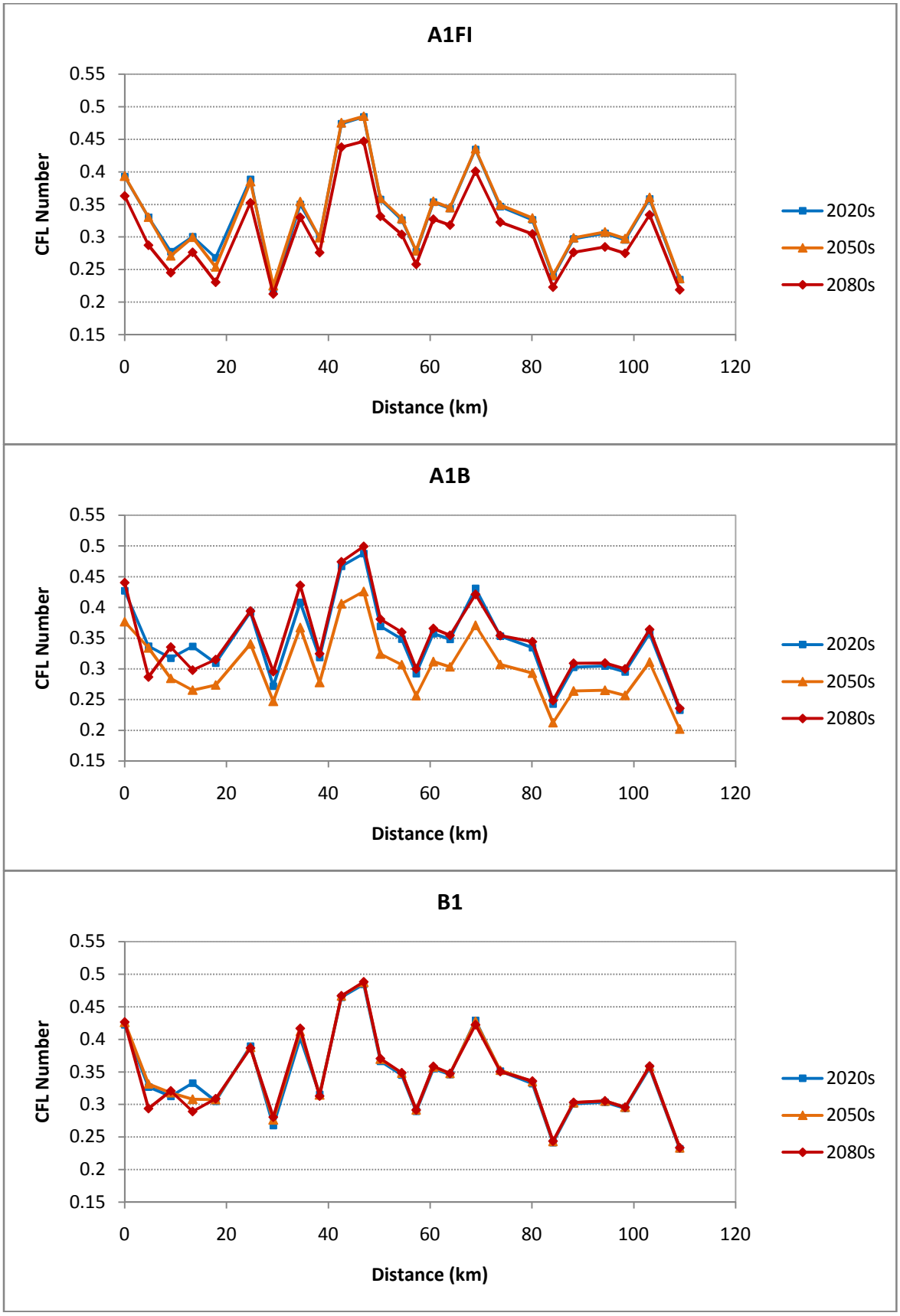

Figure C1: Variation of CFL number for the simulation of different scenarios

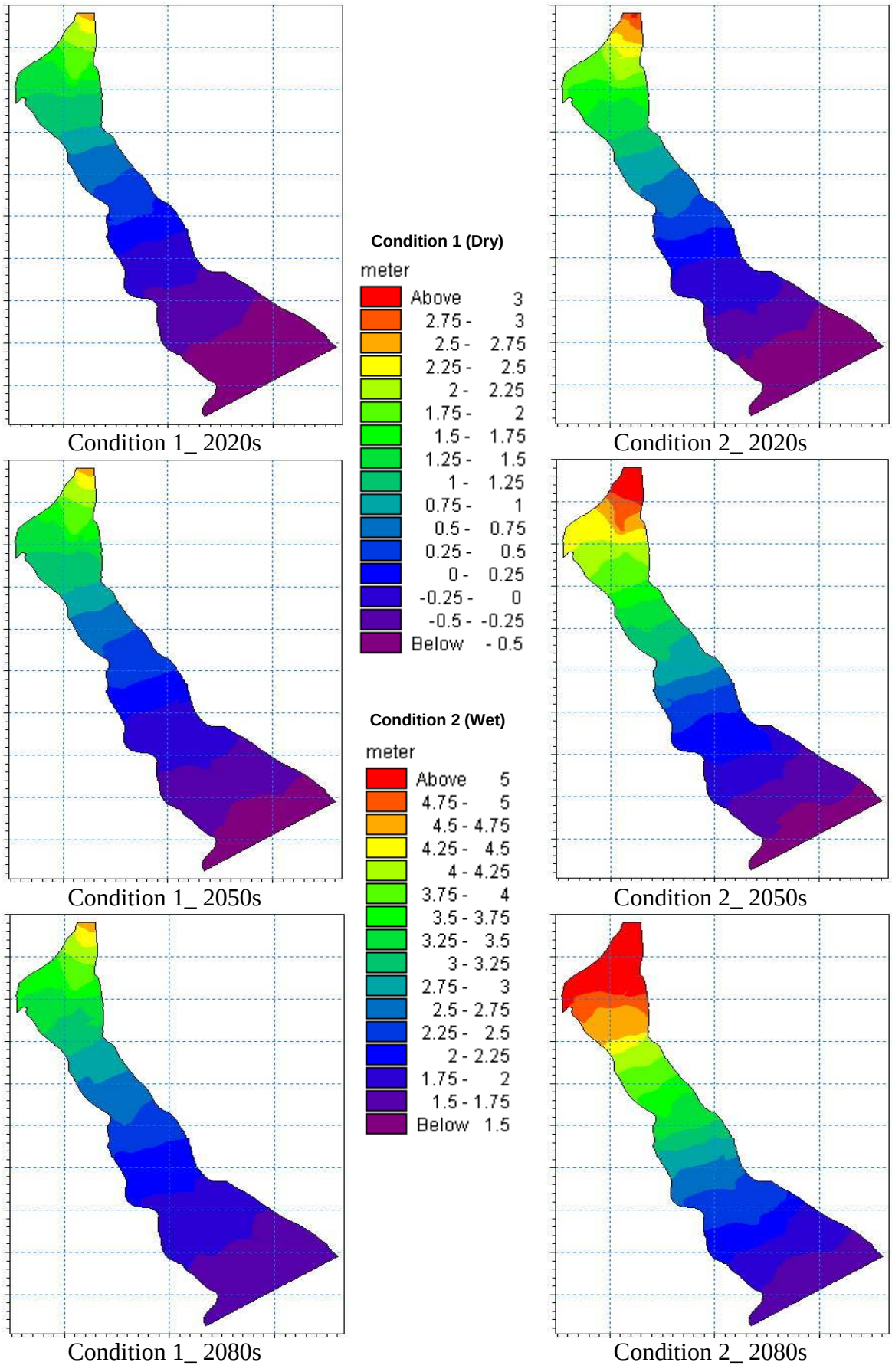

Figure C2a: Water level variation of scenario A1FI for different periods

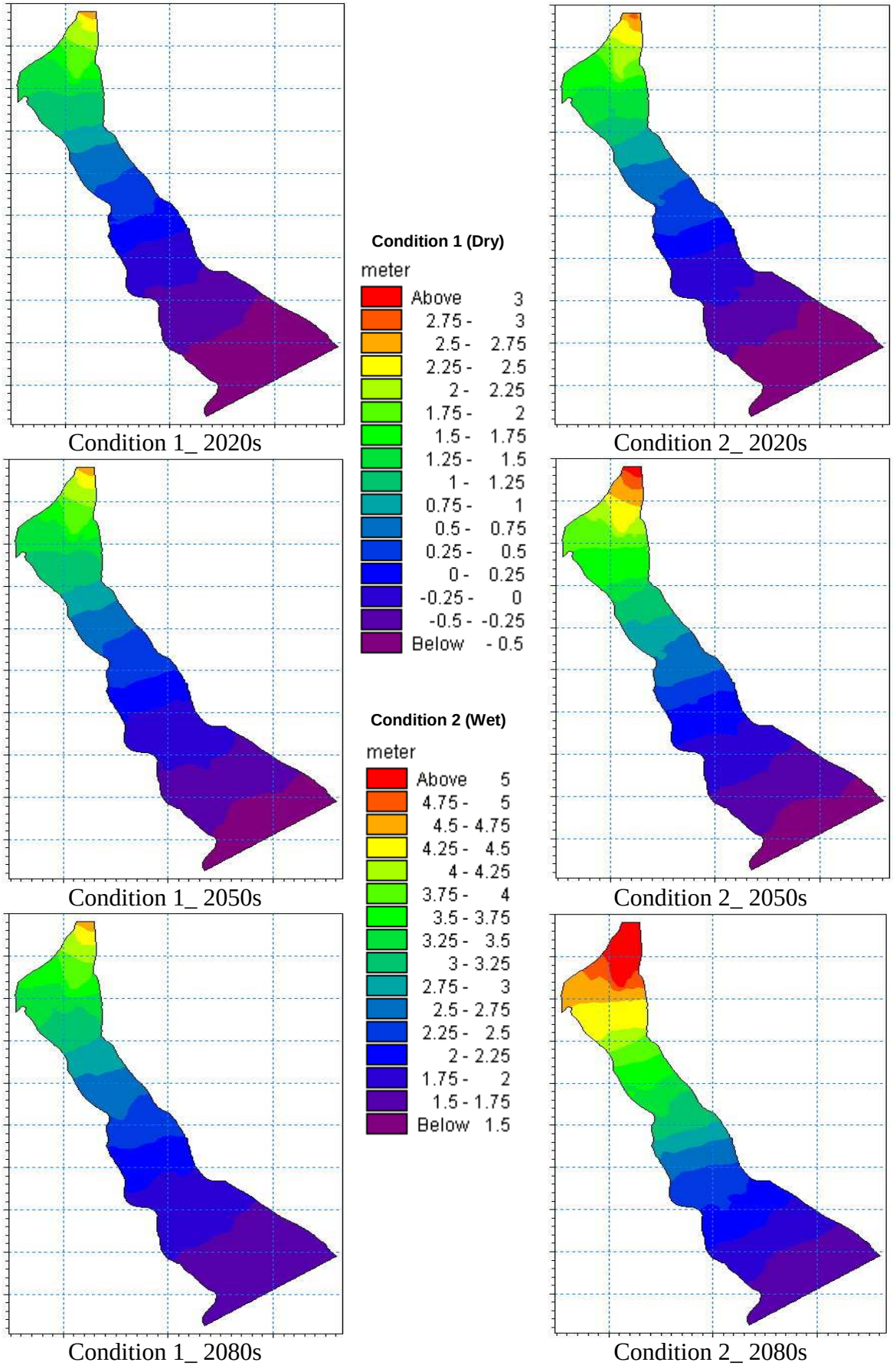

Figure C2b: Water level variation of scenario A1B for different periods

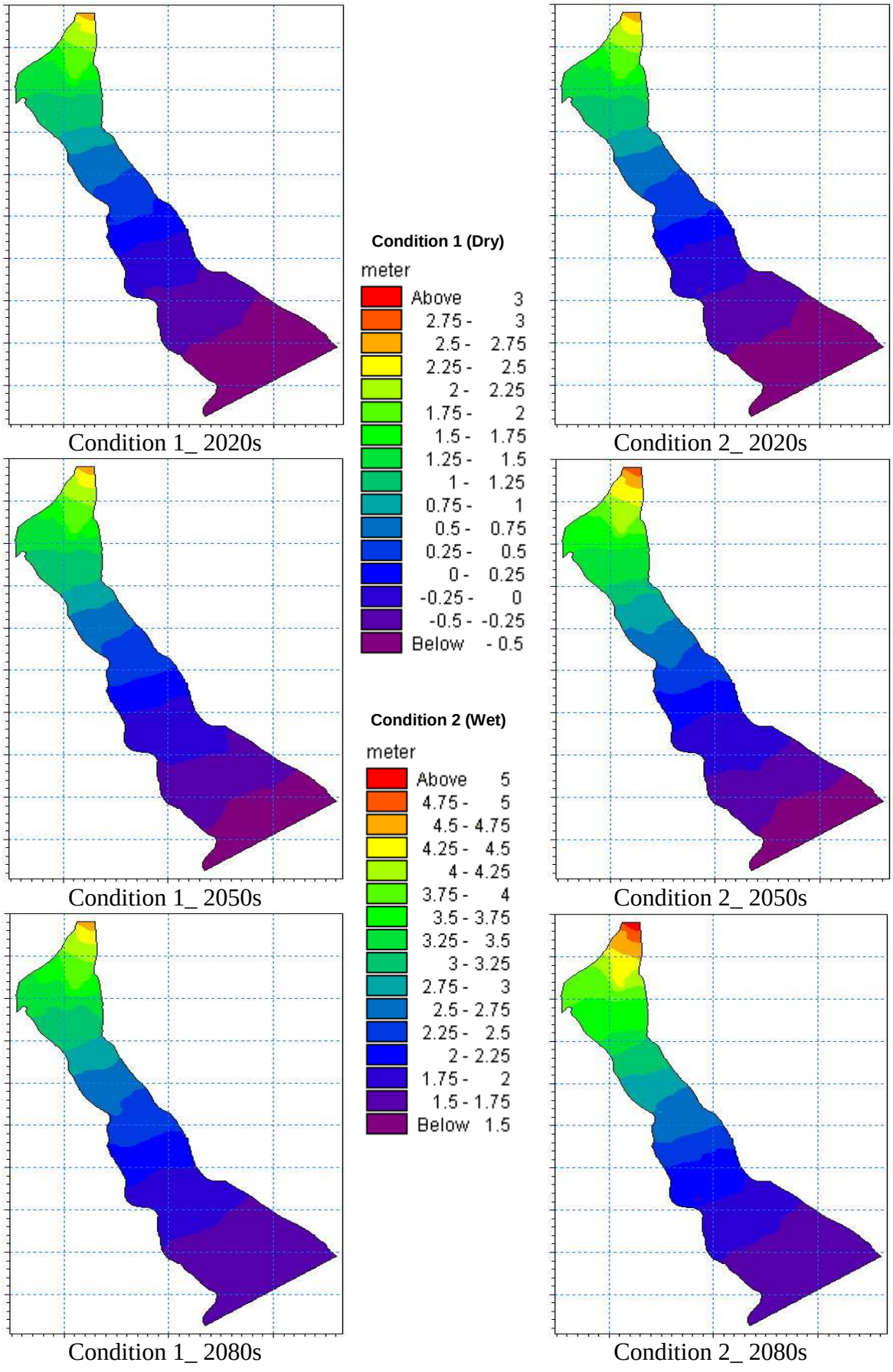

Figure C2c: Water level variation of scenario B1 for different periods